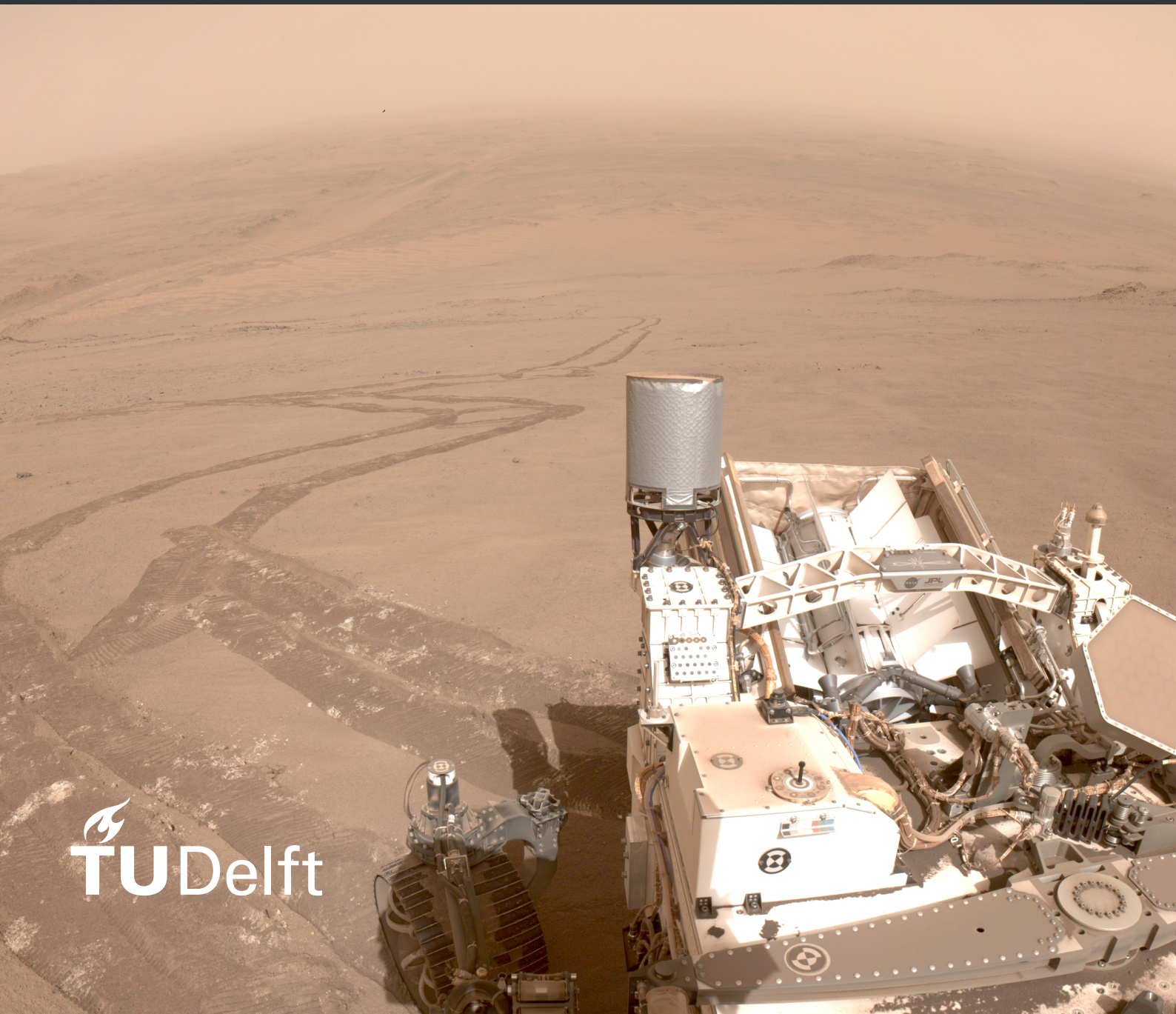


Gravity and Granular Matter

An Analysis of How Gravity Affects the Angle of
Repose of Granular Matter Through its
Avalanching Process

Nicolas Fosséprez



Gravity and Granular Matter

An Analysis of How Gravity Affects the Angle of Repose of Granular Matter Through its Avalanching Process

Thesis report

by

Nicolas Fosséprez

to obtain the degree of Master of Science
at the Delft University of Technology
to be defended publicly on February 17, 2025 at 13:30

Thesis committee:

Chair: Dr. Ir. W. van der Wal
Supervisor: Dr. S. J. de Vet
External examiner: Dr. Ir. B. Root
Place: Faculty of Aerospace Engineering, Delft
Project Duration: April, 2024 - February, 2025
Student number: 4558073

An electronic version of this thesis is available at <https://repository.tudelft.nl/>.

Faculty of Aerospace Engineering · Delft University of Technology

Cover Picture: Tracks shown in this image indicate the slipperiness of the terrain Perseverance has encountered during its climb up the rim of Jezero Crater. The image was taken by one of rover's navigation cameras on Oct. 11. 2024 (Credits: NASA/JPL-Caltech)



Copyright © Nicolas Fosséprez, 2025
All rights reserved.

Preface

This master thesis concludes my long journey at the TU Delft. Together with the literature study, this thesis report represents a personal challenge, cumulating over a year of work. The study of granular materials, rooted in planetary science, highlights the interdisciplinary nature of space engineering and its vast range of applications.

The topic of the angle of repose was, by far, not covered in class. It was therefore a challenge to dive into this new topic, while developing a scientific mindset of curiosity, self-questioning and critical thinking. I am grateful to have gotten the opportunity to work on such a project, and I will carry the skills gained over the last years into my future endeavours.

The hypo-/hypergravity experiments discussed in this thesis were obtained by the thesis supervisor dr. Sebastiaan de Vet during his own MSc thesis in 2009. The hypogravity experiments were supported by the Netherlands Space Office (grants SRON PB 09/001 and 2009-0142/TVD). We like to acknowledge the European Space Agency (ESA) for their support of the hypergravity experiments and specifically thank Alan Dowson and Jack van Loon from the ESA TEC-MMG LIS Lab for providing support for the Large Diameter Centrifuge at ESTEC in Noordwijk.

I am grateful for all the guidance and feedback I received during this project. I am thankful to my family and to my friends for their support during all those years. You definitely made this journey an enjoyable one.

*Nicolas Fosséprez
Delft, January 2025*

Summary

The study of planetary bodies enables scientists to apply the insights obtained from studying natural processes on Earth to understand the origins of other planets and vice versa. Geomorphology is therefore central to uncovering the history of Earth and the Solar System. In particular, the angle of granular terrain slopes, defined by the angle of repose, helps distinguish the environments in which these features formed. These concepts are applicable from natural processes to industrial domains involving granular matter. Experimental studies have isolated variables influencing the angle of repose, such as particle size, shape, and interstitial fluids. Gravity is the primary factor when studying planetary bodies, and only few studies have studied its effects on the angle of repose.

The literature shows that the relationship between gravity and the angle of repose remains inconclusive. The field has not been sufficiently explored to establish whether the differing findings are contradictory or complementary. The gap in the literature is identified as the lack of consensus between studies due the missing common framework for analysing the relationship between gravity and the angle of repose. The research objective of this research is to help interpreting the contradictions between studies by studying avalanches in granular materials. To this end, the main research question is defined: *How does gravity affect the angle of repose of granular materials through the mechanics of avalanching?*

This study utilises the raw video data from experimental campaigns conducted by S. de Vet prior to this study: hypergravity avalanching experiments performed in a centrifuge, covering effective gravity levels from 1g to 20g. The granular materials tested include glass beads, volcanic sand and river sand. Additionally, two mixtures were analysed: a glass-volcanic mixture displaying particle segregation and a river-volcanic mixture exhibiting particle stratification. The materials were poured into Hele-Shaw cells with varying opening diameters to study avalanches during pile formation, which were recorded on video using cameras.

A method was first developed to measure variables affecting the angle of repose from the videos of the experiments of S. de Vet. Priority was given to measuring the angles of repose, and the discharge flow. A detailed procedure was designed, which includes camera calibration, frame extraction, slope edge detection using a Canny edge detector, and angle measurement using linear regression. The method was validated on the camera used for hypergravity experiments with an accuracy of 3%. After implementation, raw data from the experiments in hypergravity with 3mm and 5mm cell openings were analysed, pre-processed to exclude low-quality sections and outliers using the 2σ -method, and refined for further interpretation.

The data analysis observed the “heartbeat graphs”, a novel visualization showing the evolution of the angle of repose (AoR) over time, revealing cyclic or stable trends that depend on experimental conditions. De Vet & Van den Boomgaard explored the use of the heartbeat graphs concept to study avalanching in Hele-Shaw cells (de Vet, *personal communication*) prior to this study, and its application was reintroduced in this research. Gravity and discharge flow were found to influence the AoR, with gravity also directly affecting discharge flow. At lower gravity levels (1g-5g), the mean AoR increases, stabilising at higher gravity levels (5g-20g). The discharge flow affects the standard deviation of the AoR, which serves as an indicator of the avalanching regimes. Higher discharge flows shift the regimes from discrete to transition, to rolling. The avalanching regime influences how gravity and discharge flow affect the AoR; from discrete to rolling regime, the mean AoR increases and stabilises at a material-dependent value, unaffected by gravity and discharge flow. Differences between static and dynamic AoR suggest distinct particle flow states along the slope, sometimes within the same regime. The observations on the mean AoR also apply to the static and dynamic AoR.

At first glance, the findings of this research appear to contradict previous studies, but closer examination reveals that differences in experimental conditions and avalanching regimes hinder comparability. The Froude number, introduced by Brucks et al. (2007), is identified as a critical parameter for standardising results across varying gravity regimes and experimental setups. By considering avalanching regimes as proxies for the Froude number, this research suggests that all studies may be observing a similar pattern

on the relationship between the AoR and gravity. However, most studies do not report Froude numbers, highlighting a critical gap in the literature.

Finally, it is concluded that the resulting relationship between gravity and the angle of repose in hypergravity answers the research questions. The comparison to literature extends this relationship to hypogravity levels, hypothesising that the relationship may take a “V-shaped” curve over the full range of gravity levels: the AoR is higher in low hypogravity due to cohesive forces, decreases near 1g as these forces weaken, increases again between 1g and 3g because of greater particle compaction induced by the stronger gravity, and finally stabilizes at 5g and above as avalanching regime transitions to a rolling regime. Validation of this hypothesis requires incorporating the Froude number across studies as a unified framework to reconcile findings. The research successfully achieves its objective by providing a path forward to bridge gaps in the literature. While the scope was limited to measuring the angle of repose from experimental video data, several recommendations are made for future research to expand on this work and improve methodological accuracy and robustness.

Contents

Preface	ii
Summary	v
List of Figures	xiv
List of Tables	xviii
I Literature Review & Research Definition	2
1 Introduction	4
2 Literature Review	6
2.1 Granular Materials & Angle of Repose	6
2.1.1 Properties & Forces on Granular Materials	6
2.1.2 Definitions of the Angle of Repose.	7
2.1.3 Experimental Methods to Study the Angle of Repose	8
2.1.4 Angle of Repose in Granular Mixtures.	8
2.1.5 Summary of Section 2.1	9
2.2 Studies on Gravity	12
2.2.1 Methods for Studying the Effect of Varying Gravity	12
2.2.2 Findings on the Effect of Gravity on the Angle of Repose in Literature	14
2.2.3 Discussion of the Literature on the Angle of Repose & Gravity	21
2.3 Summary of Chapter 2	21
3 Research Questions and Project Plan	24
3.1 Research Objective & Research Questions	24
3.1.1 Research Hypotheses	24
3.1.2 Sub-Research Questions	26
3.2 Research Plan	26
3.3 Summary of Chapter 3	26
II Method, Results & Discussion	30
4 Experimental Data	32
4.1 Experimental Setup	32
4.1.1 Hypergravity Experiments	32
4.1.2 Hypogravity Experiments.	33
4.2 Materials Tested in the Experiments	33
4.3 Raw Experimental Data	34
4.4 Summary of Chapter 4	35
5 Data Analysis Method	36
5.1 How Parameters Are Defined in the Literature	36
5.2 Parameter Selection for this Study	38
5.3 Data Analysis Method & Implementation	40
5.3.1 Numerical Implementation	40
5.3.2 Overview of the Logic	41
5.3.3 Part 0: Calibration	41
5.3.4 Part 1: Image Generation	42
5.3.5 Edge Detection Algorithm	42

5.3.6	Part 2: Optimisation of Edge Detection Parameters	43
5.3.7	Part 3: Angle of Repose Measurement	44
5.3.8	Discharge Flow Measurement	44
5.4	Method Verification & Validation	45
5.4.1	Verification	45
5.4.2	Validation	45
5.5	Non-Measured Parameters	46
5.6	Overview of Experiments Analysed	47
5.7	Data Pre-Processing	48
5.7.1	Filtering Inaccurate Measurements	48
5.7.2	Outlier Removal	49
5.8	Summary of Chapter 5	49
6	Experimental Results	52
6.1	Evolution of the Angle of Repose over Time	52
6.1.1	Introduction to the Heartbeat Graph	52
6.1.2	Heartbeat Graph Results	55
6.2	Distribution of Angle of Repose Values	61
6.3	Effects of Gravity & Discharge Flow on Angle of Repose	68
6.3.1	Relation Between Gravity & Discharge Flow	68
6.3.2	Effect of Gravity and Discharge Flow on Mean Angle of Repose	70
6.3.3	Effect of Gravity & Discharge Flow on the Standard Deviation of the Angle of Repose	74
6.4	Effects of Avalanching Regimes	78
6.4.1	Definition of Avalanching Regimes	79
6.4.2	Standard Deviation of Angle of Repose Against Discharge Flow per Avalanche Regimes	80
6.4.3	Mean Angle of Repose Against Gravity & Discharge Flow per Avalanche Regime	81
6.5	Effects on Static & Dynamic Angles of Repose	83
6.5.1	Defining and Measuring Static & Dynamic Angles of Repose	84
6.5.2	Effects of Gravity, Discharge Flow & Avalanching Regime on Static & Dynamic Angles of Repose	85
6.6	Additional Observations on Particle Separation	87
6.7	Summary of Chapter 6	87
7	Discussion	90
7.1	Interpretation of the Key Findings	90
7.2	Comparison to the Literature	91
7.2.1	Studies with a Significant Relationship	92
7.2.2	Studies with No Significant Relationship	93
7.2.3	Discussion of the Additional Observations on Particle Sorting	96
7.3	Summary of Chapter 7	97
III	Closure	100
8	Conclusions	102
8.1	Addressing the Research Questions & Hypotheses	102
8.2	Contributions to the Literature	105
8.3	Achievement of Research Objectives	105
9	Recommendations	106
	References	109
A	Method Validation Results	110
B	Detailed Research Results	112
B.1	Heartbeat Graphs of the Angle of Repose	113
B.2	Discharge Flow Against Gravity	122
B.3	Mean Angle of Repose against Gravity & the Discharge Flow	123

B.4	Standard Deviation of the Angle of Repose against Gravity & the Discharge Flow	125
B.5	Mean Angle of Repose Against Discharge Flow & Gravity per Avalanche Regimes	129
B.6	Static & Dynamic Angles of Repose	131
C	Effect of Gravity on Particle Separation	134

Nomenclature

List of Abbreviations

2D	Two-dimensional
3D	Three-dimensional
AoR	Angle of Repose
DEM	Discrete Elements Method
ESA	European Space Agency
fps	Frames per second
g-level	Gravity level
HD	High Definition
ISS	International Space Station

List of Symbols

δ	Flowing layer thickness
λ	Stratification layer wavelength
ω	Angular velocity
σ	Standard deviation
θ	Angle of Repose
θ	Pixel gradient direction
c_x, c_y	Optical centers (in x and y directions)
d	Average particle diameter
f	Discharge flow
f_x, f_y	Focal length (in x and y directions)

Fr	Froude number
Fr_{surf}	Froude number at the flow surface
g, g_0	Gravitational acceleration at the Earth surface assumed to be 9.80665m/s^2
G, G_x, G_y	Pixel intensity gradient (in horizontal x and vertical y directions)
g_{eff}	Effective gravitational acceleration
H	Hele-Shaw cell height
k_1, k_2, k_3	Radial distortion coefficients
L	Hele-Shaw cell length
p_1, p_2	Tangential distortion coefficients
R	Radius of the rotating drum
R^2	Linear regression coefficient of determination
R_0	Avalanche layer thickness
T	Stratification layer thickness
t	Time
u	Flow velocity
v	Avalanche velocity
v'	Kink velocity
W	Hele-Shaw cell width

List of Figures

2.1	Example of segregation in a mixture of large glass beads and small sand grains by Makse et al. (1998).	9
2.2	Example of stratification in a mixture of small glass beads and large sand grains by Makse et al. (1998).	9
2.3	Correlation between the Angle of Repose and the Froude number (Brucks et al., 2007). . .	15
2.4	As the Froude number increases, avalanche regime changes: discrete avalanche (empty triangle), alternating between discrete avalanching and rolling (plain triangle), rolling (empty circle), cascading (empty square), and centrifuging (plain diamond) (Brucks et al., 2007). . .	15
2.5	Measured AoR against gravity levels for glass beads at a nominal drum rotation speed of 6.75rpm (Klein and White, 1990).	15
2.6	The measured AoR for the glass beads, plotted against a dimensionless parameter $1/\sqrt{G}$. The best fit line is plotted, for a regression R^2 of 0.845 (Klein and White, 1990).	15
2.7	(a) An example of how the AoR was measured in the experiment of Marshall <i>et al.</i> In this setup, the moving block is applying pressure from the right side of the picture. (b) Resulting measurements of the AoR at different gravity levels, with error bars (Marshall et al., 2018).	16
2.8	Slope shape after the avalanche for glass grains at different gravity levels. The top shows the binarised shape at each gravity level, the bottom shows the original view of the experiment by the camera (Hofmeister et al., 2009).	17
2.9	Angle of the steepest part of the slope (square), and its position as measured from the top ridge (triangle), per gravity level. These measurements were performed in the experiment with glass beads. The arrow indicates an estimated value (Hofmeister et al., 2009).	17
2.10	Angle of repose in the hourglass experiments with basalt spheres per gravity level. Error bars denote the range between left and right angles (Hofmeister et al., 2009).	17
2.11	Angle of repose against particle diameter for glass beads. The plain squares are the numerical predictions by Elekes <i>et al.</i> , the other symbols are results from other studies (Elekes and Parteli, 2021).	19
2.12	Angle of repose against particle diameter at varying gravity levels for glass beads (Elekes and Parteli, 2021).	19
4.1	The Large Diameter Centrifuge at ESTEC (Photo: ©ESA)	33
4.2	Test setup used for the hypergravity experiments.	33
4.3	Microscope pictures of the material species used in this research (de Vet, 2010)	34
5.1	Stages of the dynamics of stratification. Definitions of the angles of repose in (c) (Makse et al., 1998).	37
5.2	Definition of the zones and angles of repose in the case of segregation (with a sample from Makse et al. (1998)).	39
5.3	Definition of the zones and angles of repose in the case of stratification (with a sample from Makse et al. (1998)).	39
5.4	Overview of the workflow of the methodology to measure the variables from the experimental data.	41
5.5	Sample triangles filmed on the cameras to validate the slope angle measurements.	46
5.6	Example of slope angle measurements and associated R^2 values over time, prior to data cleaning.	48
5.7	Example of slope angle measurements and associated R^2 values over time, after data filtering based on the threshold value of $R^2 > 0.997$	49
5.8	Example of outlier values in the measurements and cleaning using a 2σ rule.	49

6.1	Example of a heartbeat graph showing the evolution of the angle of repose during the pile formation. The discrete avalanching regime clearly shows the cyclic reactive pattern between the upper and lower AoR as the avalanche travels along the slope.	53
6.2	Example of a heartbeat graph in rolling avalanching regime, where no cyclic reactive pattern is observed between the upper and lower AoR.	54
6.3	Example of the heartbeat graphs of three experiments performed for the same parametric conditions: volcanic sand, opening of 3mm, gravity level of 1g.	54
6.4	Illustration of shapes that the granular slope is expected to take. The shape can be described as Straight, Concave, Convex or Irregular.	55
6.5	Heartbeat graphs of glass beads in varying gravity acceleration, with a 3mm opening.	56
6.6	Heartbeat graphs of glass beads in varying gravity acceleration, with a 5mm opening.	56
6.7	Heartbeat graphs of river sand in varying gravity acceleration, with a 5mm opening.	57
6.8	Heartbeat graphs of volcanic sand in varying gravity acceleration, with a 3mm opening.	58
6.9	Heartbeat graphs of volcanic sand in varying gravity acceleration, with a 5mm opening.	58
6.10	Heartbeat graphs of the glass-volcanic mixture in varying gravity acceleration, with a 3mm opening.	59
6.11	Heartbeat graphs of the glass-volcanic mixture in varying gravity acceleration, with a 5mm opening.	59
6.12	Heartbeat graphs of the river-volcanic mixture in varying gravity acceleration, with a 3mm opening.	60
6.13	Heartbeat graphs of the river-volcanic mixture in varying gravity acceleration, with a 5mm opening.	60
6.14	Distribution of the angle of repose of glass beads on the upper and bottom halves of the slope when varying gravity and the cell opening.	62
6.15	Distribution of the angle of repose of river sand on the upper and bottom halves of the slope when varying gravity, with a 5mm opening.	63
6.16	Distribution of the angle of repose of volcanic sand on the upper and bottom halves of the slope when varying gravity and the cell opening.	64
6.17	Distribution of the angle of repose of the glass-volcanic mixture on the upper and bottom halves of the slope when varying gravity and the cell opening.	65
6.18	Distribution of the angle of repose of the river-volcanic mixture on the upper and bottom halves of the slope when varying gravity and the cell opening.	66
6.19	Discharge volume flow against gravity for varying materials	69
6.20	Mean AoR against gravity of glass beads	70
6.21	Mean AoR against gravity of volcanic sand	70
6.22	Mean AoR against discharge flow of glass beads	71
6.23	Mean AoR against discharge flow of volcanic sand	71
6.24	Average overall angle of repose of the glass-volcanic mixture against gravity and the discharge volume flow, with varying cell opening.	71
6.25	Average upper angle of repose of the glass-volcanic mixture against gravity and the discharge volume flow, with varying cell opening.	72
6.26	Average bottom angle of repose of the glass-volcanic mixture against gravity and the discharge volume flow, with varying cell opening.	72
6.27	Average overall angle of repose of the river-volcanic mixture against gravity and the discharge volume flow, with varying cell opening.	73
6.28	Standard deviation against gravity of glass beads	75
6.29	Standard deviation against gravity of volcanic sand	75
6.30	Standard deviation in the angle of repose against the discharge flow. Plotted for the overall slope, for all materials and all openings.	76
6.31	Scatter plot of the standard deviation in the angle of repose against the discharge flow. This is for the overall slope, for all materials and all openings.	77
6.32	Images of the discrete avalanching regime. The avalanching layer is thin compared to the pile height. The blue arrow points at the avalanche front which moves from its highest point (in the first image) to the bottom of the pile (in the last image). Each snapshot is taken less than a second apart.	79

6.33 Images of the rolling avalanching regime. The avalanching layer is a continuous flow of particles from the top to the bottom of the pile. Each snapshot is taken less than a second apart.	79
6.34 Images of the transition avalanching regime. The upper half of the slope has a continuous flow of particles. The blue arrow points at the avalanche front which moves from its highest point at the middle of the slope (in the first image) to the bottom of the slope (in the last image). Each snapshot is taken less than a second apart.	80
6.35 Scatter plot of the standard deviation in the angle of repose against the discharge flow. Avalanche regimes are identified. This is for the overall slope, for all materials and all openings.	81
6.36 Mean AoR against gravity of glass beads	82
6.37 Mean AoR against gravity of volcanic sand	82
6.38 Mean AoR against discharge flow of glass beads	82
6.39 Mean AoR against discharge flow of volcanic sand	82
6.40 Average overall angle of repose of the river-volcanic mixture against gravity and the discharge volume flow, with varying avalanching regimes.	83
6.41 Example of detected peak values of static and dynamic AoR in a discrete regime	85
6.42 Example non-detected peak values of static and dynamic AoR in a rolling regime	85
6.43 Static and Dynamic AoR against gravity and discharge for glass beads	86
6.44 Static and Dynamic AoR against gravity and discharge for the glass-volcanic mixture	87
7.1 Hypothetical relationship between the angle of repose and gravity in the hypergravity regime.	91
7.2 V-shaped relationship between gravity and the angle of repose.	96
B.1 Heartbeat graphs of glass beads in varying gravity acceleration, with a 3mm opening.	113
B.2 Heartbeat graphs of glass beads in varying gravity acceleration, with a 5mm opening.	114
B.3 Heartbeat graphs of river sand in varying gravity acceleration, with a 5mm opening.	115
B.4 Heartbeat graphs of volcanic sand in varying gravity acceleration, with a 3mm opening.	116
B.5 Heartbeat graphs of volcanic sand in varying gravity acceleration, with a 5mm opening.	117
B.6 Heartbeat graphs of the glass-volcanic mixture in varying gravity acceleration, with a 3mm opening.	118
B.7 Heartbeat graphs of the glass-volcanic beads in varying gravity acceleration, with a 5mm opening.	119
B.8 Heartbeat graphs of the river-volcanic mixture in varying gravity acceleration, with a 3mm opening.	120
B.9 Heartbeat graphs of the river-volcanic mixture in varying gravity acceleration, with a 5mm opening.	121
B.10 Discharge volume flow against gravity for each material	122
B.11 Average overall angle of repose against gravity and the discharge volume flow, with varying cell opening, for glass beads.	123
B.12 Average overall angle of repose against gravity and the discharge volume flow, with varying cell opening, for river sand.	123
B.13 Average overall angle of repose against gravity and the discharge volume flow, with varying cell opening, for volcanic sand.	123
B.14 Average overall angle of repose against gravity and the discharge volume flow, with varying cell opening, for the glass-volcanic mixture.	124
B.15 Average upper angle of repose against gravity and the discharge volume flow, with varying cell opening, for the glass-volcanic mixture.	124
B.16 Average bottom angle of repose against gravity and the discharge volume flow, with varying cell opening, for the glass-volcanic mixture.	124
B.17 Average bottom angle of repose against gravity and the discharge volume flow, with varying cell opening, for the river-volcanic mixture.	125
B.18 Scatter plot of the standard deviation in the angle of repose of glass beads against gravity and the discharge flow, for varying openings.	125
B.19 Scatter plot of the standard deviation in the angle of repose of river sand against gravity and the discharge flow, for varying openings.	126

B.20 Scatter plot of the standard deviation in the angle of repose of volcanic sand against gravity and the discharge flow, for varying openings.	126
B.21 Scatter plot of the standard deviation in the angle of repose of the river-volcanic mixture against gravity and the discharge flow, for varying openings.	126
B.22 Scatter plot of the standard deviation in the angle of repose of the glass-volcanic mixture against gravity and the discharge flow, for the overall slope for varying openings.	127
B.23 Scatter plot of the standard deviation in the angle of repose of the glass-volcanic mixture against gravity and the discharge flow, for the upper slope for varying openings.	127
B.24 Scatter plot of the standard deviation in the angle of repose of the glass-volcanic mixture against gravity and the discharge flow, for the bottom slope for varying openings.	127
B.25 Scatter plot of the standard deviation in the angle of repose against the discharge flow. This is for the overall slope, for all materials and all openings.	128
B.26 Scatter plot of the standard deviation in the angle of repose against the discharge flow. This is for the upper half of the slope, for all materials and all openings.	128
B.27 Scatter plot of the standard deviation in the angle of repose against the discharge flow. This is for the bottom half of the slope, for all materials and all openings.	129
B.28 Average overall angle of repose against gravity and the discharge volume flow, with varying avalanching regimes, for glass beads.	129
B.29 Average overall angle of repose against gravity and the discharge volume flow, with varying avalanching regimes, for the river sand.	130
B.30 Average overall angle of repose against gravity and the discharge volume flow, with varying avalanching regimes, for the volcanic sand.	130
B.31 Average overall angle of repose against gravity and the discharge volume flow, with varying avalanching regimes, for the glass-volcanic mixture.	130
B.32 Average overall angle of repose against gravity and the discharge volume flow, with varying avalanching regimes, for the river-volcanic mixture.	131
B.33 Static and Dynamic AoR against gravity and discharge for glass beads.	131
B.34 Static and Dynamic AoR against gravity and discharge for river sand.	132
B.35 Static and Dynamic AoR against gravity and discharge for volcanic sand.	132
B.36 Static and Dynamic AoR against gravity and discharge for the glass volcanic mixture.	132
B.37 Static and Dynamic AoR against gravity and discharge for the river volcanic mixture.	133
C.1 Visual changes in the particle stratification patterns in the river-volcanic sand mixture when varying the gravity level (from 1g to 5g) for cells with a 3mm opening on the left, and a 5mm opening on the right.	135
C.2 Visual changes in the particle stratification patterns in the river-volcanic sand mixture when varying the gravity level (from 10g to 20g) for cells with a 3mm opening on the left, and a 5mm opening on the right.	136
C.3 Visual changes in the particle segregation patterns in the glass beads-volcanic sand mixture when varying the gravity level (from 1g to 5g) for cells with a 3mm opening on the left, and a 5mm opening on the right.	138
C.4 Visual changes in the particle segregation patterns in the glass beads-volcanic sand mixture when varying the gravity level (from 10g to 20g) for cells with a 3mm opening on the left, and a 5mm opening on the right.	139

List of Tables

2.1	Definitions of the angle of repose across literature, with the test setups, mixture types and avalanching regimes used.	11
2.2	Main studies on the effect of gravity on the angle of repose of granular materials, with their experiment setup and variables considered	13
2.3	Main findings of the studies on the effect of gravity on the angle of repose of granular materials.	20
4.1	Properties of the material species used during the hypogravity and hypergravity experiments	34
4.2	Overview of the experiments conducted in the hypergravity environment. "Yes" means that the experiment was performed and "No" means that the experiment was either not performed or that its data could not be retrieved.	35
5.1	Definition of variables to measure from the experimental data. Each parameter is defined and assigned with a symbol, units, and a priority-level.	40
5.2	Triangles dimensions	46
5.3	Overview of the experimental data analysed to generate data. "Yes" means that the experiment was analysed and "No" means that the experiment was not.	47
6.1	Overview of the avalanching regimes observed in the experimental videos for all parametric conditions.	80
7.1	Main findings of the studies on the effect of gravity on the angle of repose of granular materials, including the findings of this research research. The conclusions of each study are coloured as follows: in green a negative relationship; in yellow an insignificant relationship; in red a positive relationship; white for additional conclusions on the relationship.	95
8.1	Overview of the research hypotheses verification, highlighting the hypotheses that are accepted (green) and rejected (red).	104
A.1	Validation results for the measuring accuracy for the angle of repose, performed with various cameras.	110

Part I

Literature Review & Research Definition

Introduction

Much can be learned from the landscapes of our planetary neighbours, like the Moon and Mars. Their terrains, shaped by meteorite impacts, volcanic processes, and the forces of wind, water, or ice, reveal their history through physical forms and patterns (Kleinhans, 2005). Studying the planets of the Solar System allows scientists to apply the knowledge of the natural processes happening on Earth to learn about their origins, and vice-versa. Geomorphology is therefore at the core of understanding the history of the Earth and the Solar System.

Marks of wind, water, and ice appear in features like dunes, gullies, canyons, and deltas (Braat et al., 2024, Kleinhans, 2005). As the water, wind and ice move over rock, they gradually erode it, separating small particles that flow along with them. These particles eventually settle and form sediment layers, which then undergo lithification as they accumulate. Though Mars has lost its surface water, the preserved landforms provide planetary scientists with evidence of its past presence (Braat et al., 2024, Kleinhans, 2005). One way to differentiate the environments where these features developed is through their slope angles, characterized by the angle of repose. This angle is vital in understanding the flow properties of granular materials (Al-Hashemi and Al-Amoudi, 2018). The angle of repose does not only apply to the study of natural processes but also to that of industrial processes like pharmaceutical manufacturing, food processing and storage, construction materials production, and additive manufacturing to name a few (Al-Hashemi and Al-Amoudi, 2018). This last one will become relevant in the future lunar exploration and its use of in-situ resources to build structures¹ (Cesaretti et al., 2014).

Reproducing these natural phenomena with complete accuracy in a lab is challenging. Scientists have developed experimental setups to isolate variables influencing the angle of repose, such as particle size, shape, and the presence of an interstitial fluid between particles (Al-Hashemi and Al-Amoudi, 2018). Yet, the role of one parameter is still inconclusive. This parameter is gravity, which varies greatly across planetary bodies. Gravity has often been assumed to have little to no effect on the angle of repose (Kleinhans et al., 2011). This position was based on the assumption that the friction force and weight were the only two forces applied to the particles avalanching along a slope, and that the effect of gravity cancels out when calculating the force equilibrium on each particle. However, advancements in understanding particle interactions such as cohesive forces have led scientists to reconsider these assumptions, as gravity would therefore not cancel out with friction and affect the angle of repose (Kleinhans et al., 2011). Approximately a dozen studies have investigated gravity's impact on the angle of repose, with mixed outcomes. Some findings indicate an increase in the angle under varied gravity, others a decrease, and some no significant effect (Klein and White, 1990, Kleinhans et al., 2011, Marshall et al., 2018). This inconsistency could stem from differences in experimental setups and varying definitions of the angle of repose across studies (Al-Hashemi and Al-Amoudi, 2018). The problem is that these contradictory findings are taken out of their laboratory context to be applied to field observations. Studies like that of Atwood-Stone and McEwen (2013) observe variations in the slopes of dunes on Mars measured from satellite imagery, find variations in a range of 5° , and conclude that gravity has no effect on the angle of repose because their observations are in similar range to terrestrial dunes. This conclusion can be supported by studies like that of Marshall et al. (2018), who find a similar range in the variations of the slope angle values and conclude that gravity has no significant effect on the angle of repose. However,

¹Regolith-Polymer 3D Printing, visited on 11/11/24. <https://technology.nasa.gov/patent/KSC-TOPS-88>

other studies like that of Elekes and Parteli (2021) observe an effect of gravity which significantly varies the angle of repose within a range of 5° .

Because of the clear lack of consensus among the studies in the literature, it is too early to use the assumptions on the effect of gravity on the angle of repose to infer the geomorphology of planetary bodies. This thesis intends to help move towards a consensus across the literature, by studying the angle of repose of granular materials in varying gravity environments, and answers the following research question:

How does gravity affect the angle of repose of non-cohesive granular materials through the mechanics of avalanching?

The answer to this research question is developed throughout this thesis report. An overview of the current knowledge of the angle of repose across the literature is given in Chapter 2 to provide the reader with the required background knowledge. The research objective, research questions and hypotheses are then laid out in Chapter 3 with a research plan. This plan is then executed throughout the following chapters, where the experimental data used for the research is presented in Chapter 4. The method used to measure the various parameters from the experimental data is detailed in Chapter 5. All measured parameters are then analysed to infer their relations to each other in Chapter 6. These results are compared to other studies from the literature in Chapter 7. Finally, the conclusions of this study are presented in Chapter 8, and a series of recommendations for further research are given in Chapter 9.

2

Literature Review

A literature review was performed in the initial phase of this thesis research, covering the topics of granular materials, their angle of repose and gravity. This chapter provides a summary of the findings of the literature review, which lays the ground to identify a research objective and research questions for this thesis (done in the following Chapter 3).

In Section 2.1, the general properties of granular materials are synthesised to better understand how they are classified, measured and compared to each other. The angle of repose is then looked at in particular to further understand its role in the avalanching mechanics of granular materials.

Finally, the main studies on the topic of how gravity affects the angle of repose are explored in Section 2.2 to identify their findings, their agreements or disagreements, and how one can further contribute to this topic.

2.1. Granular Materials & Angle of Repose

A **granular material** is an ensemble of solid particles of a one kind of material. Mixtures of different kinds of granular materials can be found in nature. The size of the particles can vary from one micrometer to a couple meters in size. Their shape varies based on the structure of each material and the particle environment. Different forces act on the particles, and because of this wide variety in particle shape and size, all particles are not affected equally by those forces (Al-Hashemi and Al-Amoudi (2018)).

This section provides a basic understanding of the concepts around the angle of repose. Section 2.1.1 introduces the general properties of granular materials and the main forces affecting the particles. Section 2.1.2 explores the different definitions that have been given to the angle of repose in the literature. Section 2.1.3 presents how the angle of repose is studied in practice, through various experimental methods. Section 2.1.4 dives into the new properties that can be observed when multiple granular materials are mixed together.

2.1.1. Properties & Forces on Granular Materials

Forces on Granular Materials

Two of the main forces acting upon granular particles are gravity and friction (Kleinhans et al., 2011). **Gravity** depends on the distance between two particles and their masses. **Friction** depends on the normal force acting through the point of contact between two particles in contact, and a linear friction coefficient which is material-dependent. The friction force therefore depends on the slope of a pile of granular material, as it changes the angle at which the particles touch each other. The role of friction is to act against gravity to let the particles pile on top of each other until a point where gravity becomes stronger than friction and the pile falls down. If gravity and friction are the only forces acting on particles, then the maximum angle of the slope at which the pile becomes unstable and crumbles does not depend on gravity. This is because the friction force is by definition equal to the component of the particle weight normal to the contact point. Solving the equation for when weight and friction are in equilibrium shows that it can be simplified to an equation independent of the weight term (and therefore gravity). This conclusion relies on the main assumption that gravity and friction are the main forces acting on the particles. It was often accepted in literature, but was later proven to not be correct for all particle sizes as the assumption that

other forces such as cohesive forces could be ignored is wrong (Kleinhans et al., 2011; Elekes and Parteli, 2021).

Various other forces act on the particles and they can be grouped as the **cohesive forces** (or cohesive factors). The **Van der Waals forces** act at a molecular scale, originating from fluctuations in the electron clouds of molecules (Margenau, 1939). The **electrostatic force** (or Coulomb force) arises from the electric charge of atoms and molecules. Described by Coulomb's law, it is effective at very small distances. The **capillary actions** (and force) is a behaviour of liquids moving through tight spaces. Surface tension is a natural tendency of liquid molecules to attract each other and keep a tension force at the liquid borders. Surface tension and other attractive forces are factors of the capillary actions. For granular materials, the capillary actions highlight the importance of the relation between the particles and the interstitial fluid, like air or water for example (Butt and Kappl, 2009).

The intensity of the cohesive forces introduced in this section varies depending on the particle size, on the interstitial fluid and gravitational environment. Cohesive forces are generally predominant and stronger for very small particles (micrometer scale), or when gravity is low, or when the particles are in fluids with a strong viscosity (Ozaki et al., 2023).

Physical Properties of Granular Materials

Granular materials are often differentiated based on their physical properties. The **particle shape** can vary in terms of size, roundness and surface roughness among others (Maroof et al., 2020). **Dilatancy** is the tendency of the granular material to either increase or decrease in volume when under pressure as the particles better align and interlock. The movement of particles in an avalanche involves dilatancy, which separates the particles and reduces the contact forces between them (Kleinhans et al., 2011).

2.1.2. Definitions of the Angle of Repose

The **angle of repose** (AoR) is a property of granular material often used to describe the angle of the slope of a pile of granular material, and it is studied in various contexts. In industrial and agricultural processes, it is used for the stocking of granular goods like corn for example, where the structural integrity of the pile has to remain under control (Al-Hashemi and Al-Amoudi, 2018). In geomorphological studies, the AoR is used to understand the formation of dunes, deltas, or avalanche slopes among others (Kleinhans et al., 2011). For the latter, the AoR is a parameter in the stability of slopes and the prediction of avalanches (Al-Hashemi and Al-Amoudi, 2018).

Various definitions have been given to the angle of repose in literature. The main reason is that each definition depends on the context of the research: which angle is being studied, what experimental setup is being used, *etc.* The general concept of the angle of repose is that it is the angle of the slope of a granular material. However, the behaviour of granular materials is complex and there is no such thing as a unique and constant slope angle. The shape of a granular pile is not always a straight line. It therefore matters to define precisely where the angle is measured along the slope. A straight slope may have a single angle, but a curved slope will have a varying angles. Then, it also depends whether the angle is measured while material is being poured or not, whether the slope is static or dynamic.

When particles are added to a pile of granular material, either naturally transported by air, water or ice, or either artificially poured on top, the particles add up and the slope of the pile becomes steeper. Each pile can only sustain a certain quantity of material before its weight overcomes the friction forces which kept the pile stable. An avalanche then occurs, bringing some of the top particles to the bottom until the slope becomes stable to grow steep again. This cycle with a visibly clear maximum and minimum slope angle is called **discrete avalanching regime**. When the mass flow of particles being poured increases, the avalanches become a continuous flow of material rolling down the slope, the cycle is not visible anymore and is called **rolling regime**. When the flow of material is even bigger, the slope takes a clear non-linear shape as the avalanches enter the **cascading regime** (Cheng and Zhao, 2017). There are very few studies measuring the AoR in this regime, most probably because of this non-linear irregular shapes making it difficult to define an angle consistently. In a discrete avalanching regime, two main angles can be identified. As the pile builds up, the slope will reach its steepest point before it becomes unstable and avalanches. After the avalanche, the slope angle decreases until it is stable again. These maximum and minimum angles are respectively called **static** and **dynamic** AoR by Kleinhans et al. (2011), or **upper static** and **lower static** AoR by Cheng and Zhao (2017). In the rolling regime, the slope tends to take a continuous

linear shape with a constant angle. This is the angle of repose as defined by Klein and White (1990), or the **dynamic** AoR by Cheng and Zhao (2017). This here shows how the literature gives various definitions for similar concepts, with Kleinhans et al. (2011) and Cheng and Zhao (2017) giving two different definitions for the dynamic angle of repose for example.

2.1.3. Experimental Methods to Study the Angle of Repose

There exist various ways to study the angle of repose of granular material. When focusing on the avalanching process, three main types of experimental methods can be identified. These are the rotating cylinders, the Hele-Shaw cells and the fixed funnel methods. Each allows to observe a specific aspect of the phenomenon but comes with its own limitations.

The **rotating cylinders** test setup, also called rotating drum or tumbler, has been used in the studies of Kleinhans et al. (2011) and Klein and White (1990) among others. It usually consists of a cylinder made of a transparent material. It is put on its side such that the circular faces are perpendicular to the "ground".

The **fixed funnel** method consists in pouring the granular material out of a funnel on a base (often unlimited in size) to build up a pile. With the fixed funnel in particular, the pouring mass flow can be adjusted with the funnel diameter and the height between the funnel and the tip of the pile (Nakashima et al., 2011).

A **Hele-Shaw cell** is a thin transparent box in which the granular material is poured. What is particular about the Hele-Shaw cell is that the width of the box is rather thin. The small gap between the parallel plates aims to simulate a 2-dimensional flow. If the cell is too thin, particles may easily get stuck and build bridges strong enough to hold material above the bottom surface of the cell. If the cell is too wide, the particles on the sides will experience more drag and wall effects than those at the center, and the avalanche will display a 3-dimension behaviour instead of the intended 2-dimension, which can falsify the observations (Koeppel et al., 1998). Once filled, the cell can additionally be tilted to create discrete avalanches, like in the study by Grasselli and Herrmann (1997).

2.1.4. Angle of Repose in Granular Mixtures

Two phenomena occur to mixtures of granulate materials during avalanching, related to their angles of repose. Namely segregation and stratification. **Segregation** occurs because of the difference in inertia between particles, as the particles with lower inertia tend to come to a rest first while the particles with more inertia continue their avalanching motion (Hutton et al., 2004). The separation between both materials can be clearly visible, as in Figure 2.1. **Stratification** occurs in addition to segregation when the different materials also have different angles of repose. The material with the smaller AoR will create a first layer on top of which the other material will deposit, creating a repetitive pattern of layers (Hutton et al., 2004), see an example in Figure 2.2. The segregation can be observed in rotating drums experiments (Hutton et al., 2004), but stratification is typically observed in a Hele-Shaw cell setup. In the Hele-Shaw cell experiment, the stratification patterns depend on a certain combination of the flow rate of the material in the setup and the width of the cell setup. This was studied by Koeppel et al. (1998) who inferred that the material dilatancy occurring during the avalanche allowed certain particles to fall in between the others. As particle separation is a naturally occurring phenomenon, it is therefore important to understand the relations between angles of repose, avalanches and particle sorting in order to infer about the formation of geomorphological structures on planetary bodies.

In the study by Makse et al. (1997), stratification was not always observed, but segregation was always present. By varying the particle parameters, they found that the mean particle size and the individual angle of repose (defined as the smallest angle of the pile at rest, related to the particle shape) play an important role in stratification. In all cases of segregation, the smaller particles were found closer to the centre of the pile, while the larger particles would roll to the edge and base of the pile. If the AoR of the larger particles was larger than the AoR of smaller particles, then stratification would only occur. These results were found for a variety of particle size ratio. Makse et al. (1997) propose a physical explanation behind the stratification that at first the particles form a "kink" over which they pose themselves. First the small grains sieve through the larger ones and form the bottom layer. The larger grains then lay on top of it. This makes the kink move up the slope until the highest point, where the slope angle becomes too steep and an avalanche occurs. In that avalanche, the process is repeated and the layers of the stratification develops. Makse *et al.* then find a relationship to predict the wavelength λ between a pair of layers. It depends on the downwards velocity of the avalanche v , the upwards velocity of the kink v' and the thickness of the

layer of falling avalanching grains R_0 , such that $\lambda = R_0(v + v')/v'$. This study by Makse *et al.* is therefore not only interesting for its observations on the relation between the angle of repose and particle separation, but also for its detailed description of the avalanche mechanics.

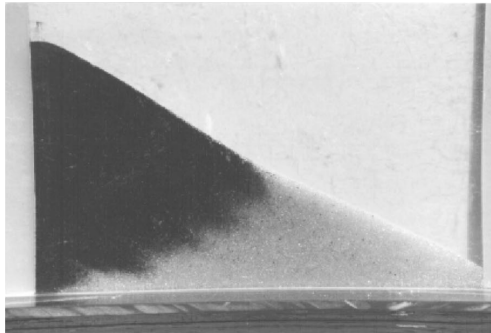


Figure 2.1: Example of segregation in a mixture of large glass beads and small sand grains by Makse *et al.* (1998).

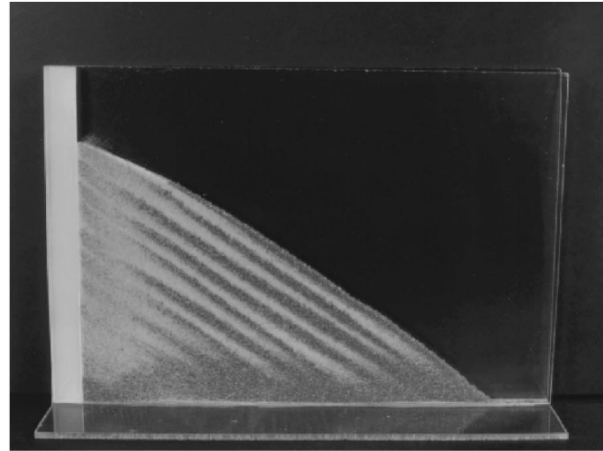


Figure 2.2: Example of stratification in a mixture of small glass beads and large sand grains by Makse *et al.* (1998).

In Makse *et al.* (1998), a high speed camera was used to capture the dynamics of the avalanching and stratification process. They define three different phases studied: the avalanche down the slope, the formation of the kink at the bottom of the slope, and uphill motion of the kink. In this study, more attention is paid to the velocity of the grains avalanching, the velocity of the kink moving up, and the wavelength. The experiment is similar to their previous study. A Hele-Shaw cell of fixed dimensions is used to pour granular mixtures at varying flow rates. First the individual AoR of each material was measured. They found that the particle shape was the main influence on the AoR, with the more rough and irregularly-shaped particles having a higher AoR than the regular spherical ones. This holds for the size range of macro particles. Micro and sub-micrometre sized particles behave more cohesively and therefore have a higher AoR. The study was therefore limited to macro-sized particles. Makse *et al.* developed analytical relations to predict the angles or repose of the different stratified layers (as they might differ from that of the individual materials), the velocities of the granular flow down the slope and the kink formation up the slope. The main variable is the flux rate of particles being poured at the top, and the cell dimensions are also used as input. Analytically, they find that the upward velocity of the kink is linearly dependent to the rate of collisions between static and rolling grains, and the thickness of the avalanching flow (which depends on the input flux). The velocity of the avalanche should have a gradient along its thickness. The mean velocity of the avalanche is also linearly dependent on these two parameters, although with a different coefficient. They find that the wavelength of stratified layers is therefore also linearly dependent on the thickness of the avalanche, hence on the input flux. These findings were tested experimentally. The experiments confirm that there is a linear velocity profile along the avalanche thickness with the faster particles at the top of the layer. Therefore the mean velocity is linearly dependent on the avalanche thickness. They finally find that the upward velocity of the kink is also linearly dependent on the avalanche thickness and it is almost the same as the avalanche velocity.

2.1.5. Summary of Section 2.1

This section introduced various concepts about granular materials. A granular material is an ensemble of many particles of matter, ranging in size from very small to large macro particles, with varying shapes and structural properties per material. Many forces apply to granular material and the intensity of each force varies depending on the size of the particles. The main ones are the gravity, friction, Van der Waals, electrostatic and capillary forces, but more forces can act and become predominant depending on the conditions around a particle. Granular material can be contractive or dilative depending on how its volume changes under applied stress.

Most of the studies on the angle of repose observe the avalanching process of the material, which can take on different regimes depending on the experiment: discrete, rolling or cascading. Various experimental setups can be used to study avalanches in granular materials. When there is enough material to form a pile, the granular matter takes on a slope of an angle usually comprised between a minimum and a maximum. The angle of the slope is often called angle of repose, but the actual definition used in studies varies per study. More specific names are given to the angle of repose: static, dynamic, dilation, maximum, minimum, etc. These names may change from one study to another to appropriately suit the event being observed, or the experimental setup. An overview of the definitions of the AoR can be seen in Table 2.1.

Table 2.1: Definitions of the angle of repose across literature, with the test setups, mixture types and avalanching regimes used.

Study	Setup	Material Mixture	Avalanche Regime	Angles	Definition
Kleinhans et al., 2011	Rotating cylinders	Homogeneous	Discrete	Static	Highest stable angle before avalanche
			Discrete	Dynamic	Lowest stable angle after avalanche
			Discrete	Dilation	Difference between static and dynamic
Cheng and Zhao, 2017	Rotating cylinders	Homogeneous	Rolling	Dynamic	Constant slope angle
			Discrete	Upper Static	Highest stable angle before avalanche
			Discrete	Lower Static	Lowest stable angle after avalanche
			Discrete	Dynamic	Average between upper and lower static AoR
Klein and White, 1990	Rotating cylinders	Homogeneous	Rolling	Angle of repose	Constant slope angle
Brucks et al., 2007	Rotating cylinders	Homogeneous	Rolling	Dynamic	Constant slope angle
Koeppel et al., 1998	Hele-Shaw cell	Heterogeneous	Discrete	Static	Angle the slope of the pile takes after avalanche for an individual material
				Maximum	Highest stable angle before avalanche
				Critical	Lowest stable angle after avalanche
Grasselli and Herrmann, 1997	Hele-Shaw cell	Homogeneous	Discrete	Angle of repose	Angle that the slope naturally takes after the material is poured
				Static	Highest stable angle before avalanche
				Dynamic	Lowest stable angle after avalanche
Makse et al., 1998	Hele-Shaw cell	Heterogeneous	Discrete	Angle of repose	Smallest angle of the pile at rest

2.2. Studies on Gravity

From all the studies on the angle of repose, ten have looked into the effects of gravity on the angle of repose. These studies aimed to better understand how the geomorphological and industrial processes would change when happening on other planets, in the context of planetary exploration. The results of those studies are presented and discussed in this section, along with the methods that were used to find them.

Section 2.2.1 presents the methods, experimental and non-experimental, used to study the angle of repose under varying gravity. Section 2.2.2 dives into the findings of each of the main studies on the topic of gravity and the angle of repose. Section 2.2.3 discusses the findings of the various studies and identifies a gap in the literature.

2.2.1. Methods for Studying the Effect of Varying Gravity

There is no one way to study the effect of gravity on granular matter. Overall, to reduce the effective gravity acceleration, the experimental setup has to be put in some kind of free fall. This is done in drop towers, parabolic flights or aboard the ISS for example (Ozaki et al., 2023). The parabolic flight allows to vary the effective gravity in hyper- and hypogravity regimes depending on its trajectory. The drop tower only allows for the setup to be in free fall (assuming that there is effectively a vacuum in the tower). In order to perform an experiment at a gravity level in between 0 and 1g, then a centrifuge can be combined to it like Hofmeister et al. (2009) did. The centrifuge allows create a desired effective gravity acceleration based on its rotation speed. It can therefore also be used to test in a hypergravity regime. A main limitation from these testing environments is the time in reduced gravity, which is in the order of seconds in a drop tower to the order of single minutes in a parabolic flight. An experiment only has a few seconds in a drop tower before it reaches the bottom. An airplane has to pitch up before flying too low towards the ground. The reduced gravity time is a factor to consider when designing these types of experiments. For example, Kleinhans et al. (2011) observed that their avalanches under water happened much slower than for those with air as an interstitial fluid. Only being able to fly an experiment in orbit like on the ISS would allow for virtually unlimited time under reduced gravity.

Various experimental setups were used across studies. Rotating drums were used by Brucks et al. (2007), Klein and White (1990) and Kleinhans et al. (2011) for their ability to repeat the experiment without requiring a manual reset, which would take time. This allows to maximise the data gathering and duplication of data in such short time frames. In a similar way, Hofmeister et al. (2009) chose to use a tilting box setup. The fixed funnel setup was chosen by Nakashima et al. (2011), Hofmeister et al. (2009) and Elekes and Parteli (2021) as they were more interested in the pile formation than the avalanching process itself. Marshall et al. (2018) and Karapiperis et al. (2020) chose to use the passive failure setup because it allows to measure many granular properties and coefficients in a single experiment. This allowed to study the effect of gravity on each parameter all at once, an efficient choice.

The definition of the angle of repose seem to be somewhat consistent per type of setup used. The AoR is measured at the centre of the slope in rotating drums. Brucks *et al.* and Klein *et al.* observe a constant AoR due to the rolling regime of their experiments, while Kleinhans *et al.* observe a static and dynamic AoR due to the discrete avalanching regime of their experiment. Experiments using the fixed funnels or the passive failure measure the AoR at the bottom of pile once it has stabilised. Only Hofmeister *et al.* measured the AoR while the pile was forming, as it is measured in the hourglass experiment on the deposited pile in the bottom chamber. Not much is said about how the angle is defined, but it is measured before the sides of the granular pile reach the walls, hence it is measured in its dynamic environment. A summary of the test setups used in the reviewed articles can be seen in Table 2.2.

Table 2.2: Main studies on the effect of gravity on the angle of repose of granular materials, with their experiment setup and variables considered

Study	Setup	Environment	Variables	G-level	Avalanche Flow Regime
Brucks <i>et al.</i> 2007	Rotating Drums	Centrifuge	Gravity	1-25	Rolling
Klein and White 1990	Rotating Drums	Parabolic flight	Gravity, Materials	0, 0.5, 1	Rolling
Nakashima <i>et al.</i> 2011	Fixed Funnel	Parabolic flight	Gravity, Funnel Angles	1/6, 1/2, 1, 2	Discrete
Marhsall <i>et al.</i> 2018	Passive Failure	Parabolic flight	Gravity	0, 0.17, 0.38, 1	Discrete
Hofmeister <i>et al.</i> 2009	Fixed Funnel	Drop tower + centrifuge	Gravity, Material	0.01-0.3	Discrete
	Tilting Box	Drop tower			
Elekes <i>et al.</i> 2021	DEM Fixed Funnel	Numerical	Gravity, Particle Size	0.06, 0.17, 0.38, 1, 3, 10, 30, 100	Discrete
Karapiperis <i>et al.</i> 2020	DEM Passive Failure	Numerical	Gravity	0, 0.17, 0.38, 1	Discrete
Kleinhans <i>et al.</i> 2011	Rotating Drums	Parabolic flight	Gravity, Materials	0.1, 0.38, 1	Discrete
Study	Material type	Particle Size (mm)	Particle Shape	Interstitial Fluids	Froude number
Brucks <i>et al.</i> 2007	Glass beads	0.53	Spherical	Air	Various
Klein and White 1990	Glass beads	1.35	Spherical	Air	0.056 - 0.0056
	Montery Sand	0.4	Irregular		0.011 - 0.0011
Nakashima <i>et al.</i> 2011	Toyoura Sand	0.1-0.6	Irregular	Air	NA
Marhsall <i>et al.</i> 2018	Sand	0.83-1.98	Irregular	Air	NA
Hofmeister <i>et al.</i> 2009	Basalt	0.4-0.6	Spherical	Vacuum	NA
	Glass	0.1-0.2	Spherical		
	Sand	0.2-0.6	Irregular		
	Sand	0.1-0.3	Irregular		
Elekes <i>et al.</i> 2021	Glass beads	1E-3 - 1E4	Spherical	Air	NA
Karapiperis <i>et al.</i> 2020	Sand	0.83-1.98	Irregular	Air	NA
Kleinhans <i>et al.</i> 2011	Gravel	2.4	Irregular	Water, Air (70% humidity)	NA
	Glass beads	0.6, 2	Spherical		
	Sand	0.6, 0.21	Irregular		

2.2.2. Findings on the Effect of Gravity on the Angle of Repose in Literature

This section dives into the main studies on the angle of repose and gravity. It reflects on each study individually first, before discussing on the entire literature in the following Section 2.2.3. It is important to understand the context surrounding each study as it explains how they made assumptions on the mechanisms at play, and why they chose to experiment on specific materials and test setups. Each of these decisions impacts the limitations of the experiment, which explains why certain behaviours are observed or not. For each study, a description is therefore given on their research questions, assumptions, setup, definitions of angle of repose and results. A summary overview is given in Table 2.3 at the end of this section.

Experimental Studies

Brucks et al. (2007) is the only experimental study on the AoR performed in hypergravity. Granular material was tested in a rotating cylinder setup, which was installed in a centrifuge to vary the effective gravity between 1 and 25 times the Earth gravity level. The material studied is glass beads. The material flows in a rolling avalanching regime. Therefore, the angle of repose measured is called the dynamic AoR, which is the angle of the linear slope at its centre. Brucks *et al.* first find that the AoR increases with the drum rotational speed. They also find that the AoR decreases with increasing gravity. Brucks *et al.* provide a dimensionless scaling for the effect of gravity, called the Froude number. The Froude number is a ratio between two forces applied on the granular material. It is the ratio between the centrifugal force due to the tumbler rotation and the effective gravitational force of the environment. The Froude number is therefore a property unique to the rotating drum setup. They find that for the same Froude number, the granular material can reach steeper angles of repose for greater ratios R/d , where R is the drum radius and d the particle average diameter. For smaller Froude numbers ($\sim 10^{-6}$) the angles all collapse to an asymptotic value, as can be seen in Figure 2.3. Brucks *et al.* argue that for these Froude numbers, where the material is under discrete avalanching regime, the AoR is controlled by the particle size rather than by the drum radius. From the findings of Brucks *et al.*, the Froude number can be related to the avalanche flow regime, as they are both dictated by gravity and the centrifugal force of the drum. At a fixed gravity level, the Froude number is linearly dependent on the cylinder radius and on the square of the angular velocity. Hence at small Froude numbers, the avalanching regime is discrete. As the Froude number increases, the regime becomes rolling, then cascading, and eventually the centrifugal force is so large that all particles are stuck to the periphery of the drum. This can be seen in Figure 2.4. When keeping the Froude number constant, it is observed that the avalanching regime is not dictated by gravity, but rather by the Froude number itself. Brucks *et al.* also find that the thickness of the flowing layer increases during the avalanche just enough to let the particles move down the slope, but the thickness is independent on gravity when the Froude number is kept constant. This is important with regards to other studies on dilatancy or particle sorting among others. The final finding by Brucks *et al.* is very interesting as it explains how the Froude number can be linked to other studies who don't necessarily use a rotating cylinder setup, nor the same flow regimes as Brucks *et al.*, and allow to better compare findings across studies. In the context of the rotating cylinder setup, the Froude number is defined by Equation 2.1, with the angular velocity ω , and the effective gravitational acceleration g_{eff} :

$$Fr = \frac{\omega^2 R}{g_{eff}} \quad (2.1)$$

Brucks et al. (2007) claim that the Froude number relates across studies through the surface flow velocity during avalanching. The Froude number at the surface of any flow would follow Equation 2.2:

$$Fr_{surf} = u^2 / \delta g_{eff} \quad (2.2)$$

where u is the flow velocity and δ is the flowing layer thickness. In the particular case of the tumbler, the surface Froude number follows Equation 2.3:

$$Fr_{surf} = (R^3 / 4\delta^3) Fr \quad (2.3)$$

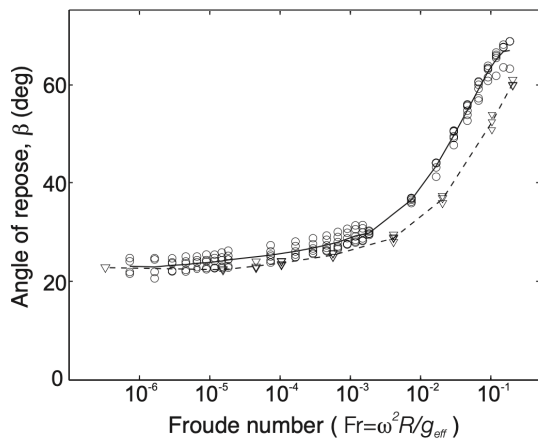


Figure 2.3: Correlation between the Angle of Repose and the Froude number (Brucks et al., 2007).

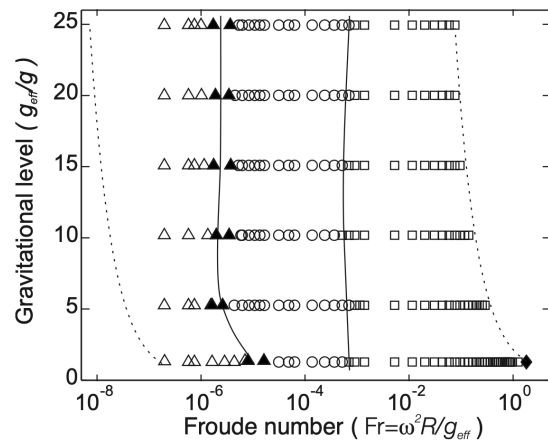


Figure 2.4: As the Froude number increases, avalanche regime changes: discrete avalanche (empty triangle), alternating between discrete avalanching and rolling (plain triangle), rolling (empty circle), cascading (empty square), and centrifuging (plain diamond) (Brucks et al., 2007).

Klein and White (1990) studied the effect of varying gravity on the angle of repose. Klein *et al.* measured the changes in angle repose of granular material while performing parabolas in an airplane to vary the effective gravity. Klein and White (1990) first measured variations in AoR when changing the rotation speed of their rotating drum setup. They observed an increase in AoR when increasing the speed for both materials. This behaviour was also observed by Brucks et al. (2007), except that Klein *et al.* consider that the change in AoR is negligible over the tested rpm range, despite measuring a change in AoR of about 2°. They then performed their experiments in parabolic flights aboard a KC-135 of NASA. During the reduced gravity phase, the gravity varied "uniformly" between 0g and 0.5g (Klein and White, 1990). The data was recorded during the whole flight which produced measurements of the AoR in a changing gravity varying from 0g-1.8g (1.8g was during the pull-up phase to initiate the parabola and during the pull-out phase to terminate the parabola). They found that the dynamic AoR (θ) increases with a reducing gravity following the relation: $\theta = a + b\sqrt{1/g}$ with a and b being constant angles (in degrees) varying per material (Figure 2.5 and Figure 2.6). They explain that the reduced gravity reduces the interparticle normal loads, which would increase the particle coefficients of friction and therefore increase the angle of repose. They observed that the round glass particles were more sensitive to changes in gravity than the rough sand particles.

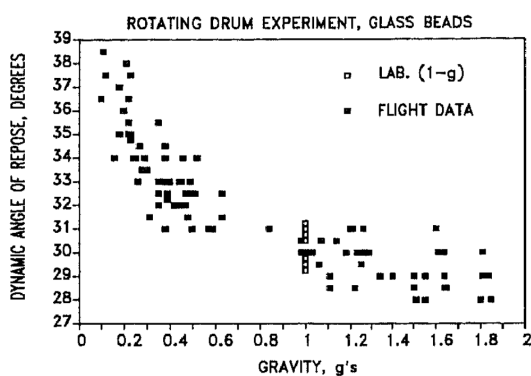


Figure 2.5: Measured AoR against gravity levels for glass beads at a nominal drum rotation speed of 6.75rpm (Klein and White, 1990).

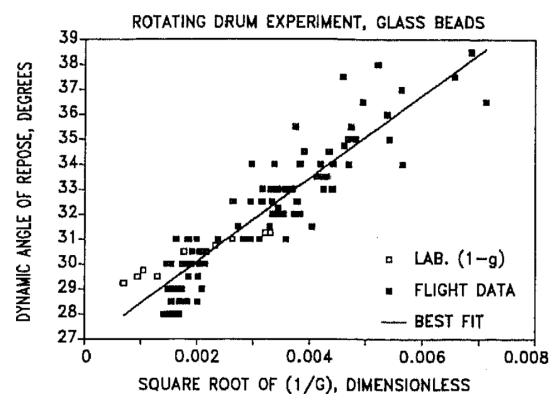


Figure 2.6: The measured AoR for the glass beads, plotted against a dimensionless parameter $1/\sqrt{G}$. The best fit line is plotted, for a regression R^2 of 0.845 (Klein and White, 1990).

The angle of repose was also studied by Nakashima et al. (2011) under low gravity. The purpose of the study was to develop a DEM simulation tool to analyse the locomotion of future rovers on the Moon, and to validate it experimentally. Nakashima et al. (2011) found that the AoR is independent on gravity. The data presented shows variations between each experiment. When averaging the results, the averages do not show a correlation with gravity. There is a significant standard deviation of $2^\circ - 3^\circ$ per each gravity level. This goes against other research which said that the AoR does vary with gravity, like Klein and White (1990) or Brucks et al. (2007). The main difference is that the test setup is not the same: a fixed funnel against rotating drums. In this fixed funnel experiment by Nakashima *et al.*, the AoR is measured twice: once while the sand is being poured and once after being poured. This does not necessarily correspond to the angles of repose identified in rotating drums. In addition, there can be large differences between the angles measured on the left side and right side of the pile (sometimes over 6°). These can be the result of many variables. Perturbations external to the experiment could have been the source of one side of the pile to avalanche. Or the material selected could have been too cohesive. Nakashima *et al.* do not explain these discrepancies and instead immediately conclude that there is just no effect from gravity. A study with more material types and a larger array of gravity levels comprised between 0g and 1g would provide a stronger case to these conclusions.

Marshall et al. (2018) performed a different kind of experiment on the topic. They studied the changes in strength properties of soil under different gravity levels, to infer about how the soil strength would behave on other planets. The strength properties studied were the peak friction angle, the residual friction angle, the angle of repose, and the peak dilatancy angle. During the parabolic flights of Marshall et al. (2018), various gravity levels were flown at: three at martian gravity (0.38g), two at lunar gravity level (0.17g), five at terrestrial gravity level (1g) and 20 at near 0g. The measurements of the AoR were only performed at the martian, lunar and terrestrial gravity levels. Marshall *et al.* measured no significant change in AoR across the range of gravity levels, with a standard deviation of about 2° (see Figure 2.7(b)). These results were verified numerically by Karapiperis et al. (2020) who also did not find a significant correlation between gravity and the AoR.

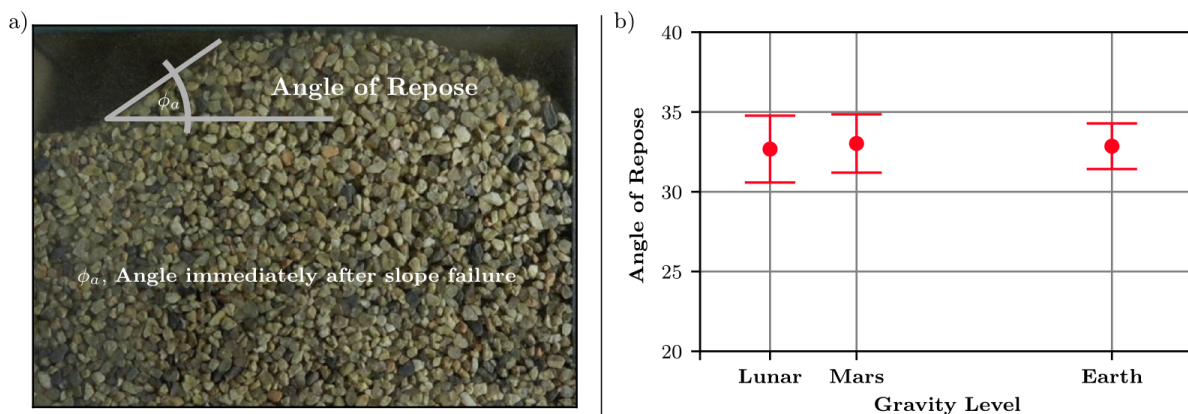


Figure 2.7: (a) An example of how the AoR was measured in the experiment of Marshall *et al.* In this setup, the moving block is applying pressure from the right side of the picture. (b) Resulting measurements of the AoR at different gravity levels, with error bars (Marshall et al., 2018).

Hofmeister et al. (2009) performed a series of experiments focused on the effect of gravity on properties of granular materials. The experimental setup consisted of a quasi-2D hourglass and a tilting box setup. Both setups were tested in a drop tower to counter the effects of the Earth gravity, and a centrifuge created an artificial gravity. The tested materials were basalt spheres, glass spheres and two types of sand grains. From the tilting box experiment of Hofmeister et al. (2009), it is observed that when reducing gravity, the avalanche time increases, the width of the avalanche decreases and the steepest part of the avalanche increases (see Figure 2.8 and Figure 2.9). It appears that they observed some cohesive behaviour at very low gravity levels, with irregular slope shapes. The granular mass flow was also measured and it appears to be decreasing for a decreasing gravity. The angle of repose is measured in the hourglass experiment on the deposited pile in the bottom chamber. Not much is said about how the angle is defined,

but it is measured before the sides of the granular pile reach the walls, hence it is measured in its dynamic environment. They observe that the AoR increases for a decreasing gravity, and the rate at which it increases also increases for decreasing gravity. This could hint towards observing the same behaviour as in Klein and White (1990) or Elekes and Parteli (2021). As can be seen in Figure 2.10, the AoR decreases at very low gravity levels close to 0. Not much data or argumentation is provided to explain this observation. One could suppose that cohesive forces are the driving forces on the particles for this very low gravity, hence the granular pile could take irregular shapes where it would not make sense to measure any kind of angle of repose.

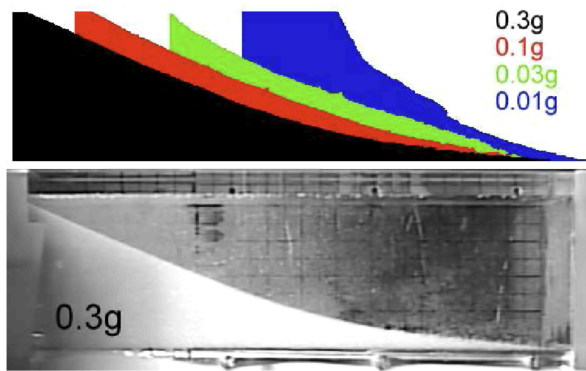


Figure 2.8: Slope shape after the avalanche for glass grains at different gravity levels. The top shows the binarised shape at each gravity level, the bottom shows the original view of the experiment by the camera (Hofmeister et al., 2009).

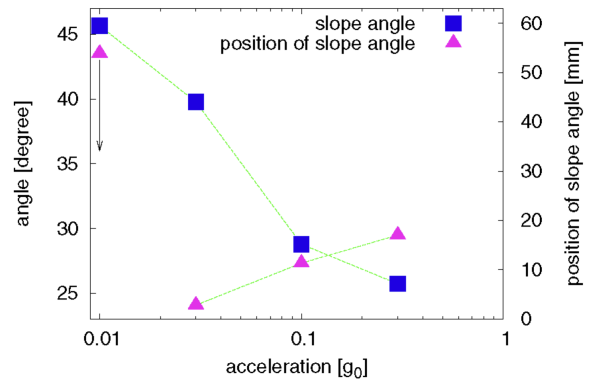


Figure 2.9: Angle of the steepest part of the slope (square), and its position as measured from the top ridge (triangle), per gravity level. These measurements were performed in the experiment with glass beads. The arrow indicates an estimated value (Hofmeister et al., 2009).

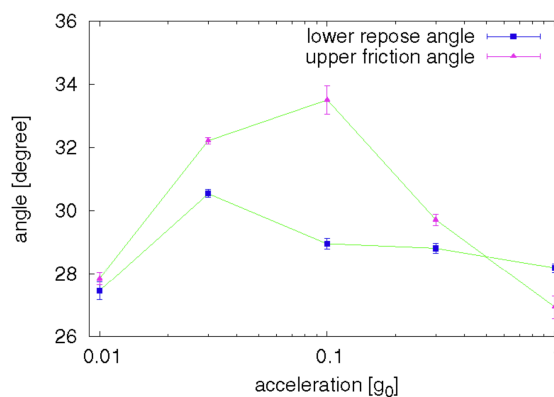


Figure 2.10: Angle of repose in the hourglass experiments with basalt spheres per gravity level. Error bars denote the range between left and right angles (Hofmeister et al., 2009).

The experiment of Kleinhans et al. (2011) was performed in parabolic flights where the g -levels were varied to 0.1 g , 0.38 g and 1 g . The materials selected were 2.4mm gravel, 2mm glass beads, 0.6mm glass beads, 0.21mm sand and 0.6mm sand. The interstitial fluids used were air and water (fully submerged). In total, nine combinations of material and interstitial fluids were tested in the rotating drums setup. Two different angles of repose were measured: the static and dynamic AoR. The static AoR is defined as the maximum angle the slope will take before it starts avalanching. The dynamic AoR is the lowest angle the slope will take right after avalanching and being stable again. It is said to be "dynamic" as it is formed from a dynamic process. Having these two distinct angles of repose is also a result of the discrete avalanching

regime of the experiment. Kleinhans et al. (2011) studied the effect of gravity on the angle of repose of granular material. They defined two hypotheses to validate in their study. The first hypothesis of Kleinhans et al. (2011) is that the static angle of repose would increase with a decreasing gravity force. It is based on the assumption that the other forces acting on particles (Van der Waals, electrostatic, etc.) would not change with the reduction of gravity. Kleinhans *et al.* also do not aim to study the effect of these other forces in details, but rather use them in the discussion of the observations and the possible interactions between the experiment and the tested material. My interpretation of the driving assumption behind this first hypothesis is that the static friction force does not only depend on the applied load, hence with a lower gravity, the weight of the particles decreases more than the static friction force does. Therefore a steeper slope angle is required for the particles' weight to overcome the friction and initiate movement. The second hypothesis of Kleinhans et al. (2011) is that the dynamic angle of repose would become smaller with a decreasing gravity force. The main assumption behind this is that under a lower gravity, the moving flow of particles would become more dilated, which would reduce friction and allow the material to settle at a smaller angle of repose. Intuitively, under a lower gravity, the particles from upper layers are less "pushed down" against the lower layers. Therefore while falling along the slope, the particles experience a lesser acceleration downwards and can travel further horizontally. The particles will experience less contacts with other particles, hence less friction. With the particles being more separated from one another, the flow would effectively be more dilated. A smaller (more horizontal) slope angle would be required for the friction forces to overcome gravity and stop the motion. Therefore the dynamic AoR would become smaller under reduced gravity. The results show that the two hypotheses defined by Kleinhans et al. (2011) are correct. The static angle of repose increases as gravity decreases. The dynamic angle of repose decreases as gravity decreases. It is further observed that the dynamic AoR decreases more than the static AoR increases. The dilation angle therefore increases with decreasing gravity. This relation is not linear, it appears to be stronger than linear with decreasing gravity. Kleinhans *et al.* do advise to further study this correlation. The results do not show a dependence on the interstitial fluid. Materials display the same AoR in air or under water. Only the avalanching time is longer in water due to higher viscosity of water. In air, particles are in the free-fall regime. In water, the particles are either in a viscous or inertial regime depending on the particle size and effective gravity.

Numerical Methodologies

Elekes and Parteli (2021) developed a particle-based DEM (Discrete Elements Method) model to predict the angle of repose, the sliding and rolling friction, and van der Waals forces. The main variables are the particle size and the gravity level. The model simulates the formation of a particle conical pile after being poured on a flat surface from a fixed funnel. The flow regime would correspond to a discrete avalanche regime. The angle of repose is measured at the base of the conical pile (to be precise: at the base of the isosceles triangle with same surface area as the pile). The DEM model used in this study is a model that was first developed in 1979 and has been improved over the years and studies in order to better simulate granular particles, their interactions and the forces acting on them. Two main behaviours are observed in the work of Elekes and Parteli (2021): the AoR increases for smaller particle diameters, and the AoR increases for decreasing gravity. As can be seen in Figure 2.11, the effect of particle size shows that the AoR distribution follows an asymptote for larger particles down to about the millimetre range. Then the AoR increases to large angles as the particle diameter further decreases. This behaviour can at least be described until the range of tens of micrometres ($10^{-5}m$), before the material behaves cohesively. Elekes and Parteli (2021) validate these predictions with the observations of nine other studies. The predictions for the effect of gravity is that for decreasing gravity, the slope of the AoR distribution (for varying diameter) increases. This means that the AoR increases when reducing gravity for a fixed particle diameter. This would confirm the finding of Klein and White (1990) and that of Kleinhans et al. (2011) for the static AoR. Now the different experiments used in these studies do not allow for a direct comparison of their results. Elekes *et al.* then develop an analytical relation between the AoR, gravity (g) and particle diameter (d). They find that the tangent of the AoR scales with $1 + \frac{1}{d\sqrt{g}}$. They further develop these relations to understand how the cohesiveness of the matter changes. They then compare their results to those of experimental studies. While not being able to directly compare the results due to the different test setups and angle definitions, they are able to compare the observed behaviour by explaining the increase in material cohesiveness in lower gravity, which would explain the increases in (static) angles of repose. The study by Elekes and Parteli (2021) provides a good understanding of how gravity and particle diameter affect the AoR. Little is said about the effect of the particle pouring flux, which had been

observed to affect results in previous studies. The lack of a good method to compare results from different experiment setups makes it difficult to relate this study to observations in other setups or in nature. Elekes *et al.* validated their simulator with the results of various other studies for the case under Earth gravity, but not for under other gravity levels (probably due to the lack of data available). Following studies should focus on validating the predictions under non-Earth gravity levels.

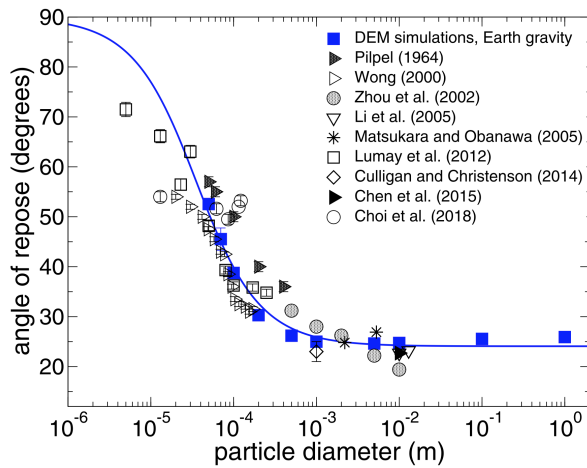


Figure 2.11: Angle of repose against particle diameter for glass beads. The plain squares are the numerical predictions by Elekes *et al.*, the other symbols are results from other studies (Elekes and Parteli, 2021).

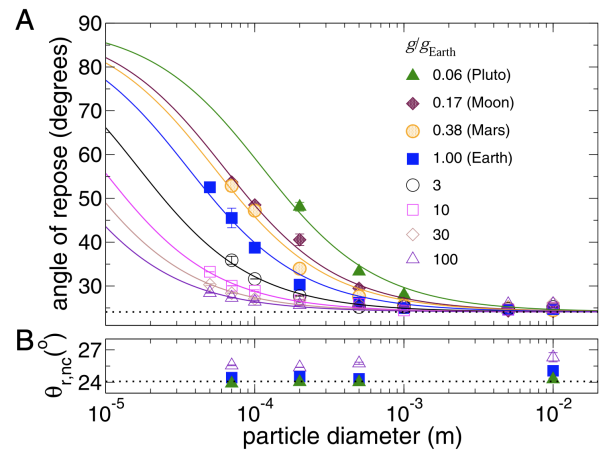


Figure 2.12: Angle of repose against particle diameter at varying gravity levels for glass beads (Elekes and Parteli, 2021).

The numerical study by Karapiperis *et al.* (2020) follows the experimental study done by Marshall *et al.* (2018). The study by Karapiperis *et al.* provides a DEM simulation of the experiment by Marshall *et al.* The simulation recreates the exact same setup as the physical experiment, with a passive failure test of sand under the gravity levels experienced during the parabolic flights. The simulation was developed on a similar base as that of Elekes and Parteli (2021) but then use a variant method called level-set DEM (LS-DEM) which can capture arbitrary grain shapes represented as level set functions (Karapiperis *et al.*, 2020). Karapiperis *et al.* (2020) find that the results of the simulation only slightly differ from reality, and even fall into the variation range of each other's results. They therefore similarly conclude that there is no significant correlation between the angle of repose and gravity, as the AoR appears to stay constant. The friction angle appears to slightly increase with decreasing gravity. The conclusions of this study were to be expected, knowing it was essentially performed by the same group of people, who probably used the same literature survey for both studies and therefore the same assumptions on the effect of gravity on the AoR. It would have been more interesting to see how this numerical study could have been performed more independently from the study by Marshall *et al.* (2018) in order to challenge their results.

To best capture this section, an overview of each study with the definition of the angle of repose they studied and their results can be seen in Table 2.3. Where the colours group the studies who found similar findings, green for those who found a negative relationship between gravity and the AoR, red for those who found a positive relationship between gravity and the AoR, and yellow for those who found no significant relationship.

Table 2.3: Main findings of the studies on the effect of gravity on the angle of repose of granular materials.

Study	Angles	Definition Angle of Repose	Results/Conclusions
Brucks <i>et al.</i> 2007	AoR	Mid Slope Angle	The AoR decreases with increasing g-level
Klein and White 1990	Dynamic AoR	Mid Slope Angle	Dynamic AoR increases with decreasing g-level, varying with the reciprocal of the square root of the g-level
Nakashima <i>et al.</i> 2011	Dynamic AoR	Angle at the bottom of the cone during pouring	The AoR is independent on varying g-level
	Static AoR	Angle at the bottom of the cone after pouring	
Marhsall <i>et al.</i> 2018	AoR	Angle at the bottom of the slope after avalanche	The AoR is independent on varying g-level
	Dilatancy	Change in volume due to applied stress	The dilatancy angle increases when reducing g-level
Hofmeister <i>et al.</i> 2009	AoR	Mid Slope Angle	The AoR increases with decreasing g-level
Elekes <i>et al.</i> 2021	AoR	Angle at the bottom of the cone after pouring	The AoR increases with decreasing g-level
			The AoR varies with $\frac{1}{d\sqrt{g}}$
Karapiperis <i>et al.</i> 2020	AoR	Angle at the bottom of the slope after avalanche	The AoR is independent on varying g-level
Kleinhans <i>et al.</i> 2011	Static AoR	Highest before avalanche	Static AoR increases with decreasing g-level
	Dynamic AoR	Smallest after avalanche	Dynamic AoR decreases with decreasing g-level

2.2.3. Discussion of the Literature on the Angle of Repose & Gravity

The results are as varied as what the studies used for test setups, avalanche flow regimes and granular material. Both Klein *et al.* and Brucks *et al.* used drums rotating fast enough to have a rolling avalanche regime, they both used similar materials, and both found a similar relation with gravity. Klein *et al.* found it for the hypogravity levels, and Brucks *et al.* for the hypergravity regimes. The simulations of Elekes *et al.* confirm these observations with their simulations, although they simulated a different type of experiment. For the particle size range used by Klein *et al.* and Brucks *et al.*, Elekes *et al.* find that the variation in AoR should be in the order of less than 5° compared to Earth gravity, which is less than the experimental observations. Kleinhans *et al.* also observe the static AoR increase under lower gravity. Elekes *et al.* explain these observations by a possible increase in material cohesiveness under low gravity.

Now, Kleinhans *et al.* observed a decrease in dynamic AoR under reduced gravity. They actually found that the dynamic AoR decreases more than the static AoR increases. The experiment by Kleinhans *et al.* had a discrete avalanching regime, while Klein *et al.* and Brucks *et al.* both were in rolling regime. Cheng and Zhao (2017) demonstrated that in between both regimes, what Klein *et al.* and Brucks *et al.* call the dynamic AoR can be approximated as the average of the upper and lower AoR in discrete avalanches (which Kleinhans *et al.* call static and dynamic AoR respectively). Therefore, if the dynamic AoR decreases more than the static AoR, the average of both must also decrease. In that sense, the results of Kleinhans *et al.* contradict the others. It also contradicts the predictions of Elekes *et al.*, who defined the angle of repose as the angle at the bottom of the pile after being poured and stabilised, which has a similar definition as the dynamic AoR of Kleinhans *et al.* This also contradicts the results of Marshall *et al.* and Nakashima *et al.* They both defined their AoR as the angle at the bottom of the pile once stabilised. They do not observe a significant correlation between gravity and changes in AoR. Although, their standard deviations are in the order of a few degrees, which could be the expected change to be observed according to the predictions by Elekes *et al.* In addition, as Elekes *et al.* show, smaller particles are more affected by cohesive forces than the size ranges used in the reviewed studies. Smaller particles often have a greater AoR and the effect of gravity as predicted by Elekes *et al.* should be more visible. The same experiments with smaller particles might show more significant or different results.

The work of Kleinhans *et al.* did not close the gap on the understanding of how gravity affects the AoR. It actually displayed another way of which gravity shapes granular material, and it might have opened the door for new possibilities. With the contradicting results of all the studies analysed here, could it be that other factors were not taken into account such as external perturbations like vibrations for example, which are typical in flying aircraft? Experiments with discrete avalanching regimes could be more sensible to these perturbations which might create instability and initiate unwanted avalanches. This also highlights the difficulty of performing experiments on the effect of gravity. Experiments are limited by the testing environment, such as parabolic airplanes, drop towers, centrifuges or the ISS. These experiments restrict the size of the experimental setup, or the sample size as running these experiments can be expensive.

Most of the studies chose to study only one or two material types and it can be criticised that these studies did not infer enough about the effects of material properties on their measurements. The choice of using a small number of materials in the study is worth a discussion. On the one hand, there are already many variables affecting the AoR. Therefore, when studying the effect of gravity, using a single material allows to control for the effect of the material properties, as it can be assumed that they stay constant even when gravity changes. The problem arises when using two materials, like Klein and White (1990) did. They found a statistical relation between gravity and the AoR for each material tested, but each equation was different from another. How can the effect of gravity be described now that the effects of material properties were not accounted for? This is where a study across a range of materials can provide an answer. There exists a variety of studies of the effect of material properties on the AoR. While all the effects are not fully understood (a dedicated literature study should be done for this), there is enough literature to support the evidence of the effect of material properties on the AoR. It certainly would require more work, but using these studies to infer and control for the effects of material properties would allow to better isolate the effects of gravity on the AoR.

2.3. Summary of Chapter 2

This chapter provides an overview of the key findings of the literature surrounding this research. First, an introduction to granular materials is given, covering the main properties used to characterise these

materials, and the major forces acting on the particles over their range of size. From these characteristics, the angle of repose is explored further through some of the main studies on the topic, which show how different types of experimental and numerical studies exist to analyse the effect of specific variables. One main lesson is that there is no unique definition of the angle of repose across the literature, as it is adapted to suit the specific experimental setup or phenomenon of each study. Then, the literature on the effect of gravity on the angle of repose is looked at. The focus on gravity as a variable is chosen because it puts the angle of repose (used in industrial and geomorphological applications) in the context of planetary exploration, as gravity is one of the main varying parameters from one planet to another. The literature review shows that there is no consensus among studies on how gravity affects the angle of repose. Some find that the angle of repose decreases when gravity increases, some find that it increases when gravity increases, and other find that there is no significant dependence between them. The lack of consensus arises from various reasons. One is the fact that in this very niche topic with few studies, all studies have used differing experimental setups tested within the restricted capabilities of hyper- and hypogravity test facilities (centrifuges, drop towers, parabolic aircraft, *etc.*), which also meant that it was difficult to generate enough data for significant results. They used different materials tested under different avalanching regimes and therefore defined the angle of repose differently. In conclusion, the topic of gravity and the angle of repose has not been explored enough yet to tell whether certain studies are right and others are wrong, or whether their findings may overlap and build towards a common understanding of the very complex mechanisms behind how gravity affects the angle of repose.

This research aims to improve the understanding of how gravity affects the angle of repose and progress towards a consensus in the field. Next, in Chapter 3, research objectives and research questions are defined, along with a plan to guide the research of this thesis.

Research Questions and Project Plan

This chapter presents the thesis research project objectives. Based on the gap in the literature identified in the previous chapter, it first defines the main research question with sub-research questions to shape the answer in Section 3.1, then lays out hypotheses to validate in order to provide an answer to the research questions. Finally, an overview of the approach used in this research is presented in Section 3.2. The details of the experiments, the methodology, results and conclusions of the research are presented in the following chapters of this report.

3.1. Research Objective & Research Questions

In Chapter 2, it was concluded that there is a lack of consensus in the literature on gravity and the angle of repose. On the one hand the lack of consensus can be due to the studies not using a common and consistent experimental method. On the other hand, it can be due to inconsistent choices of materials studied, the avalanching regimes used, or the limitations in number of data points for significant results linked to the complexity of testing in hyper- and hypogravity. This research aims to further explore the intricacies between gravity and the angle of repose to help bridge the gap between the studies on the topic, building towards a better global understanding. Therefore, the research objective of this study is the following.

Research Objective

The objective of this thesis research project is to help establish which studies made correct inferences as to how gravity affects the angle of repose of granular material, by observing changes in the mechanics of their avalanches over a range of varying gravity levels.

The research objective will be achieved by answering the main research question of the thesis.

Main Research Question

How does gravity affect the angle of repose of non-cohesive granular materials through the mechanics of avalanching?

The main research question is quite broad and does not guide how the research should be performed. A scientific method should therefore be followed throughout this research. To this end, a series of hypotheses can be defined based on certain assumptions, which will be tested to help build a complete answer to the main research question. This will be done during the research project by comparing them to observations from experiments.

3.1.1. Research Hypotheses

In the literature review of Chapter 2, the paper by Kleinhans et al. (2011) was identified, where they defined two hypotheses to validate in their study. The first hypothesis of Kleinhans et al. (2011) is that the static angle of repose would increase with a decreasing gravity force. It is based on the assumption that the other forces acting on particles (Van der Waals, electrostatic, etc.) would not change with the reduction

of gravity. Kleinhans *et al.* also do not aim to study the effect of these other forces in details, but rather use them in the discussion of the observations and the possible interactions between the experiment and the tested material. An interpretation of the driving assumption behind this first hypothesis is that the static friction force does not only depend on the applied load, hence with a lower gravity, the weight of the particles decreases more than the static friction force does. Therefore a steeper slope angle is required for the particles' weight to overcome the friction and initiate movement. The second hypothesis of Kleinhans *et al.* (2011) is that the dynamic angle of repose would become smaller with a decreasing gravity force. The main assumption behind this is that under a lower gravity, the moving flow of particles would become more dilated, which would reduce friction and allow the material to settle at a smaller angle of repose. Intuitively, under a lower gravity, the particles from upper layers are less "pushed down" against the lower layers. Therefore while falling along the slope, the particles experience a lesser acceleration downwards and can travel further horizontally. The particles will experience less contacts with other particles, hence less friction. With the particles being more separated from one another, the flow would effectively be more dilated. A smaller (more horizontal) slope angle would be required for the friction forces to overcome gravity and stop the motion. Therefore the dynamic AoR would become smaller under reduced gravity. In their results, Kleinhans *et al.* found that both their assumptions were correct. Other studies found the same relations in their results for the angle of repose, based on similar assumptions (Elekes and Parteli, 2021; Klein and White, 1990; Brucks *et al.*, 2007). Assuming that the relations found by Kleinhans *et al.* (2011) are correct, the following hypotheses can be defined.

- **Hypothesis 1:** A decrease in gravity leads to an increase in angle of repose.
- **Hypothesis 2:** A decrease in gravity leads to an increase in static angle of repose.
- **Hypothesis 3:** A decrease in gravity leads to a decrease in dynamic angle of repose.

In addition to finding that the angle of repose increases when gravity decreases, Elekes and Parteli (2021) found that the particle size also affects the strength of the change in AoR. Small particles are more affected than large particles. The reason for this is that the cohesive forces are relatively much stronger than gravity for smaller particles (orders of magnitude smaller in size) than for large particles, where gravity is predominant. The following hypothesis is therefore defined.

- **Hypothesis 4:** The effect of gravity on the angle of repose is stronger for smaller particles than for larger ones.

During their experiments with rotating drums, Brucks *et al.* (2007) defined an important variable: the Froude number $Fr = \omega^2 \frac{R}{g_{eff}}$, with the drum angular velocity ω , the drum radius R , and the effective gravitational acceleration g_{eff} . They found that the Froude number was the characteristic parameter to differ between the avalanching regimes. As the Froude number increases, the granular material went from discrete avalanching regime, to rolling, to cascading, with a transition phase in between each. Brucks *et al.* found that when keeping the gravity-level constant and increasing the drum angular velocity (hence increasing the Froude number), the angle of repose would increase. The inverse relation was also found, that for a constant angular velocity, increasing gravity (hence decreasing the Froude number) would decrease the angle of repose. With this, it can be assumed that when the avalanching transitions from discrete, to rolling, to cascading, the associated Froude number increases. In turn, this means that if gravity is kept constant, an increase in the angle of repose should be observed. This will be tested through the following hypothesis.

- **Hypothesis 5:** The mean angle of repose is smaller in discrete avalanching regime than in rolling regime, and it is smaller in rolling regime than in cascading regime ($AoR_{Discrete} < AoR_{Rolling} < AoR_{Cascading}$).

To summarize this section, all research hypotheses are captured in the box below.

Research Hypotheses

- H1:** A decrease in gravity leads to an increase in angle of repose.
- H2:** A decrease in gravity leads to an increase in static angle of repose.
- H3:** A decrease in gravity leads to a decrease in dynamic angle of repose.
- H4:** The effect of gravity on the angle of repose is stronger for smaller particles than for larger ones.
- H5:** The mean angle of repose is smaller in discrete avalanching regime than in rolling regime, and it is smaller in rolling regime than in cascading regime.

3.1.2. Sub-Research Questions

By validating the research hypotheses defined in the previous section, a series of associated sub-research questions will be answered throughout the following chapters of this thesis research report. By the end, answering each research question will help provide a complete answer to the main research question. The sub-research questions are the following.

Sub-research Questions

- R1:** How does gravity affect the mean angle of repose?
- R2:** How does gravity affect the static angle of repose?
- R3:** How does gravity affect the dynamic angle of repose?
- R4:** How does the effect of gravity on the angle of repose change between smaller particles and larger ones?
- R5:** How is the average angle of repose affected when transitioning between discrete avalanching, rolling and cascading regimes?

3.2. Research Plan

With the research objective, hypotheses and research questions defined, an overview will be given in this section of the research plan followed during the thesis. To provide context surrounding this research, the raw data for this research reuses video data which was produced during experiments performed by de Vet (2010), who supervised this thesis research. The experiments studied series of avalanches of granular materials in varying gravity environments. Performed in a Hele-Shaw cell, these would allow to study the angle of repose over the various test conditions. This is detailed further in Chapter 4. A Hele-Shaw cell has not yet been used to study the effect of gravity on the angle of repose making this an interesting opportunity for new insight. The availability of this data is an opportunity to get a head-start in this research and not have to perform the experiments, which allows to spend more time on the analysis of the data in the given time-span of the thesis project.

With the experiments already performed, this project focuses on the development of a method for the measurement of the angle of repose over time over all the experiments. As the observation of the avalanching mechanics is a visual process, the raw experimental data is in the form of videos. The method therefore aims to create a database of measurements of the angle of repose and various other variables over time, for each experiment. The design and validation of the method are detailed in Chapter 5.

Comparing the various measurements allows to establish how the variables relate to each other in their varying environment. Testing the validity of these results allows then to answer the various research questions, which is done in Chapter 6.

Finally, these results are linked to the literature on the angle of repose and gravity to see how it may add to, validate or conflict with the other studies. This is discussed in Chapter 7, before the research conclusions are drawn in Chapter 8.

3.3. Summary of Chapter 3

This chapter follows the review of the literature on the effect of gravity on the angle of repose where a lack of consensus was identified as the main gap in the literature. This gap will be addressed in this study by reaching the research objective defined in this chapter, which is to help establish the correctness in the

findings of other studies by observing avalanches in granular materials. To this end, the main research question will be answered, which concerns how gravity affects the angle of repose. With the breadth of this research question, a series of sub-research questions were defined to help build a complete answer to the main research question. Each sub-research question will verify its corresponding hypothesis, which is defined based on the current knowledge of the angle of repose and gravity. A research plan is then proposed to carry out the thesis and meet the research objectives. This plan is based on the availability of experimental data which was gathered in experimental campaigns prior to this research. How this experimental data was gathered is detailed in the following Chapter 4.

Part II

Method, Results & Discussion

4

Experimental Data

The previous chapter defined the research objectives of this research. The outlined research plan is based on the opportunity to analyse experimental data which was studied in the past prior to this study. This chapter provides a detailed background on the gathered raw data. Section 4.1 details the experimental setups used. Section 4.2 details which materials were used in the experiments along with their material properties. Finally, Section 4.3 provides an overview of the parametric conditions gathered for later analysis in this research.

4.1. Experimental Setup

Experiments were conducted by de Vet (2010) to produce the raw data. One of these sets was in the hypergravity regime. All sets tested the same materials but required a slightly different setup to accommodate the different test environments.

4.1.1. Hypergravity Experiments

The hypergravity experiments were conducted at the Large Diameter Centrifuge at the European Space Agency (ESA) ESTEC centre in Noordwijk (the Netherlands). The experiment is installed in a test cell attached to one of the arms of the centrifuge (one of the red boxes in Figure 4.1). The rotation of the centrifuge generates a centrifugal acceleration $a_{centrifuge}$ on the experiment which depends on the angular velocity of the centrifuge ω , and the distance R between the centre of the centrifuge and the position of the test cell along the centrifuge arm following Equation 4.1:

$$a_{centrifuge} = \frac{\omega^2}{R} \quad (4.1)$$

The experiment is subject to the effective gravitational acceleration g_{eff} , which is a combination of the gravitational acceleration of the Earth g , and the centrifugal acceleration as per Equation 4.2:

$$g_{eff} = \sqrt{a_{centrifuge}^2 + g^2} \quad (4.2)$$

The effective gravity levels were varied throughout the experiments at 2g, 3g, 5g, 10g, 15g and 20g. Experiments at 1g were also conducted, although this meant that the centrifuge was not rotating.



Figure 4.1: The Large Diameter Centrifuge at ESTEC (Photo: ©ESA)

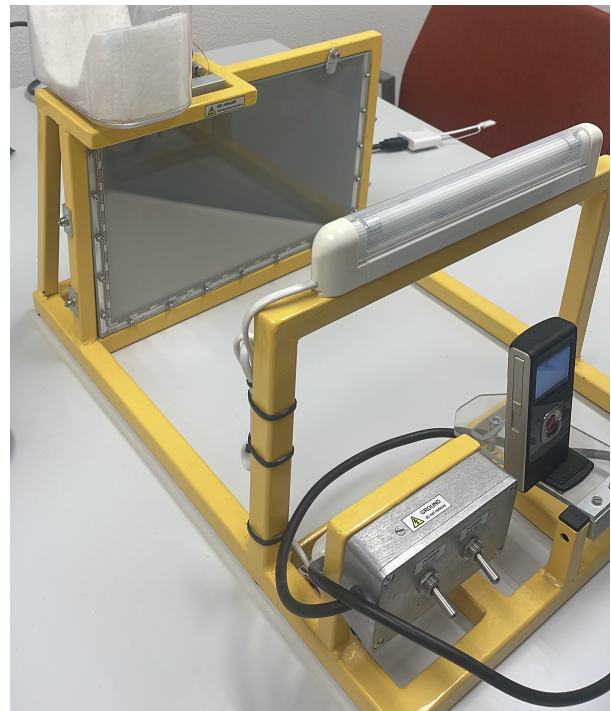


Figure 4.2: Test setup used for the hypergravity experiments.

The Hele-Shaw cell used in these experiments was made of transparent acrylic. It is a 30cm by 20cm (length - height) rectangular cell, with a width of 7.5mm to be about fifty times the average particle size. A digital camera was used to film the experiments. The camera is a Cisco Flip Video U32120B UltraHD Video Camera, which records videos with a resolution of 1280x720 pixels, and a frame rate of 50fps. The camera was installed perpendicular to the test setup as can be seen in Figure 4.2. The materials are poured into the cell through a circular opening. The opening diameter was varied throughout the experiments to also study the impact that a larger opening (and hence a greater discharge flow of particles) would have on the experiment. The hole diameter was varied from 3mm, to 4mm and 5mm.

4.1.2. Hypogravity Experiments

A series of similar experiments with Hele-Shaw cells were performed in hypogravity in parabolic flights. These experiments used a slightly different setup from that of the hypergravity experiments with a different video camera. The data analysis pipeline developed for this research (detailed in Chapter 5) requires calibration material to process the data. The calibration material of the camera used for the parabolic flights experiments was not available for this research and the experiments in the hypogravity environment were therefore not analysed.

4.2. Materials Tested in the Experiments

Five different materials were used in the experiments (de Vet, 2010). Three were homogeneous and two were mixtures of two of the homogeneous species. Note that in all tests, the interstitial medium was air. The species and materials were the following.

- Glass beads of industrial origin, with a sample size between $412 - 512 \mu\text{m}$. The beads have a spherical shape (see Figure 4.3a).
- Volcanic sand, originated from Java (Indonesia). Sieving the sample results in a particle size distribution of $250 \mu\text{m}$ at D50, and $320 \mu\text{m}$ at D90¹. The grains have an irregular shape with sharp edges (see Figure 4.3b).

¹This means that 50% of the sample was smaller or equal to $250 \mu\text{m}$, and 90% of the sample was smaller or equal to $320 \mu\text{m}$.

- River sand, of unknown origin. Sieving the sample results in a particle size distribution of $180\mu\text{m}$ at D50, and $290\mu\text{m}$ at D90. The grains have an irregular shape with sharper edges than the glass beads, however less than the volcanic sand (see Figure 4.3c).
- One mixture of glass beads and volcanic sand, with 50% of each species.
- One mixture of river sand and volcanic sand, with 50% of each species.

The characteristics of the species used in the experiments are summarised in Table 4.1.

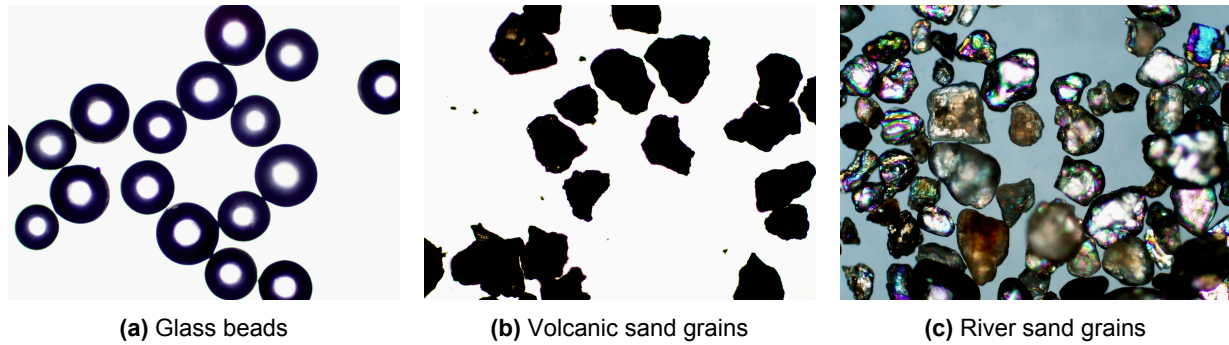


Figure 4.3: Microscope pictures of the material species used in this research (de Vet, 2010)

These mixtures were chosen to observe particle sorting. Indeed, following the mechanisms well described by Makse et al. (1998), mixtures of materials of different sizes and individual angles of repose can result in the observation of particle separation. In the Glass-Volcanic mixtures, the glass beads are on average larger than the volcanic sand grains. The rounder shape of the glass beads means that its individual angle of repose is expected to be smaller than that of the volcanic sand. In a mixture where the larger particles have the lower angle of repose, particle segregation can be observed. The glass beads should end up towards the bottom of the pile. In the River-Volcanic mixtures, the river sand grains are on average smaller than the volcanic sand grains. The irregular shape with sharper edges of the volcanic grains means that its individual angle of repose is expected to be greater than that of the river sand. In a mixture where the larger particles have the greater angle of repose, particle stratification can be observed. It is expected that the two sand species will form repeating layers of each individual material.

Table 4.1: Properties of the material species used during the hypogravity and hypergravity experiments

Species	Origin	Size	Shape
Glass Beads	Industrial	$412 - 512\mu\text{m}$	Spherical
River Sand	Unknown	$180\mu\text{m}$ at D50 $290\mu\text{m}$ at D90	Irregular
Volcanic Sand	Java, Indonesia	$250\mu\text{m}$ at D50 $320\mu\text{m}$ at D90	Strongly Irregular

4.3. Raw Experimental Data

During the experimental campaigns, each material type was poured in its Hele-Shaw cell while the gravity acceleration was varied between runs. The main variables changed during the experiments were therefore the effective gravity, the type of material and the diameter of the cell opening. For each combination of conditions, the experiment is repeated 3 times to minimise the effect of local errors and variations which could produce outliers. An overview of all the experiments conducted is presented in Table 4.2, where "Yes" means that the experiment was performed and "No" means that the experiment was either not performed or that its data could not be retrieved.

Table 4.2: Overview of the experiments conducted in the hypergravity environment. "Yes" means that the experiment was performed and "No" means that the experiment was either not performed or that its data could not be retrieved.

Experiment	g-level	Cell opening (mm)	Material				
			Glass Beads	River Sand	Volcanic Sand	Glass-Volcanic	River-Volcanic
Centrifuge	1	3	Yes	No	Yes	Yes	Yes
	2		Yes	No	Yes	Yes	Yes
	3		Yes	No	Yes	Yes	Yes
	5		Yes	No	Yes	Yes	Yes
	10		Yes	No	Yes	Yes	Yes
	15		Yes	No	Yes	Yes	Yes
	20		Yes	No	Yes	Yes	Yes
	1	4	No	Yes	No	No	No
	2		No	Yes	No	No	No
	3		No	Yes	No	No	No
	5		No	Yes	No	No	No
	10		No	Yes	No	No	No
	15		No	Yes	No	No	No
	20		No	Yes	No	No	No
	1	5	Yes	Yes	Yes	Yes	Yes
	2		Yes	Yes	Yes	Yes	Yes
	3		Yes	Yes	Yes	Yes	Yes
	5		Yes	Yes	Yes	Yes	Yes
	10		Yes	Yes	Yes	Yes	Yes
	15		Yes	Yes	Yes	Yes	Yes
	20		Yes	Yes	Yes	Yes	Yes

4.4. Summary of Chapter 4

This chapter provided a detailed background on the production of the experimental data of this research. An experimental campaign in hypergravity was performed in a centrifuge, over a range of effective gravity accelerations from 1g to 20g. The materials tested in the experiments include glass beads with an average diameter of $462\mu\text{m}$ and spherical shape, volcanic sand with an average diameter of $250\mu\text{m}$ and a rough irregular shape, and river sand with an average diameter of $180\mu\text{m}$ and a shape smoother than the volcanic sand but more irregular than the glass beads. Two mixtures were also tested from these pure species. The first is a glass-volcanic mixture which displays particle segregation. The second is a river-volcanic sand mixture which displays particle stratification. The granular materials were poured in a Hele-Shaw cell to observe the avalanches happening along the pile formation. The main parameter of the Hele-Shaw cell varied during the experiments was the opening diameter of the hole through which the material was poured into the cell. The avalanches were recorded on video using a camera, and calibration material was recorded. Each experimental condition was tested three times to record redundancy in the data.

Not all recordings from the experimental videos of 2010 could be recovered for analysis in this research. An overview of which parametric conditions were recovered is given in Table 4.2. This experimental data contains detailed information on the avalanche mechanics and the angle of repose. The following Chapter 5 details how this information is retrieved to generate data such that it can later be used to answer the research question.

5

Data Analysis Method

The previous chapter detailed the experiments in which various granular materials were poured in Hele-Shaw cells in hypergravity regimes. The mechanics of the avalanches were captured on video and this raw experimental data has been made available for analysis for the purpose of this research. By measuring various parameters from this data, it will be possible to objectively describe how the avalanching mechanics evolve when changing the gravitational environment and answer the research questions of this research. This chapter has the following structure:

- Section 5.1 explores which parameters have been studied in the literature and how they were measured.
- In Section 5.2, the parameters to be measured in this research are defined based on the research questions to be answered, and based on the variables used in other studies such that the results can later be compared.
- Section 5.3 details the method that is implemented in this study, and how the variables are measured step-by-step.
- Then, Section 5.4 describes how the method is validated for accurate results.
- Section 5.5 covers why certain parameters could not be measured in this study.
- Section 5.6 gives an overview of which experiments were eventually used to produce data from the method described in this chapter.
- Finally, Section 5.7 details how the data was pre-processed to remove inaccurate measurements and outliers such that it can be analysed in the following Chapter 6.

5.1. How Parameters Are Defined in the Literature

Many parameters can be measured from the experimental videos and it may be difficult to choose which ones to focus on. Looking at the variables studied in the literature (reviewed in Chapter 2) provides insight into what to measure and how, because measuring the variables in a consistent manner will allow to later generate results comparable to the other studies. This is done in this section.

It was identified in the literature review that there is no single definition of the angle of repose. Rather, the definition is often adapted to the type of experiment and setup used in each study. It was often defined as the angle of the slope of a pile of granular material either just before, during, or after an avalanche had occurred. The angle of repose was also found to have an influential role in the apparition of particle sorting, a behaviour specific to granular mixtures. It is mostly studied in Hele-Shaw cells, which is the setup also used in the gravity experiments of this research. After being poured, a mixture could display segregation and have both materials on separate sides of the cell, or it could display stratification and make a complex pattern of repeating layers of each material. During the literature study, certain papers were identified studying particle sorting, namely Makse et al. (1997), Makse et al. (1998), Koeppe et al. (1998) and Grasselli and Herrmann (1997). While they did not look at the effect of gravity, they did study the angle of repose in Hele-Shaw cells. Hele-Shaw cells have not been used yet in the context of studying gravity. It is therefore important to use a coherent method to measure the angle of repose. These studies are re-explored in this section to understand what parameters were identified and how they were measured.

The slope angle of the granular pile is a main observable parameter across studies, often described by the **angle of repose**. As particles pile up on each other, the slope angle varies depending on which material is beneath the upper particles. In a mixture of two materials, Makse et al. (1998) recognise up to five angles of repose measured once the particles stabilise. Each angle is denoted $\theta_{\alpha,\beta}$ where α is the particle on top of the other particle β . The large particles are denoted as 2 and the small ones as 1. This means that four angles are measured: θ_{11} small particles on top of small particles; θ_{12} small particles on top of large particles; θ_{21} large particles on top of small particles; θ_{22} large particles on top of large particles. θ_{11} and θ_{22} are therefore the individual angles of repose of the pure species. All these angles of repose are measured in degrees and can be seen in Figure 5.1.

When segregation occurs, see Figure 2.1, Makse et al. (1998) only identify two angles of repose which are the AoR of the pure species θ_{11} and θ_{22} . When stratification occurs, see Figure 2.2, then the four angles θ_{12} , θ_{21} , θ_{11} and θ_{22} can be identified. The fifth AoR defined by Makse et al. (1998) is the angle of the slope surface θ_0 . It is measured above the stratification layers, not above the extremities of the pile where one can find the pure species (small particles on the top, large particles at the bottom). Since there are thin layers of both species, the effective angle of the slope at its surface will not necessarily be θ_{22} nor θ_{11} , but rather a value in between (Makse et al., 1998). Koeppe et al. (1998) measured the AoR of the individual materials and then of the mixture, measuring a different angle depending on which material would be on top of the other. It is unclear where those angles were measured on the slope, it could be assumed that it was measured at the center. Contrary to Makse et al., Koeppe et al. do not recognise that the slope of the pile is not a straight line. They only measure one angle at the centre where the stratification occurs, and not various angles along the slope.

The **velocity** of the avalanche and the kink along the slope in cm/s is measured by Makse et al. (1997), which is an important factor of the slope formation. The velocities of the avalanche and kink affect the layer formation, and therefore affect the pattern wavelength (Makse et al., 1998).

The **mass flow** f of particles being poured in the cell is measured in g/s by Koeppe et al. (1998) as it affects the apparition of the stratification. Above a threshold mass flow, the particle sorting simply does not occur at all. Below the threshold, particle sorting can occur, and the mass flow does not seem to affect the pattern shape (Koeppe et al., 1998). It is unclear how Koeppe et al. measure the mass flow, but one could imagine a system where the particles are poured from a container separate from the Hele-Shaw cell, and the cell itself sits on a scale to measure the increase of mass over time.

The **cell dimensions** are the first parameters measured in almost each study as it is expected that the cell shape affects the particle sorting in multiple ways. Makse et al. (1997) measure the cell gap in mm (the horizontal width), the horizontal length and vertical height of the side plates in mm . Koeppe et al. (1998) and Grasselli and Herrmann (1997) also measure and control the cell width. The cell width is an important factor affecting the particle stratification pattern, as Koeppe et al. found that an increase cell width leads to a decrease in the layer wavelength and layer amplitude (how effectively separated the grains are inside a layer).

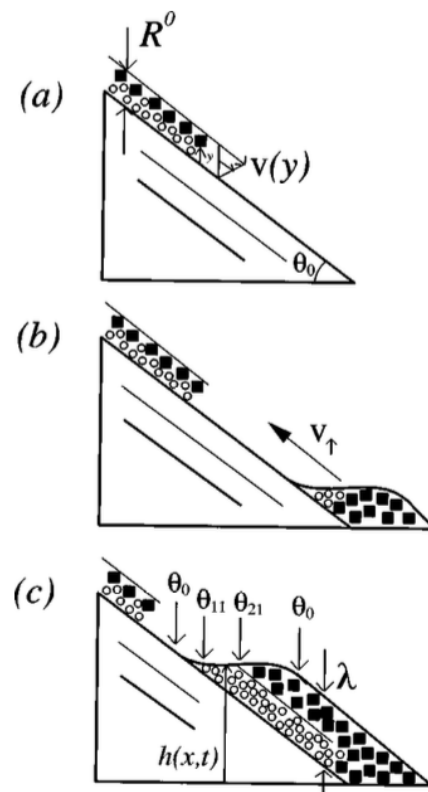


Figure 5.1: Stages of the dynamics of stratification. Definitions of the angles of repose in (c) (Makse et al., 1998).

5.2. Parameter Selection for this Study

The previous section provided insight on how other studies defined and measured their parameters related to the angle of repose and particle sorting in Hele-Shaw cells. The research question aims to measure the effect of gravity on the angle of repose through the avalanching mechanisms. Additionally, particle sorting is expected to be observed from the non-homogeneous mixtures used in this study, which can provide additional insight on the changes in the avalanching mechanics. The objective of this section is to build a list of variables to be measured from the raw experimental data, with an identification of which ones are essential to building an answer to the research question, and which ones are more of a "nice to have".

To begin, the **effective gravitational acceleration** g_{eff} experienced by the system is the main variable of the research questions and is therefore required to be measured. The effective gravitational acceleration is the downwards acceleration that objects inside the test cell experience from their environment (the parabolic plane or the centrifuge). This acceleration was accurately measured during the experiments, and the acceleration is computed differently for the experiments in the parabolic flights than in the centrifuge. This was detailed in Chapter 4. The gravitational acceleration is expressed in m/s^2 , or in g as a ratio of the standard gravitational acceleration experienced at the Earth surface (assuming $g = 9.80665m/s^2$). The measurements of this parameter were documented as part of the experimental data of S. de Vet and were given with the raw data.

Then, all research questions concern the angle of repose. From the various definitions given in the literature, Makse et al. (1998) has the most precise definitions of the various angles to measure ($\theta_{11}, \theta_{22}, \theta_{12}, \theta_{21}$). There are certain cons to using those angles. The first is that they are used to describe the avalanche kink shape and the layer formation in the stratification of mixtures. The rest of the literature never used this many various angles, but rather a more global angle representing the whole slope at specific times. Using the angles defined by Makse *et al.* might not yield easily comparable results. The second main con to using these definitions of the AoR is that they capture a phenomenon at very small scale. The camera resolution might not be high enough to properly discern particle grains, or the front of the avalanche and kink.

The angles of repose will therefore be defined along the definitions of Koeppel et al. (1998), Grasselli and Herrmann (1997) and Kleinhans et al. (2011). The **angle of repose** θ is defined as the angle of the slope at any given time. It is measured as the angle between the best-fitting straight line along the edge of the slope and the base of the pile (considered to be horizontal). The **static angle of repose** θ_{static} is defined as the steepest angle of repose before an avalanche occurs. The **dynamic angle of repose** $\theta_{dynamic}$ is defined as the lowest angle of repose after an avalanche occurs, when the grains are at rest. These definitions of static and dynamic AoR follow the definitions given by Grasselli and Herrmann (1997) and Kleinhans et al. (2011). Fitting a straight line onto the slope may not be capturing its non-linear shape the best. Splitting the slope into more sections allows to fit multiple shorter straight lines and better capture a curved slope, although each straight line will be more affected by local irregularities. More straight lines also means that more measurements have to be performed in total. For this research, the slope will be represented by one single line capturing the overall slope ($\theta_{overall}$), which is also what most other studies did in the literature. The angle of the slope is not taken from the highest point of the slope to the lowest, but rather over a section best capturing the side of the slope. This is because the top of the slope flattens and rapidly changes its shape due to the constant pouring of new material on it. The bottom of the edge shows a strong flattening as an effect of the presence of the bottom floor of the Hele-Shaw cell. The fallen material there spreads and flattens the foot of the slope. To this end, the angle of the slope will only be measured on a section which does not show these flattening effects (see Figure 5.3). This may be defined arbitrarily per experience, although the same zone will be consistently used across experiments.

In addition to a single overall slope, each slope will also be segmented into two sections (an upper and a bottom section) with one representative slope angle each (θ_{upper} and θ_{bottom}). A large difference between θ_{upper} and θ_{bottom} would show that the overall slope is showing a curved shape and having these two sections will provide more representative measures. This should also reflect the individual angles of repose to be observed in case of segregation like in the work of Makse et al. (1998) (see Figure 5.2).

The **particle sizes** is one of parameters required to answer sub-research question **R4**. This cannot be measured visually from the experimental footage. It has however been measured through sieving and documented at the time of the experiments.

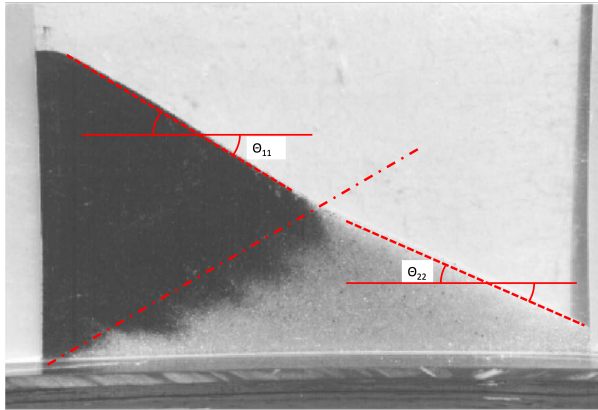


Figure 5.2: Definition of the zones and angles of repose in the case of segregation (with a sample from Makse et al. (1998)).

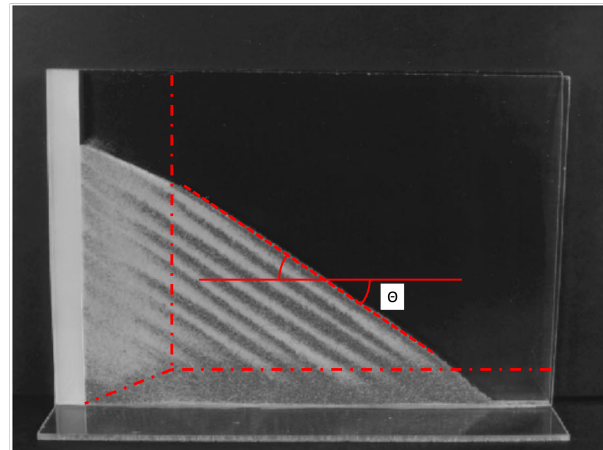


Figure 5.3: Definition of the zones and angles of repose in the case of stratification (with a sample from Makse et al. (1998)).

The **avalanching regimes** are a parameter to answer sub-research question **R5**. Brucks et al. (2007) defined the discrete, rolling and cascading avalanching regimes which depended on the Froude number. The Froude number itself related to the avalanche thickness and velocity.

The **velocities** of the avalanche front down the slope and the kink up the slope were measured by Makse et al. (1998) by tracking the position of the particles along the slope over time. This should require to identify the position of the front and kink and compute its change over time. As the measurements were taken at a certain frame rate in the experiment, each frame represents a point in time. While the resolution might be high enough to identify the avalanche front and kink, tracking the position of the front manually is an arduous and inconsistent. A better method should be found, otherwise it can be considered optional to measure the velocity of the avalanche as there exist other ways to qualify the avalanching regimes.

The particle **discharge flow** is the flux of particles being poured into the cell. Quantified as a mass flow or volume flow, it could be measured as the change in mass in the cell over time, or change in volume occupied in the cell over time. Koeppe et al. (1998) showed that the discharge mass flow affects the particle sorting formation in a discrete manner, where there is no sorting above a threshold in-flux. Brucks et al. (2007) also observed that the changes in regime were related to the change in particle flux being cycled into the avalanches. One could imagine that in an environment where gravity is a variable, the discharge flow would vary due to the change of the acceleration which brings the particles down towards the slope. It can therefore be interesting to observe changes in discharge flow in the experiment. If the avalanche thickness or velocity cannot be measured, the discharge flow should be measured to somehow track the changes in Froude number and the associated changed in avalanching regimes. Those three parameters are considered optional to measure, as long as measuring at least one or two of them is sufficient to qualify the avalanching regimes.

Finally, the **cell dimensions** (length, height, width) were not varied throughout the experiments. The values for these parameters can be found in the experiment documentation or they can be measured on the experimental setup itself. While this parameter was kept constant across the experiments, it is deemed required to measure and document these parameters for the reproducibility of the experiments.

To summarize this section, Table 5.1 presents the selected parameters, along with their definition, symbol, units used, and the priority to be measured in order to answer the research questions. A strategy and method need to be defined to measure these parameters on the experimental data.

Table 5.1: Definition of variables to measure from the experimental data. Each parameter is defined and assigned with a symbol, units, and a priority-level.

Parameters	Symbol	Unit	Definition	Priority
Gravitational Acceleration	g_{eff}	$m/s^2 ; g$	Effective gravitational acceleration experienced by the system. If expressed in g units, then $g = 9.80665m/s^2$ assumed (gravitational acceleration at the Earth surface).	Required
AoR Overall Slope	θ	$^\circ$	Angle of the overall slope at any time.	Required
AoR Upper Half of the Slope	θ_{upper}	$^\circ$	Angle of the stabilised slope after avalanche, for a pure species of larger particles.	Required
AoR Bottom Half of the Slope	θ_{bottom}	$^\circ$	Angle of the stabilised slope after avalanche, for a smaller particles on top of larger particles.	Required
Static AoR	θ_{static}	$^\circ$	Angle of the stabilised slope after avalanche, for a larger particles on top of smaller particles.	Required
Dynamic AoR	$\theta_{dynamic}$	$^\circ$	Angle of the stabilised slope after avalanche, measured at the surface over the stratified layers.	Required
Particle Size	d	mm	Average particle size of the material species.	Required
Velocity	v	mm/s	Velocity of the avalanche layer front going down the slope, and of the kink building up the slope.	Optional
Discharge Flow	f	g/s or cm^3/s	Input of granular material into the system over time.	Optional
Cell Length	L	mm	Horizontal length of the Hele-Shaw cell.	Optional
Cell Height	H	mm	Vertical height of the Hele-Shaw cell.	Optional
Cell Width	W	mm	Horizontal distance between the two plates of the Hele-Shaw cell.	Optional

5.3. Data Analysis Method & Implementation

The parameters identified in the previous section now have to be measured from the raw experimental data practically. The priority is on measuring the most required parameters that can be found in the experimental data. This is mainly the angle of repose (for its various definitions). The other optional parameters may be computed from the same data measured for finding the AoR, or will have a dedicated measuring process. To this end, a step-by-step method is implemented. This method is described in this section.

5.3.1. Numerical Implementation

It was decided to make use of the power of computers to analyse not a single frame in a whole experiment but rather have the ability to rapidly analyse many frames. This leads to the production of many data points from a single experiment in its test conditions. One of the common issues discovered in the literature is that it was difficult to generate enough data points to make statistically significant conclusions about the relation of gravity on the angle of repose due to the practical limitations of testing in hypo- and hypergravity.

To this end, it was decided to implement the measuring methods into a single tool. The tool required to analyse the experimental data is a series of programs developed in Python. Python 3.11 is chosen for its capabilities in terms of image processing, feature detection, data analysis and visualisation, and because of the author's familiarity with the language.

5.3.2. Overview of the Logic

In practice, how is an angle measured on the Hele-Shaw cell? From this dynamic process, one wants to freeze an instant in time and draw two lines on this still image. One line represents what has to be measured, like a tangent to a curve or a straight line best representing a set of points. The other line is a reference, like the horizon, against which the first line of interest will be measured. Then, like in school, one can use a protractor and tell how big the angle is.

When implementing this manual process into a numerical one, the same approach is followed. The first step is to calibrate the camera, to make sure that the image it captures through its lenses is not deformed and correctly represents reality. Then, the video is cut into its individual frames and each one of them is saved as a single picture that can be analysed. Then, the computer has to detect where the edge of the slope is and draw a line through it. Finally, it measures the orientation of the line compared to a reference line and computes the angle between them. This allows to generate data points for each frame of each video that can later be analysed to infer about the processes at play. This is only an overview of the process, which is visually represented in the workflow diagram in Figure 5.4. The details of each step of the process are given in the following sections.

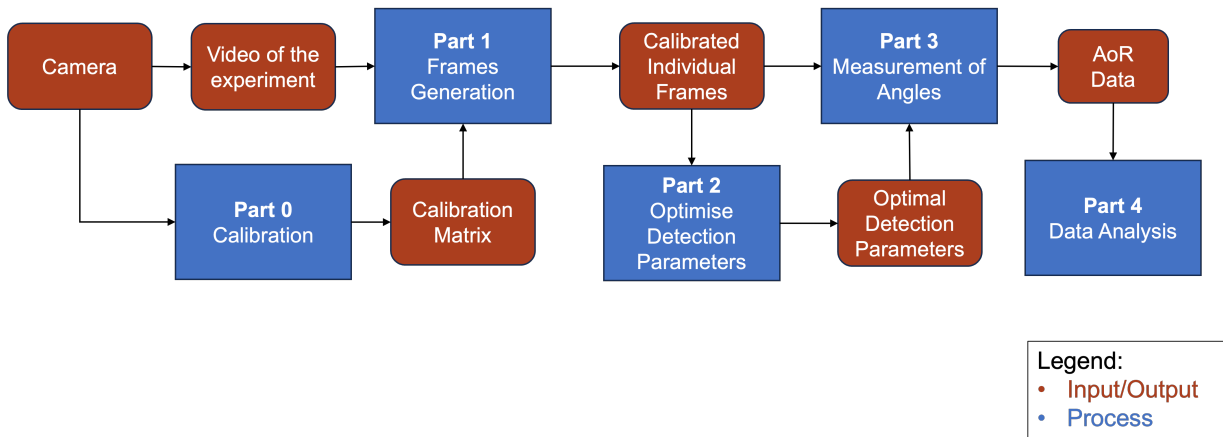


Figure 5.4: Overview of the workflow of the methodology to measure the variables from the experimental data.

5.3.3. Part 0: Calibration

Each camera setup uses different sets of lenses which vary in shape, size and position inside the camera. Each camera also runs different software to process the light information into a digital version. The output video of a camera is a "projection" of reality and may look very different, which can be problematic when using the videos to infer about reality. Calibration is therefore an essential part of the process, as it applies modifications to the output video by modifying it to look like what it should look like in reality.

For measuring angles, the most important aspect is that straight lines in reality stay straight lines in the video, pointing in the same direction. The calibration will therefore move the video pixels in such way that they form the original lines again by applying mathematical transformations to them. This uses the (Linear) Pinhole Camera model, which is a mathematical model which allows to translate how the light coming from a 3D object gets bended through the system of lenses inside the camera onto the 2D pixels of the camera sensor. It is a mathematical transformation which defines matrices to capture the internal properties of the camera (the *intrinsic matrix*) and its external properties (the *extrinsic matrix*) about its relative position to the object being filmed. The *camera matrix* can be taken from the intrinsic matrix and follows Equation 5.1:

$$\text{Camera Matrix} = \begin{pmatrix} f_x & 0 & c_x \\ 0 & f_y & c_y \\ 0 & 0 & 1 \end{pmatrix} \quad (5.1)$$

with as intrinsic parameters the focal length f_x and f_y , and the optical centres c_x and c_y (in x and y respectively). The camera matrix is therefore used to map points of a 3D object to each pixel of the camera

sensor. A matrix to one camera assembly (the sensor and its lens). This allows to compute how much an image is being distorted by a camera. The main distortions affecting a camera are radial distortion, tangential distortion, and some combinations like barrel distortions. These can be corrected with a mapping software return to a true picture.

In Python, the OpenCV library¹ comes with built-in functions to compute the calibration matrix and the distortion coefficients k_1, k_2, p_1, p_2 and k_3 (k_1 : Radial distortion coefficient; k_2 : Radial distortion coefficient; p_1 : Tangential distortion coefficient; p_2 : Tangential distortion coefficient; k_3 : Radial distortion coefficient (higher-order term)). The calibration is done by filming a chessboard pattern with the camera and running the calibration algorithm on the footage. The algorithm identifies the corners between the black and white squares of the pattern and computes the distances between them. From those distances, it is able to compute the camera matrix and distortion coefficients, all together called the *calibration parameters*.

The chessboard pattern is used because the high contrast between the black and white corners makes it easier for the software to detect them. Then, as the squares have side of equal length, the corners should respectively be at the same distance from their neighbour corners in perpendicular directions. If not, this is a sign of a distortion. When calibrating the camera with OpenCV, it happens that the distortion coefficients are not good on the first try. Barrel distortion appeared to often still be present after the first correction. An additional optimisation loop was implemented in the design to optimise the distortion coefficients to make barrel distortion disappear until the distances between the chessboard corners are as close to being constant as possible. The computed camera calibration parameters only have to be computed once and can then be applied any footage recorded with that camera to fix the image.

5.3.4. Part 1: Image Generation

After filming the experiments and computing the calibration parameters of the camera, the videos could be split into individual frames. Because avalanches are a dynamic process, it means that the value of the angle of repose over time may vary. It is therefore necessary to "freeze" an instant in time to measure the value of the AoR at that instant. Other studies often waited for a time where the pile would be at rest to make a measurement. However, a video is a series of still pictures recorded and displayed at a high enough frame rate for the human brain to interpret it as a moving phenomenon. Therefore, recording a video of the avalanches allows to analyse it a many more instants in time rather than waiting for the process to halt.

The camera used in the hypergravity experiments recorded at a frame rate of 50 frames per second. This means that up to 50 images per second were recorded. The video is then later divided into its individual frames, and each frame is then calibrated and saved individually before analysis.

Recording a video to then later split it into its individual frames may seem less efficient than shooting a burst of individual pictures at a similar frame rate. There is a loss of picture quality when recording the footage as a video and then transforming it again. However, cameras may be limited in how long they can shoot a burst of images, and may not do so at the same frame rate as a video can. Additionally, the compressed video file requires less storage space than the individual images would, offering more flexibility and more possibilities for performing the experiments again or for long periods of time.

5.3.5. Edge Detection Algorithm

The main task performed in the following parts of the process is the detection of the edge of the slope for the measurements of its angle with the horizon. The slope of the material is identified by detecting its edge against the background of the Hele-Shaw cell. The edge detection is done with the use of a Canny edge detector. This method was introduced by Canny (1986) and consists of the following steps:

1. Application of a Gaussian filter.
2. Computation of the intensity gradient per pixel.
3. Hysteresis Thresholding.

First, a Gaussian filter is applied to remove the noise of the original image, effectively blurring the image. Then, the Canny algorithm applies four filters to detect edges in the horizontal, vertical and diagonal

¹https://docs.opencv.org/4.x/dc/dbb/tutorial_py_calibration.html (visited on 30/10/24)

directions of a pixel. The gradient returned is the first derivative in the horizontal (G_x) and vertical (G_y) direction of the intensity of each pixel. The intensity is the light intensity. The gradient has for amplitude G :

$$G = \sqrt{G_x^2 + G_y^2} \quad (5.2)$$

and for direction

$$\Theta = \text{atan2}(G_y, G_x) \quad (5.3)$$

Edges of objects reflect light differently (between a foreground and a background) and there should be a strong gradient at an edge (Ritter and Wilson, 2001). Finally, two thresholds are defined (one high and one low) and applied to the gradients to reduce noise and remove unwanted edges. Any point above the high threshold is a *primary point* and will be kept in the result image. Points in between the high and low threshold will only be kept in the result image if they are connected to the primary point (either directly or through other points which are somehow connected to the primary point) which forms a line of connected points. Other points between the two thresholds that are not connected to a primary point are discarded. Any point below the low threshold is discarded, even if it is somehow connected to a primary point (Ritter and Wilson, 2001).

This detector was chosen due to its wide popularity and use. Much online advice and tutorials pointed towards this method. The Python OpenCV library has built-in functions to implement the Canny edge detector². This detector was the first one implemented in the tool. Through its validation (which is detailed in a further section), it showed accurate results and it was therefore decided to keep it. No trade-off was performed between this method and others as the objective of this study is not to design the most precise or efficient tool, but to study the physics of the edges detected by the tool. It is therefore sufficient to have a design which performs with enough precision to detect edges and measure angles.

It should be noted that because the Canny edge detector detects gradients in intensity, it only looks at the amount of light of each pixel, and not at other factors such as colours. This means that if two neighbour objects of different colours have the same light intensity, the Canny edge might not detect the edge, while the human eye would be able to identify the edge based on the colour difference. The Canny edge detector therefore effectively sees each image in "black and white". This is important for the design of experiments to be filmed to generate the raw data, as a good choice of environment is one where there is a strong gradient between the material edge and its background.

5.3.6. Part 2: Optimisation of Edge Detection Parameters

The edge detection algorithm is mostly sensible for changes in gradients of light intensity. It is therefore crucial to provide an image which will show the edge of the slope under the best conditions.

For this, some image processing is introduced to modify the image. The first parameter defined is a search zone: a section of the image where the edge of the slope appears throughout the video, such that other unwanted edges (of the walls of the cell for example) are not detected. Then, multiple parameters allow to change the contrast of the image to clearly distinct the edge of the material from its background. Sometimes a binarisation to black and white is used. This means that all pixels under a certain threshold are changed to pure black, and the ones above the threshold are changed to pure white. Finally, the hysteresis thresholding parameters (the high and low threshold) for the Canny edge detector are also defined. The various materials have different colours and therefore different light reflections. It is essential to find a combination of parameters to improve the intensity gradient at the edge for each material.

The bottom of the Hele-Shaw cell is defined as the reference horizon for the granular pile in the cell. It would sometime happen that the cell appears tilted in the image. This can happen due to a misalignment of the camera horizon with respect to the bottom of the cell. If not corrected, this would add a bias to all measurements of the angle later on. To correct this, the angle of the bottom of the cell with respect to the camera frame was measured by manually fitting a straight line through points along the bottom line, and measuring the tilt angle.

This step of the process requires manual input to assess of the quality of the detection capabilities of the algorithm based on the given parameters. Each experiment video may vary in lighting conditions, material,

²https://docs.opencv.org/4.x/da/d22/tutorial_py_canny.html (Visited on 25/10/24)

tilt of the setup, etc. Therefore, the set of parameters is individually tested for satisfying results on a couple of frames of the video. The parameters are then saved in a separate file that will be used to later analyse all frames of the video with those optimised parameters.

5.3.7. Part 3: Angle of Repose Measurement

With the set of individual calibrated frames and the optimal edge detection parameters, the program can now analyse each frame to measure the angle of repose. For each image, it runs the Canny edge detection algorithm and identifies a cloud of points (pixels) that belong to the edge of the slope.

A straight line is fitted over the cloud of points through linear regression and applying the least squares method to find the best fitting straight line. The least squares method minimises the distance between the line and all the points of the cloud. In the X-Y coordinate of the image, the line follows Equation 5.4:

$$y = m * x + c \quad (5.4)$$

where m is the slope of the line, and c an offset. The slope of the line can be translated into an angle θ in degrees using trigonometry, following Equation 5.5:

$$\tan(\theta) = \frac{\Delta y}{\Delta x} = m \quad (5.5)$$

This is done for a one straight line that fits the whole cloud of points at first to calculate the overall angle of repose $\theta_{overall}$. Then, the cloud is divided into two groups by splitting the horizontal axis of the search zone at its middle. All the points on the left of the middle are part of the *upper* half of the slope, and all others are part of the *bottom* part of the slope. This assumes that the slope always decreases when going from left to right in the image, which is a correct assumption as the material was always poured from the top left edge of the cell. This allowed to fit a straight line in the upper half and compute the upper AoR, θ_{upper} , and similarly for the bottom half to compute the bottom AoR, θ_{bottom} .

These angles are measured in the X-Y reference frame of the image where the X-axis is the horizon, which does not necessarily align with the real horizon of the experiment. The angle with the horizon (bottom of the Hele-Shaw cell) was computed in Part 2 and the angles of repose are then compensated for the tilt between the image and the horizon. This provides a measure of the angle of repose measured over three sections of the slope for each frame. As the frame rate of each camera is known, this data provides a value of the AoR over time, where the time step between two consecutive frames is calculated following Equation 5.6:

$$\Delta t = \frac{1}{frame\ rate} \quad (5.6)$$

After this part, the data produced is analysed in Part 4 to generate results. These results still require to be pre-processed (Section 5.7), before being explored in Chapter 6.

5.3.8. Discharge Flow Measurement

The one variable that was measured from the experimental data but without using the edge detection data is the discharge flow. The discharge flow was not measured during the experiments as a change of the mass in the system over time, which is quite complex to measure directly on the system. However, it can be measured visually from the experimental videos. This is done by tracking the change over time of the volume occupied by the granular material inside the cell. To be precise, the change in area occupied by material is tracked over time. The Hele-Shaw cell is a quasi 2D cell, with a known width. The camera is placed perpendicular to the cell and hence does not have a perspective on the depth of the material inside the cell. Therefore, it is assumed that the volume occupied by the material is equal to the visible area occupied by the material multiplied by the known depth of the cell.

These measures were not performed for every frame of an experimental video. Each cell has measurement marks along its left and bottom wall in centimetres. For each video, the time is noted when the material starts being poured as it reaches the bottom of the cell. Then, at a later time step, the occupied area is computed by measuring how far the pile extends along the marked X-Y axes. The area is assumed to be that of the triangle inside the cell. This assumes that the slope is a straight line connecting the points where the slope intersects with the X and Y axes of the cell. This is known to not be correct, as the slope

is not a straight line and clearly displays a curved flattening at the top of the pile and at the foot of the pile. The discharge flow is therefore computed as the change in volume divided by the time difference between the two time steps, expressed in cm^3/s . This provides an average discharge flow based on the assumption that it is constant over time, which may not be correct.

However, while this is an inaccurate method to measure the discharge flow, no other method was found and it is the best available at the time of this research. It may not be a correct measure of the discharge flow, it is still considered to be the best indication of it.

5.4. Method Verification & Validation

The method was verified for its functionalities and validated for the accuracy of its measurements. This is described in this section.

5.4.1. Verification

For each step in the processes laid out in Figure 5.4, unit tests were performed to verify that the functions were computing the right information. This was mostly done through printing statements in Python of the parameters calculated to assess if they had the correct format and desired information. Functional tests were then performed at each individual process level (Part 0, Part 1, etc.) to assess if all the functions of the process could run together without running into errors and by producing the expected output.

Once that multiple processes were created and verified on their own, integration tests were conducted to verify the functioning of the process as a whole. This was done by running one process after the other in various conditions of the parameters, and the assessment focused on the suitability of the output of a first process being used as the input of a following process.

The last verification step was a system test of the whole process. A sample data would be used to go through all the various processes until the desired final output of measurements data was created. The apparition of bugs and errors was tracked, and it was assessed whether the output was of the expected form. The correctness of the measurement was assessed in the Validation of the tool, which is explained in the next section.

When errors were identified, they would be immediately corrected in the code. The whole verification process would be performed again up to the level at which the error was identified: unit test → functional test → integration test → system test.

5.4.2. Validation

The method was validated at various points in the process. The first validation is done in Part 0 with the calibration of the camera. The calibration parameters were computed from footage of multiple pictures of chessboard patterns taken at different places in the picture frame. The parameters should be computed to best suit all pictures. After the image was corrected for any camera distortion, a validation step was implemented in the code. This step would identify the corners of the chessboard patterns and assess of their relative position to each other. The calibration of the image may have scaled the image up or down, which is not an issue. However, leftover distortions are not acceptable. The main distortion that was often left after a first round of calibration was the barrel distortion. For this specifically, the value of k_1 and k_2 (radial distortion coefficients) was varied in a given range to find the best improvement in the calibration quality. The best combination of parameters would be the one for which the ratio of the vertical distances and the horizontal distances between the chessboard corners would be as close to 1 as possible. The best calibration settings were then saved for usage on the raw footage. The suitability of the calibration on the final measurements of the method would be validated at a later stage.

The second point of validation was performed in Part 2 for the selection of the edge detection parameters. The set of parameters would be tested on multiple sample images of a single video. The detected edge could be plotted over the image to overlay it on the edge of the material. If the detected edge visually corresponded to what the human eye considered to be the real edge, then the parameters were good enough. It was also important that no noise was being detected by the edge detection algorithm. This could be due to certain noisy points displaying a strong enough intensity gradient to be considered part of the edge while they were physically far from it. Iterations of the detection parameters allowed to reduce the probability of this to occur.

The main validation of the method was the validation of the correctness of its measurements of the angle of repose. For this a set of triangles of varying sizes were filmed with the camera (see Figure 5.5). Each triangle was a right angle triangle for which the bottom and vertical side could be used as reference axes to compensate any tilt between the triangle and camera frame. The varying lengths of the base and side of the triangle allowed to vary the slope of eleven triangles (see Table 5.2). The range of angles covered should encompass the expected range of angles of repose to be observed in the materials, based on the observations from other experiments in the literature.

Table 5.2: Triangles dimensions

Triangle	Base (mm)	Height (mm)	Slope (deg)
1	57.5	57	44.7
2	67	57	40.4
3	79	57	35.8
4	85.5	57	33.7
5	51	94	61.5
6	51	69	53.5
7	51	57	48.2
8	172	64.5	20.6
9	172	52.5	17.0
10	172	41	13.4
11	172	27	8.9

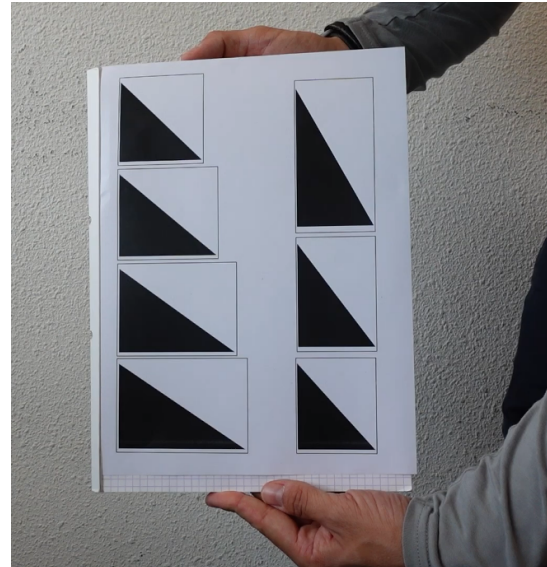


Figure 5.5: Sample triangles filmed on the cameras to validate the slope angle measurements.

The process of filming calibration footage and triangles with a camera, and then processing the footage to measure the slope angles was performed on a variety of cameras. One was a Sony ZV-1 (a general consumer point-and-shoot camera), one was an action camera GoPro Hero 8 which typically displays a strong barrel distortion because of its wide angle, and the last one was the Cisco Flip Video U32120B UltraHD Video Camera used in the hypergravity experiments. Different calibration settings were tested on each camera and the best results were kept. These can be seen in Table A.1 in Appendix A.

From the validation results, it can be seen that the attempts on the Sony and GoPro achieved an average error of 1.2% and 1% respectively, which translates to an error in the angle of 0.31° and 0.19° respectively. These results are quite satisfying, mostly for the GoPro considering that the original footage had strong barrel distortion straight out of the camera. The Cisco Flip camera used in the hypergravity experiments achieved less accurate measurements than the two other cameras. One reason for this is that the technology of the Cisco camera is at least ten years older than the others. Its sensor has a lower resolution than the other, and might not profit from the processing capabilities that the more recent cameras have. The lower resolution used on the Cisco may be the main reason for the lower accuracy. Nonetheless, the best results were found to have a 3% average error of 0.6° . The error is smaller for the bigger angle values above $\sim 30^\circ$, where there is a 1.1% average error of 0.45° . This will be taken into account when interpreting the measurement results. The validation results represent the accuracy of the results. However, the consistency of the accuracy was not tested for validation. The measuring process with the triangles requires a manual input, which is time-consuming. To test the consistency of the results, the slope of a same shape should be measured over many pictures.

5.5. Non-Measured Parameters

Not all parameters could be measured. Measuring a certain variable requires to find a method to compute its value from the experimental data, to develop and implement this method, and to validate that the

measurements are accurate. This is a time-consuming process. If the parameter does not appear in the experimental data, new experiments should be performed to capture the parameter, and organising these experiments is also time-consuming.

The velocity of the avalanche front was not measured directly. It could be detected by the Canny edge detector and some processing would probably allow to identify its location from one frame to another. This was however not implemented in this research. A secondary method to find the velocity could be to see how the angle of repose changes due to the passing of this kink. This would require to know the distance over which the angle was measured, which was unfortunately not recorded during the measurements generation. The velocity is not required to answer the research questions. Its purpose would be to compute the Froude number among others (further discussed in Chapter 7 and Chapter 9).

5.6. Overview of Experiments Analysed

An overview was given in Chapter 4 which showed the parametric conditions for which data was captured (see Table 4.2). In addition, parts of the recovered data could not be analysed either.

It was decided to focus on analysing the 3mm and 5mm opening series from the hypergravity experiments. This was decided because the gap in the range of discharge flows between the highest flow achieved in the 3mm series is quite close to the lowest flow achieved in the 5mm series. This allows to practically cover a wide range of discharge flow without having a large gap in between the two series. The range of discharge flows in the 4mm series would have overlapped with those of the other series.

The 4mm series was only performed on the river sand though, whose 3mm footage could also not be recovered. Analysing the 4mm series for the river sand would have provided a wider range of discharge flow data for this particular material, but it was eventually not analysed due to time constraints. It is left as a recommendation to analyse the river sand experimental data with a 4mm opening, or to reproduce the experiment with a 3mm opening.

To summarise this section, only the hypergravity data for cell openings of 3mm and 5mm were observed for all materials, except for the river sand where there is only data for the 5mm opening. An overview is given in Table 5.3.

Table 5.3: Overview of the experimental data analysed to generate data. "Yes" means that the experiment was analysed and "No" means that the experiment was not.

Experiment	g-level	Cell opening (mm)	Material				
			Glass Beads	River Sand	Volcanic Sand	Glass-Volcanic	River-Volcanic
Centrifuge	1	3	Yes	No	Yes	Yes	Yes
	2		Yes	No	Yes	Yes	Yes
	3		Yes	No	Yes	Yes	Yes
	5		Yes	No	Yes	Yes	Yes
	10		Yes	No	Yes	Yes	Yes
	15		Yes	No	Yes	Yes	Yes
	20		Yes	No	Yes	Yes	Yes
	1	4	No	No	No	No	No
	2		No	No	No	No	No
	3		No	No	No	No	No
	5		No	No	No	No	No
	10		No	No	No	No	No
	15		No	No	No	No	No
	20		No	No	No	No	No
	1	5	Yes	Yes	Yes	Yes	Yes
	2		Yes	Yes	Yes	Yes	Yes
	3		Yes	Yes	Yes	Yes	Yes
	5		Yes	Yes	Yes	Yes	Yes
	10		Yes	Yes	Yes	Yes	Yes
	15		Yes	Yes	Yes	Yes	Yes
	20		Yes	Yes	Yes	Yes	Yes

5.7. Data Pre-Processing

The first step before analysing from the results is to clean the data to only keep the valid measurements. Two main problems are tackled in this section: inaccurate measurements (Section 5.7.1) and outliers (Section 5.7.2).

5.7.1. Filtering Inaccurate Measurements

First, the inaccurate measurements are removed. A look at the measurements of the angle of repose (AoR) over time shows that the measurement are sometimes far off their expected value. This is seen in Figure 5.6a by strong changes in the slope angle of over 10° in a very short time. By comparison, the video data did not show any behaviour where the slope has this kind of dynamics.

As previously mentioned, the angle is computed from the slope of a straight line fitted through the points belonging to the edge of the slope. The coefficient of determination R^2 from this linear regression can be used as an indicator of the fitness of the line to match the slope edge. An R^2 value close to 1 means that the straight line is a good fit. The closer to 0, the worse the fit is. Plotting the R^2 value over time like in Figure 5.6b shows where the linear regression had a good fit with the slope edge. It can be seen that the AoR seems to diverge strongly when R^2 reaches values below 0.9.

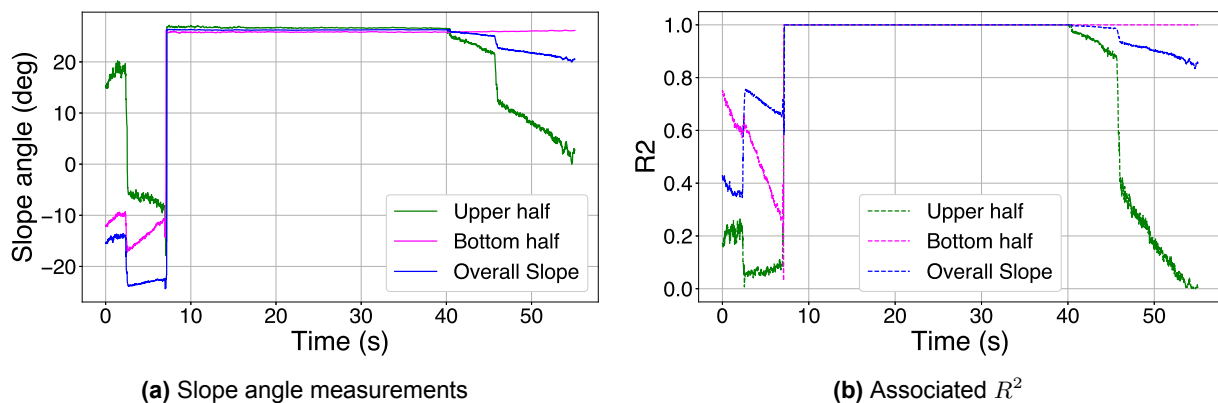


Figure 5.6: Example of slope angle measurements and associated R^2 values over time, prior to data cleaning.

A lower R^2 can be associated to a higher variance of the data around the straight line. This means that the Canny edge detector incorrectly detected points that did not belong to the edge, and included them in the linear regression to compute the slope angle, which falsified the measurement. Therefore, it is decided to keep sections of the data for the which the associated R^2 is as close to 1 as possible. The minimum threshold is set at $R^2 = 0.997$, which allows to keep large portions of the measurements of every experiment. This value is chosen arbitrarily because it appeared that the R^2 value would either be above 0.997 (like the central straight section in Figure 5.6b) or it would diverge far off to lower values (like the extremity sections in Figure 5.6b). This was observed across many of the experiments and the threshold was therefore set at $R^2 = 0.997$, above which measurements would be considered valid.

The invalid sections with an R^2 value below the threshold are then removed from the data of each experiment. From the example given in Figure 5.6, the raw measurements from Figure 5.6a are filtered to only keep the correct section, which results in valid measurements like in Figure 5.7a. Accordingly, the initial plot of R^2 over time in Figure 5.6b becomes Figure 5.7b after filtering, where it only displays R^2 values above the threshold. Note that for both Figure 5.7a and Figure 5.7b,

An important consequence of data filtering is the significant shortening of the duration of each experiment. Although the same experimental conditions were repeated three times, the filtered data for each experiment differs in length, as R^2 values vary over time. For instance, an experiment originally lasting 60s might be reduced to 40s, while another attempt under identical conditions might shrink to 25s. Originally, all repeated experiments began under the same initial conditions. However, due to the removal of early data (as shown in Figure 5.6 and Figure 5.7), the filtered data no longer align in time or initial conditions. In

practice, this means that at $t = 0$ s in the plots, repeated experiments may start with more or less material already in the cell.

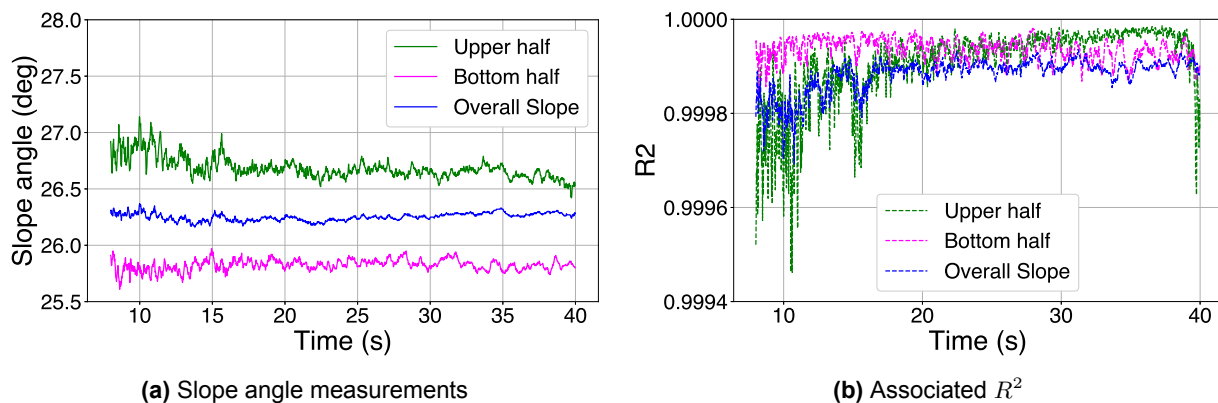


Figure 5.7: Example of slope angle measurements and associated R^2 values over time, after data filtering based on the threshold value of $R^2 > 0.997$.

5.7.2. Outlier Removal

The second main problem encountered in the data is the presence of outliers at certain individual points, like in Figure 5.8a. These outliers were removed using the two standard deviation rule (2σ -method), which identified the outliers lying outside 2 standard deviations (2σ) from the mean. The removal of outliers resulted in cleaned measurements like in Figure 5.8b.

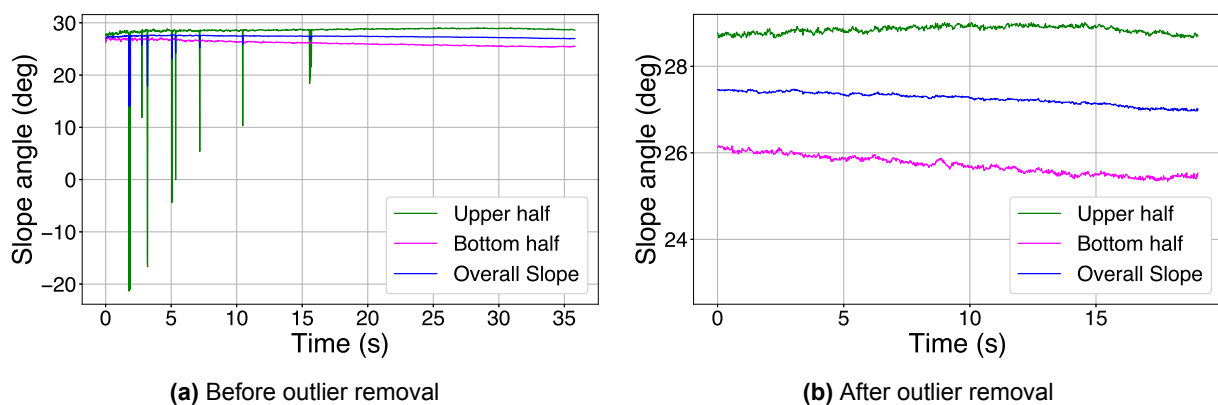


Figure 5.8: Example of outlier values in the measurements and cleaning using a 2σ rule.

5.8. Summary of Chapter 5

This chapter details the various parameters which have to be measured in the experimental data to answer the research questions of the thesis. It first identifies the parameters that were used in the literature to study the avalanches of granular materials in Hele-Shaw cells, which is the experimental setup also used in this research. The main parameters identified were the angle of repose, the velocity of the avalanche flow, the mass flow of particles being poured into the cell, and the cell dimensions. It was also identified that these parameters were not measured in the same manner across studies. Then, the parameters that would be required to answer the research questions of this report are identified. In addition to the parameters found from the literature review, the effective gravitational acceleration, the particle size, and the particle discharge flow are identified. A level of priority is associated to each parameter to provide an order of importance in measuring certain parameters. The angles of repose are the major parameter to be measured.

A detailed method is laid out on how to measure the angles of repose from the experimental data. It starts by finding the calibration parameters of the camera to ensure the correct capture of real features

in the image. The individual frames are then extracted from the video and calibrated. Parameters are then found to optimise the detection of the edge of the granular slope. This is then used to analyse all the frames, identify the edge of the slope and fit a straight line to it (or to a section of it) and measure the angle between this line and the horizon, which is the angle of repose. This method is then verified, and validated by measuring shapes of known slope angle. The camera used in the hypergravity experiments has an accuracy of 3% (average error of 0.6°) which should be taken into account when analysing the results.

After the method was implemented, the raw experimental data was analysed to produce all the measurement datasets. In the end, all experiments run in hypergravity with a cell opening of 3mm and 5mm were analysed. This data was pre-processed to only keep sections of each experiment where the R^2 associated to the linear regression was above a minimum threshold value. Any outliers were also removed from the data based on the 2σ -method. The results of these measurements are detailed in the following Chapter 6.

Experimental Results

The method implemented in the previous Chapter 5 was applied to the raw experimental data set. The produced measurements are presented in this chapter through visual representations in various graphs. Many parameters are analysed throughout this chapter to understand how they influence each other. Trying to do so for all parameters at once could lead to confusion. To this end, this chapter presents the following logic.

- In Section 6.1, the raw measurements of the angle of repose over time are first presented through the introduction of a new type of graph: the “heartbeat” graph. This enables qualitative comparisons of the change in angle of repose over time between the materials.
- In Section 6.2, the distribution of the angle of repose of each material is analysed quantitatively to support the observations from the heartbeat graphs.
- In Section 6.3, examines the separate effects of gravity and discharge flow on the average angle of repose. By the end of the section, the standard deviation of the angle of repose is identified to best capture the changes in avalanching regime.
- In Section 6.4, the types of avalanching regimes are defined quantitatively and their effect on the angle of repose is analysed. This provides a comprehensive view of how the effects of gravity and the discharge flow on the angle of repose change depending on the type of avalanching regime.
- In Section 6.5, the focus is laid on the static and dynamic angles of repose to see how these extreme values of the angle of repose (the maximum and minimum) are affected by others variables.

An important note to the reader on this chapter is that its writing style follows an inductive reasoning approach. It begins with detailed observations on the results which lead to identifying patterns and building up general conclusions. For readers who want a quick overview, red summary boxes of the conclusions are presented at the end of each section. The intention is that by the end of this chapter, the reader will have enough understanding of the mechanisms at play, preparing them for the later discussion of the findings in comparison to the literature in Chapter 7.

6.1. Evolution of the Angle of Repose over Time

The pre-processed data is used to analyse key measurements, focusing on changes in the angle of repose (AoR) during experiments. These changes, plotted over time, illustrate the evolution of the slope formation observed in the experimental videos. This section introduces a new type of graph, the *Heartbeat Graph* (Section 6.1.1), which is used to analyse changes in AoR over time for different materials (Section 6.1.2): glass beads, river sand, volcanic sand, the glass-volcanic mixture, and the river-volcanic mixture. The insights from the heartbeat graphs are summarised at the end of the section. This section only displays the graphs of the relevant results. All results can be found in Appendix B, Section B.1.

6.1.1. Introduction to the Heartbeat Graph

The analysis tool measured the angle of repose of the granular slope for each experiment video. Three angles were measured: one for the overall slope, one for the upper half of the slope and one for the bottom half. Each video contained hundreds to thousands of frames which were analysed. As each frame was

filmed at a constant frame rate of 50fps, each AoR data point can be plotted over time as there is a $\frac{1}{50}$ s step between each measurement.

Plotting the angle of repose (AoR) against time (see Figure 6.1 and Figure 6.2) has not yet been explored in the literature. This type of graph, referred to as a “heartbeat graph”, resembles the shape of an electrocardiogram and metaphorically represents the lifecycle of avalanches bringing the granular pile to life. The graph is used to identify patterns in the AoR over time, including cyclic signals, trends in the mean, variations around the mean, noise, and more. Together with experimental videos, these patterns provide a deeper understanding of particle behaviour and their interactions.

The example heartbeat graph in Figure 6.1 shows the typical cycles that can be observed in a discrete avalanching regime, when the avalanche front and kink are visible. There is a clear cyclic pattern. There is even a reactive pattern between the upper and bottom half of the slope as the particles pile up at the top of the slope slowly increasing the angle of the upper half, while the bottom half has a somewhat constant slope at the same time. Then the avalanche occurs and travels quickly down the slope, which creates a spike down for the upper half, and a spike up in the bottom half a little later. The spike is quite short as the kink bounces back to the top of the slope, bringing the bottom half to a plateau again and the upper half back to its increasing slope angle.

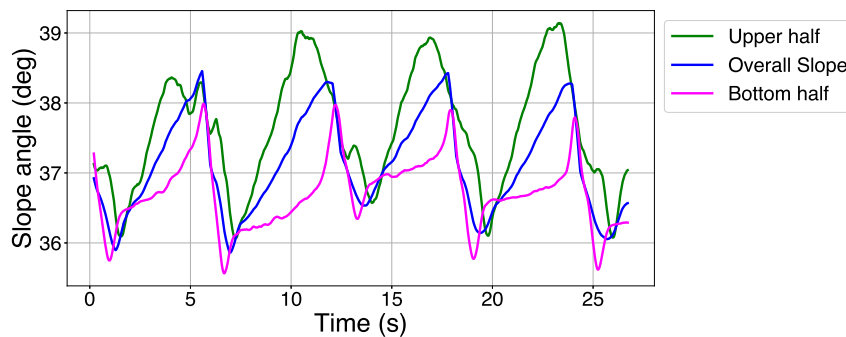


Figure 6.1: Example of a heartbeat graph showing the evolution of the angle of repose during the pile formation. The discrete avalanching regime clearly shows the cyclic reactive pattern between the upper and lower AoR as the avalanche travels along the slope.

In Figure 6.2, there is no cyclic pattern like in Figure 6.1. This can be expected from an avalanching regime where the avalanche of particles is a constant-like fluid flow. Small variations in the value can be attributed to noise in the measurements.

All heartbeat graphs use a rolling mean (moving average) smoothing to enhance readability. This does not impact the conclusions regarding the amplitude of variations or noise in the plots. Any exceptions will be explicitly noted when necessary.

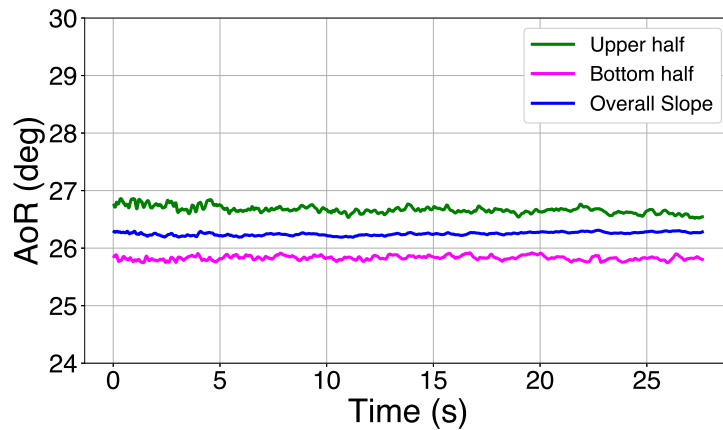


Figure 6.2: Example of a heartbeat graph in rolling avalanching regime, where no cyclic reactive pattern is observed between the upper and lower AoR.

Each experiment was repeated three times for data redundancy, as illustrated in Figure 6.3 for volcanic sand experiments with a 3mm opening at 1g gravity. The graphs differ in length and initial values due to the data pre-processing described in Section 5.7, which retain only sections of accurate measurement.

For the heartbeat graphs discussed in this section, it is assumed that one of the three graphs can be chosen as representative, since all display similar patterns. However, for further analyses in this chapter involving mean AoR values and distributions, data from all three experiments are combined, as they share the same parametric conditions.

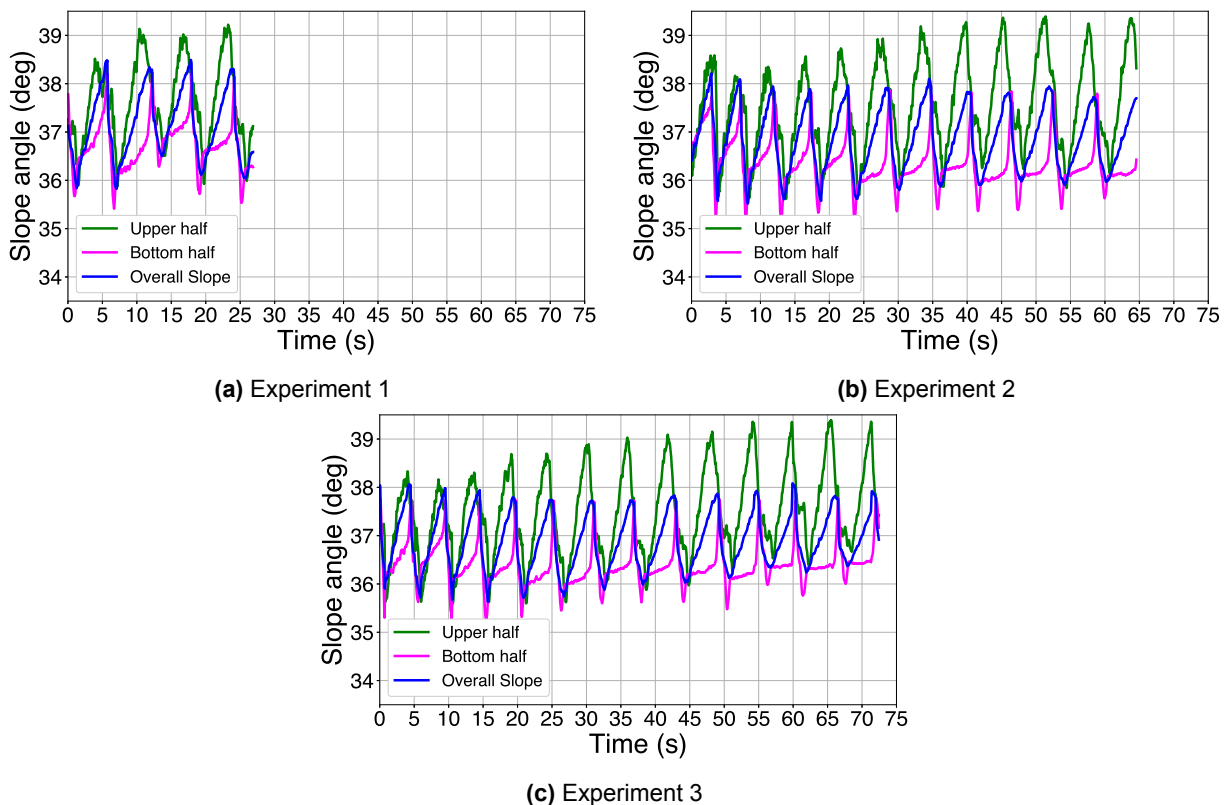


Figure 6.3: Example of the heartbeat graphs of three experiments performed for the same parametric conditions: volcanic sand, opening of 3mm, gravity level of 1g.

In the following sections, representative heartbeat graphs are shown for each material based on their

distinctive patterns. Additionally, only graphs relevant to the discussion are included in this chapter, with all plots available in Appendix B.

As a final note, the shape of the granular slope is frequently referenced in the following sections. To aid visualization, Figure 6.4 illustrates typical slope shapes. The slope shapes can be described using the following terms:

- **Straight:** A straight line with a constant slope angle.
- **Concave:** Curved outward; the upper slope is less steep than the bottom.
- **Convex:** Curved inward; the upper slope is steeper than the bottom.
- **Irregular:** An uneven shape; specific descriptions are provided when needed.

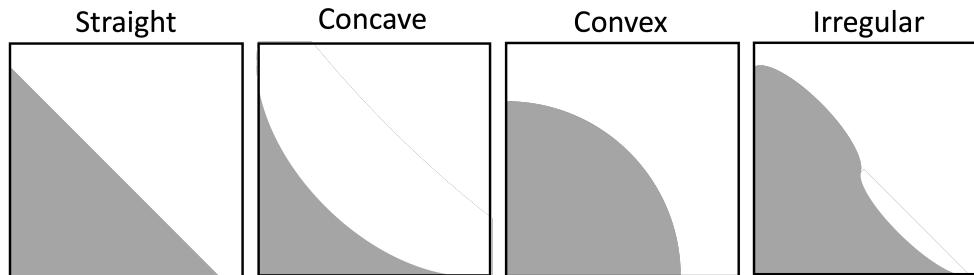


Figure 6.4: Illustration of shapes that the granular slope is expected to take. The shape can be described as Straight, Concave, Convex or Irregular.

6.1.2. Heartbeat Graph Results

This section analyses the heartbeat graphs for all tested materials: glass beads, river sand, volcanic sand, the glass-volcanic mixture, and the river-volcanic mixture. Key heartbeat graphs are analysed for each material and each cell opening size, and the findings are captured in a summary box at the end of this section. The analyses focus on the effects on the angle of repose due to **time**, **gravity**, **opening size**, **material type** and **avalanching regime**.

The heartbeat graphs for **glass beads** with a 3mm opening are shown in Figure 6.5. At 1g (Figure 6.5a), the overall AoR cycles between 24.5° and 25° . The upper and bottom AoR values overlap, with periodic, discrete peaks that increase in amplitude as the pile forms. At 2g (Figure 6.5b), the overall AoR is at least 1° higher than at 1g. The upper and bottom AoR values no longer overlap. Because the upper half is on average 1.5° steeper than the bottom half, the slope takes a more concave shape. The peak amplitudes are larger for the bottom half, indicating a more pronounced avalanche front. Over time, the mean AoR of both halves shows a decreasing trend, as the slope elongates and becomes less steep on average. At 20g (Figure 6.5c), the overall AoR further increases, reaching up to 26.5° . The separation between the upper and bottom AoR values widens, and discrete avalanches occur more frequently with greater randomness.

The heartbeat graphs for **glass beads** with a 5mm opening are shown in Figure 6.6. The main observations compared to the 3mm series (Figure 6.5) are that the AoR values are higher on average, and that the amplitude of the cycles has drastically decreased and appears noisier. At 1g (Figure 6.6a), the upper and bottom AoR are constant and do not overlap. The upper half is 1° steeper than the bottom half, giving the slope a concave shape. At 2g (Figure 6.6b), the overall AoR increases by at least 1° , with no overlap between the upper and bottom AoR values. Over time, the bottom AoR shows a decreasing trend, while the upper AoR slightly increases. As the pile lengthens, the slope becomes increasingly concave. These observations also apply to higher gravity levels.

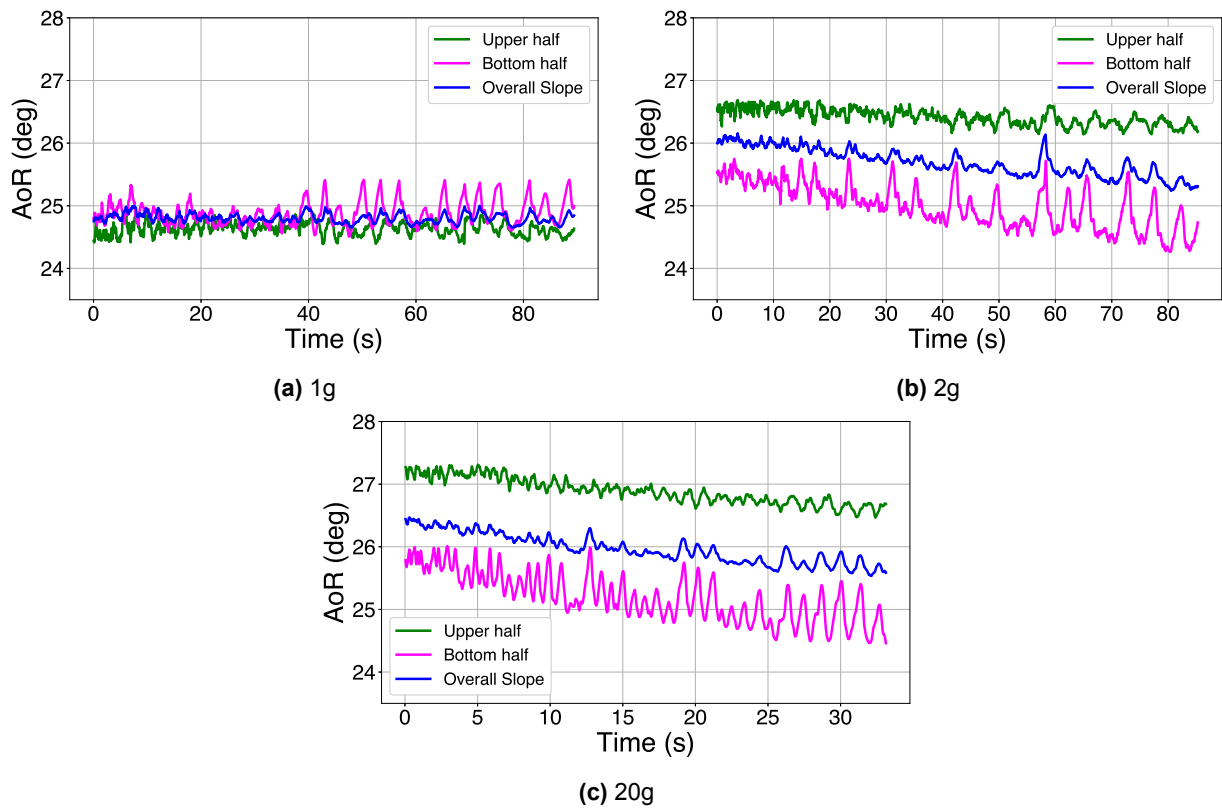


Figure 6.5: Heartbeat graphs of **glass beads** in varying gravity acceleration, with a 3mm opening.

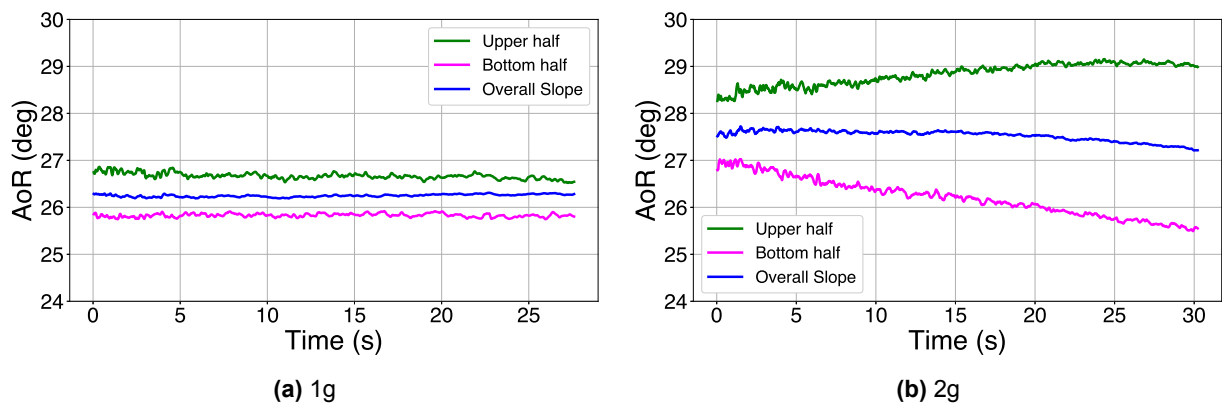


Figure 6.6: Heartbeat graphs of **glass beads** in varying gravity acceleration, with a 5mm opening.

The **river sand** was tested only with a 5mm opening. The heartbeat graphs are presented in Figure 6.7. At 1g (Figure 6.7a), the upper and bottom AoR overlap and fluctuate chaotically between 34° and 35.5° . At 2g and above (Figure 6.7b), the plots no longer overlap. The overall AoR increases compared to 1g, ranging from 35.5° to 36.5° . Over time, the upper AoR increases while the bottom AoR remains constant, resulting in a more concave slope. At 20g (Figure 6.7c), the overall AoR is slightly higher, ranging from 36° to 37° . With increasing gravity, noise in the AoR values diminishes, indicating smoother material flow down the slope.

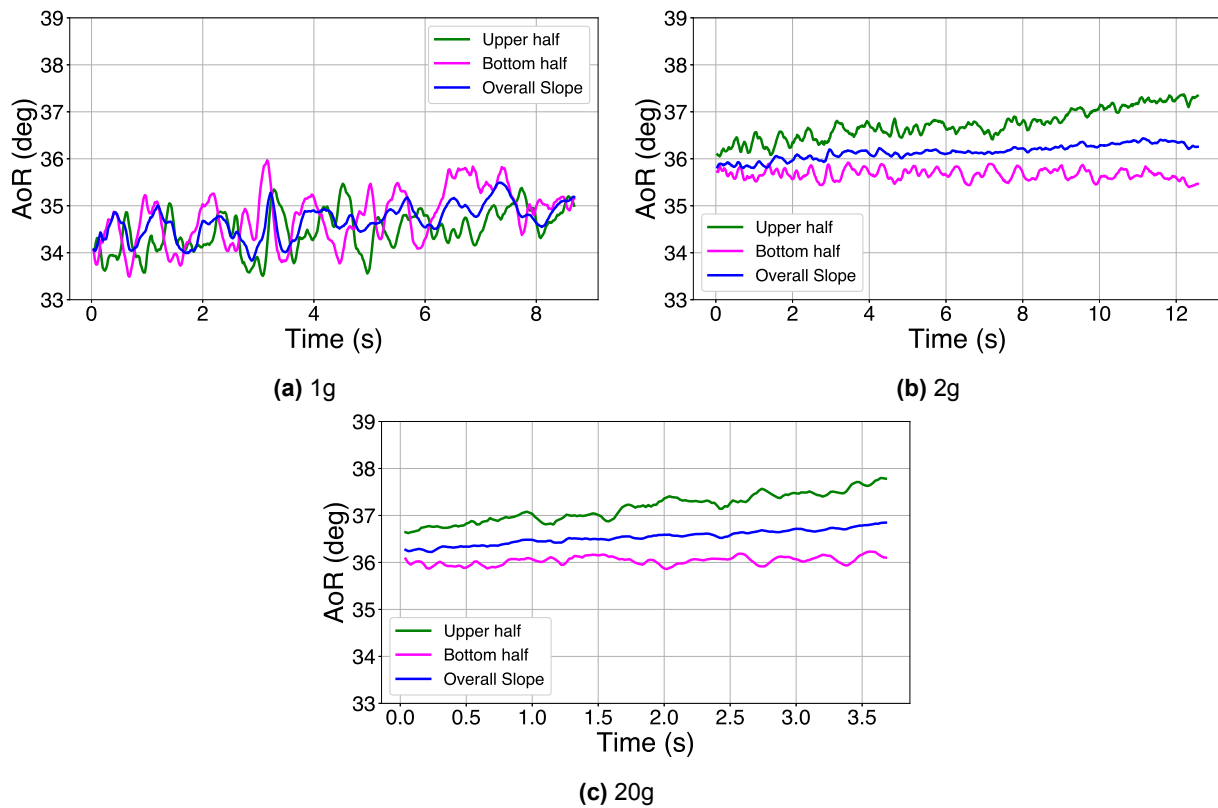


Figure 6.7: Heartbeat graphs of **river sand** in varying gravity acceleration, with a 5mm opening.

The heartbeat graphs for **volcanic sand** with a 3mm opening are shown in Figure 6.8. These graphs show a distinct behaviour compared to the previous materials. At 1g (Figure 6.8a), the AoR cycles between 35.5° and 38° , with overlapping upper and bottom values. Initially, the bottom AoR peaks higher than the upper AoR, but over time, the upper AoR surpasses the bottom, which gradually decreases. A responsive interaction is observed: the bottom AoR forms a plateau before spiking sharply upward and downward as the avalanche passes. At 20g (Figure 6.8b), AoR values increase by approximately 1° , exceeding 40° , while maintaining the same overlapping and responsive behaviour as at 1g. This could exemplify a discrete avalanching regime.

The heartbeat graphs for **volcanic sand** with a 5mm opening are shown in Figure 6.9, illustrating a transition in heartbeat patterns. At 1g (Figure 6.9a), the upper and bottom AoR overlap but display a more chaotic pattern as the pile grows. The mean AoR increases over time, making the slope steeper. At 2g and above (Figure 6.9b), the upper and bottom AoR no longer overlap, with an average difference of about 1° , resulting in a concave slope. The mean AoR values remain constant over time. At 20g (Figure 6.9c), the overall behaviour and cycle amplitude remain unchanged.

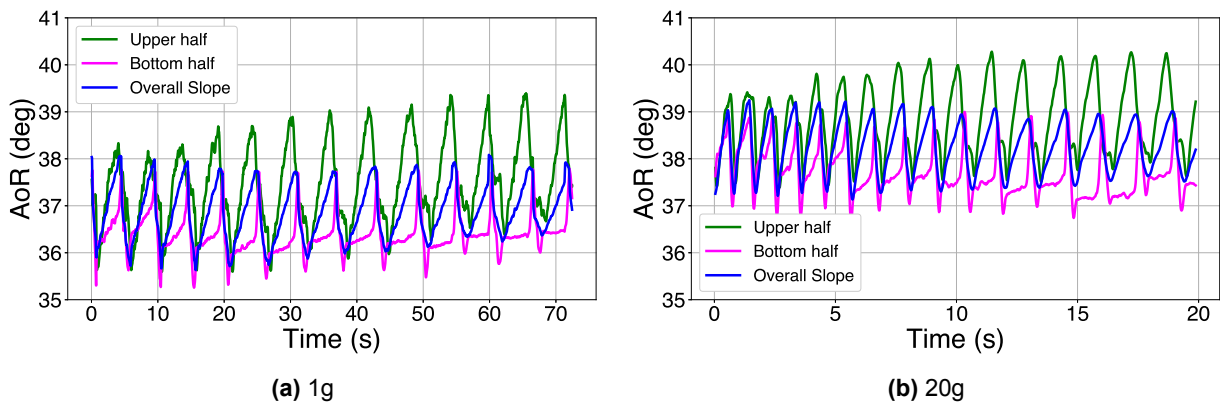


Figure 6.8: Heartbeat graphs of **volcanic sand** in varying gravity acceleration, with a 3mm opening.

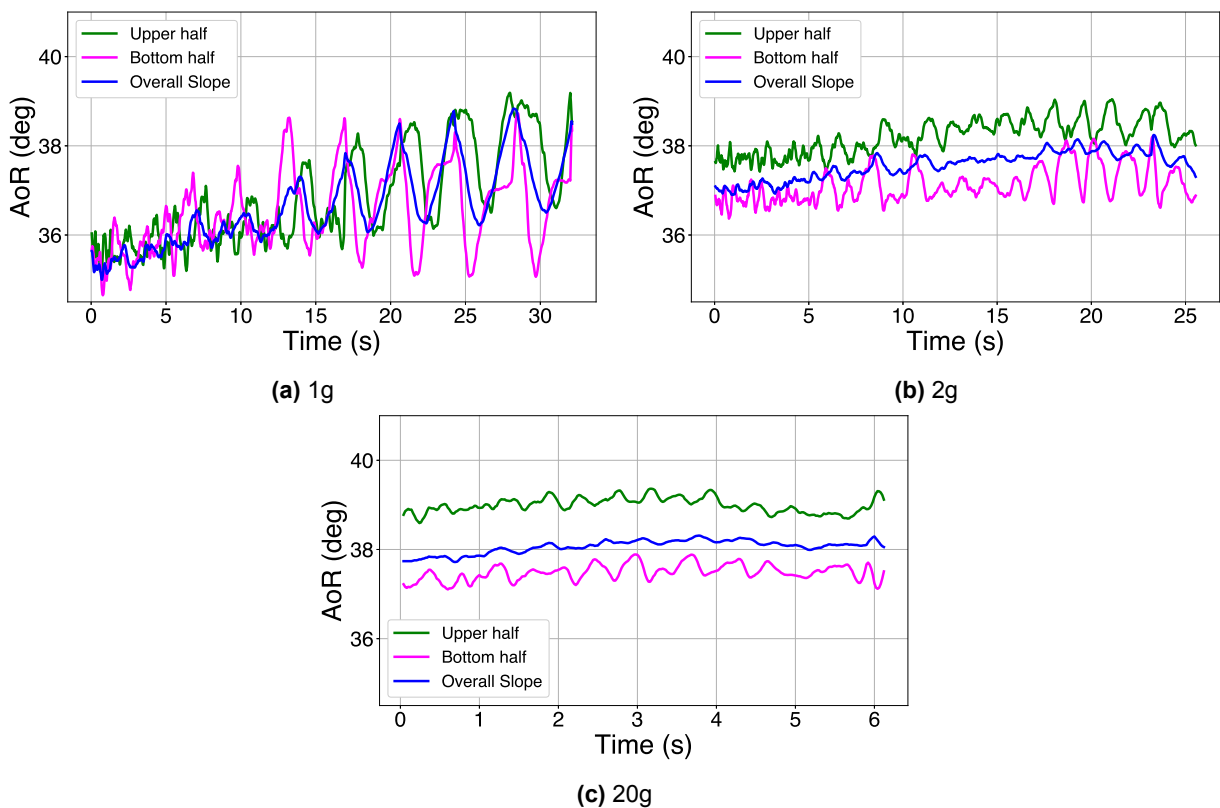


Figure 6.9: Heartbeat graphs of **volcanic sand** in varying gravity acceleration, with a 5mm opening.

The heartbeat graphs for the **glass-volcanic** mixture with a 3mm opening are shown in Figure 6.10. The patterns differ slightly from the previous materials. At 1g (Figure 6.10a), the average AoR cycles between 33° and 34° . The upper and bottom AoR have an average difference of about 5° , sign of a strong concavity. The AoR pattern appears cyclic between the upper and bottom AoR. At 20g (Figure 6.10b), the average AoR initially increases by about 0.5° compared to 1g but shows a decreasing trend over time. The cycle frequency increases with gravity.

The heartbeat graphs for the **glass-volcanic** mixture with a 5mm opening are shown in Figure 6.11. At 1g (Figure 6.11a), the AoR values remain similar but show fewer cyclic variations compared to the 3mm opening. At 2g and higher (Figure 6.11b), the avalanches transition to a regime with significantly reduced amplitude, indicating a more fluid-like behaviour of the avalanching particles. This trend persists across higher gravity levels.

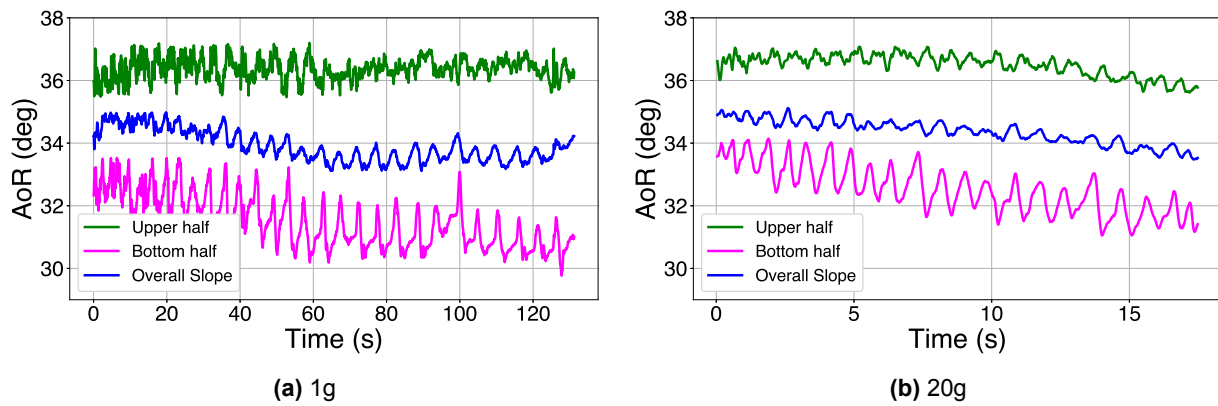


Figure 6.10: Heartbeat graphs of the **glass-volcanic mixture** in varying gravity acceleration, with a 3mm opening.

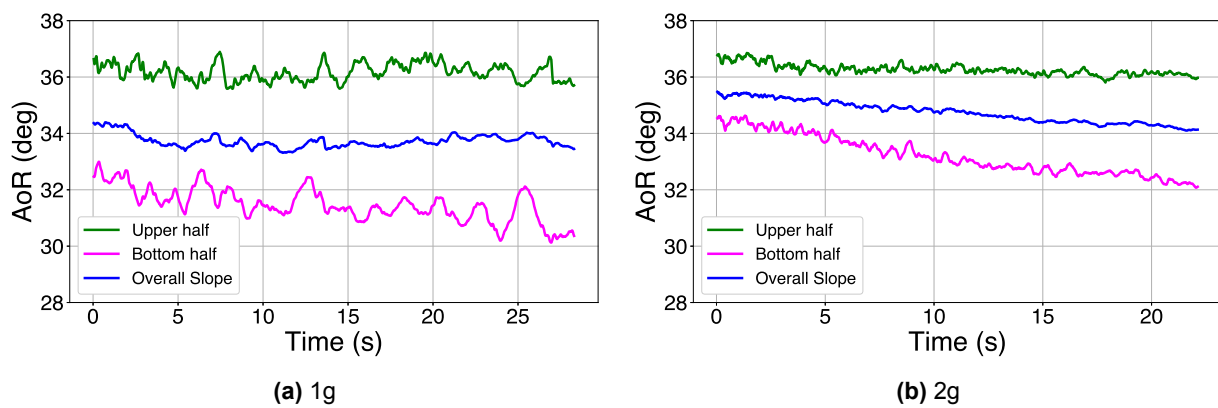


Figure 6.11: Heartbeat graphs of the **glass-volcanic mixture** in varying gravity acceleration, with a 5mm opening.

The heartbeat graphs for the **river-volcanic** mixture with a 3mm opening are shown in Figure 6.12,. These graphs show a similar behaviour to that of the volcanic sand (Figure 6.8). At 1g (Figure 6.12a), the overall AoR is about 36.5° . The upper and bottom AoR overlap. The cycles are discrete and responsive between the upper and bottom AoR, indicating a discrete avalanching regime. Similar to the volcanic sand, the bottom AoR initially reaches higher values than the upper AoR, but over time, the upper AoR surpasses the bottom. At 20g (Figure 6.12b), the AoR values increase by approximately 1° on average. The cycle frequency increases while the amplitude decreases.

The heartbeat graphs for the **river-volcanic** mixture with a 5mm opening are shown in Figure 6.13. At 1g (Figure 6.13a), the avalanches begin transitioning into a different regime, with cycles becoming more irregular. At 2g (Figure 6.13b), the overall AoR increases, and the upper and bottom AoR values diverge, creating a concave slope. At 20g (Figure 6.13c), the cycle amplitude decreases, becoming noise, which suggests fluidisation of the avalanching flow.

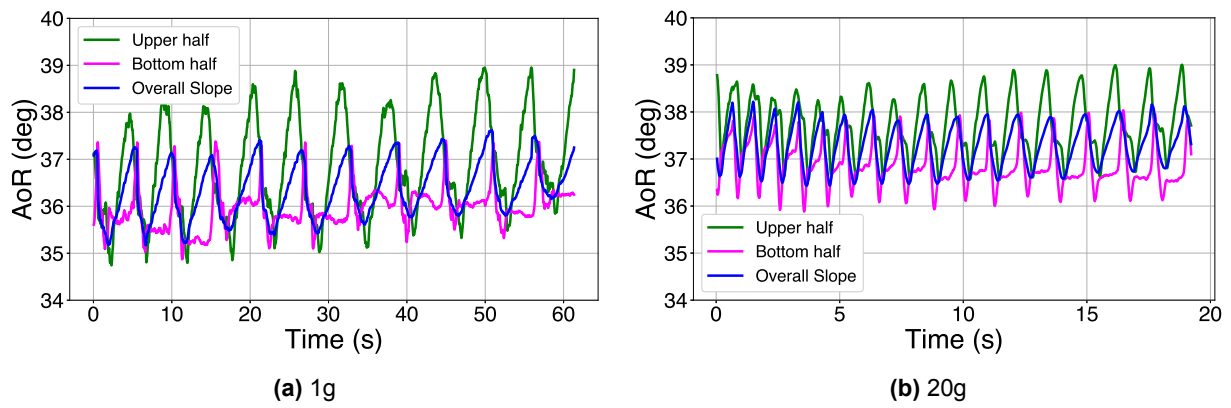


Figure 6.12: Heartbeat graphs of the **river-volcanic mixture** in varying gravity acceleration, with a 3mm opening.

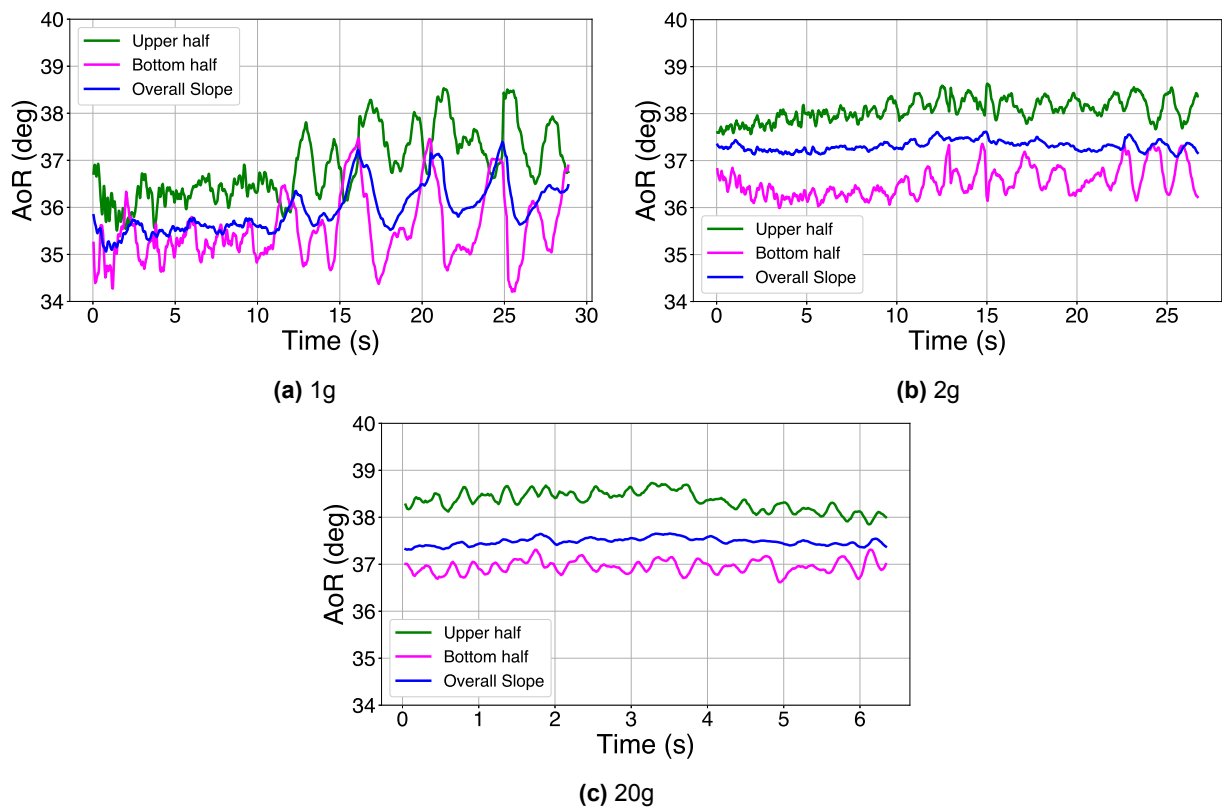


Figure 6.13: Heartbeat graphs of the **river-volcanic mixture** in varying gravity acceleration, with a 5mm opening.

Summary of the Findings from the Heartbeat Graphs

Effect of time:

- The angle of repose (AoR) typically varies over time.
- Depending on the avalanching regime, this variation may occur in cycles of increasing and decreasing values or exhibit negligible fluctuations.
- There can also be increasing or decreasing trends in the average value of these cycles.
- The timing of AoR measurements is crucial, as it affects the expected value of the observation.

Material-specific behaviours:

- The glass beads exhibit relatively cyclic avalanching with a small opening (3mm). The amplitude of the peaks strongly diminishes with larger openings (5mm), indicating a transition to more fluid flow.
- The river sand shows chaotic and overlapping AoR values at 1g, but as gravity increases, noise decreases and the slope stabilises, suggesting smoother flow.
- The volcanic sand displays a cyclic and responsive pattern with the 3mm opening. With the 5mm opening, the flow regime appears more chaotic at 1g and transitions to smoother behaviour at higher gravity.
- The glass-volcanic mixture is similar to the glass beads. The upper and bottom AoR always diverge. The heartbeat is cyclic with the 3mm opening, but the amplitude strongly reduces with the 5mm opening.
- The river-volcanic mixture behaves like the volcanic sand with the 3mm opening, with the discrete cycles. With the 5mm opening, it becomes more fluid like the river sand, with the decreased amplitude.

Effect of gravity:

- The general trend of increasing gravity is that it consistently raises the mean angle of repose (AoR) across all materials, with more pronounced effects at lower gravity levels (e.g., 1g to 2g) than at higher levels (e.g., 2g to 20g).
- A higher gravity increases the cycle frequency while reducing the amplitude of variations. This was mostly observed for materials where the upper and bottom AoR were divergent (not overlapping).
- When increasing gravity, the upper and bottom AoR values tend to diverge, forming concave slope profiles. This separation is especially evident in mixtures and volcanic sand.

Effect of the opening size:

- Smaller openings (3mm) lead to higher AoR amplitudes and more pronounced cyclic variations.
- Larger openings (5mm) tend to reduce amplitude and smooth out cyclic patterns, particularly under higher gravity.

Regime transitions:

- At low gravity levels (1g), many materials exhibit avalanching regimes characterised by periodic, responsive cycles. As gravity increases, transitions to smoother, fluid-like behaviours are observed.

6.2. Distribution of Angle of Repose Values

In the heartbeat graphs from Section 6.1, an increase in gravity often led to an increase in the angle of repose and variations in the amplitude of avalanching cycles depending on the material. However, these graphs are not ideal for quantitatively characterizing these trends.

To address this, “heatmap” plots are introduced. These plots show the upper and bottom angles of repose (AoR) plotted against each other, with each point representing their values at a specific time. The overall

slope AoR is excluded since it represents an average of the upper and bottom halves. The heatmaps are intended to be used in combination with the heartbeats to infer the behaviour of the particles. This approach highlights the relationship between the two halves of the slope.

In this section, the heatmaps are analysed in detail for each material, and the findings are then captured in a summary box at the end. The analyses focus on the effects on the angle of repose due to **gravity**, **opening size**, **material type** and **avalanching regime**.

Distribution of the Angle of Repose of Glass Beads

The distributions of the upper and bottom AoR values for the glass beads are shown in Figure 6.14.

With the 3mm opening (Figure 6.14a), the average AoR of the upper half increases from 24.75° to 26.5° when gravity increases from 1g to 2g and reaches 27° at 20g, showing only a marginal 0.5° increase between 2g and 20g. The variance in the upper AoR remains relatively constant with gravity. In contrast, the bottom half shows a smaller average AoR increase, from 25° at 1g to 25.5° at 20g. However, its variance grows, ranging from 1° at 1g to 2° at higher gravity levels.

The behaviour is similar in the 5mm series (Figure 6.14b). At 1g, both upper and bottom AoR display a small variance in a range of 0.5° . The average AoR is of 26.75° for the upper half and 25.75° for the bottom half. These values align with the higher gravity levels of the 3mm series (Figure 6.14a). When increasing gravity, the average AoR increases for both the upper and bottom slopes and stabilises between 2g and 20g. For the upper half, the average AoR increases from 26.75° at 1g to 29° at 2g and higher. The variance is in a range of 1° , slightly larger than at 1g. For the bottom half, the average AoR increases from 25.75° at 1g to 26.5° at 2g and higher. The variance is in a range of 2° , much larger than at 1g, and larger than the variance of the upper half for the same gravity levels.

The takeaways concern the change in average AoR and the change in variance of the AoR. The change in variance can be explained by two phenomena. The first is a moving average AoR trend at higher gravity levels, evident in heartbeat graphs of glass beads (Figure 6.5c and Figure 6.6b). The second is changes in the amplitude of AoR peaks with increasing gravity (Figure 6.5 and Figure 6.6). As these two phenomena cannot be distinguished from the heatmap alone, interpretations rely on combined insights from the heatmaps and the heartbeat graphs of Section 6.1.

With a 3mm opening, the upper half of the slope increases in steepness when gravity increases, more than the bottom half. The variance of both halves is explained by their heartbeat graphs (Figure 6.5) with the decreasing trend of their average values. The variance of the bottom AoR is larger because of its larger peak amplitude. With a 5mm opening, the overall slope increases in steepness. From the heartbeat graphs (Figure 6.6), the variance of the upper AoR is explained by the increasing trend of its average AoR, while the variance of the bottom AoR is explained by a decreasing trend. The AoR of both halves displayed a negligible peak amplitude.

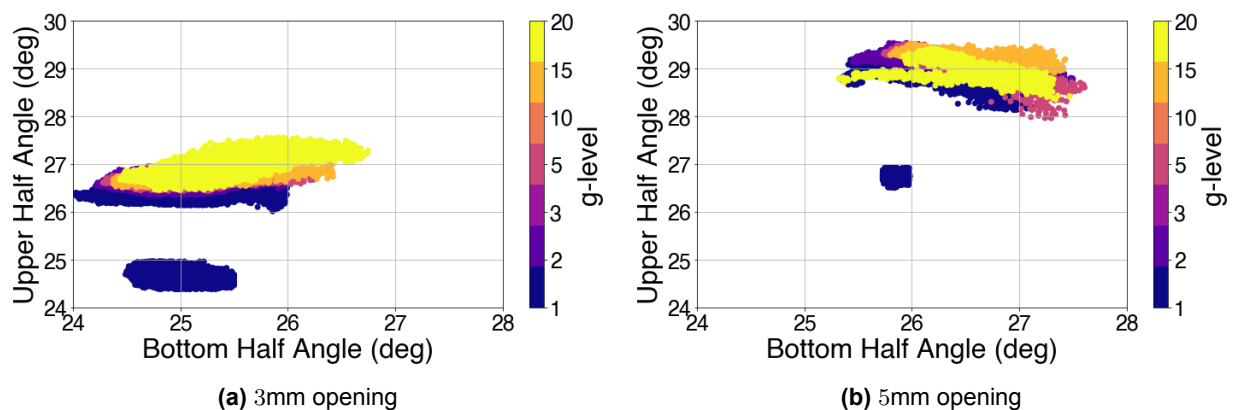


Figure 6.14: Distribution of the angle of repose of **glass beads** on the upper and bottom halves of the slope when varying gravity and the cell opening.

Distribution of the Angle of Repose of River Sand

The distribution of the upper and bottom AoR values for the river sand are shown in Figure 6.15.

The distributions are for a 5mm opening. At 1g the upper and bottom halves are widely spread around an average of 35.5° . At 20g, the average AoR of the upper half is of 37° and the average bottom AoR is 36° . The variance of the upper half is in a range of 2.5° , much larger than the bottom half variance which is in a range of 0.5° .

With a 5mm opening, the overall slope increases in steepness. From the heartbeat graphs of river sand (Figure 6.7), the variance of the upper AoR is explained by the increasing trend of its average AoR, while the variance of the bottom AoR is explained by a decreasing trend. The AoR of both halves displayed a negligible peak amplitude.

The main takeaways are that when gravity increases, the overall slope increases in steepness. From the heartbeat graphs (Figure 6.7), the wide variance at 1g is explained by the large amplitude of the AoR values combined with a slightly increasing trend of the average. At higher gravity levels, the amplitude in the AoR of both halves becomes negligible, which explains the small variance observed on the bottom AoR. However, the variance of the upper AoR is explained by an increasing trend of its average.

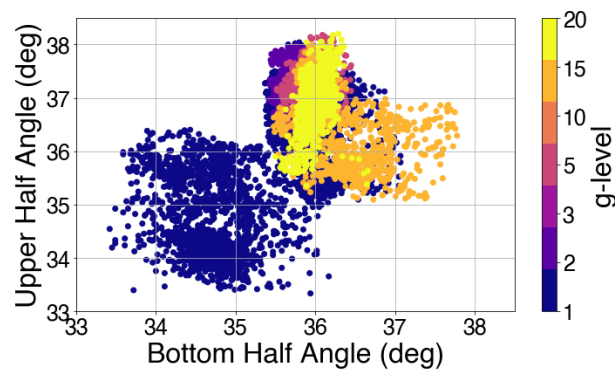


Figure 6.15: Distribution of the angle of repose of **river sand** on the upper and bottom halves of the slope when varying gravity, with a 5mm opening.

Distribution of the Angle of Repose of Volcanic Sand

The distribution of the upper and bottom AoR values for the volcanic sand are shown in Figure 6.16.

With the 3mm opening (Figure 6.16a), the average AoR of both slope halves increases with gravity. For the upper half, it rises from 37.5° at 1g to 38.5° at 20g, while for the bottom half, it increases from 36.5° to 37.75° . The increase rises rapidly between 1g and 2g and then stabilises in the higher gravity levels. The variance changes slightly with gravity. At 1g, the upper and bottom halves have ranges of 4° and 3.5° , respectively, which decrease to 3.5° and 3° at 20g.

The observations are different with the 5mm opening (Figure 6.16b). At 1g, the average AoR and variance range are close to the values observed for 3mm (Figure 6.16a). For gravity levels of 2g and above, the average AoR increases to 39° and 37.5° for the upper and bottom AoR respectively, which is similar to the values of the 3mm opening. However, the variance has reduced on both halves of the slope. It has reduced from a range of 4.5° and 4° at 1g for the upper and bottom halves respectively, to 1° and 1.5° at 20g.

The main takeaways are that with a 3mm opening, the slope becomes steeper with an increasing gravity while maintaining the same avalanche regime. This takes place between 1g and 2g and then stabilises in the higher gravity levels. With the 5mm opening, the slope similarly becomes steeper with an increasing gravity, however with a change in avalanching regime. The decrease in variance is explained by the decrease in the amplitude of the AoR around a constant value for both halves of the slope, which is visible in the heartbeat graph of the volcanic sand (Figure 6.9). The passage of the avalanche front becomes less visible at higher gravity levels.

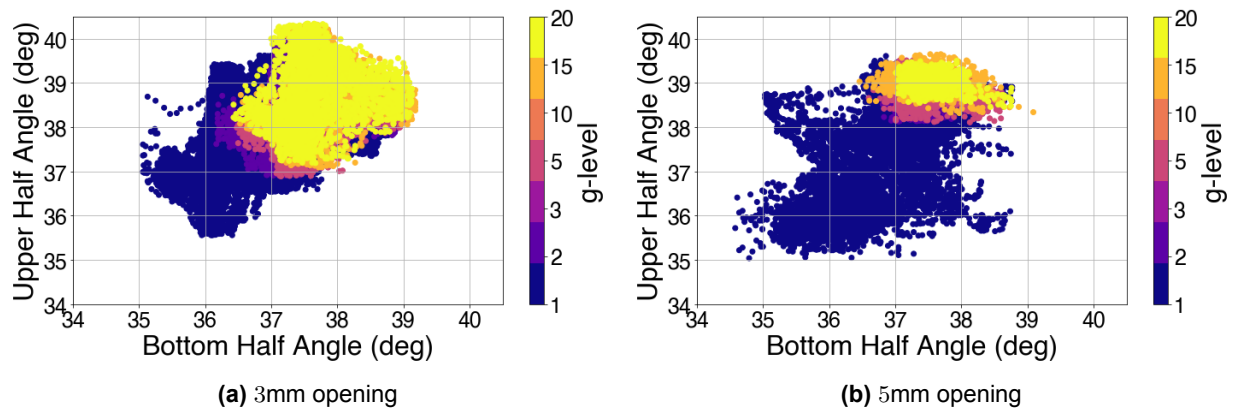


Figure 6.16: Distribution of the angle of repose of **volcanic sand** on the upper and bottom halves of the slope when varying gravity and the cell opening.

Distribution of the Angle of Repose of Glass-Volcanic Mixture

The distribution of the upper and bottom AoR values for the glass-volcanic mixture are shown in Figure 6.17.

With the 3mm opening (Figure 6.17a), the average AoR of both slope halves increases with gravity. For the upper half, it rises from 35.75° at 1g to 36.5° at 20g, while for the bottom half, it increases from 31.5° to 32.5° . The variance decreases slightly with gravity. At 1g, the upper and bottom halves have ranges of 3° and 4° , respectively, which decrease to 2.5° and 3.5° at 20g.

The observations contrast with the 5mm opening (Figure 6.17b). At 1g, the average AoR of the upper and bottom halves are 36.25° and 32.5° , respectively. For gravity levels of 2g and above, the average AoR increases to 36.75° and 33.25° for the upper and bottom AoR respectively. The variance strongly reduces for the upper and bottom halves of the slope from a range of 3° and 4.5° at 1g respectively, to 1.25° and 2.5° at 20g. The bottom AoR always has a larger variance than the upper half.

The main takeaways are that with a 3mm opening, the slope becomes slightly steeper with an increase in gravity, with a slight decrease in variance. It can be seen how the upper half of the slope is on average about 4° steeper than the bottom half of the slope, indicative of the concave slope shape. With the 5mm opening, the slope similarly becomes steeper. This affects the bottom half more than the upper half. The decrease in variance with the 3mm opening is explained by the decrease in the amplitude of the AoR with a decreasing trend for both halves of the slope, which is visible in the heartbeat graph of the glass-volcanic mixture (Figure 6.10). With the 5mm opening, the amplitude in the AoR is negligible and the variance is explained by a decreasing trend mostly present in the bottom AoR (Figure 6.11). The passage of the avalanche front becomes less visible at higher gravity levels as the avalanching regime transitions into a continuous flow, and the slope shape becomes more concave over time.

The glass-volcanic mixture displays particle segregation in the experiments, where the volcanic sand is located mostly in the upper half of the pile, and the glass beads at the bottom. Visible particle separation is later shown in Section 6.6. The AoR values (θ) reached in the mixture do not correspond to those of the pure species. The AoR of the volcanic sand in the upper half of the mixture is smaller than the in its pure species. And the AoR of the glass beads at the bottom of the mixture is larger than that of its pure species.

$$\theta_{volcanic} > \theta_{glass-volcanic_{upper}} > \theta_{glass-volcanic_{bottom}} > \theta_{glass} \quad (6.1)$$

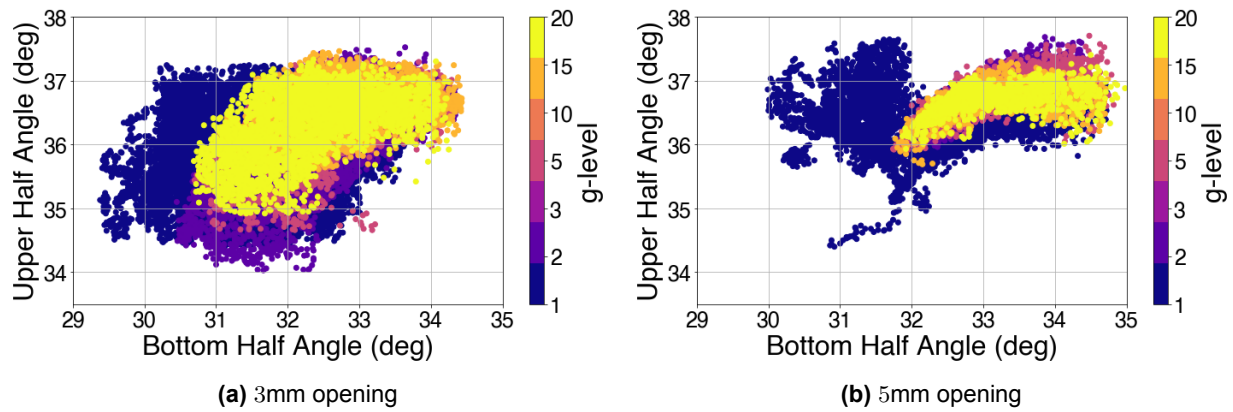


Figure 6.17: Distribution of the angle of repose of the **glass-volcanic mixture** on the upper and bottom halves of the slope when varying gravity and the cell opening.

Distribution of the Angle of Repose of River-Volcanic Mixture

The distribution of the upper and bottom AoR values for the river-volcanic mixture are shown in Figure 6.18. The observations for this mixture are similar to those for the volcanic sand.

With the 3mm opening (Figure 6.18a), the average AoR of both slope halves increases with gravity. For the upper half, it rises from 37° at 1g to 38° at 20g, while for the bottom half, it increases from 36.5° to 37°. The increase rises rapidly between 1g and 2g and then stabilises in the higher gravity levels. The variance decreases slightly with gravity. At 1g, the upper and bottom halves have ranges of 4.5° and 3°, respectively, which decrease to 3° and 2.5° at 20g.

The observations differ with the 5mm opening (Figure 6.18b). At 1g, the average AoR is close to the value observed for 3mm (Figure 6.18a), although with a larger variance. The average AoR of the upper and bottom halves are 36° and 35.5°, respectively. For gravity levels of 2g and above, the average AoR increases to 39° and 37.5° for the upper and bottom AoR respectively, which is similar to the values of the 3mm opening. However, the variance strongly reduced on both halves of the slope. It has reduced from a range of 6° and 5° at 1g for the upper and bottom halves respectively, to 1° and 1.5° at 20g.

It can be concluded that with a 3mm opening, the slope becomes steeper with an increasing gravity while maintaining the same avalanche regime. This takes place between 1g and 2g and then stabilises in the higher gravity levels. With the 5mm opening, the slope similarly becomes steeper with an increasing gravity, however with a change in avalanching regime. The decrease in variance is explained by the decrease in the amplitude of the AoR around a constant value for both halves of the slope, which is visible in the heartbeat graph of the river-volcanic mixture (Figure 6.13). The passage of the avalanche front becomes less visible at higher gravity levels as the avalanching regime transitions into a continuous flow.

The river-volcanic mixture displays particle stratification in the experiments, where both individual materials formed repetitive layers. Visible particle separation is later shown in Section 6.6. The AoR values (θ) reached in the mixture are found to be in between those of the pure species.

$$\theta_{volcanic} > \theta_{river-volcanic} > \theta_{river} \quad (6.2)$$

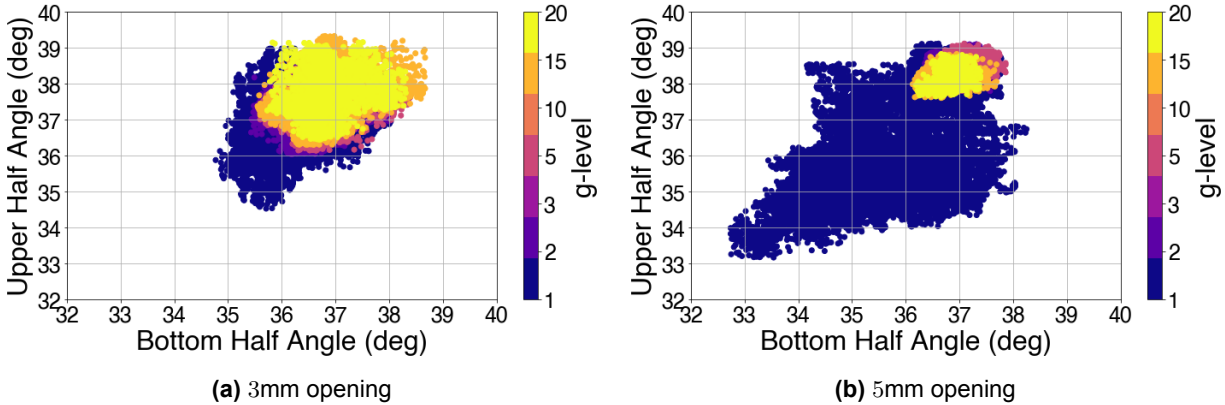


Figure 6.18: Distribution of the angle of repose of the **river-volcanic mixture** on the upper and bottom halves of the slope when varying gravity and the cell opening.

Summary of the Findings from the Distributions of the Angles of Repose

Use of the heatmap to infer on the angle of repose (AoR):

- It allows to quantitatively assess the distribution of the AoR.
- The conclusions on the variance in the AoR cannot be taken from the heatmap alone. Using both the heatmap and the heatmap graphs is required.

Material-specific behaviours:

- The glass beads exhibit steeper slopes with increasing gravity. With the 3mm opening, the larger peak amplitudes cause higher variance in the bottom half. The 5mm opening results in negligible peak amplitudes in both halves.
- The river sand displays a consistent steepening with gravity. The wide variance at 1g is due to large a AoR amplitude, and the variance decreases at higher gravity.
- The volcanic sand shows that its slope steepens between 1g and 2g and stabilises at higher gravity levels with a 3mm opening. There is a transition to a more fluid avalanching regime with decreasing variance at higher gravity levels for a 5mm opening. The avalanche front therefore becomes less visible as gravity increases.
- The glass-volcanic mixture with a 3mm opening exhibits a slight increase in steepness and slight decrease in variance due to a downward AoR trend. The 5mm opening results in a negligible AoR amplitude, and the strong decreasing trend in the bottom half increases slope concavity.
- The river-volcanic mixture behaves similar to the volcanic sand, as its slope steepens between 1g and 2g and stabilises at higher gravity levels. The decrease of the amplitude of the AoR results in a decrease in variance, indicative of a transition to a more fluid avalanching flow.
- Mixtures showed that the average values of the AoR lies in between that of the pure species they are made of.

$$\theta_{volcanic} > \theta_{glass-volcanic_{upper}} > \theta_{glass-volcanic_{bottom}} > \theta_{glass} \quad (6.3)$$

$$\theta_{volcanic} > \theta_{river-volcanic} > \theta_{river} \quad (6.4)$$

Effect of gravity:

- Increasing gravity generally leads to steeper slopes across all materials and mixtures.
- The effect of gravity on the variance depends on the material and the avalanching regime. The regimes often transition around 1g with a 5mm opening.

Effect of the opening size:

- The smaller 3mm opening lead to small changes in variance with gravity. The bottom half often displayed a variance as large or larger than the upper half.
- The larger 5mm opening lead to visible changes with gravity, mostly between 1g and 2g. The decrease of the AoR amplitude at higher gravity levels was visible in the change in variance.

Regime transitions:

- A transition from cyclical avalanching to continuous flow regimes occurs with increasing gravity, exhibited by all materials but particularly in the volcanic sand and the mixtures.
- The transition is mostly visible in the variance decrease at higher gravity, due to the reduced amplitude in the AoR. This results in smoother avalanching processes, making the avalanche front less visible.

6.3. Effects of Gravity & Discharge Flow on Angle of Repose

The results from Section 6.1 and Section 6.2 have shown so far that there is an increase in the average values of the angles of repose when increasing gravity. The amplitude of the variance varies with gravity and the cell opening, which indicates changes in avalanching regimes along the slope.

The measurements of the angle of repose (AoR) with a 3mm or 5mm opening differ a lot for the same gravity levels. This indicates that the change of opening affects the distribution of the angle of repose. It can be seen in all heartbeat graphs (Section 6.1) that the overall experiment time is shorter in the 5mm series than in the 3mm, and even more at higher gravity levels. A similar amount of material poured in a shorter amount of time means that the discharge flow should be increasing. The discharge flow was not yet analysed as a variable. This section analyses the results further, by adding the perspective of the particle discharge flow.

This section has the following structure. First, Section 6.3.1 examines the correlation between gravity and the discharge flow, based on the experimental data. Section 6.3.2 then explores the distinct effects of gravity and the discharge flow on the mean angle of repose. Finally, Section 6.3.3 introduces the standard deviation of the angle of repose as a parameter to analyse the influence of gravity and the discharge flow on its variance.

6.3.1. Relation Between Gravity & Discharge Flow

Theoretical Relationship Between Gravity and Discharge Flow

This section begins by exploring the theoretical relationship between gravity and the discharge flow. The discharge flow represents the quantity of particles poured into the cell over time and can be measured as the volume of particles added per second. One factor influencing discharge flow is the velocity at which particles fall through the opening. Gravity, as the primary force acting on the particles, determines their falling velocity. This velocity depends on gravity as described by Equation 6.5:

$$\Delta v = g_{eff} * \Delta t \quad (6.5)$$

where Δt is the time interval (in seconds) between a particle starting from rest and passing through the opening. Consequently, discharge flow is directly influenced by gravity.

The discharge flow also depends on the area of the opening, as a larger opening allows more particles to fall through simultaneously. The experiments used circular openings with diameters of 3mm and 5mm. The discharge flow, expressed in cm^3/s , is proportional to the product of the falling velocity and the opening area following Equation 6.6:

$$\text{Discharge Flow} \propto \text{Area} * \text{velocity} \quad (6.6)$$

Combining these relationships, the discharge flow can in theory be expressed as a function of gravity following Equation 6.7:

$$\text{Discharge Flow} \propto \text{Area} * g_{eff} \quad (6.7)$$

Empirical Relationship Between Gravity & Discharge Flow

Following the theoretical predictions, the relationship between gravity and the discharge flow is now explored empirically. The discharge flow measured in the experimental data is plotted against gravity in Figure 6.19, showcasing the observed relationship between the two variables.

As shown in Figure 6.19a, the discharge flow increases with gravity. Notably, the slope of this increasing trend is steeper for the larger 5mm opening compared to the 3mm opening, which highlights the dependency on the opening area. This behaviour is consistent across all materials, with the detailed plots provided in Section B.2.

The river sand, however, lacks data for the 3mm opening, preventing direct comparisons with the other materials (Figure 6.19b). Nevertheless, its 5mm series exhibits behaviour similar to the other materials, albeit with irregularities likely caused by inaccuracies in the measurements of the discharge flow.

Interestingly, the relationship between the discharge flow and gravity appears to deviate from the predicted linear behaviour. Instead, the data suggests a less-than-linear relationship, such as Equation 6.8:

$$\text{Discharge Flow} \propto \sqrt[3]{g_{eff}} \quad (6.8)$$

where the discharge flow depends on gravity raised to a power smaller than 1, alongside other contributing factors.

This correlation between gravity and the discharge flow must be considered when analysing the effects of gravity on avalanching mechanics. While the exact relationship is not determined here, confirming this correlation is sufficient for the analyses in the following sections.

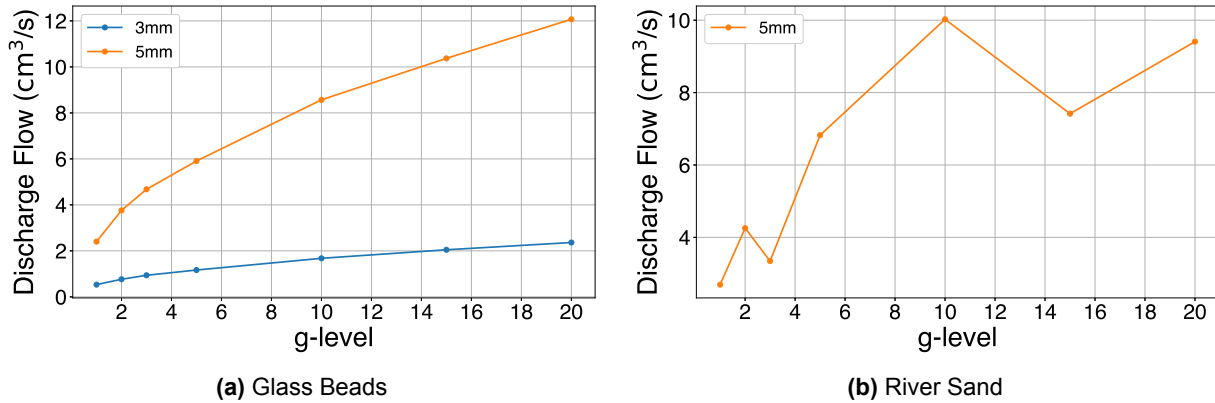


Figure 6.19: Discharge volume flow against gravity for varying materials

Summary of the Findings from the Relationship Between Gravity and Discharge Flow

Theoretical Insights:

- The discharge flow represents the input of material over time in the Hele-Shaw cell. It can be expressed as an increase in material volume over time (in cm³/s), which is proportional to the product of the particle falling velocity and the opening area.
- Gravity influences particle velocity, which can be expressed as:

$$\Delta v = g_{eff} * \Delta t \quad (6.9)$$

- Theoretically, the discharge flow is therefore expected to have a linear relationship with gravity:

$$Discharge\ Flow \propto Area * g_{eff} \quad (6.10)$$

Empirical Observations:

- The discharge flow increases with gravity, but the observed trend is less-than-linear, suggesting:

$$Discharge\ Flow \propto \sqrt{x} g_{eff} \quad (6.11)$$

- The larger openings (at 5mm) exhibit steeper increases in discharge flow compared to smaller openings (at 3mm), highlighting the dependence on opening area.
- Consistent behaviour is observed across all materials, except for river sand, which lacks 3mm data and shows minor irregularities in the 5mm series due to measurement inaccuracies.

Key Implications:

- The correlation between gravity and the discharge flow is sufficient for analysing avalanching mechanics, even without determining the exact functional relationship.
- The dependence of discharge flow on both gravity and opening area must be considered in subsequent analyses.

6.3.2. Effect of Gravity and Discharge Flow on Mean Angle of Repose

The heartbeat graphs (Section 6.1) detailed the angle of repose over time, while the heatmaps (Section 6.2) illustrated changes in its distribution with gravity, revealing an increase in the mean angle of repose (AoR) values with gravity. This section examines the general trends between the mean AoR, gravity, and discharge flow by plotting these variables for each material.

The focus here is on the effects of gravity and discharge flow on the entire AoR distribution, characterised by its mean and standard deviation. This section addresses the mean AoR, while Section 6.3.3 explores the standard deviation. The mean AoR is calculated as the average of the combined measurements from the three repeated experiments conducted under specific conditions (material, gravity, and cell opening). The focus is on the AoR of the overall slope, as it should reflect the combined behaviour of the upper and bottom halves. If this assumption is not true, the upper and bottom halves of the slope are analysed in the plots.

Effect of Gravity on the Mean Angle of Repose

For the angle of repose of glass beads, it can be seen in Figure 6.20 with a 3mm opening that when increasing gravity, the AoR rapidly increases from 1g to 2g, and then stabilises at higher gravity levels. The same behaviour is observed for the 5mm opening, however the whole plot is shifted upwards by 1.5° over all gravity levels.

Similarly, the volcanic sand in Figure 6.21 shows that the mean AoR rapidly increases with gravity when going from 1g to 5g, and it then plateaus for the higher gravity levels. The difference here is that when going from the 3mm to the 5mm opening, the mean AoR is only slightly affected, as it decreases by less than 0.25° on average.

Going from the 3mm to the 5mm opening induces a change in the mean AoR distribution of some materials like the glass beads (Figure 6.20) but not the volcanic sand (Figure 6.21). This change can be associated to the discharge flow which is higher with the 5mm opening at the same gravity levels.

The effect of **gravity** on the mean AoR is described by its rapid increase from 1g to about 5g followed by a plateau at higher gravity levels. This is observed across materials (see Section B.3).

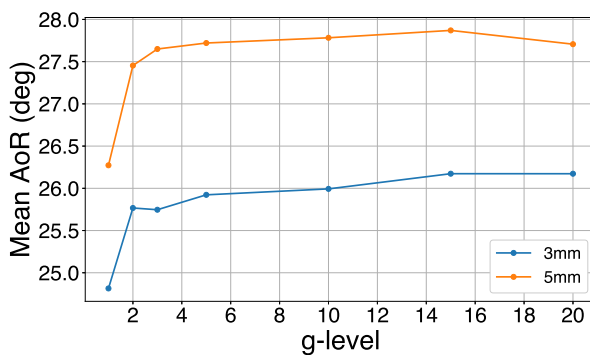


Figure 6.20: Mean AoR against gravity of glass beads

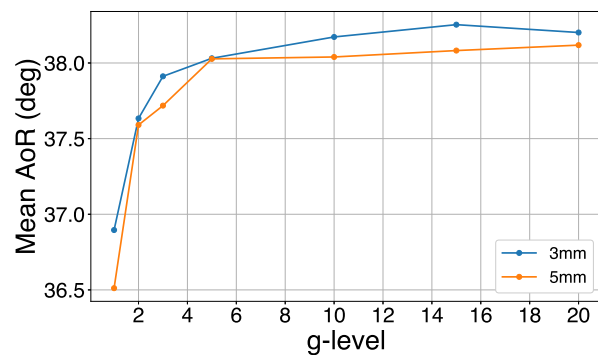


Figure 6.21: Mean AoR against gravity of volcanic sand

Effect of Discharge Flow on the Mean Angle of Repose

Plotting the mean AoR against the discharge flow for glass beads (Figure 6.22) makes an almost continuous transition from 3mm to 5mm. It has the steep increases where gravity goes from 1g to 2g, and then stabilises. Looking at the effect of the discharge flow on the mean AoR of volcanic sand in Figure 6.23, it can be seen that there is no continuity between the 3mm and 5mm series, despite the volume flow values being continuous from the end of the 3mm set to the beginning of the 5mm set.

This supports what was just observed in Figure 6.20 that changing the cell opening from 3mm to 5mm induces an increase in the mean AoR distribution. This is observed in materials like the glass beads and the glass-volcanic mixture. For the same gravity level, the mean AoR is significantly higher with the 5mm opening than with the 3mm one. This increase is therefore only dependent on the **discharge flow** which

increased with the cell opening. This is however not clearly observed for volcanic sand (Figure 6.21) and the river-volcanic mixture where only gravity affects the mean AoR.

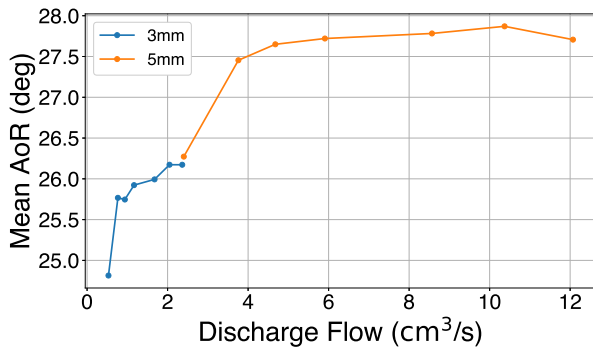


Figure 6.22: Mean AoR against discharge flow of glass beads

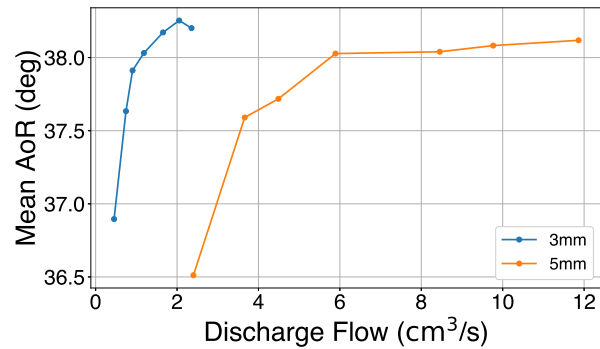
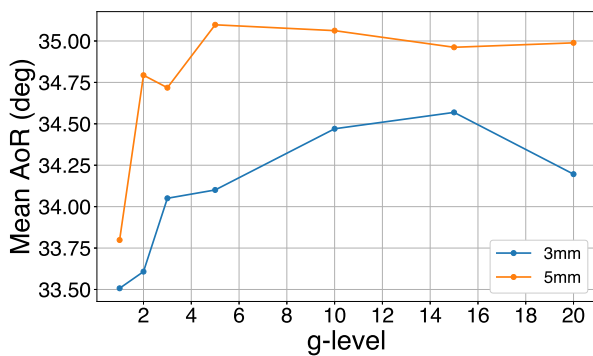


Figure 6.23: Mean AoR against discharge flow of volcanic sand

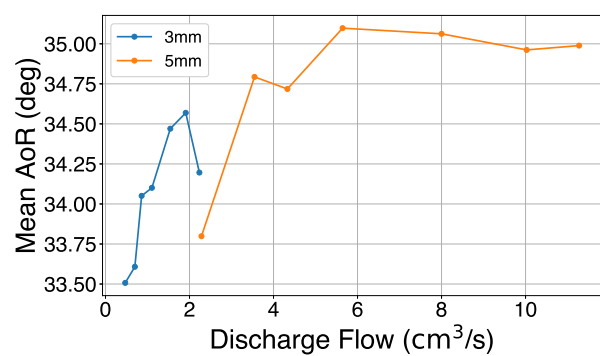
Effect of the Avalanching Regime Observed in Mixtures

The glass-volcanic and river-volcanic mixtures displayed behaviours with small differences compared to their pure species. The mean AoR of the **glass-volcanic mixture** is not only plotted for the overall slope (Figure 6.24), but also for the upper (Figure 6.25) and bottom halves (Figure 6.26) of the slope to better isolate observations.

The mean AoR for the overall slope against gravity (Figure 6.24a) increases rapidly in the lower gravity levels and then stabilises in the higher levels. Like for the glass beads (Figure 6.20), the plot is moved upwards in the 5mm series as it reaches higher values of angle of repose than in the 3mm series for the same gravity levels. The mean AoR against the discharge flow (Figure 6.24b) shows a relation that is somewhere between that of the volcanic sand (Figure 6.23) and of the glass beads (Figure 6.22), the two species composing the mixture. The mean AoR increases with the discharge flow, but it is not as continuous as for the glass beads. This shows that both gravity and the discharge flow have a strong influence on the overall slope. Looking at the overall slope does not show new observations. However, looking at the upper and bottom halves of the slope separately does reveal new observations.



(a) Mean AoR against gravity



(b) Mean AoR against discharge flow

Figure 6.24: Average overall angle of repose of the **glass-volcanic mixture** against gravity and the discharge volume flow, with varying cell opening.

The mixture displayed visible particle segregation in the experiments, the upper half therefore mostly consisted of volcanic sand and the bottom half of glass beads.

The mean AoR of the upper half does not vary much when varying gravity (Figure 6.25a), it seems to plateau in a range of less than 1° . Moving from the 3mm to the 5mm opening has an observable effect of

increasing all values by about 0.5° . It can be seen in Figure 6.25b that the AoR is mostly dependent on the discharge flow, as the plot is almost continuous, which is similar to the glass beads (Figure 6.22).

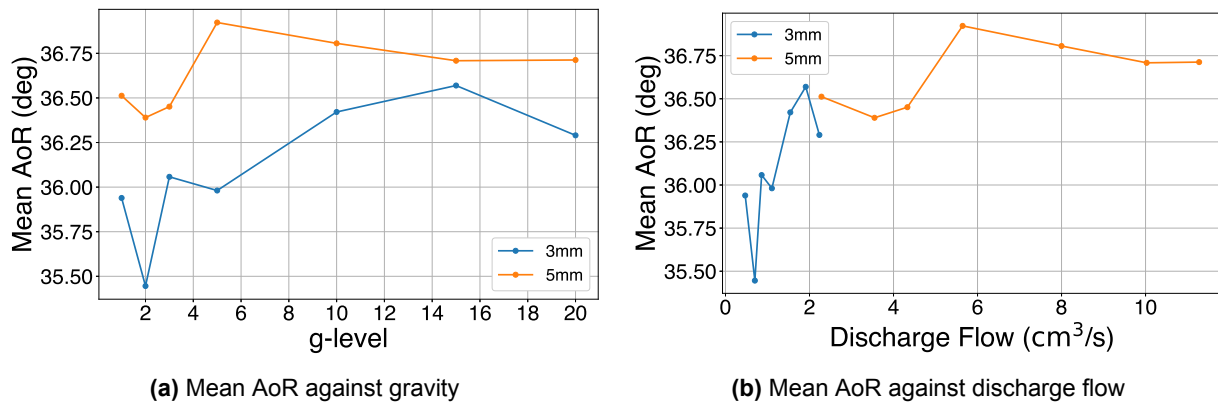


Figure 6.25: Average **upper** angle of repose of the **glass-volcanic mixture** against gravity and the discharge volume flow, with varying cell opening.

For the bottom half of the slope, the same relation between the mean AoR and gravity is observed (Figure 6.26a), and the effect of the discharge flow is strong as the curve moves upwards by 0.5° except at 1g where there is almost no effect. From the plot of the AoR against the discharge flow in Figure 6.26b, it can be seen that there is a stronger change in lower volume flows. It is discontinuous between the 3mm and 5mm openings, behaving like for the volcanic sand (Figure 6.23). However, a transition happens after $4\text{cm}^3/\text{s}$, where the AoR stabilises.

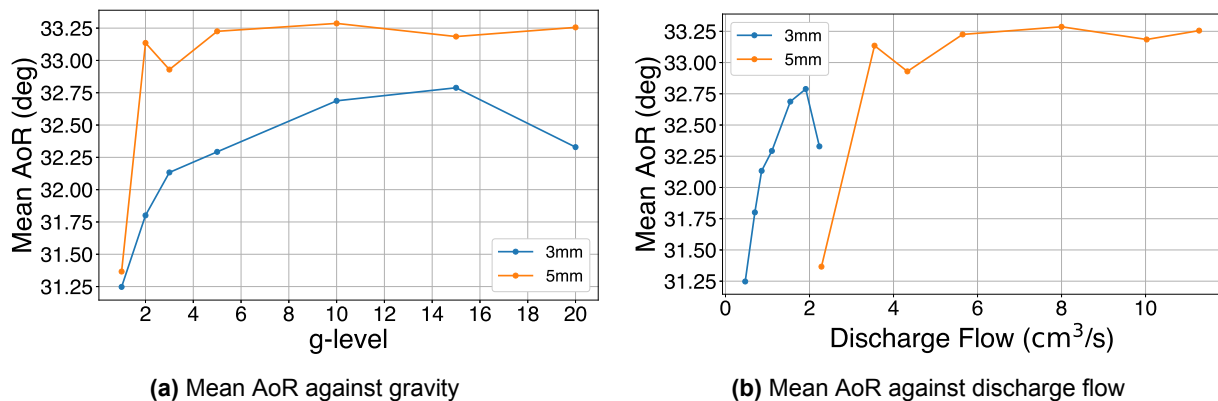


Figure 6.26: Average **bottom** angle of repose of the **glass-volcanic mixture** against gravity and the discharge volume flow, with varying cell opening.

The main observation from the glass-volcanic mixture is that the upper half made of volcanic sand behaves more like the pure glass species, and the bottom half behaves more like the volcanic species. It was observed in Figure 6.17b that with the 5mm opening, the upper half transitioned into a more fluid flow as it had a smaller variance in the higher gravity levels. The small variance was also observed for the pure species of glass beads (Figure 6.14b), which could indicate that they are in a similar avalanching regime. The behaviours observed in the plots of the mean AoR against the discharge flow could therefore be dictated by the **avalanching regime**, and not by the material specifically.

Then, the mean AoR of the **river-volcanic mixture** is plotted against gravity (Figure 6.27a) where a steep increase of the AoR can be observed from 1g to 5g, followed by a plateau in the higher gravity levels. While the 5mm mean AoR at 1g is lower than at 3mm, the 5mm values rapidly increase and are about 0.5° higher than for the 3mm series in the upper gravity levels, until they stabilise at a similar value.

The mean AoR against the discharge flow (Figure 6.27b) shows a pattern similar to that of the volcanic sand (Figure 6.23) at first sight, with the strong discontinuity from the end of the 3mm series and the beginning of the 5mm. However, the AoR values in the 5mm series reach higher values from 2g onwards than in the 3mm series, and then stabilise. A transition happens between 1g and 2g in the 5mm opening where gravity has the predominant effect on the mean AoR before the transition, after which the neither variable has the predominant effect. This contrasts with the volcanic sand where only gravity had an effect on the mean AoR.

Looking back at Figure 6.18b, it can be seen that at 1g, before the transition, the values have a wide variance. The variance drastically reduces and concentrates around a mean value at 2g and higher, which shows that the particles have transitioned into a different avalanching regime, with a more fluid flow.

The main observation from the river-volcanic mixture is that the avalanching regime transition happening with the 5mm opening after 1g stabilises the mean AoR at a constant value, unaffected by gravity and the discharge flow. Similar to the glass-volcanic mixture, this could indicate that the **avalanching regime** dictates whether gravity or the discharge flow have the predominant effect on the AoR.

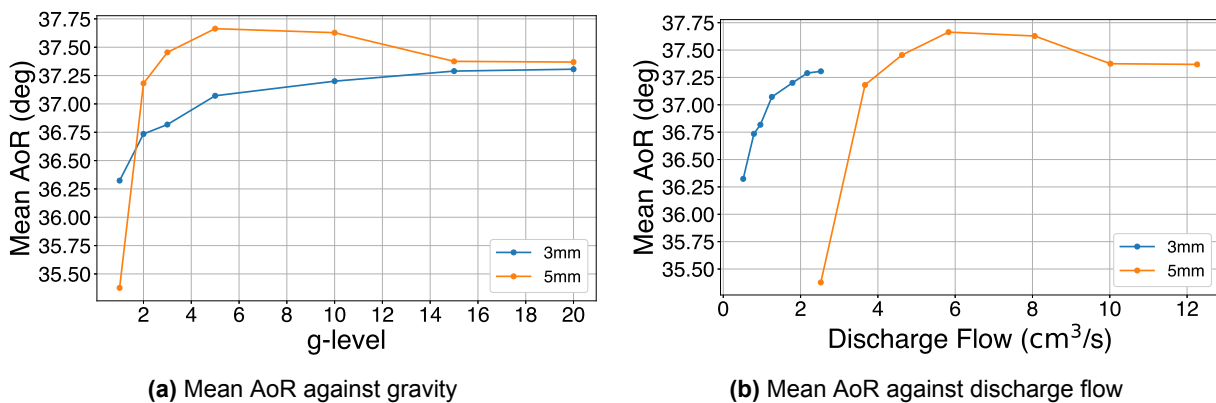


Figure 6.27: Average overall angle of repose of the **river-volcanic mixture** against gravity and the discharge volume flow, with varying cell opening.

Summary of the Findings on the Effects of Gravity and Discharge Flow on Mean Angle of Repose

Effect of gravity:

- An increase of gravity in the lower levels from 1g to 5g (depending on the material) increases the mean AoR.
- At higher gravity levels 5g to 20g, the mean AoR stabilises and gravity has little to no effect.

Effect of the discharge flow:

- Increasing the discharge flow by increasing the opening from 3mm to 5mm has a predominant increasing effect on the mean AoR for materials like the glass beads and the glass-volcanic mixture.
- The discharge flow has little to no effect on the mean AoR of materials like the volcanic sand and the river-volcanic mixture.

Effect of avalanching regimes

- A regime transition is observed in the higher discharge flow values with the 5mm opening and gravity level of 2g and higher for materials like the river-volcanic mixture, and the glass-volcanic mixture.
- In more fluid regimes, gravity and the discharge flow lose their affect on the mean AoR, which stabilises at a constant value.
- The mixtures displayed that they do not necessarily behave like their original pure species. The effects of gravity and the discharge flow on the mean AoR are dictated by the type of avalanching regime.

6.3.3. Effect of Gravity & Discharge Flow on the Standard Deviation of the Angle of Repose

The variance of the angle of repose (AoR) around its mean has been observed to change with the varying environmental conditions of the experiment. It was so far referenced qualitatively but will be analysed quantitatively in this section, using the standard deviation (σ). Before calculating the standard deviation of the angle of repose of a certain experiment, its distribution over time (the heartbeat graph) is de-trended.

The heartbeat plots (Section 6.1) show that the AoR often oscillates around its mean value, but in several experiments the value of the mean also changed over time as the pile was forming. This is a trend in the heartbeat plot, which would induce a bias in the standard deviation if not accounted for. De-trending the signal means that the trend is quantified and subtracted from the signal. Here, a linear fit was used as a trend as it seemed qualitatively good enough for the observed trends in the heartbeat graphs. Quantifying the trend with a polynomial fit, or a moving average is left as a recommendation for future studies. After de-trending, the standard deviation is computed and expressed in degrees, which allows to quantify on average by how much the angle of repose varies around its mean value.

This section analyses the standard deviation of the AoR (σ_{AoR}) by plotting it against gravity and the discharge flow to characterize their individual effects. Each scatter plot point represents the standard deviation of the overall slope AoR for a single experiment after de-trending, plotted against the corresponding gravity level or discharge flow. Points are colour-coded by cell opening, and since each experiment was repeated three times, three points exist for each experimental condition.

The standard deviation was calculated for individual experiments rather than for combined measurements of repeated experiments, as done in Section 6.3.2. This approach avoids the averaging effect, which could reduce accuracy, and provides a denser scatter, better illustrating the distribution of the standard deviation.

Effect of Gravity on the Standard Deviation of the Angle of Repose

From the plots for the glass beads in Figure 6.28, it can be seen that the standard deviation does not vary with increasing gravity. The values are lower for the 5mm opening than for the 3mm, highlighting a dependency on the discharge flow. The glass-volcanic mixture displays a similar behaviour (Section B.4).

For the volcanic sand (Figure 6.29), the standard deviation displays a rapid decrease from 1g to 2g, followed by a plateau. The direct effect of passing from the 3mm set to the 5mm set is that the plot is shifted down by 0.4° , however the distribution holds the same shape. The shape of the distribution can be attributed to gravity, while the downward shift of the values can be attributed to the increase of discharge flow. This is also observed for the river sand and river-volcanic mixture (Section B.4).

Therefore, **gravity** has a limited effect on the standard deviation across all materials, with only a notable decrease observed from 1g to 2g for certain materials. Beyond this, gravity shows no significant impact.

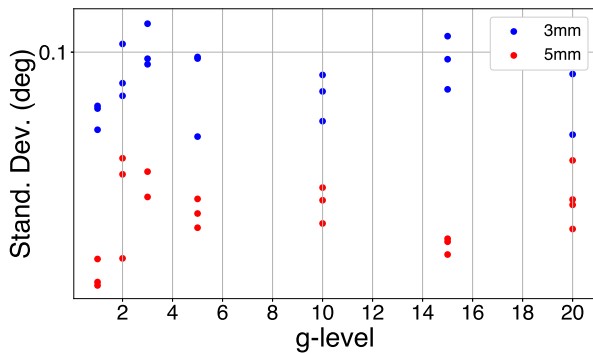


Figure 6.28: Standard deviation against gravity of glass beads

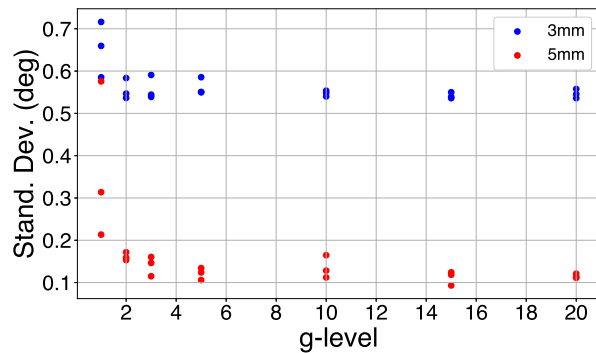


Figure 6.29: Standard deviation against gravity of volcanic sand

Effect of Discharge Flow on the Standard Deviation of the Angle of Repose

To compare the effect of the discharge flow across materials, the standard deviation of the angle of repose is plotted for all materials into a combined comparative overview in Figure 6.30.

In contrast to gravity, the **discharge flow** strongly influences the standard deviation. As the discharge flow increases, the standard deviation decreases sharply and stabilises at lower values. This relationship often follows a stepwise pattern, with periods of steep decline followed by plateaus, potentially indicating transitions in flow regimes. These stepwise trends were observed in the volcanic sand, the river-volcanic mixture, and the bottom half of the slope in the glass-volcanic mixture.

The volcanic sand and the river-volcanic mixture exhibit similar distributions, with the highest standard deviation values around 0.55° . The glass beads have the lowest standard deviation values, consistently below 0.1° . Overall, the standard deviation shows a sharp decrease at low discharge flow rates and stabilises around 0.1° as the discharge flow increases. This displays the effect of **material properties** on the standard deviation. At low discharge flow rates, materials with more irregular particle shapes (e.g., volcanic sand, river-volcanic mixture) tend to have higher standard deviation values compared to rounder materials (e.g., glass beads, glass-volcanic mixture), which exhibit the lowest values. However, as the discharge flow increases, all standard deviation values converge toward a similar constant value.

The opening sizes of 3mm and 5mm are not differentiated in Figure 6.30. Plots of the standard deviation against the discharge flow with identified opening size can be found in Section B.4. In Figure 6.30, all points from the 5mm series yielded discharge flows above $2\text{cm}^3/\text{s}$. In the plot, this includes most of the points distributed nearly vertically and the plateau at the higher discharge flows. The vertical distribution in the range between $2\text{cm}^3/\text{s}$ to $3\text{cm}^3/\text{s}$ is where most materials exhibited a noticeable change of flowing regime.

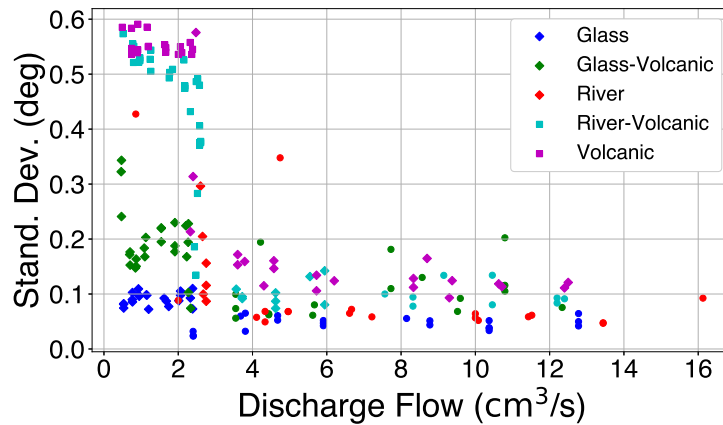


Figure 6.30: Standard deviation in the angle of repose against the discharge flow. Plotted for the overall slope, for all materials and all openings.

When comparing the standard deviation distributions for the upper and bottom halves of the slope, noticeable differences emerge.

On the upper half (Figure 6.31a), the distribution resembles that of the overall slope (Figure 6.30), but the plateau stabilises at a higher value of approximately 0.2° instead of 0.1° . For volcanic sand and the river-volcanic mixture, the standard deviation decreases significantly with increasing discharge flow, dropping from 0.7° to 0.2° . This steep decline suggests a transition in the flow regime on the upper halves of their slopes. In contrast, the standard deviation for other materials decreases only slightly, by about 0.1° , indicating a weaker effect.

On the bottom half (Figure 6.31b), the standard deviation values span a broader range. The glass beads exhibit a more pronounced decrease in standard deviation compared to the upper half, declining from 0.25° at low discharge flow to 0.1° at higher discharge flow. In contrast, the decrease in standard deviation for volcanic sand and the river-volcanic mixture is less significant than that observed on the upper half, indicating a weaker regime transition for these materials.

The differences between the two slope halves highlight key takeaways. On the upper half, the lower standard deviation values indicate that higher discharge flows induce a transition to a more fluid regime. This behaviour may result from the upper half's proximity to the constant particle pouring source, which likely favours more continuous flow conditions. On the bottom half, the higher standard deviation values across the discharge flow range suggest that the bottom half experiences more cyclic flow, influenced by the presence of avalanche fronts.

The differences between the upper and bottom halves imply that transitions in avalanching regimes do not occur instantaneously across the entire slope. Instead, the maximum height of the avalanche front and kink may initially reach most of the slope length. But gradually, this maximum height propagates downward as the discharge flow increases. Additionally, the material properties, particularly particle shape, likely influence the discharge flow rate required to fully transition the avalanching regime across the slope.

The avalanching regime appears to be an influential parameter on the angle of repose and its effect are not yet quantified. This is done in the following Section 6.4.

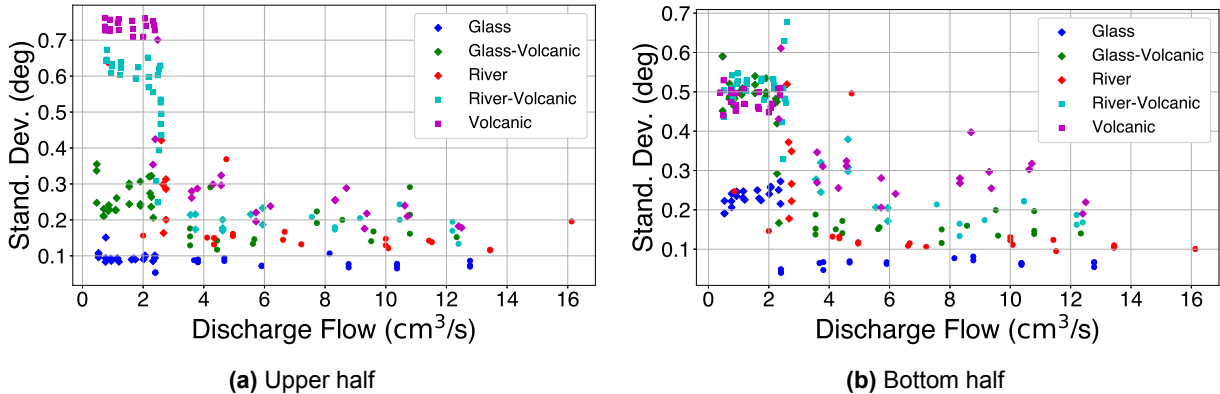


Figure 6.31: Scatter plot of the standard deviation in the angle of repose against the discharge flow. This is for the overall slope, for all materials and all openings.

Summary of the Findings on the Effects of Gravity and Discharge Flow on the Standard Deviation of the Angle of Repose

Effect of Gravity:

- Gravity has a limited effect on the standard deviation of the angle of repose.
- A steep decrease in standard deviation occurs when gravity increases from $1g$ to $2g$ for most materials, except glass beads and the upper slope half of the glass-volcanic mixture.
- Beyond $2g$, gravity shows no significant effect across all materials.

Effect of the Discharge Flow:

- The discharge flow has a strong influence on the standard deviation.
- The standard deviation decreases sharply as the discharge flow increases and stabilises at lower values.
- This relationship often follows a stepwise pattern (declines followed by plateaus), suggesting a transition point in flow regimes. These are mostly observed in materials like volcanic sand, the river-volcanic mixture, and the bottom half of the glass-volcanic mixture.
- A noticeable regime transition typically occurs in the range of $2\text{--}3\text{cm}^3/\text{s}$.

Material-Specific Behaviours:

- Irregularly shaped particles (e.g., volcanic sand, river-volcanic mixture) exhibit higher standard deviation values at low discharge flow rates.
- Rounder particles (e.g., glass beads, glass-volcanic mixture) display the lowest standard deviation values at all discharge flow rates.
- At high discharge flow rates, all materials exhibit convergence toward similar, stable standard deviation values.

Observations on Each Slope Half:

- On the upper half, the lower standard deviation values indicate more fluid flow regimes at higher discharge flows. The proximity to the particle source likely favours more continuous flow conditions, reducing variability.
- On the bottom half, the higher standard deviation values suggest a more cyclic flow due to the presence of avalanche fronts. The variability decreases less significantly compared to the upper half.
- The differences between the two halves indicate that the avalanching regime transitions are not instantaneous across the entire slope. Avalanche fronts and kinks are initially visible on the entire slope length, but the maximum height reached propagates downwards as discharge flow increases.
- Material properties, especially particle shape, may influence the discharge flow rates required for regime transitions.

6.4. Effects of Avalanching Regimes

The avalanching regimes introduced in Chapter 2 affect the mechanics of the slope formation. The measurements of the angle of repose is analysed through the lens of the avalanching regimes in this section to infer on its influence.

This is done through the following section structure. First, Section 6.4.1 introduces the definitions of the different avalanching regimes observed in the experiments. Then, Section 6.4.2 quantifies the definitions of avalanching regimes by associating to the definitions a value of the standard deviation of the angle of repose, which were explored in Section 6.3.3. Finally, Section 6.4.3 re-analyses the effects of gravity and the discharge flow on the mean angle of repose (studied in Section 6.3.2) however from the perspective of the avalanching regimes this time.

6.4.1. Definition of Avalanching Regimes

The concept of avalanching regimes is well defined by Brucks et al. (2007), who identified three primary regimes: discrete, rolling, and cascading, with transition phases in between. These regimes were established in the context of experiments performed in a rotating cylinder. In this setup, the material at the bottom of the cylinder is continually cycled back to the top of the pile. In the discrete regime, which occurs at low angular velocities, avalanches are discrete events in time. The slope becomes unstable when it reaches a critical steep angle, initiating an avalanche. The avalanche stops when the material stabilises at a lower angle. At higher angular velocities, the rolling regime appears, characterized by a continuous avalanche and a slope with a quasi-linear, constant angle. Finally, at the highest angular velocities, the cascading regime appears. This regime features continuous avalanches, but the slope takes on a strongly non-linear, S-shaped profile. In the context of the Hele-Shaw cell, the material discharged from the pile is analogous to the material at the bottom of the rotating cylinder being returned to the top. Despite the differing experimental setups, the same principles of avalanching behaviour can be applied. Brucks et al. (2007) found that the Froude number, a dimensionless ratio of inertial to gravitational forces, determines which regime applies to the material. This insight provides a unifying framework for understanding avalanching behaviour across experimental setups.

Similar to the work of Brucks et al. (2007), various avalanching regimes were observed in the experiments conducted for this research. The definitions used here are chosen to align with those of Brucks *et al.* as far as possible. The **Discrete** regime was observed and is best described by the work of Makse et al. (1998). In this regime, particles pile up at the top of the slope until it becomes too steep and unstable. The slope then avalanches with a distinct front, building a small pile at the bottom until the kink moves up the slope, nearly reaching the top. This behaviour is illustrated in Figure 6.32. The avalanche front is easy to identify in a moving video. The front is however difficult to observe in still images, which are still the best way to show the experiment in this report.

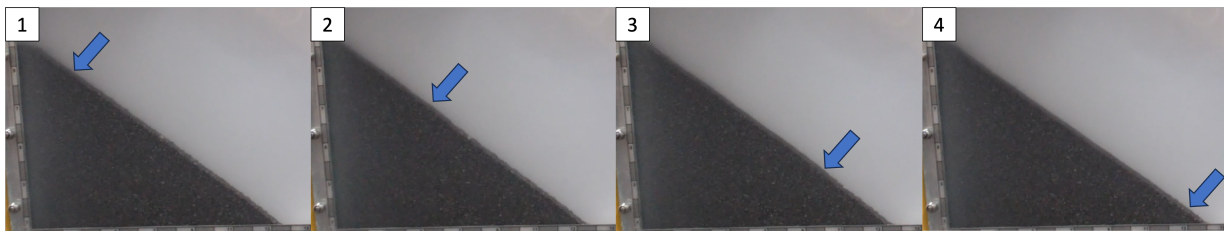


Figure 6.32: Images of the discrete avalanching regime. The avalanching layer is thin compared to the pile height. The blue arrow points at the avalanche front which moves from its highest point (in the first image) to the bottom of the pile (in the last image). Each snapshot is taken less than a second apart.

The **Rolling** regime was observed too, where there is no avalanche front or kink formation. There is only a constant flow of material along the slope, as can be seen in Figure 6.33.

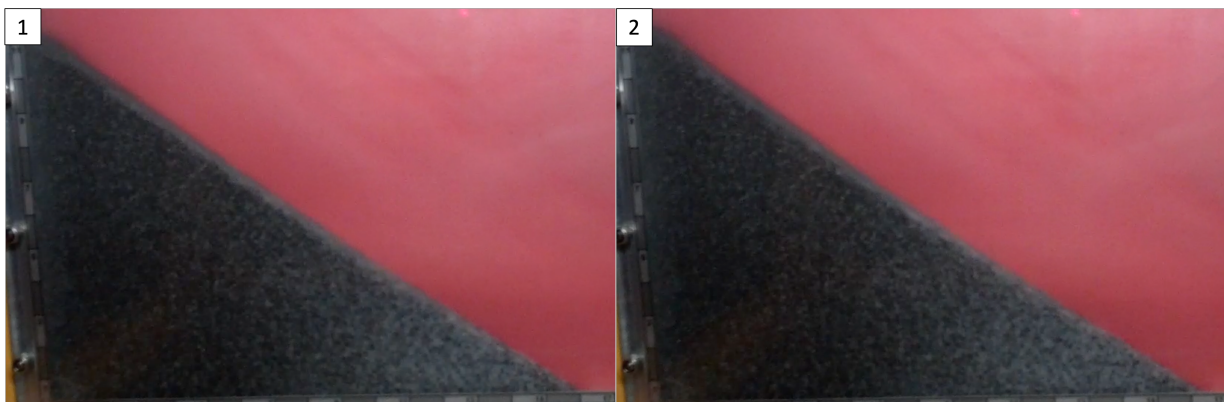


Figure 6.33: Images of the rolling avalanching regime. The avalanching layer is a continuous flow of particles from the top to the bottom of the pile. Each snapshot is taken less than a second apart.

A **Transition** regime was observed as well in between the discrete and rolling regimes. Brucks et al. (2007) find in their experiments that this state tends to alternate between both other regimes. However, the transition regime behaves differently in the Hele-Shaw cell and the definition used in this research slightly differs from that of Brucks *et al.*

In this transition regime, the avalanche front and kink are less clearly visible than for the discrete regime, and do not move as much up the slope as before. The upper section of the slope would be in rolling regime and the bottom part in discrete regime. This can be seen in Figure 6.34. The higher the discharge flow, the less high the kink reaches up. The transition regime means that the upper and bottom halves might each be in a different regime.

Between the rolling and cascading regime, Brucks et al. (2007) see no transition into cascading. In this research, no cascading regime (as defined by Brucks *et al.*) was observed in the experiments .

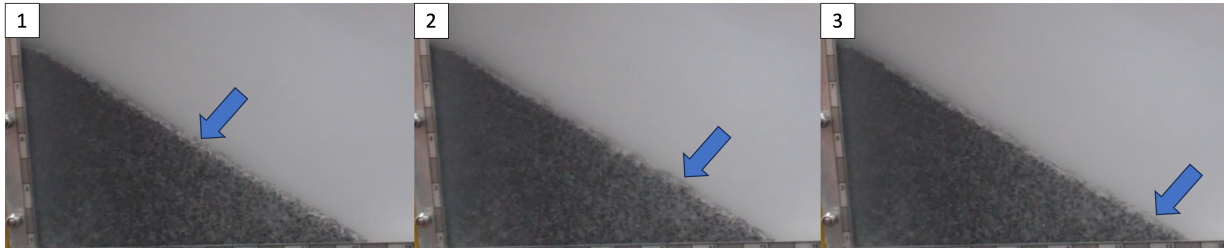


Figure 6.34: Images of the transition avalanching regime. The upper half of the slope has a continuous flow of particles. The blue arrow points at the avalanche front which moves from its highest point at the middle of the slope (in the first image) to the bottom of the slope (in the last image). Each snapshot is taken less than a second apart.

After defining the avalanching regimes, each experimental video was reviewed to determine the regime exhibited during each experiment. An overview of the avalanching regime for each experiment, along with its parametric conditions, is presented in Table 6.1. This information is then linked to the measurement data in Section 6.4.2 and Section 6.4.3 to analyse its impact on avalanche mechanics.

Table 6.1: Overview of the avalanching regimes observed in the experimental videos for all parametric conditions.

Experiment	g-level	Cell opening (mm)	Material				
			Glass Beads	River Sand	Volcanic Sand	Glass-Volcanic	River-Volcanic
Centrifuge	1	3	Transition	n.a.	Discrete	Transition	Discrete
	2		Transition	n.a.	Discrete	Transition	Discrete
	3		Transition	n.a.	Discrete	Transition	Discrete
	5		Transition	n.a.	Discrete	Transition	Discrete
	10		Transition	n.a.	Discrete	Transition	Discrete
	15		Transition	n.a.	Discrete	Transition	Discrete
	20		Transition	n.a.	Discrete	Transition	Discrete
	1	5	Rolling	Transition	Transition	Transition	Discrete
	2		Rolling	Rolling	Transition	Rolling	Transition
	3		Rolling	Rolling	Transition	Rolling	Transition
	5		Rolling	Rolling	Transition	Rolling	Transition
	10		Rolling	Rolling	Transition	Rolling	Rolling
	15		Rolling	Rolling	Transition	Rolling	Rolling
	20		Rolling	Rolling	Transition	Rolling	Rolling

6.4.2. Standard Deviation of Angle of Repose Against Discharge Flow per Avalanche Regimes

In Section 6.3.3, the standard deviation of the angle of repose was plotted against the discharge flow (Figure 6.30). This graph is revisited in this section in Figure 6.35, now including the identified avalanche regimes.

Note that the 3mm and 5mm openings are omitted from Figure 6.35 and subsequent plots. Instead, the avalanching regimes are highlighted. Although the cell opening is a variable in the experiments, it primarily influences the discharge flow and avalanching regimes, which in turn affect the angle of repose. The following analyses focus on characterizing the effects of discharge flow and avalanching regimes separately, making cell opening irrelevant to the remaining graphs.

In Figure 6.35, experiments in the discrete regime happen at low discharge flow and have a high standard deviation of about 0.55° . This concerns the volcanic sand and the river-volcanic mixture.

The transition zone is identified at low discharge flow values, with an average standard deviation value of 0.15° . Materials with a relatively rounder shape like the glass, river sand and glass-volcanic mixture transition before a discharge flow of $3\text{cm}^3/\text{s}$, whereas the volcanic sand and river-volcanic mixture of more irregular shape transition after the discharge flow rate of $3\text{cm}^3/\text{s}$.

The rolling regime is observed at discharge flow rates above $3\text{cm}^3/\text{s}$, with an average standard deviation of 0.1° or less. At sufficiently high discharge flow rates, this regime applies to all materials except volcanic sand.

These observations suggest that the standard deviation of the angle of repose can serve as a proxy for identifying the avalanching regime, as the avalanche location on the graph reflects the regime. However, identifying regimes within the transition phase remains challenging, introducing some uncertainty. Despite this limitation, the method provides a sufficiently reliable approximation for the purposes of this research.

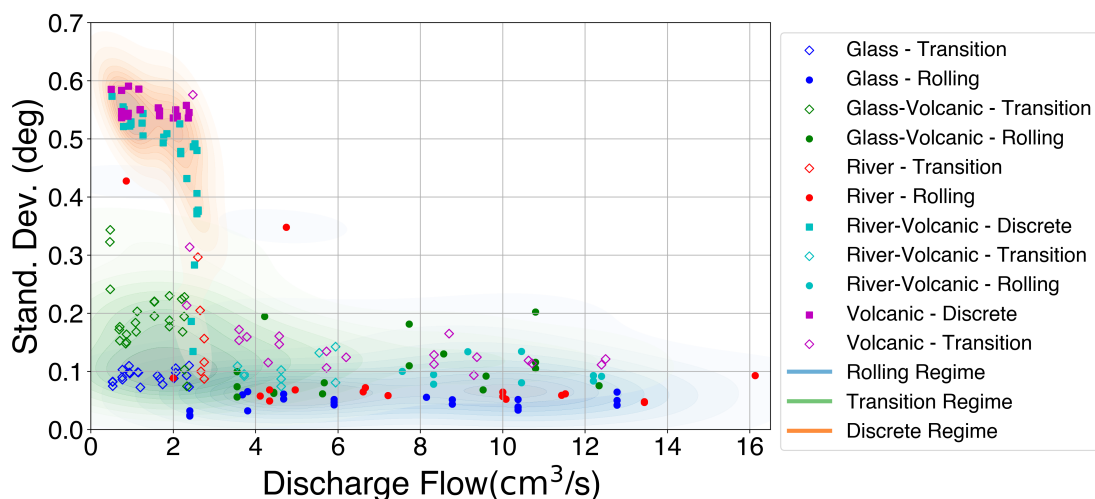


Figure 6.35: Scatter plot of the standard deviation in the angle of repose against the discharge flow. Avalanche regimes are identified. This is for the overall slope, for all materials and all openings.

6.4.3. Mean Angle of Repose Against Gravity & Discharge Flow per Avalanche Regime

In Section 6.3.2, the mean value of the angle of repose was plotted for each material against gravity and the discharge flow. These graphs are revisited in this section in with the addition of the identified avalanche regimes. A selection of graphs are joined to the discussion of this section, and all other graphs can be seen in Section B.5.

Effect of Gravity on the Mean Angle of Repose

Plotting the mean angle of repose against gravity with the highlighted avalanching regimes leads to similar conclusions on the effect of **gravity**.

In the discrete and transition regimes, increasing gravity from 1g to about 5g (depending on the material) leads to increase in the mean AoR. It then stabilises at higher gravity levels. In the rolling regime however, gravity has no visible effect on the mean AoR. This can be seen for glass beads in Figure 6.36 and volcanic sand in Figure 6.37.

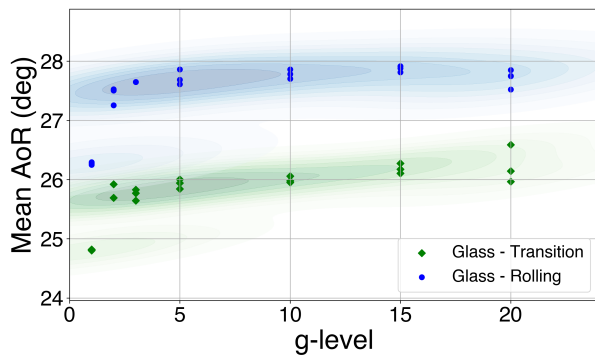


Figure 6.36: Mean AoR against gravity of **glass beads**

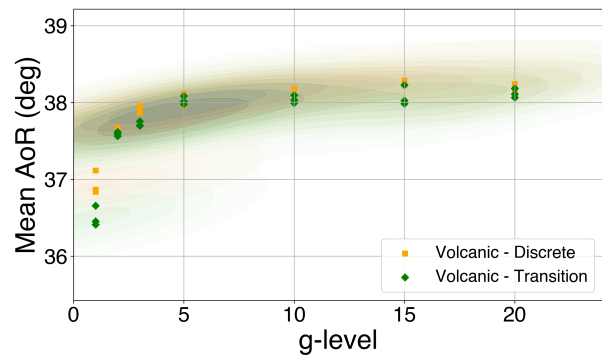


Figure 6.37: Mean AoR against gravity of **volcanic sand**

Effect of Discharge Flow on the Mean Angle of Repose

When plotting the mean angle of repose against the **discharge flow** with the highlighted avalanching regimes, the main observations of the effect of the discharge flow still hold. It can be seen in Figure 6.39 that in discrete and transition regimes, the higher discharge flows lead to a higher mean AoR. In the rolling regime however (Figure 6.38), the discharge flow has no significant effect on the mean AoR.

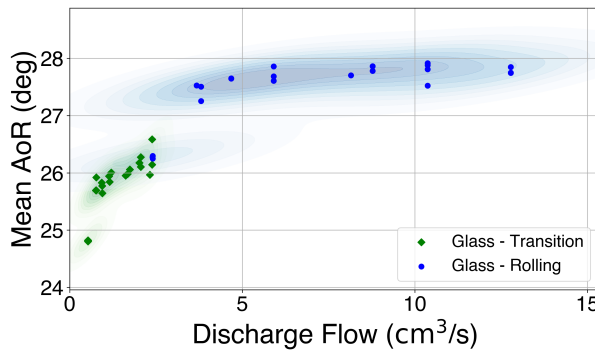


Figure 6.38: Mean AoR against discharge flow of **glass beads**

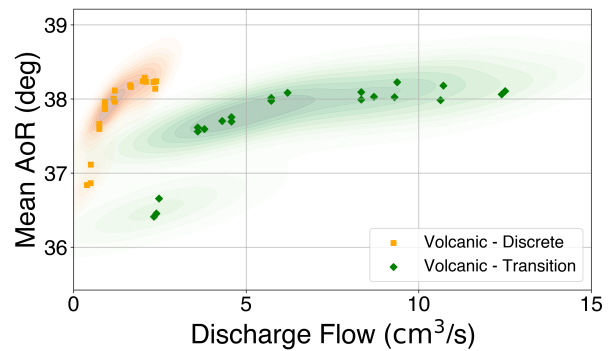


Figure 6.39: Mean AoR against discharge flow of **volcanic sand**

Effect of Avalanching Regimes on the Mean Angle of Repose

Increasing the discharge flow induces a change in the avalanching regime from discrete, to transition, to rolling (Figure 6.40b). The change from the transition regime to the rolling regime often leads to an increase in the mean AoR (Figure 6.39), and both gravity and the discharge flow lost their effect on the AoR. The **avalanching regime** does not appear to have a direct effect on the value of the AoR itself, but rather on the strength of the effect of gravity and the discharge flow on the AoR.

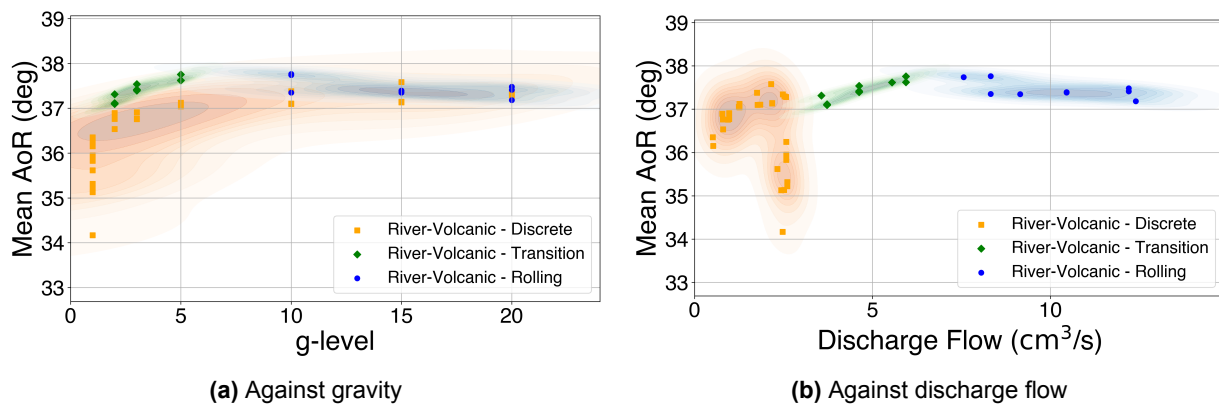


Figure 6.40: Average overall angle of repose of the **river-volcanic mixture** against gravity and the discharge volume flow, with varying avalanching regimes.

Summary of the Findings on the Effects of the Avalanching Regimes on the Mean Angle of Repose

Effect of gravity:

- In the discrete and transition regimes, increasing gravity in the lower levels from 1g to 5g (depending on the material) raises the mean AoR.
- At higher gravity levels 5g to 20g, the mean AoR stabilises and gravity has little to no effect.
- In the rolling regime, gravity has no effect on the mean AoR.

Effect of the discharge flow:

- Increasing the discharge flow induces a change in the avalanching regime from discrete, to transition, to rolling.
- In the discrete and transition regimes, a higher discharge flow increases the mean AoR for most materials, except volcanic sand and the river-volcanic mixture, where it has little to no effect.
- In the rolling regime, the discharge flow has no effect on the mean AoR.

Effect of avalanching regimes:

- The type of regime does not directly affect the mean AoR but influences the strength of the relationships between gravity, discharge flow, and the mean AoR.
- In the rolling regime, neither gravity nor discharge flow affects the mean AoR, which stabilises at a material-dependent value.

6.5. Effects on Static & Dynamic Angles of Repose

The static and dynamic angles of repose (AoR) are the subject of one of the research questions. They were introduced in Chapter 2 as other studies focused on these two angles to describe avalanches.

This section analyses the effects of the experimental variables on the static and dynamic angles of repose. To this end, Section 6.5.1 first defines the static and dynamic angles of repose in the context of the experiments performed in this research. Then, a method to measure the static and dynamic AoR is also presented in Section 6.5.1. Finally, Section 6.5.2 analyses the effects of gravity, discharge flow and avalanching regimes on the mean values of the static and dynamic AoR, following the approach used in the previous Section 6.4.3.

6.5.1. Defining and Measuring Static & Dynamic Angles of Repose

This section first provides definitions of the static and dynamic AoR in the context of this research. It then details how these angles were measured in the experimental data.

Definition of Static & Dynamic Angles of Repose

The definitions used for the static and dynamic AoR in this research are designed to make the results of the experiments comparable to other studies in the literature that specifically examined static and dynamic angles of repose, such as Kleinhans et al. (2011).

The **Static** angle of repose is defined by Kleinhans et al. (2011) as the steepest slope angle before an avalanche. It is therefore measured in this research as the maximum peak AoR value in the avalanching cycles. The static AoR is measured on the upper half of the slope, where avalanches originate, to provide higher and more accurate values than if measured over the entire slope. This definition applies to the discrete and transition regimes, where cycles are visible.

The **Dynamic** angle of repose is defined by Kleinhans et al. (2011) as the lowest slope angle after an avalanche at which the slope stabilises. It is therefore measured in this research as the minimum peak AoR value in the avalanching cycles. The dynamic AoR is measured on the bottom half of the slope, where particles stabilize after avalanching, yielding lower and more accurate values than measurements over the entire slope. This definition applies to the discrete and transition regimes.

In the rolling regime, distinct avalanching cycles are not observed. Therefore, the static and dynamic angles of repose are approximated as the average AoR values measured on the upper and bottom halves of the slope, respectively.

Method for Measuring Static & Dynamic Angles of Repose

The method used to detect the peak values in the measurements is two-fold. First, a rolling mean was used to smoothen the plot. Then, a prominence based algorithm¹ detects all local peaks and only retains the true peaks from local noise, based on the distance between the peaks and a given threshold.

Figure 6.41 illustrates a heartbeat graph from an experiment in the discrete regime. The peaks in the cycles of the upper half of the slope are detected and used to measure the static AoR. The static AoR for the experiment is calculated as the mean of these detected values.

Similarly, peaks in the cycles of the bottom half of the slope are detected and used to measure the dynamic AoR. The dynamic AoR for the experiment is computed as the mean of these detected values.

It can be observed that these peaks do not occur simultaneously with those in the upper half. The delay reflects the time required for the avalanche front to travel from the top to the bottom of the slope.

In contrast, Figure 6.42 shows a heartbeat graph from an experiment in the rolling regime. Here, variations in AoR for the upper and bottom halves are minimal, remaining within a range of 0.2° . Peaks are too small to be identified as true maxima or minima, and the observed fluctuations are likely due to measurement noise. In this regime, the static and dynamic AoR values are measured as the average AoR values for the upper and bottom halves of the slope, respectively.

¹Peak prominence in Python (visited on 27/11/24) https://docs.scipy.org/doc/scipy/reference/generated/scipy.signal.peak_prominences.html

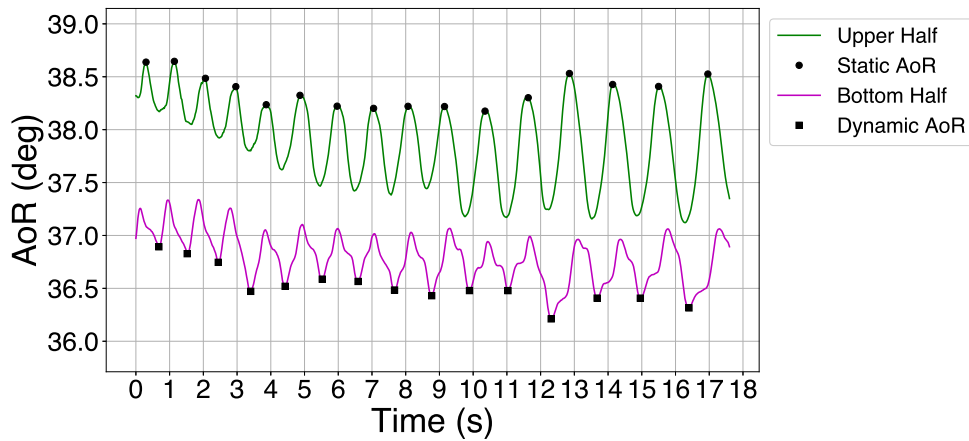


Figure 6.41: Example of detected peak values of static and dynamic AoR in a discrete regime

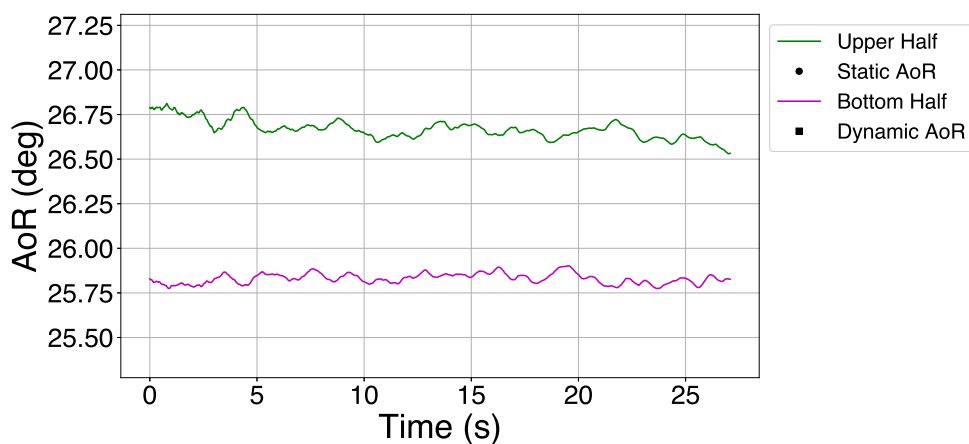


Figure 6.42: Example non-detected peak values of static and dynamic AoR in a rolling regime

6.5.2. Effects of Gravity, Discharge Flow & Avalanching Regime on Static & Dynamic Angles of Repose

Looking at the static and dynamic angles of repose with the highlighted avalanching regimes allows to see if their behaviour differ from that of the average AoR. As the static AoR is measured on the upper half of the slope and the dynamic AoR is measured on the bottom half, plotting both in the same graph will allow to observe differences between both halves.

The plots in this section follow a similar format to those in Section 6.4.3, showing the mean AoR values against gravity and discharge flow. For comparison, both the mean static AoR and mean dynamic AoR are included in the same graph. The static AoR is represented by solid dots and solid lines, while the dynamic AoR is shown with hollow dots and dotted lines. As in Section 6.4.3, the avalanching regimes are colour-coded: orange for the discrete regime, green for the transition regime, and blue for the rolling regime.

General Effects of Gravity, Discharge Flow and Avalanching Regime

Looking at the static and dynamic angles of repose does not reveal any new behaviour related to gravity, the discharge flow or and avalanching regime. The same observations as for the previous sections still hold.

In the discrete and transition regimes, increasing gravity in the lower levels from 1g to 5g (depending on the material) raises the mean static and dynamic AoR. At higher gravity levels 5g to 20g, the mean AoR

stabilises and gravity has little to no effect. In the rolling regime, gravity has no effect on the mean static and dynamic AoR.

Increasing the discharge flow induces a change in the avalanching regime from discrete, to transition, to rolling. In the discrete and transition regimes, a higher discharge flow slightly increases the mean static and dynamic AoR. In the rolling regime, the discharge flow has no effect on the mean static and dynamic AoR.

The type of avalanching regime does not directly affect the mean static and dynamic AoR but appears to influence the strength of the relationships between gravity, discharge flow, and the mean AoR. In the rolling regime, neither gravity nor discharge flow affects the mean static and dynamic AoR, which stabilizes at a material-dependent value.

Differences Between the Static and Dynamic Angles of Repose

Looking at the mean static and dynamic AoR does reveal differences in the state of each slope half. A selection of graphs are joined to the discussion of this section, and all other graphs can be seen in Section B.6.

For the glass beads, the static AoR sharply increases with gravity (Figure 6.43a) from 1g to 3g and stabilised at higher gravity levels. The dynamic AoR is constant over the whole gravity range and only slightly increases with the discharge flow (Figure 6.43b). The same behaviour is observed in both transition and rolling regimes, although the rolling regimes yields higher values of the AoR. The change in regime increases all values by 2° .

The differences between the static and dynamic plots show that both slope halves are not in the same state of transition regime, where the bottom half is closer to a rolling regime than the upper half.

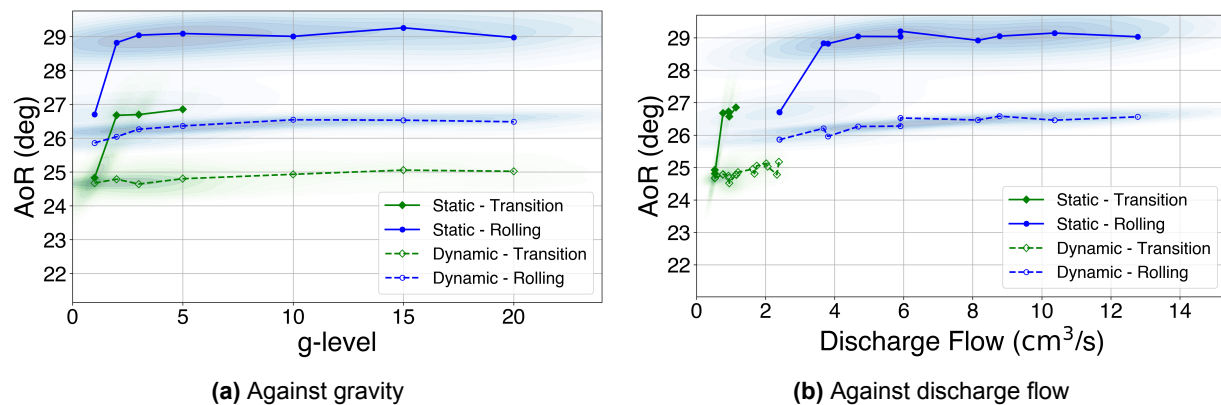


Figure 6.43: Static and Dynamic AoR against gravity and discharge for **glass beads**.

For the glass-volcanic mixture, in the transition regime, the dynamic AoR increases slightly with gravity, while the static AoR does not vary with gravity (Figure 6.44a). This shows that the bottom half of the slope (where the dynamic AoR is measured) is in a less fluid state than the upper half.

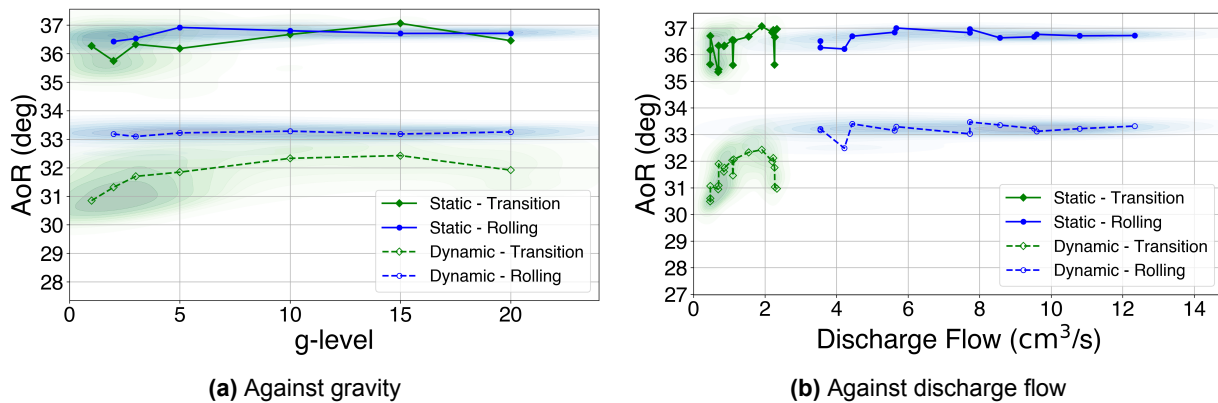


Figure 6.44: Static and Dynamic AoR against gravity and discharge for the **glass-volcanic mixture**.

Summary of the Findings on the Effects on the Static and Dynamic Angles of Repose

The findings on the static and dynamic mean angles of repose are similar to those on the mean angle of repose of the overall slope in Section 6.4.3 with regards to gravity, discharge flow and the avalanching regime.

Differences between static and dynamic AoR:

- Notable differences in the behaviours of static and dynamic AoR were observed in materials such as glass beads, river sand, and the glass-volcanic mixture.
- These differences suggest that the upper and lower slope halves may not be in identical particle flow states, even when classified as the same avalanching regime.

6.6. Additional Observations on Particle Separation

In addition to the measurements of the angle of repose and other parameters, changes in the particle separation patterns of the two mixtures tested in the experiments could also be observed. However, these observations do not help in answering the research question of this study. The observations and conclusions on the effect of gravity on particle separation are therefore included in Appendix C. The inclusion of these observations in this report is important as it still represents a significant addition to the literature to be explored more deeply in future research.

6.7. Summary of Chapter 6

In this chapter many insights were gained over the previous sections about the values of the angle of repose (AoR), its standard deviation, the avalanching regimes, gravity, and the discharge flow. These are gathered and summarised in this final section to build a clear picture of the phenomena at play.

First, the heartbeat graphs were introduced in Section 6.1. These novel graphs show the evolution of the AoR in time, which was not yet done in the literature. It highlights that:

- The angle of repose (AoR) typically varies over time.
- Depending on the avalanching regime, this variation may occur in cycles of increasing and decreasing values or exhibit negligible fluctuations.
- There can also be increasing or decreasing trends in the average value of these cycles.
- The timing of AoR measurements is crucial for the interpretation of the results.

Section 6.3 showed that two main variables of the angle of repose are gravity and the discharge flow. Gravity is the main force attracting the poured particles down onto the pile, and it therefore affects the discharge flow. This relationship was observed empirically:

- The discharge flow increases with gravity, with an observed trend less-than-linear, like Equation 6.8:

$$\text{Discharge Flow} \propto \sqrt[3]{g_{eff}} \quad (\text{Equation 6.8})$$

- The larger openings (at 5mm) exhibit steeper increases in discharge flow compared to smaller openings (at 3mm), highlighting the dependence on the cell opening area.
- Consistent behaviour is observed across all materials, indicating that this relationship is independent of the material properties.

Section 6.3 further showed that the discharge flow affects the standard deviation of the AoR. The standard deviation can be used as a proxy to quantify which avalanching regime applies to an experiment.

- The discharge flow has a strong influence on the standard deviation. This relationship often follows a stepwise pattern (declines followed by plateaus). The stabilisation of the standard deviation at a plateau indicates a change of avalanching regime.
- Differences in standard deviation are observed between the two halves of the slope. This indicates that the avalanching regime transitions are not instantaneous across the entire slope. Avalanche fronts and kinks are initially visible on the entire slope length, but the maximum height reached propagates downwards as discharge flow increases.
- Material properties, especially particle shape, influences the discharge flow rates required for regime transitions. Irregularly shaped particles (e.g., volcanic sand, river-volcanic mixture) exhibit higher standard deviation values at low discharge flow rates. Rounder particles (e.g., glass beads, glass-volcanic mixture) display the lowest standard deviation values at all discharge flow rates. At high discharge flow rates, all materials exhibit convergence toward similar, stable standard deviation values.

With the introduction of the avalanching regimes in Section 6.4, the effect of gravity, discharge flow and the avalanching regime were characterised. The following observations apply to the mean values of the AoR and also to the values of the static and dynamic AoR.

Effect of gravity:

- In the discrete and transition regimes, increasing gravity in the lower levels from 1g to 5g (depending on the material) raises the mean AoR.
- At higher gravity levels 5g to 20g, the mean AoR stabilises and gravity has little to no effect.
- In the rolling regime, gravity has no effect on the mean AoR.

Effect of the discharge flow:

- Increasing the discharge flow induces a change in the avalanching regime from discrete, to transition, to rolling.
- In the discrete and transition regimes, a higher discharge flow increases the mean AoR for most materials, except volcanic sand and the river-volcanic mixture, where it has little to no effect.
- In the rolling regime, the discharge flow has no effect on the mean AoR.

Effect of the avalanching regimes:

- The type of regime does not directly affect the mean AoR but rather influences the strength of the relationships between gravity, discharge flow, and the mean AoR.
- In the rolling regime, neither gravity nor discharge flow affects the mean AoR, which stabilizes at a material-dependent value.
- Differences in behaviours between the static and dynamic AoR suggest that the upper and lower slope halves may not be in identical particle flow states, even when classified as the same avalanching regime.

Before concluding on how these findings answer the research questions, the validity of the results will be questioned and compared against those of other studies from the literature in the following Chapter 7.

Discussion

The previous Chapter 6 detailed the results from the experiments and characterised the relationships between main variables affecting the angle of repose (AoR): time, gravity, the discharge flow and the avalanching regimes.

This chapter presents a discussion of the results from Chapter 6. Section 7.1 first discusses the interpretation of the results with regards to the physical phenomena at play. Then, Section 7.2 links the findings to the studies of the literature identified in Chapter 2.

7.1. Interpretation of the Key Findings

This section reflects on three main findings of this research: the effects of time, gravity and the discharge flow on the angle of repose. The validity of the findings is questioned, and a theoretical explanation is associated to the findings based on the known physical dynamics at play.

Effect of Time on the Angle of Repose

The first key finding is that the angle of repose (AoR) is influenced by time. This is because piles form through avalanches, causing the slope to fluctuate between maximum and minimum values.

Previous research, as outlined in Chapter 2, typically measured AoR at discrete time points to simplify sampling or accommodate practical constraints. These studies focused either on static and dynamic AoR or on a constant AoR in rolling regimes, such as in rotating drums.

While this finding is not new, this study offers a novel approach to study it, which lies in the introduction of the “heartbeat” graphs (Section 6.1.1). These graphs capture the continuous evolution of AoR over time. These graphs reveal intricate details of pile formation and avalanching mechanics that would be missed with single-point measurements. Additionally, as the pile grows over time, the slope length increases, potentially affecting the AoR values. Investigating the impact of slope length on AoR is recommended for future research.

Relationship Between Gravity & Angle of Repose

The second key finding concerns the relationship between gravity and the angle of repose. In the hypergravity environment, gravity primarily affects the angle of repose by causing a steep increase at lower gravity levels, followed by stabilization at higher gravity levels. This relationship is described by an inverse-negative form, similar in shape to Equation 7.1, where AoR is the angle of repose, g is the gravity level, and c is a material-specific constant:

$$AoR \propto \frac{-1}{g} + c \quad (7.1)$$

The validity of this relationship and its comparison to findings in the literature are discussed in Section 7.2.

This relationship (Equation 7.1), visualised in Figure 7.1, can be explained by the interaction between gravity and particle dynamics. When increasing gravity (e.g., from 1g to 5g), avalanching particles are pressed more firmly against the static layers beneath them, increasing friction and causing the particles to stop after a shorter travel distance. This results in a steeper slope. However, at a certain gravity level

(material-specific), the interlocking of particles reaches an equilibrium where the balance of friction and particle weight stabilises, leading to a constant angle of repose in the higher gravity levels (e.g., from 5g and higher).

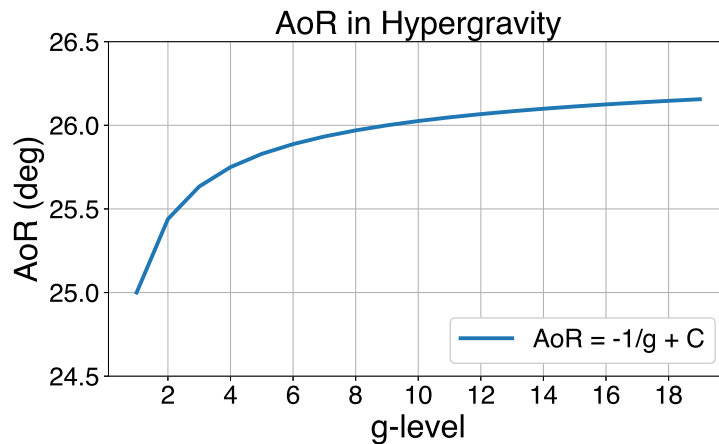


Figure 7.1: Hypothetical relationship between the angle of repose and gravity in the hypergravity regime.

Relationship Between Discharge Flow & Angle of Repose

A final key finding concerns the relationship between discharge flow and angle of repose. While results suggest that the discharge flow influences the AoR, it was experimentally demonstrated that gravity directly affects discharge flow. This raises the possibility of an indirect effect of gravity on the AoR via discharge flow, or alternatively, that discharge flow itself has no significant direct impact on the AoR.

This study did not aim to independently characterize the effect of discharge flow on the AoR. Future research should address this question, either through partial correlation analysis of the available data or by conducting experiments with precise control over the discharge flow to isolate its effects.

Despite this uncertainty, the other relationships identified remain robust. The relationship between gravity and the AoR was shown to be independent of the discharge flow in materials experiencing both discrete and transition regimes. Furthermore, the discharge flow was found to directly influence the avalanching regime, which in turn governs how gravity and the discharge flow impact the AoR. Through its effect on avalanching regimes, the discharge flow also shapes the cyclic behaviour of the AoR, as captured in the heartbeat graphs (Section 6.1.2).

7.2. Comparison to the Literature

An overview of the findings of the previous studies was given in Chapter 2. This overview is repeated in Table 7.1, expanded with the results of this research. From the studies who found a significant relationship between gravity and the angle of repose, most found a relationship where the AoR increases when gravity decreases, and vice-versa (negative relationship). Only Kleinhans et al. (2011) found a relationship between gravity and the dynamic AoR where the AoR decreases when gravity decreases (positive relationship). The findings of this research all show a negative relationship between the AoR and gravity depending on the avalanching regime and gravity level, and sometimes gravity had no effect on the AoR.

The main findings of this research are discussed against the literature in this section. The discussion addresses each paper individually, as understanding their respective backgrounds is essential to contextualise their results. This discussion is separated into two categories: against those who found a significant relationship between gravity and the AoR (Section 7.2.1), and against those who found no significant relation (Section 7.2.2). Finally, Section 7.2.3 discusses the findings of this research against the literature from the perspective of the visual observations on particle sorting.

For clarification, this research only analysed experiments in hypergravity environments. Therefore, any inference in this chapter on the behaviour of particles in hypogravity environments is based on the findings of other studies in the literature.

7.2.1. Studies with a Significant Relationship

Comparison to Brucks et al. (2007)

Brucks et al. (2007) found that the AoR increases when gravity decreases. This was tested in hypergravity regimes, in rotating drums. At first sight, it contradicts the findings of this research. However, it may depend on how the findings of Brucks *et al.* are interpreted. They defined the Froude number as the ratio of the centrifuge acceleration (which depends on the drum radius and the square of the angular velocity) and gravity. The actual finding of Brucks is that the AoR increases with the Froude number. This means that it depends on both the gravity and the rotating velocity (assuming a constant drum radius). The rotation of the drum is the main factor influencing the flux of material being poured back to the top of the pile, similar to the discharge flow. Brucks *et al.* gave a formula to relate the Froude number in a rotating drum and the Froude number in a fixed setup like a Hele-Shaw cell as per Equation 7.2:

$$Fr = \frac{\omega^2 * R}{g_{eff}} = \frac{u^2}{\delta * g_{eff}} \quad (7.2)$$

The rotating drum parameters are the angular velocity ω and the drum radius R . Different setups can compute the Froude number with the avalanche velocity u and the flowing layer thickness δ (Brucks et al., 2007). Unfortunately, the avalanche velocity required to compute the Froude number was not measured in this research and the results cannot be compared easily. However, Brucks show that higher Froude numbers are related to more fluid avalanching regimes (see Figure 2.4). The discrete regime happens at a lower Froude number than the transition regime, which happens at a lower Froude number than the rolling regime.

Brucks et al. (2007) also found that when decreasing gravity at a constant angular velocity of the drum, the Froude number increases. Correspondingly, the AoR also increased as gravity decreased, hence the AoR increased as the Froude number increased (see Figure 2.3). When the Froude number increased, the avalanching regime changed from the discrete, to rolling, to cascading avalanching regimes. The AoR therefore increased as the regimes changed in that order. In this research, it was also observed that the average AoR increased when moving from the discrete regime to the rolling regime. Therefore, the results of this research and those of Brucks *et al.* actually align.

The observations of the angle of repose at similar gravity levels differ between this research and Brucks et al. (2007), only because they were made at different Froude numbers. Computing the Froude numbers and associating them to the measurements is strongly recommended for future studies of this topic.

Comparison to Klein and White (1990)

Klein and White (1990) observed that increasing the rotation velocity of their drums at constant gravity increased the AoR, which aligns with Brucks et al. (2007) as the increase in rotation velocity increases the Froude number and therefore the associated AoR. They tested Monterey sand and glass beads in hypogravity in rolling regime. They find that the AoR increases when gravity decreases. Here, it was found for similar materials and regimes that there was no effect when varying gravity. However, as they were keeping the rotating velocity constant when reducing gravity, they were increasing the Froude number. When staying in this rolling regime (assuming it did not change into cascading regime), it should be expected to see the AoR increase following the relationship found by Brucks et al., 2007. The Froude numbers used by Klein *et al.* are unknown and it is therefore difficult to compare.

Comparison to Hofmeister et al. (2009)

Hofmeister et al. (2009) tested glass beads in a tilting box experiment in microgravity. The details of the study were not fully documented, but they found that reducing gravity increased the AoR. In lower gravity, the slope would be less extended horizontally and take a more irregular shape, indicating that cohesive forces may become predominant. No Froude numbers or information on the avalanche cycle is given here, as the measurements were taken after the entire material was done pouring. In this research, it was never observed that the slope would change the horizontal space it took. It was also found that gravity only increased the AoR in the transition regime when increasing from 1g to 3g. Both studies could extrapolate their results to one another. It could be explained that at high gravity (e.g., 20g), the particles are strongly compacted on each other and therefore pile up at a high AoR. When decreasing the gravity until 3g, no significant changes are observed. Decreasing further below 3g, and assuming a transition regime, the

AoR starts to decrease. At 1g, the rate of decrease of the AoR is more important than at 3g. The slower slope angle requires the pile to extend its horizontal footing. Decreasing below 0.3g (the first measure of Hofmeister et al. (2009)), the begins to increase the Froude number and the slope AoR is increasing again. At very low gravity, the Froude number may have increased, but more importantly the cohesive forces are becoming predominant and hold the pile at a higher average AoR, but with irregular slope shapes.

This hypothesis may connect this research to Hofmeister et al. (2009) and explain a “V-shaped” relationship between gravity and the AoR across hypogravity and hypergravity ranges. Unfortunately, this cannot be verified due to the lack of measurements of the Froude number in both studies.

Comparison to Elekes and Parteli (2021)

Elekes and Parteli (2021) performed a numerical study on a simulated fixed funnel method. They found that the angle of repose decreases when increasing gravity. This was simulated for a gravity regime from 0.06g to 100g. This clashes with the results found in this research. They found that the AoR of smaller particles is more affected by changes in gravity, and this was also observed in this research.

It is difficult to explain why the observations are contradicting, as Elekes and Parteli (2021) do not explain the effects of gravity on the pouring flux (the discharge flow). Nothing is said about how to compare their experimental setup with a Hele-Shaw cell, nor a rotating drum. As was recommended previously, associating the Froude number to the measurements of the AoR is of high interest to allow comparisons under similar conditions.

Comparison to Kleinhans et al. (2011)

Kleinhans et al. (2011) looked at the AoR of granular materials in varying environments in rotating drums in hypogravity. The materials tested included glass beads and sand. Some were performed under water and some in air. The avalanches were always in discrete avalanching regime. The static AoR was found to increase when gravity decreases. The opposite was found in this research. They based the assumption on the fact that cohesive forces would be more predominant in hypogravity and would therefore increase the effective friction force, allowing steeper slopes to form. In the hypergravity environment of this research, this assumption does not hold, as gravity (and therefore weight) is predominant on the particles. It would appear that the increase in gravity compacts the particles more into a different interlocking disposition which effectively increases the friction force and allowing a steeper slope to form. This hypothesis cannot be verified though. Kleinhans et al. (2011) then find that the dynamic AoR decreases when decreasing gravity. Similarly here, the dynamic AoR is found to increase with an increasing gravity. The assumption of Kleinhans *et al.* on this is that under a lower gravity, the avalanche layer is more dilated and the particles are less pushed against the slope, experiencing less friction and travelling further along the slope. This explanation therefore supports the results of this research.

7.2.2. Studies with No Significant Relationship

Comparison to Nakashima et al. (2011)

Nakashima et al. (2011) performed experiments with a fixed funnel in hypogravity with Toyoura sand. They measured the AoR at the base of the plate after the material was finished pouring and the pile was stable. They repeated the experiment multiple times in varying gravity regime. They found a standard deviation of $2^\circ - 3^\circ$ and the average did not seem to significantly change. They therefore concluded that there is no significant change. This is an interesting situation, as the fixed funnel may be better suited to represent natural pile formations in three dimensions without wall effects. However, in this study it was shown in the heartbeat graphs that the slope of a pile is not constant most of the time. In a discrete or transition regime, it can fluctuate within a range of over 2° between its maximum and minimum peak values. When taking a single measurement after the pile formation does not tell at which point in the cycle the measurement was performed. It is normal then Nakashima *et al.* found a standard deviation of over 2° . In their experimental results, they observe an increase of the average AoR from 1g to 2g, which aligns with the findings of this research. The average AoR reaches a minimum at 0.5g, but increases again towards $1/6g$. This could align with the observations of other studies who saw an increase in the AoR when decreasing gravity, possibly due to the cohesive forces becoming more predominant. This could support a theoretical V-shaped relationship between the AoR and gravity.

Comparison to Marshall et al. (2018) & Karapiperis et al. (2020)

Marshall et al. (2018) and Karapiperis et al. (2020) both studied the AoR in a passive failure experiment in hypogravity. In the first they performed an experiment, in the second they simulated it numerically. The AoR is measured after it stabilises at the bottom of the pile. They found similar results. They conclude that there is no effect of gravity on the AoR. This would disagree with the findings of this research. However, their work did not have enough data points to have significant results and they can therefore not conclude that there the AoR and gravity are significantly independent. With 10 measurement points, two at lunar gravity, three at martian gravity and five at Earth gravity, it shows that there are too few data points to confidently talk about an average AoR and standard deviation at each gravity level. The standard deviation at 1g is smaller than for the other gravity levels, showing how more data points reduce the uncertainty of the measurements. It is therefore not possible to conclude why the findings of their study differs from that of this study, as there are no comparable measurements.

Table 7.1: Main findings of the studies on the effect of gravity on the angle of repose of granular materials, including the findings of this research research. The conclusions of each study are coloured as follows: in green a negative relationship; in yellow an insignificant relationship; in red a positive relationship; white for additional conclusions on the relationship.

Study	Angles	Definition Angle of Repose	Results/Conclusions
Brucks <i>et al.</i> 2007	AoR	Mid Slope Angle	The AoR decreases with increasing g-level
Klein and White 1990	Dynamic AoR	Mid Slope Angle	Dynamic AoR increases with decreasing g-level, varying with the reciprocal of the square root of the g-level
Nakashima <i>et al.</i> 2011	Dynamic AoR	Angle at the bottom of the cone during pouring	The AoR is independent on varying g-level
	Static AoR	Angle at the bottom of the cone after pouring	
Marhsall <i>et al.</i> 2018	AoR	Angle at the bottom of the slope after avalanche	The AoR is independent on varying g-level
	Dilatancy	Change in volume due to applied stress	The dilatancy angle increases when reducing g-level
Hofmeister <i>et al.</i> 2009	AoR	Mid Slope Angle	The AoR increases with decreasing g-level
Elekes <i>et al.</i> 2021	AoR	Angle at the bottom of the cone after pouring	The AoR increases with decreasing g-level
			The AoR varies with $1/(d g^{1/2})$
Karapiperis <i>et al.</i> 2020	AoR	Angle at the bottom of the slope after avalanche	The AoR is independent on varying g-level
Kleinhans <i>et al.</i> 2011	Static AoR	Highest before avalanche	Static AoR increases with decreasing g-level
	Dynamic AoR	Smallest after avalanche	Dynamic AoR decreases with decreasing g-level
Fosséprez 2024	AoR	Average slope angle at any instant in time	The AoR increases with increasing g-level in discrete and transition regimes
	AoR	Average slope angle at any instant in time	The AoR is independent of the g-level in the rolling regime
	Static AoR	Highest before avalanche	The static AoR increases with increasing g-level in discrete and transition regimes
	Static AoR	Highest before avalanche	The static AoR is independent of the g-level in the rolling regime
	Dynamic AoR	Smallest after avalanche	The Dynamic AoR increases with increasing g-level in discrete and transition regimes
	Dynamic AoR	Smallest after avalanche	The Dynamic AoR is independent of the g-level in the rolling regime

Discussion of a V-shaped Relationship Between Gravity and the Angle of Repose

After discussion of the findings of this research against the rest of the literature, a hypothetical v-shaped relationship between gravity and the angle of repose could explain the differences observed between studies. This relationship is visualised in Figure 7.2.

In the hypogravity range, it was observed that the AoR decreased when gravity increased. In the gravity range closer to 0g, the granular material displays a cohesive behaviour due to the various cohesive forces being predominant. These forces hold the particles together and allow the pile to take a steeper slope. At 1g, the balance between the cohesive forces and gravity is such neither are predominant. Gravity attracts the particles towards the surface and allows the pile to spread out on the ground, giving it a less steep slope.

In the hypogravity regime, the AoR appears to be proportional to one over the square root of gravity (Klein and White, 1990, Elekes and Parteli, 2021) following Equation 7.3.

$$AoR \propto \frac{1}{\sqrt{g}} \quad (7.3)$$

In the hypergravity regime, with an increasing gravity from 1g until about 5g (depending on the material), the particles are compressed against the layers beneath them. This enforces the interlocking between particles and favours the pile to build up rather than spread on the ground, giving it a steeper shape. At higher gravity levels, the interlocking of particles reaches a maximum and the AoR will reach a plateau.

In the hypergravity regime, the AoR appears to be proportional to the negative inverse of gravity, following Equation 7.4.

$$AoR \propto \frac{-1}{g} \quad (7.4)$$

This relationship over the whole gravity range will have to be proved by future studies.

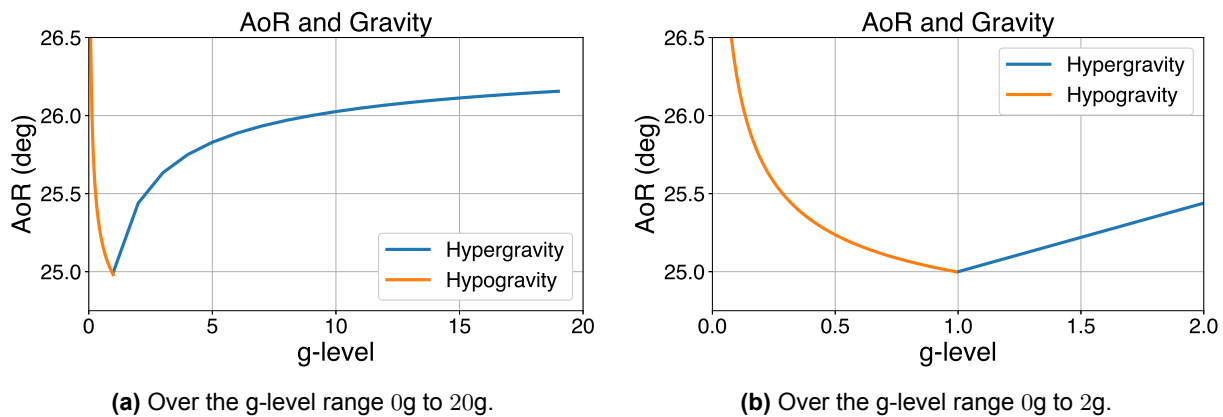


Figure 7.2: V-shaped relationship between gravity and the angle of repose.

7.2.3. Discussion of the Additional Observations on Particle Sorting

The variations in gravity visibly influenced particle sorting patterns, including stratification and segregation. These observations, detailed in Appendix C, are not directly relevant to answering the research question but illustrate the visible effects of gravity and avalanching regimes on both the angle of repose and particle sorting. While no other study in the literature has specifically examined the effect of gravity on particle sorting, the observed relationships between angles of repose, avalanching regimes, and particle sorting patterns (all influenced by gravity) can be compared to existing literature to push the discussion a step further.

In stratification, it was observed that the increasing gravity would decrease the length of the stratified layer and increase the strength of segregation in the material. The increase in discharge flow reduced the

thickness of the layers. Passing into a transition and rolling regime makes the stratification disappear. In the study of Koepe et al. (1998), it was observed that there is a threshold input mass flow (the discharge flow) above which no more stratification occurs. This can be the transition point where the avalanching regime becomes rolling. They also observe that the wavelength (the thickness of the layers) does not vary with the discharge flow. This could be true. The layer thickness was subjectively assessed from screenshots, and these should be precisely measured to take conclusions about their variations. The studies by Makse *et al.* do not assess how the gravity or the discharge flow affect the stratification patterns. They identify the avalanche velocity as a main parameter, however this was not measured in this study.

In segregation, it was observed in this research that the increase in gravity strengthens the degree of segregation between the particles. No other studies observed segregation and the findings cannot be compared.

7.3. Summary of Chapter 7

At first sight, most other studies found results contradicting those of this research. A closer look at each study sheds light on a common challenge: their results are not fully comparable due to differences in experimental conditions and avalanching regimes. The key for bridging this gap is the Froude number. As introduced by Brucks et al. (2007), the Froude number appears to be critical in standardising the results across the various studies. It makes studies in varying gravity regimes and different experimental setups comparable.

The avalanche regimes were found by Brucks et al. (2007) to be dependent on the Froude number. By using the avalanche regimes as a proxy for the Froude number, it appeared that the relationships of the AoR were aligning between this research and certain studies. It highlights that all studies may be observing a similar pattern on the relationship between the AoR and gravity. However, this hypothesis cannot be validated across the whole literature, as most studies do not report Froude numbers, underscoring a significant gap in the literature.

Finally, while many studies focus exclusively on hypogravity or hypergravity regimes, their conclusions of an asymptotic AoR at higher gravity levels may oversimplify the relationship. This research proposes a more nuanced perspective:

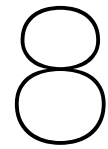
- At low hypogravity (just above $0g$), cohesive forces dominate, leading to a higher AoR. The discrete avalanching regime dominates.
- Near $1g$, the cohesive forces diminish and the resulting forces on the particles can only support the slope at a lower angle, hence the AoR decreases.
- Between $1g$ and $3g$, the AoR increases again as particle compaction and friction intensify.
- At higher gravity levels ($5g$ and above), the AoR stabilises due to strong compacting force and the avalanching transition into a rolling regime, yielding material-dependent stagnation values.

Across the whole gravity spectrum, this relationship between the angle of repose and gravity follows a **V-shaped** pattern.

This hypothesis offers a comprehensive framework for understanding behaviour of the angle of repose across gravity regimes and emphasises the need for future studies to consider both Froude numbers and avalanching regimes in their experimental designs.

Part III

Closure



Conclusions

Throughout this report, Chapter 3 defined research objectives and questions to be answered by the thesis study. Chapter 5 designed a method to analyse the available experimental data (Chapter 4), the results of which were presented in Chapter 6 and discussed in Chapter 7. This chapter reflects the research objectives and questions by linking them to the conclusions of this thesis research, and addresses the gap in the literature.

To this end, the following structure is followed. Section 8.1 evaluates the research questions and hypotheses laid out in the research plan and describes how the conclusions of this research answer these questions. Section 8.2 explores how this study addresses the identified gap in the literature. Finally, Section 8.3 concludes how the research objectives of this thesis project have been met.

8.1. Addressing the Research Questions & Hypotheses

In Chapter 3, the main research question of this research was defined:

Main Research Question

How does gravity affect the angle of repose of non-cohesive granular materials through the mechanics of avalanching?

To cover the breadth of the main research question, a series of hypotheses were laid out based on the theory from the literature on the angle of repose and gravity. These hypotheses have for purpose to aid in answering the main research question. These were the following:

Research Hypotheses

- H1:** A decrease in gravity leads to an increase in angle of repose.
- H2:** A decrease in gravity leads to an increase in static angle of repose.
- H3:** A decrease in gravity leads to a decrease in dynamic angle of repose.
- H4:** The effect of gravity on the angle of repose is stronger for smaller particles than for larger ones.
- H5:** The mean angle of repose is smaller in discrete avalanching regime than in rolling regime, and it is smaller in rolling regime than in cascading regime.

To test these hypotheses, a series of sub research question were defined:

Sub-research Questions

- R1:** How does gravity affect the mean angle of repose?
R2: How does gravity affect the static angle of repose?
R3: How does gravity affect the dynamic angle of repose?
R4: How does the effect of gravity on the angle of repose change between smaller particles and larger ones?
R5: How is the mean angle of repose affected when transitioning between discrete avalanching, rolling and cascading regimes?

These research questions can now be answered through the analysed results from Chapter 6.

The first three research questions concern how gravity affects the mean, the static and the dynamic angles of repose. These questions can be addressed collectively, as the conclusions drawn are applicable to all three. For **R1** “*How does gravity affect the mean angle of repose?*”, **R2** “*How does gravity affect the static angle of repose?*” and **R3** “*How does gravity affect the dynamic angle of repose?*”: In the discrete and transition regimes, an increase in gravity has an increasing effect on the angle of repose in the lower gravity levels of 1g to 3g. For higher gravity levels, gravity has little effect on the angle of repose. Increasing the discharge flow has an increasing effect on the angle of repose in the higher gravity levels though. In the rolling regime, neither gravity or the discharge flow has an effect on the angle of repose, and the constant angle of repose value is material dependent. This applies to the mean, static and dynamic angles of repose. A difference of a couple degrees was observed between the static and dynamic angles of repose. These could only be observed in the discrete and transition regimes. In the rolling regime, the avalanche front cannot be discerned.

This concludes that hypothesis **H1** “*A decrease in gravity leads to an increase in angle of repose.*” is **rejected**, in favour of the counter-hypothesis that *a decrease in gravity leads to a decrease in the mean AoR.*

Similarly, hypothesis **H2** “*A decrease in gravity leads to an increase in static angle of repose.*” is **rejected**, in favour of the counter-hypothesis that *a decrease in gravity leads to a decrease in static AoR.*

It can however be concluded that hypothesis **H3** “*A decrease in gravity leads to an decrease in dynamic angle of repose.*” is **accepted**.

For **R4** “*How does the effect of gravity on the angle of repose change between smaller particles and larger ones?*”, it was observed that the effect of gravity was stronger for small particles than for larger ones, as smaller particles would see a stronger increase in the angle of repose with an increasing gravity level.

The largest particles were the glass beads, followed by the volcanic sand and then the river sand. For the mixtures, it can be assumed that the average particle size is in between that of the pure species. Gravity only affects the AoR in the transition and discrete regimes. The change in average AoR for each material can be deduced over the gravity range from the plots of the AoR against gravity from Section 6.4.3. The following results answer **R4**:

- For the glass beads in transition regime, the AoR increases by 1° from 1g to 3g. It increases by 1.5° from 1g to 20g.
- For the glass-volcanic mixture in transition regime, the AoR increases by 1.2° from 1g to 3g. It increases by 1.5° from 1g to 20g.
- For the volcanic sand in transition and discrete regime, the AoR increases by 1.2° from 1g to 3g. It increases by 1.7° from 1g to 20g.
- For the river-volcanic mixture in transition regime, the AoR increases by 0.5° from 1g to 3g. In discrete regime, the AoR increases by 2° from 1g to 3g, and by 2.5° from 1g to 20g.
- The effect of gravity on the AoR cannot be estimated for the river sand as it was practically only in the rolling regime.

From these observations, it can be concluded that hypothesis **H4** “*The effect of gravity on the angle of repose is stronger for smaller particles than for larger ones*” is **accepted** in the discrete and transition regimes as the smaller particles see a stronger increase in the average AoR when increasing gravity.

However in the rolling regime, all materials observe that gravity has no effect on the AoR, hence hypothesis **H4** is **rejected** for that regime. This answers the sub-research question **R4**.

For **R5** “*How is the mean angle of repose affected when transitioning between discrete avalanching, rolling and cascading regimes?*”, it was observed that the mean angle of repose increases when going from discrete avalanching to the rolling regime, with intermediate values in the transition regime. The avalanching regime has a crucial role in defining which values and fluctuations in values are to be expected for the angle of repose. This concludes that hypothesis **H5** “*The mean angle of repose is smaller in discrete avalanching regime than in rolling regime, and it is smaller in rolling regime than in cascading regime*” is **accepted**.

Finally, an overview of the verified hypotheses is given in Table 8.1. Together, the answers to the sub research questions provide an answer to the **main research question** on various fronts. In hypergravity, the angle of repose increases with gravity in the range of 1g until 5g, and then stabilises to a constant value for higher gravity levels. This relation is affected by the avalanching regime of the particles. It is observed as described in the discrete avalanching regime and the transition phase towards the rolling regime. In the rolling regime however, gravity does not have any effect on the AoR anymore, and the AoR value is a constant material-dependent value which is higher than in the discrete and transition regimes. This is observed on both the static and dynamic angles of repose. Smaller particles exhibit a stronger effect of gravity on their AoR than materials made of larger particles. It is therefore concluded that main research question is successfully answered.

Answer to the Main Research Questions

In hypergravity, the angle of repose increases with gravity in the range of 1g until 5g, and then stabilises to a constant value for higher gravity levels. This relation is affected by the avalanching regime of the particles. It is observed as described in the discrete avalanching regime and the transition phase towards the rolling regime. In the rolling regime however, gravity does not have any effect on the AoR anymore, and the AoR value is a constant material-dependent value which is higher than in the discrete and transition regimes. This is observed on both the static and dynamic angles of repose. Smaller particles exhibit a stronger effect of gravity on their AoR than materials made of larger particles.

Table 8.1: Overview of the research hypotheses verification, highlighting the hypotheses that are accepted (green) and rejected (red).

Identifier	Hypothesis	Status	Comment
H1	A decrease in gravity leads to an increase in angle of repose.	Rejected	
H2	A decrease in gravity leads to an increase in static angle of repose.	Rejected	
H3	A decrease in gravity leads to a decrease in dynamic angle of repose.	Accepted	
H4	The effect of gravity on the angle of repose is stronger for smaller particles than for larger ones.	Accepted	For the discrete and transition regimes.
		Rejected	For the rolling regime.
H5	The mean angle of repose is smaller in discrete avalanching regime than in rolling regime, and it is smaller in rolling regime than in cascading regime.	Accepted	

8.2. Contributions to the Literature

The main gap in the literature was identified in Chapter 2 as the lack of consensus on the effect that gravity has on the angle of repose. While the results of this research initially appear to contradict existing studies, a closer comparison reveals that they may in fact observe the same underlying relationship between gravity and the angle of repose.

The lack of a common comparable parameter across experiment types and gravity levels does not allow to make definite conclusions. This research identifies the Froude number as a promising metric for interpreting results across the literature, as it accounts for both gravity levels and the material's avalanching regime.

This study makes several contributions toward addressing the identified gap. It lays the ground on how Hele-Shaw cells can be used to study the effect of gravity on the angle of repose, which had not been done so far in the literature. Additionally, it highlights the importance of incorporating the Froude number in future studies to bridge the observations in hypogravity and hypergravity.

By aligning the findings of this research with those in the literature, it becomes evident that previous studies may have observed the same relationship between gravity and the angle of repose but lacked a shared framework to interpret and compare their results. Establishing a common understanding of this relationship could unify insights across gravity regimes and experimental methods.

8.3. Achievement of Research Objectives

The research objective was defined in Chapter 3 as the following:

Research Objective

The objective of this thesis research project is to help establish which studies made correct inferences as to how gravity affects the angle of repose of granular material, by observing changes in the mechanics of their avalanches over a range of varying gravity levels.

This research identified the Froude number as the best candidate to link and compare all studies on the relationship between gravity and the angle of repose. Establishing a common framework for comparison will enable researchers to evaluate which studies have drawn accurate inferences about this relationship. Additionally, this study contributes new observations that future research can build upon to better understand how gravity influences the angle of repose in Hele-Shaw cells under hypergravity conditions. It can therefore be concluded that the research objective of this study was successfully achieved.

The findings of this research are relevant to space exploration and geomorphology. In this context, the low discharge flow associated to the natural transportation of granular matter may see discrete avalanches. While this study primarily investigated hypergravity regimes, most rocky planetary bodies operate under hypogravity conditions. With a common framework connecting the observations across the whole gravity spectrum, a general relationship will be defined between gravity, the angle of repose and avalanching regimes. Applying this relationship to observations of natural phenomena on planetary bodies will allow to validate the findings of the literature.

In industrial processes and engineering, avalanching cycles often span various regimes. Whether under Earth gravity, in centrifuges, or on other planetary surfaces, understanding how gravity and discharge flow influence the angle of repose will enable the design of more efficient processes and systems.

Recommendations

The scope of this research was confined to measuring the angle of repose using experimental video data of multiple materials tested under varying gravity conditions. Several opportunities for extending this research or enhancing its outcomes have been identified. These include exploring additional research avenues and implementing methodological improvements to enhance accuracy, efficiency, and overall robustness. These identified improvements are presented in this chapter as recommendations for future research on the topic of gravity and the angle of repose (AoR).

The following recommendations concern the **future experiments** to be performed on the topic, advising which parameters to measure and how.

- Measure all parameters required to compute the Froude number. The Froude number is essential to connect all research going ahead. Brucks et al. (2007) provide a formula to compute it in different setups than rotating drums which depend on the avalanche velocity and other parameters. In this study, the main parameter required for the computation of the Froude number which was not measured was the avalanche velocity. Implementing a method to measure the avalanche velocity across the different avalanching regimes would be a big step forward towards documenting the Froude number.
- Control the discharge flow. Controlling the discharge flow allows to separate the effects of gravity and the discharge flow. This could for example be achieved by implementing a controllable variable opening over a continuous range of opening diameters.
- Investigate the impact of slope length on the angle of repose. It was found that the AoR changes over time, as the pile builds up with the continuous inflow of material. This means that the AoR varies as the slope length increases over time. Studying the relation between slope length and AoR may be applied to the observation of slopes in the landscape of other planets, to infer on their formation for example.
- Study the changes in particle separation with gravity in further detail. The changes in particle separation due to gravity were observed in this study, however they were not explored in detail as it was not the main focus. There are certain parameters defined in the work of Makse et al. (1998) and Koeppel et al. (1998) to quantify stratification and segregation. Studying the effect on particle sorting could reveal new findings on the angle of repose and the behaviour of granular material in environments of different gravity than Earth, such as other planets.
- Repeat the experimental campaigns with more recent equipment. Camera technologies have greatly improved since 2010. During the validation of the data analysis pipeline, two consumer cameras were tested. Each camera dates from 2020 and can record footage up to a resolution of 4K. During the validation process, the accuracy of these cameras reached an average true error of 1% to 1.2% (Table A.1), which is better than the 2010 camera used in the experiments which reached at best an average true error of 3%. Nowadays, there are affordable cameras on the market that can record up to a resolution of 8K at high frame rates. This will improve the pixel density and the identification of particles in the experiment.
- Perform the experiments again with improved lighting conditions and calibration material. Artefacts from unwanted lighting sources and lack of enough calibration footage (calibration is required

specifically for the data analysis pipeline used in this research) were the main hurdles to overcome before generating data. The more work is done ahead in the process to improve the video quality, the less work is required in post-production to correct for mistakes in the camera.

- Use experimental data from the hypogravity regime. This research only studied the hypergravity environment and hypothesised on the hypogravity environment based on the findings of other studies in the literature. Studying the hypogravity environments will extend the relationship between gravity and the AoR over the whole gravity spectrum and provide an understanding supported by empirical evidence.
- Analyse the river sand experimental data with a 4mm opening, or reproduce the experiment with a 3mm opening to complete the data set across the whole material range.

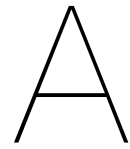
The following recommendations concern the **measurements techniques, computation methods and accuracy** of the measurements.

- Compute the individual effects of each variable on the angle of repose by performing a partial correlation analysis on the available data. This will highlight the most contributing variables and allow follow-on studies to focus more deeply on these variables.
- Improve the edge detection or angle measurement techniques. There are many numerical methods available to detect edges. New methods based on colour detection or machine learning could yield more accurate measurements.
- Improve the camera calibration. Using more advanced camera calibration techniques than those provided in the OpenCV Python library could improve the accuracy of the measurements of the angle of repose.
- Quantifying the trends in the mean AoR with a polynomial fit, or a moving average could yield more accurate measurements of the standard deviation which could be used to better define the avalanching regimes.
- Better quantification of the avalanching regimes. This would provide an objective and more reproducible method to identify the regimes and study the variable effects under each regime more accurately.

References

- Al-Hashemi, H. M. B., & Al-Amoudi, O. S. B. (2018). A review on the angle of repose of granular materials. *Powder technology*, 330, 397–417.
- Atwood-Stone, C., & McEwen, A. S. (2013). Avalanche slope angles in low-gravity environments from active martian sand dunes. *Geophysical Research Letters*, 40(12), 2929–2934.
- Braat, L., Brückner, M. Z., Sefton-Nash, E., & Lamb, M. P. (2024). Gravity-driven differences in fluvial sediment transport on mars and earth. *Journal of Geophysical Research: Planets*, 129(2).
- Brucks, A., Arndt, T., Ottino, J. M., & Lueptow, R. M. (2007). Behavior of flowing granular materials under variable g. *Physical Review E*, 75(3), 032301.
- Butt, H.-J., & Kappl, M. (2009). Normal capillary forces. *Advances in colloid and interface science*, 146(1-2), 48–60.
- Canny, J. (1986). A computational approach to edge detection. *IEEE Transactions on pattern analysis and machine intelligence*, (6), 679–698.
- Cesaretti, G., Dini, E., De Kestelier, X., Colla, V., & Pambaguian, L. (2014). Building components for an outpost on the lunar soil by means of a novel 3d printing technology. *Acta Astronautica*, 93, 430–450.
- Cheng, N.-S., & Zhao, K. (2017). Difference between static and dynamic angle of repose of uniform sediment grains. *International Journal of Sediment Research*, 32(2), 149–154.
- de Vet, S. J. (2010). *Down-wind and down-slope: Aeolian screecone formation and martian analogues*. [Unpublished Master's thesis]. Insitute for Biodiversity and Ecosystem Dynamics, University of Amsterdam.
- Elekes, F., & Parteli, E. J. (2021). An expression for the angle of repose of dry cohesive granular materials on earth and in planetary environments. *Proceedings of the National Academy of Sciences*, 118(38), e2107965118.
- Grasselli, Y., & Herrmann, H. J. (1997). On the angles of dry granular heaps. *Physica A: Statistical Mechanics and its Applications*, 246(3-4), 301–312.
- Hofmeister, P. G., Blum, J., & Heiβelmann, D. (2009). The flow of granular matter under reduced-gravity conditions. *AIP Conference Proceedings*, 1145(1), 71–74.
- Hutton, S., Forsyth, A., Rhodes, M., & Osborne, C. (2004). Effect of interparticle force on mixing and segregation of dry granular materials. *Physical Review E*, 70(3), 031301.
- Karapiperis, K., Marshall, J. P., & Andrade, J. E. (2020). Reduced gravity effects on the strength of granular matter: Dem simulations versus experiments. *Journal of Geotechnical and Geoenvironmental Engineering*, 146(5), 06020005.
- Klein, S., & White, B. (1990). Dynamic shear of granular material under variable gravity conditions. *AIAA journal*, 28(10), 1701–1702.
- Kleinhans, M. G. (2005). Flow discharge and sediment transport models for estimating a minimum timescale of hydrological activity and channel and delta formation on mars. *Journal of Geophysical Research: Planets*, 110(E12).
- Kleinhans, M. G., Markies, H., De Vet, S. J., In't Veld, A. C., & Postema, F. N. (2011). Static and dynamic angles of repose in loose granular materials under reduced gravity. *Journal of Geophysical Research: Planets*, 116(E11).

- Koepe, J., Enz, M., & Kakalios, J. (1998). Phase diagram for avalanche stratification of granular media. *Physical Review E*, 58(4), R4104.
- Makse, H. A., Havlin, S., King, P. R., & Stanley, H. E. (1997). Spontaneous stratification in granular mixtures. *Nature*, 386(6623), 379–382.
- Makse, H. A., Ball, R. C., Stanley, H. E., & Warr, S. (1998). Dynamics of granular stratification. *Physical Review E*, 58(3), 3357.
- Margenau, H. (1939). Van der waals forces. *Reviews of Modern Physics*, 11(1), 1.
- Maroof, M. A., Mahboubi, A., Noorzad, A., & Safi, Y. (2020). A new approach to particle shape classification of granular materials. *Transportation Geotechnics*, 22, 100296.
- Marshall, J. P., Hurley, R. C., Arthur, D., Vlahinic, I., Senatore, C., Iagnemma, K., Trease, B., & Andrade, J. E. (2018). Failures in sand in reduced gravity environments. *Journal of the Mechanics and Physics of Solids*, 113, 1–12.
- Nakashima, H., Shioji, Y., Kobayashi, T., Aoki, S., Shimizu, H., Miyasaka, J., & Ohdoi, K. (2011). Determining the angle of repose of sand under low-gravity conditions using discrete element method. *Journal of terramechanics*, 48(1), 17–26.
- Ozaki, S., Ishigami, G., Otsuki, M., Miyamoto, H., Wada, K., Watanabe, Y., Nishino, T., Kojima, H., Soda, K., Nakao, Y., et al. (2023). Granular flow experiment using artificial gravity generator at international space station. *npj Microgravity*, 9(1), 61.
- Ritter, G. X., & Wilson, J. N. (2001). *Handbook of computer vision algorithms in image algebra* (2nd ed.). CRC Press.



Method Validation Results

The results of the validation campaign performed on the analysis tool used to measure the angle of repose from Chapter 5 are presented in this appendix.

Table A.1: Validation results for the measuring accuracy for the angle of repose, performed with various cameras.

Camera	Shape	Real Slope (deg)	Measured Slope (deg)	True Error (deg)	True Error (%)
Sony	1	44.87	44.24	0.64	1.4%
	2	40.44	40.13	0.31	0.8%
	3	35.91	35.40	0.51	1.4%
	4	33.85	33.79	0.06	0.2%
	5	61.51	61.45	0.06	0.1%
	6	53.67	53.38	0.29	0.5%
	7	48.34	48.06	0.28	0.6%
	8	20.78	20.40	0.38	1.8%
	9	17.24	16.88	0.36	2.1%
	10	13.60	13.23	0.37	2.7%
	11	8.96	8.79	0.17	1.9%
Average				0.31	1.2%
GoPro	1	44.87	44.86	0.01	0.0%
	2	40.44	40.51	0.07	0.2%
	3	35.91	36.02	0.11	0.3%
	4	33.85	33.79	0.06	0.2%
	5	61.51	61.57	0.06	0.1%
	6	53.67	53.85	0.18	0.3%
	7	48.34	48.81	0.47	1.0%
	8	20.78	21.15	0.37	1.8%
	9	17.24	17.15	0.09	0.5%
	10	13.60	13.37	0.24	1.8%
	11	8.96	8.50	0.47	5.2%
Average				0.19	1.0%
Cisco Flip	1	44.87	45.40	0.52	1.2%
	2	40.44	39.66	0.78	1.9%
	3	35.91	36.58	0.67	1.9%
	4	33.85	33.48	0.37	1.1%
	5	61.51	61.49	0.02	0.0%
	6	53.67	53.82	0.15	0.3%
	7	48.34	47.68	0.66	1.4%
	8	20.78	21.83	1.05	5.0%
	9	17.24	17.60	0.36	2.1%
	10	13.60	14.74	1.13	8.3%
	11	8.96	9.81	0.85	9.5%
Average				0.60	3.0%

B

Detailed Research Results

All graphs and results from Chapter 6 are presented in this appendix.

- Section B.1 presents all the heartbeat graphs of every material tested.
- Section B.2 presents the plots of the discharge flow against gravity for each material.
- Section B.3 displays the mean angle of repose (AoR) against gravity and discharge flow for every material.
- Section B.4 shows the standard deviation of the AoR against gravity and discharge flow for every material.
- Section B.5 presents the mean AoR against gravity and discharge for every material again, however with the addition of the highlighted avalanching regimes.
- Section B.6 displays the mean static and dynamic AoR against gravity and discharge flow for every material.

B.1. Heartbeat Graphs of the Angle of Repose

Heartbeats of Glass Beads

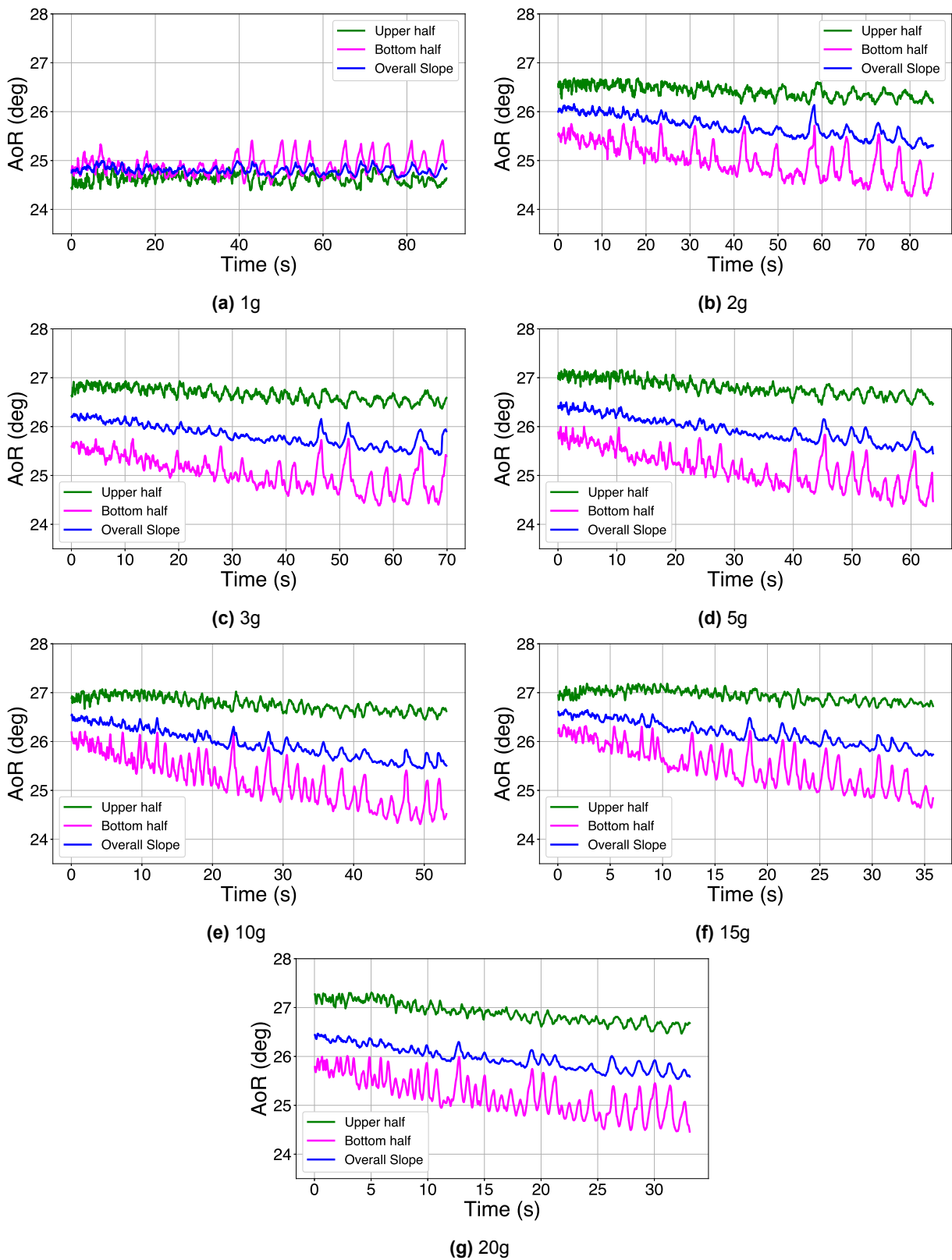


Figure B.1: Heartbeat graphs of glass beads in varying gravity acceleration, with a 3mm opening.

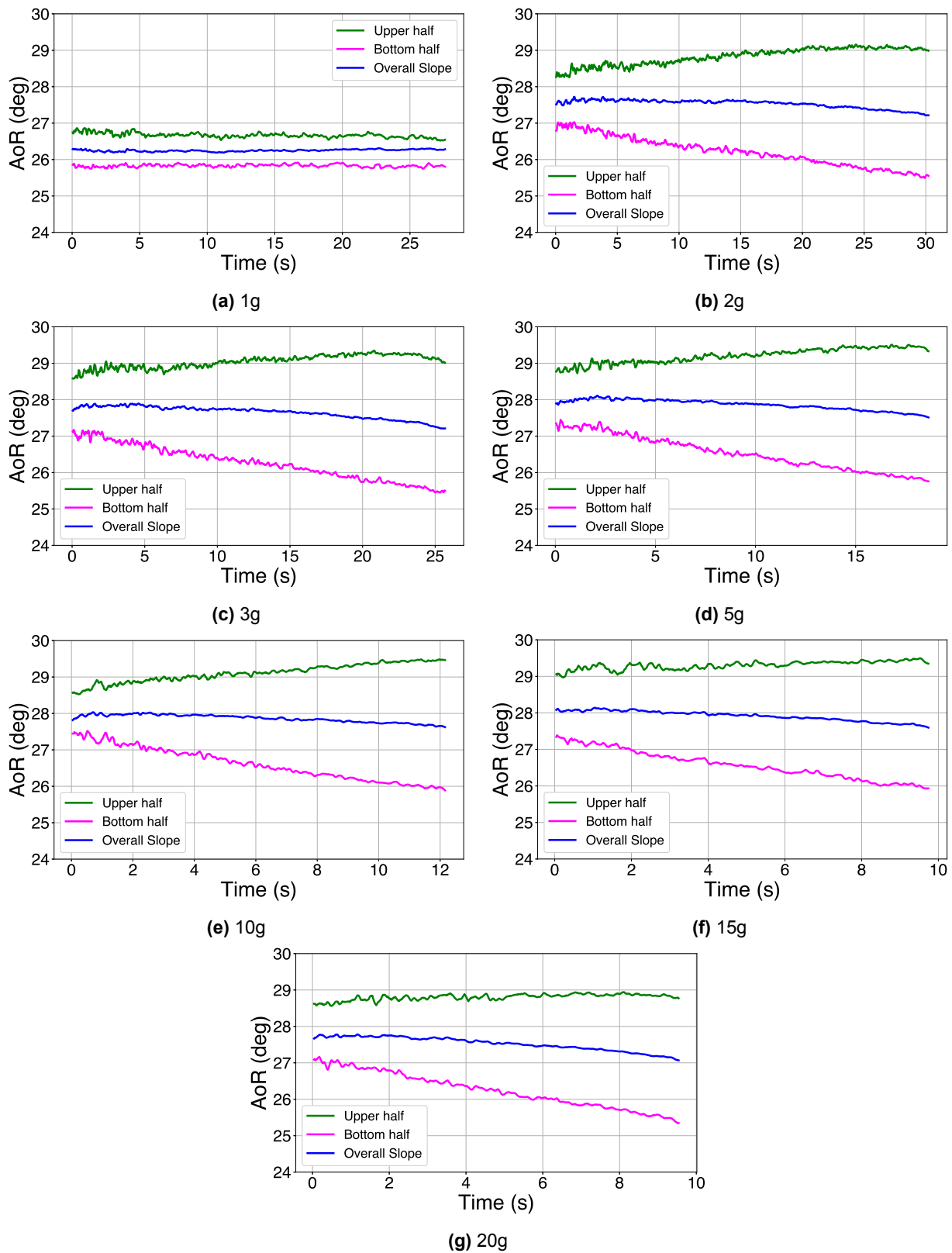


Figure B.2: Heartbeat graphs of glass beads in varying gravity acceleration, with a 5mm opening.

Heartbeats of River Sand

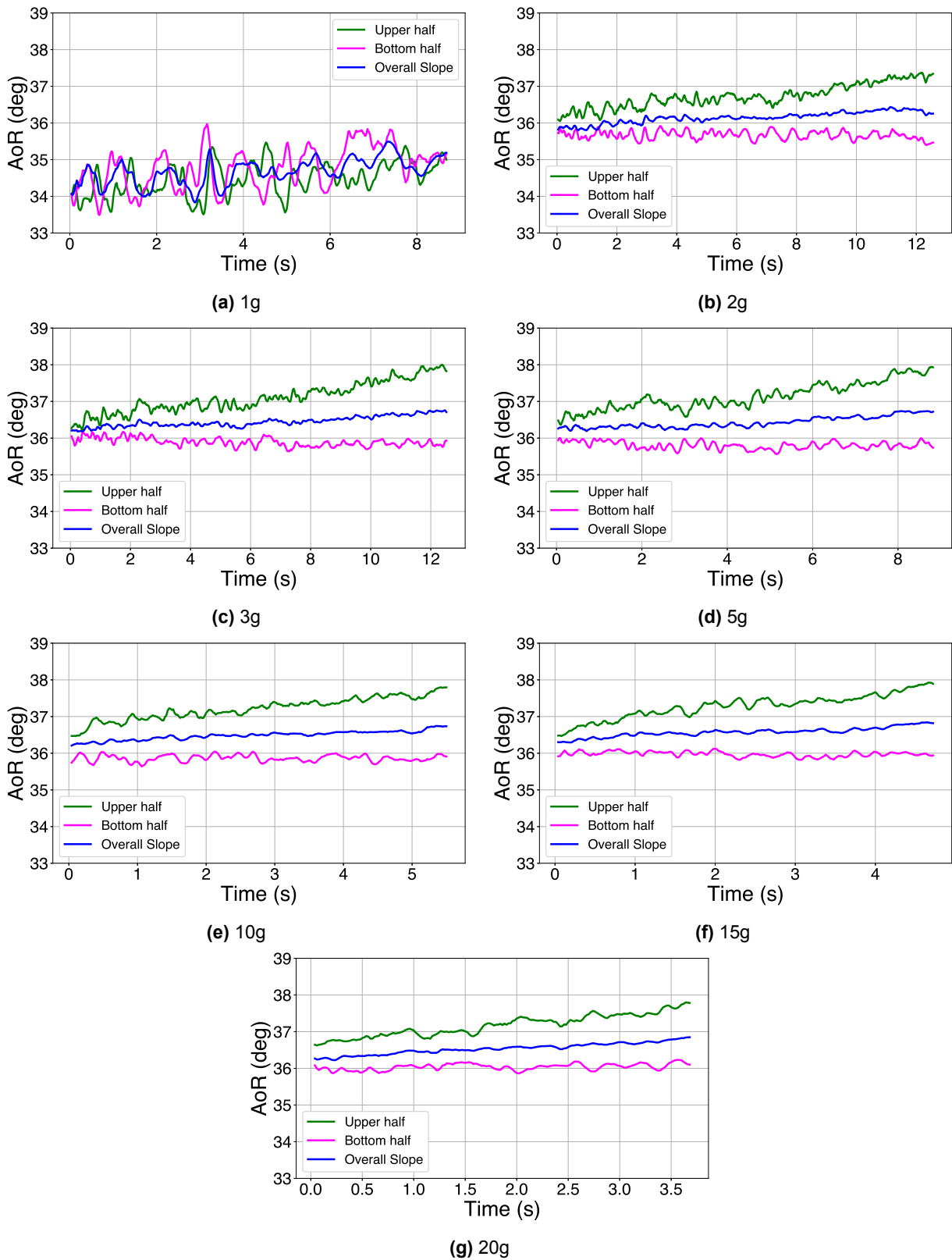


Figure B.3: Heartbeat graphs of river sand in varying gravity acceleration, with a 5mm opening.

Heartbeats of Volcanic Sand

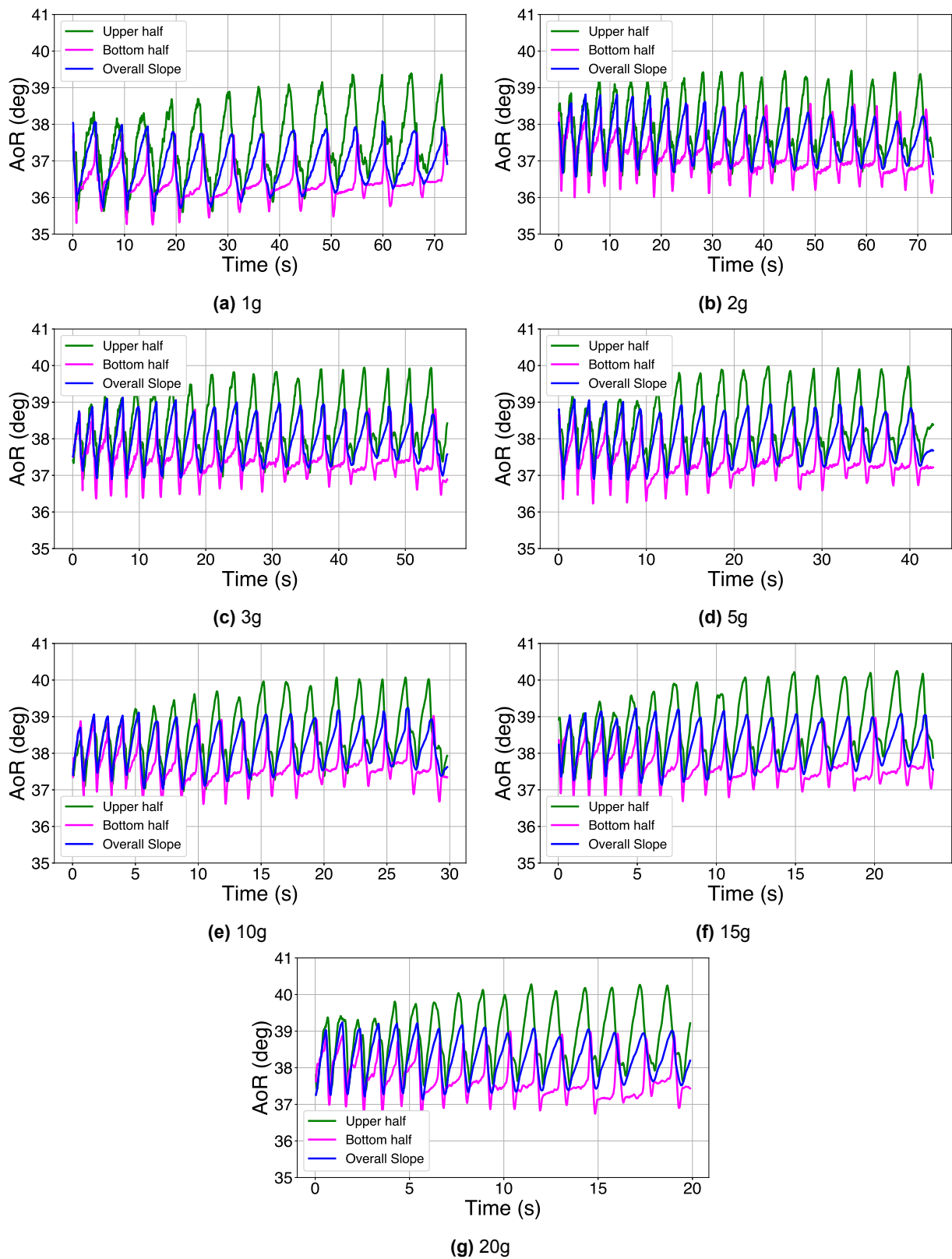


Figure B.4: Heartbeat graphs of volcanic sand in varying gravity acceleration, with a 3mm opening.

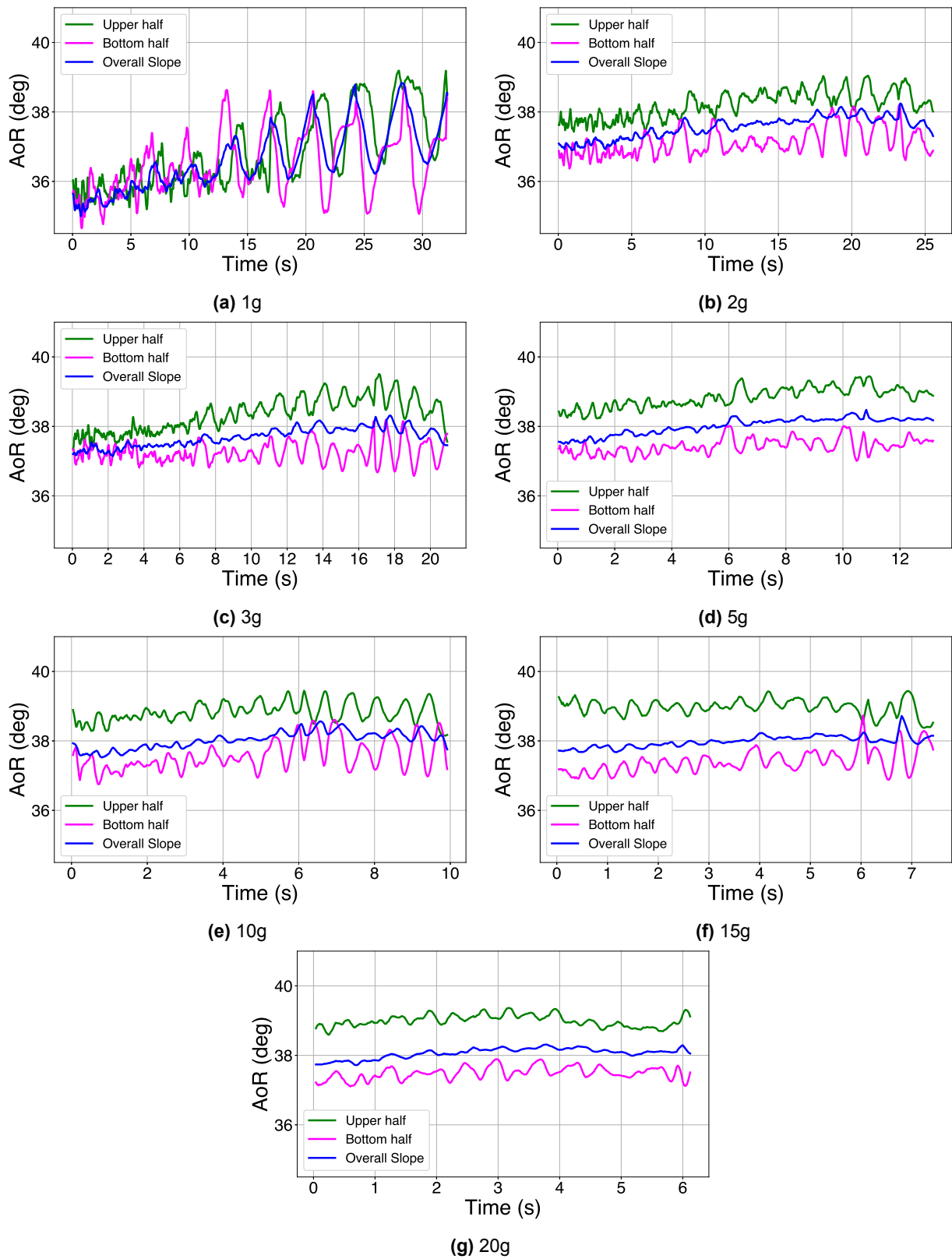


Figure B.5: Heartbeat graphs of volcanic sand in varying gravity acceleration, with a 5mm opening.

Heartbeats of the Glass-Volcanic Mixture

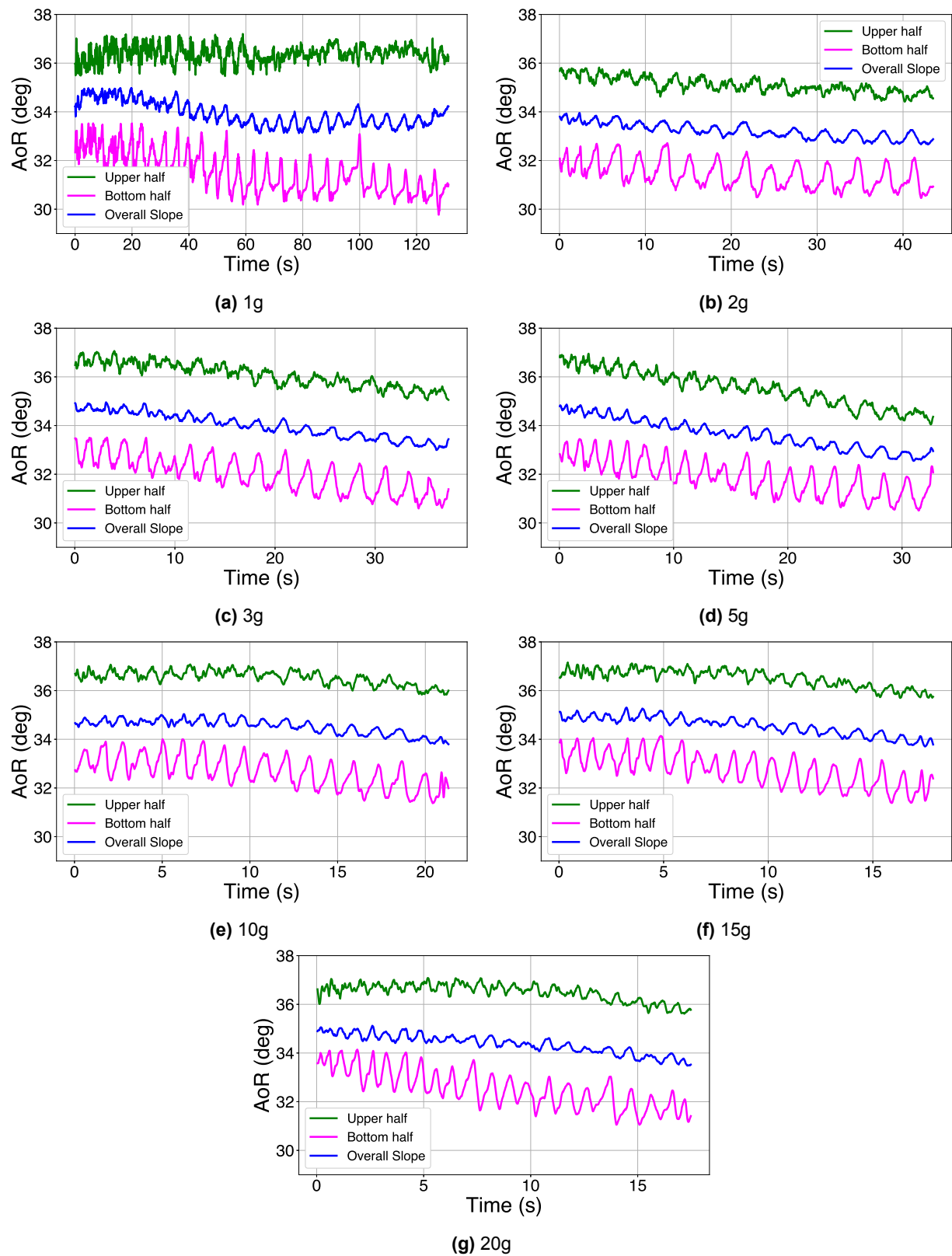


Figure B.6: Heartbeat graphs of the glass-volcanic mixture in varying gravity acceleration, with a 3mm opening.

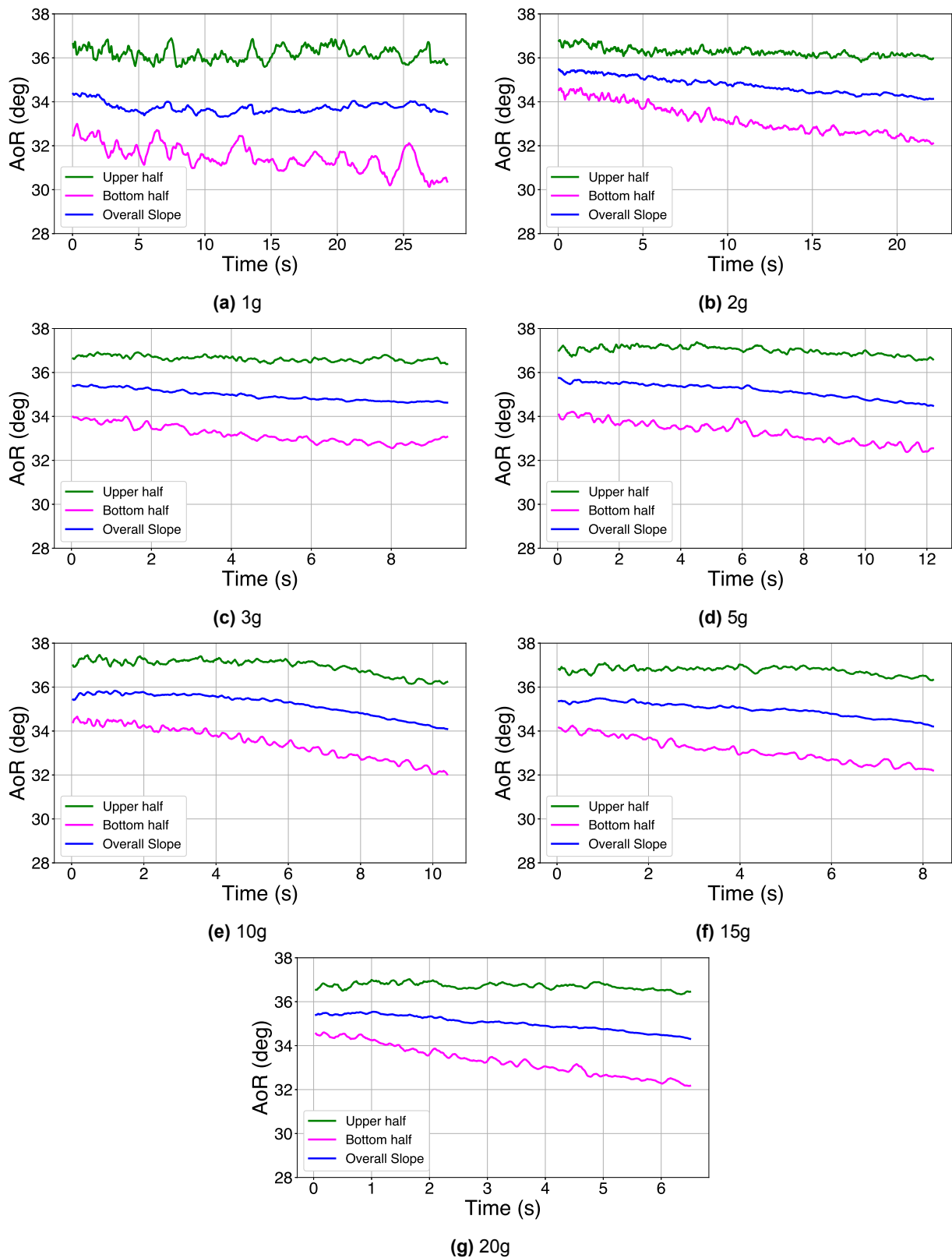


Figure B.7: Heartbeat graphs of the glass-volcanic beads in varying gravity acceleration, with a 5mm opening.

Heartbeats of the River-Volcanic Mixture

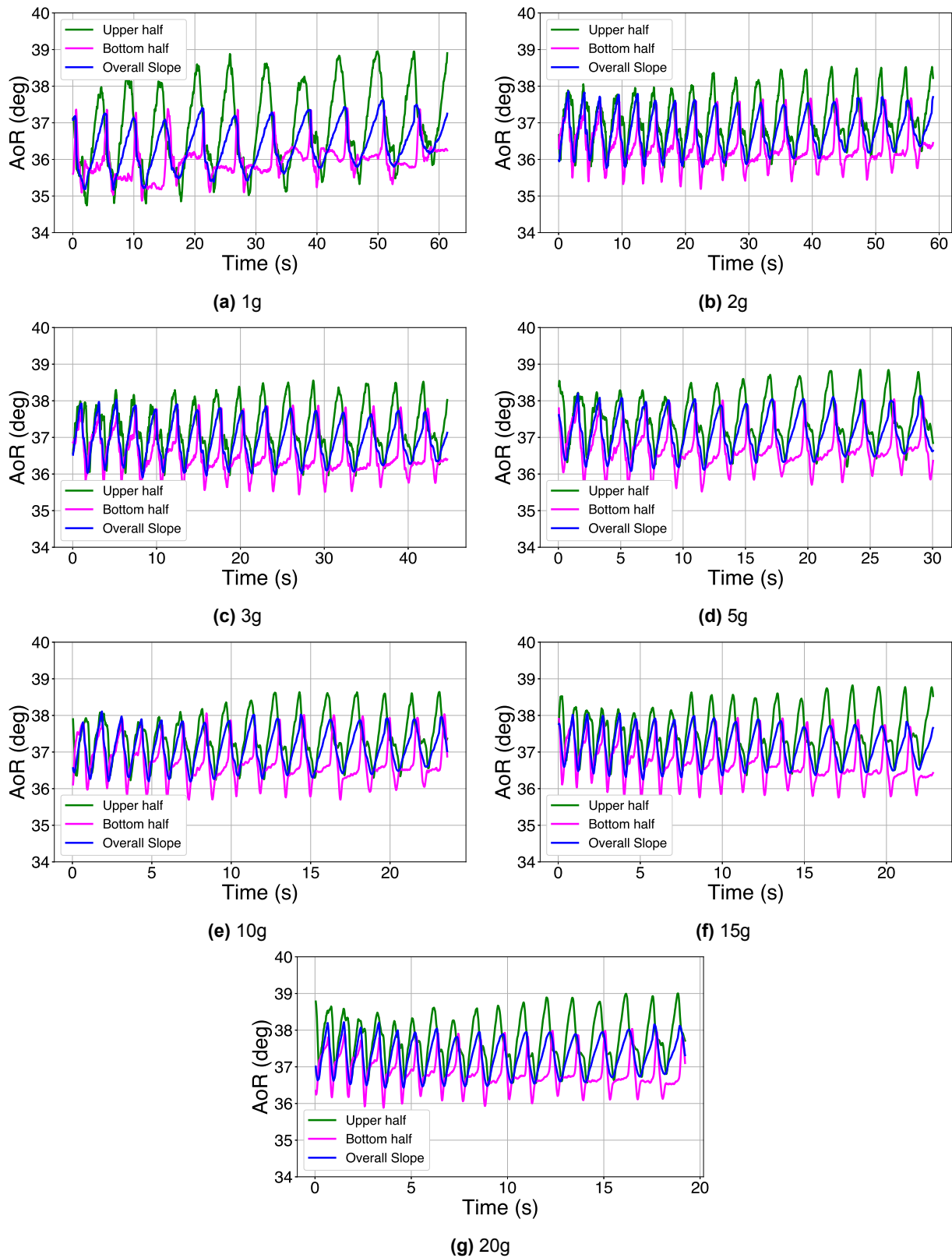


Figure B.8: Heartbeat graphs of the river-volcanic mixture in varying gravity acceleration, with a 3mm opening.

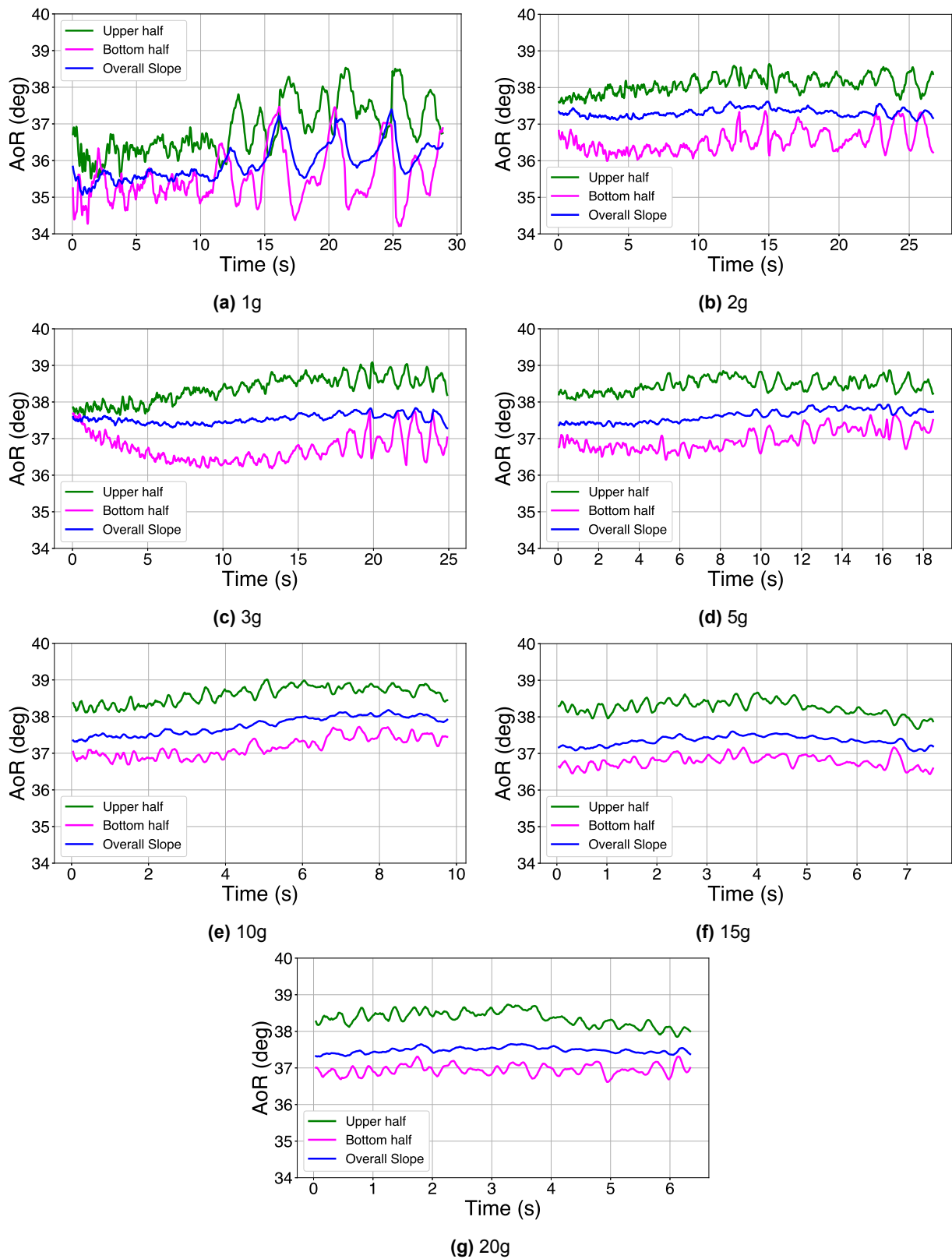


Figure B.9: Heartbeat graphs of the river-volcanic mixture in varying gravity acceleration, with a 5mm opening.

B.2. Discharge Flow Against Gravity

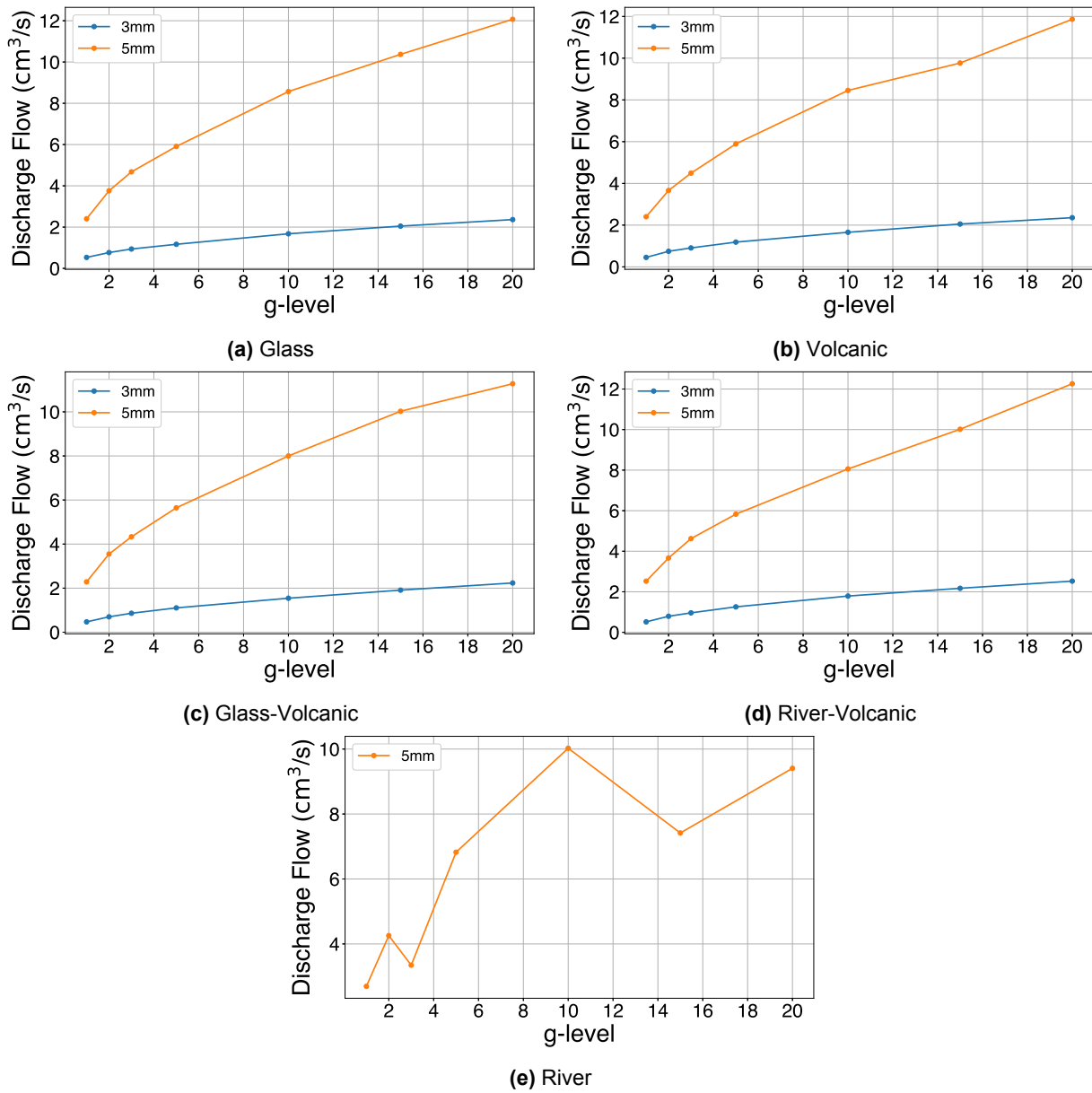
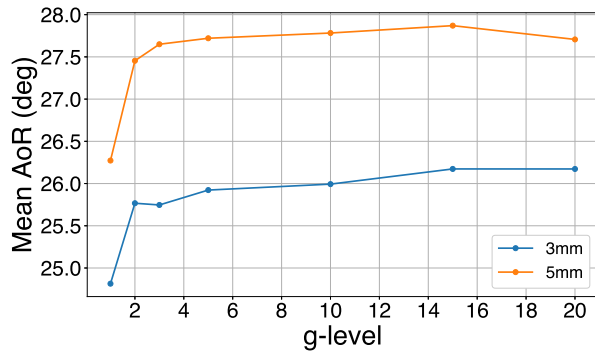


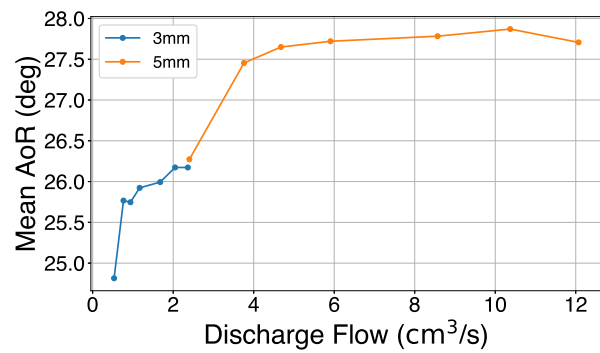
Figure B.10: Discharge volume flow against gravity for each material

B.3. Mean Angle of Repose against Gravity & the Discharge Flow

Glass Beads



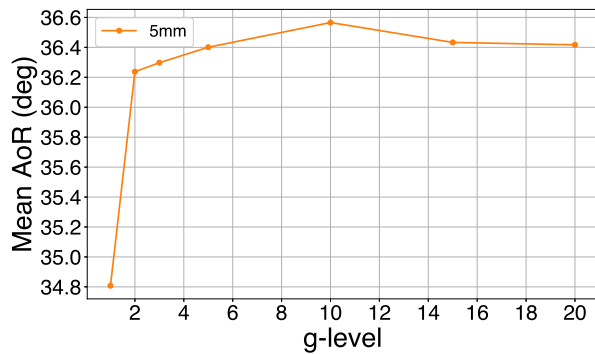
(a) Mean AoR against gravity



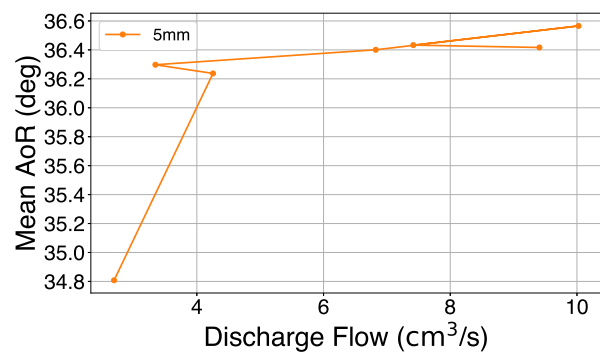
(b) Mean AoR against discharge flow

Figure B.11: Average overall angle of repose against gravity and the discharge volume flow, with varying cell opening, for glass beads.

River Sand



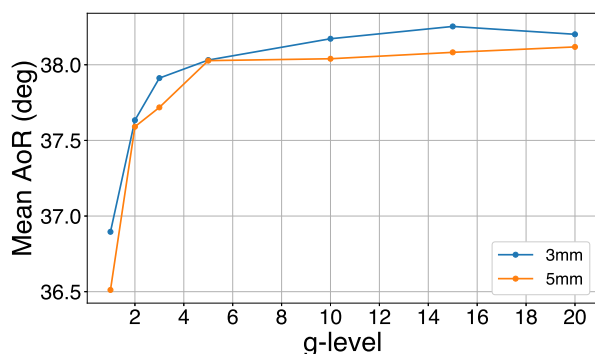
(a) Mean AoR against gravity



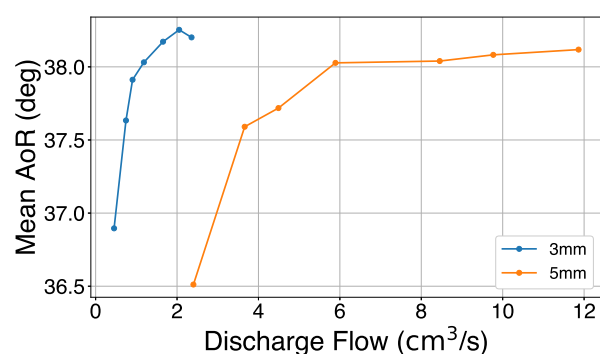
(b) Mean AoR against discharge flow

Figure B.12: Average overall angle of repose against gravity and the discharge volume flow, with varying cell opening, for river sand.

Volcanic Sand



(a) Mean AoR against gravity

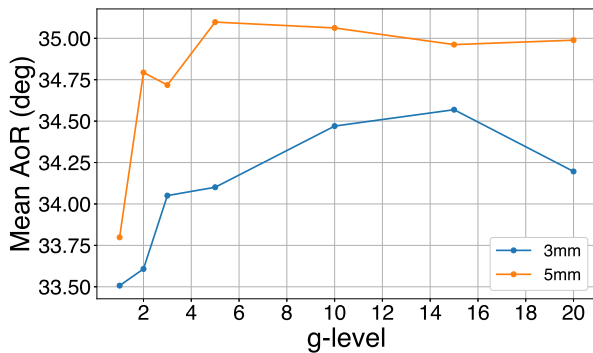


(b) Mean AoR against discharge flow

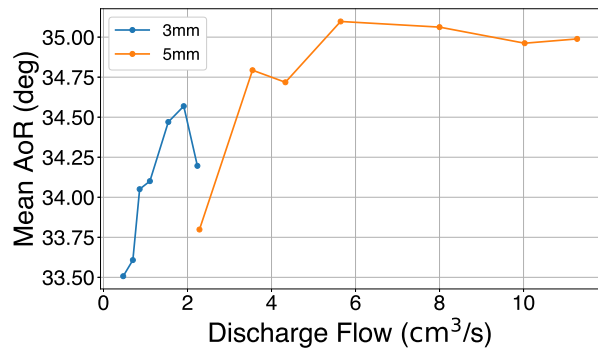
Figure B.13: Average overall angle of repose against gravity and the discharge volume flow, with varying cell opening, for volcanic sand.

Glass-Volcanic Mixture

Plots for the overall slope.



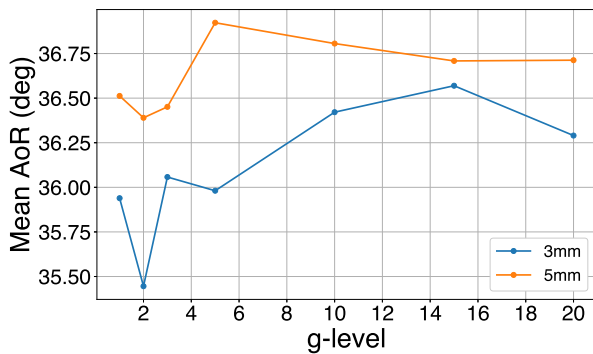
(a) Mean AoR against gravity



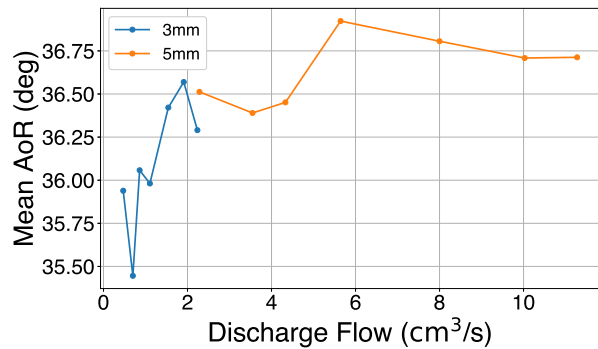
(b) Mean AoR against discharge flow

Figure B.14: Average overall angle of repose against gravity and the discharge volume flow, with varying cell opening, for the glass-volcanic mixture.

Plots for the upper half of the slope.



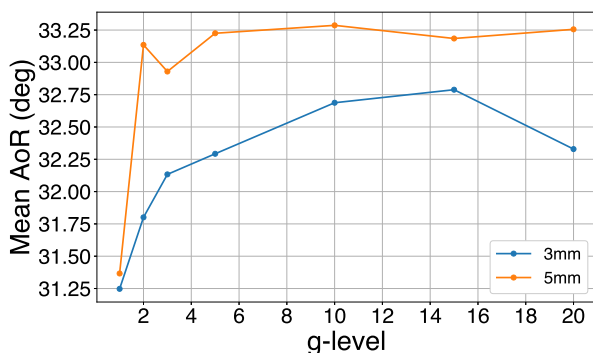
(a) Mean AoR against gravity



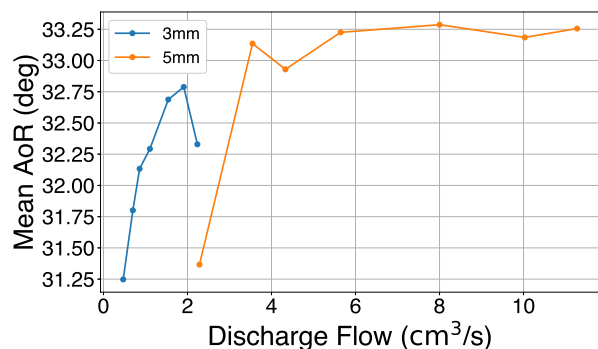
(b) Mean AoR against discharge flow

Figure B.15: Average upper angle of repose against gravity and the discharge volume flow, with varying cell opening, for the glass-volcanic mixture.

Plots for the bottom half of the slope.



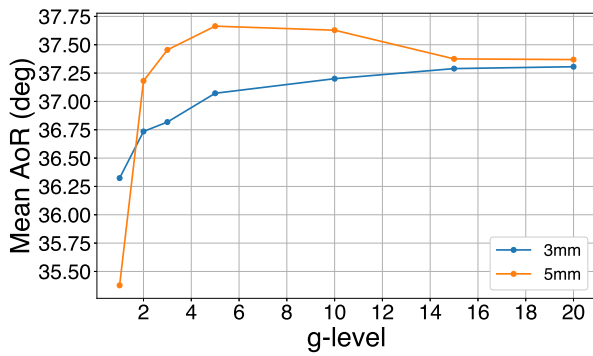
(a) Mean AoR against gravity



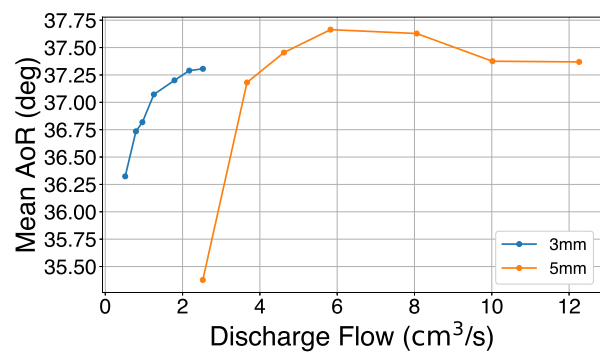
(b) Mean AoR against discharge flow

Figure B.16: Average bottom angle of repose against gravity and the discharge volume flow, with varying cell opening, for the glass-volcanic mixture.

River-Volcanic Mixture



(a) Mean AoR against gravity

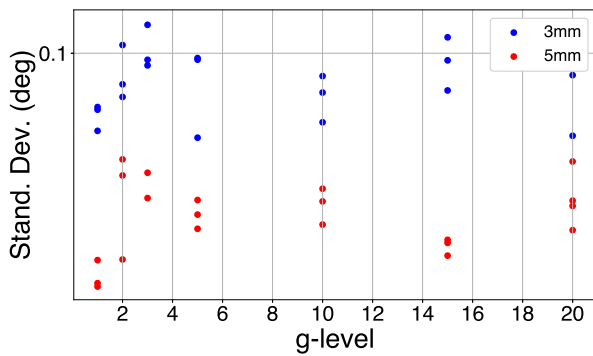


(b) Mean AoR against discharge flow

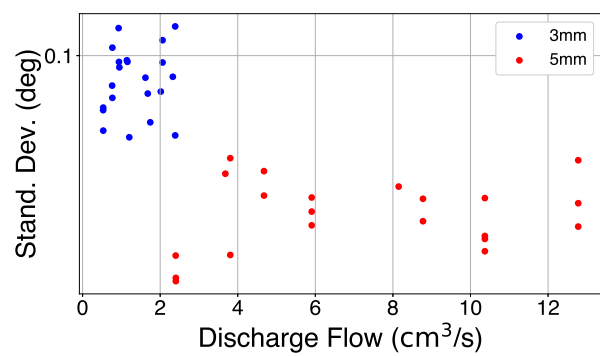
Figure B.17: Average bottom angle of repose against gravity and the discharge volume flow, with varying cell opening, for the river-volcanic mixture.

B.4. Standard Deviation of the Angle of Repose against Gravity & the Discharge Flow

Glass Beads



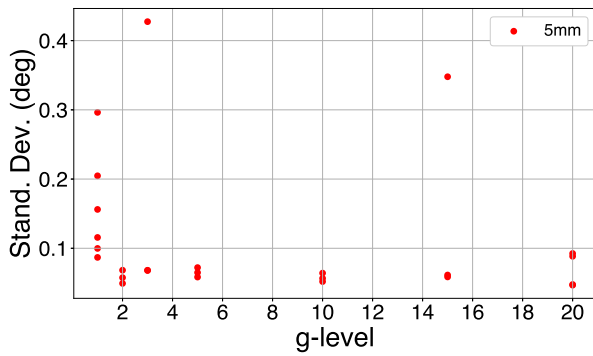
(a) Standard deviation against gravity



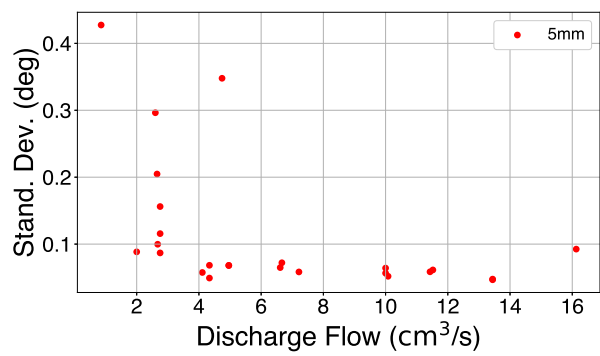
(b) Standard deviation against the discharge flow

Figure B.18: Scatter plot of the standard deviation in the angle of repose of glass beads against gravity and the discharge flow, for varying openings.

River Sand



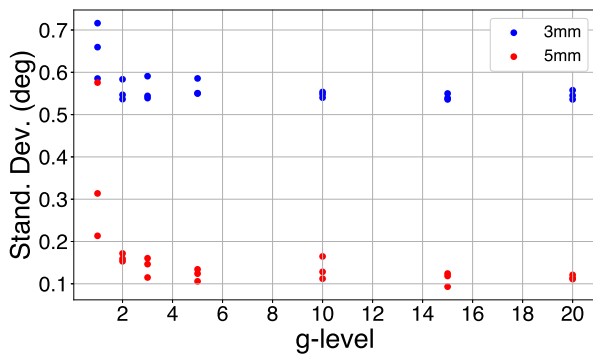
(a) Standard deviation against gravity



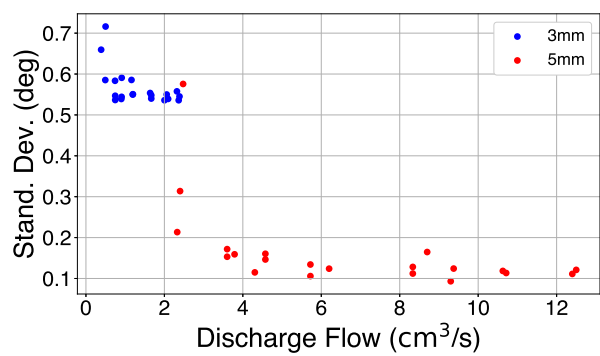
(b) Standard deviation against the discharge flow

Figure B.19: Scatter plot of the standard deviation in the angle of repose of river sand against gravity and the discharge flow, for varying openings.

Volcanic Sand



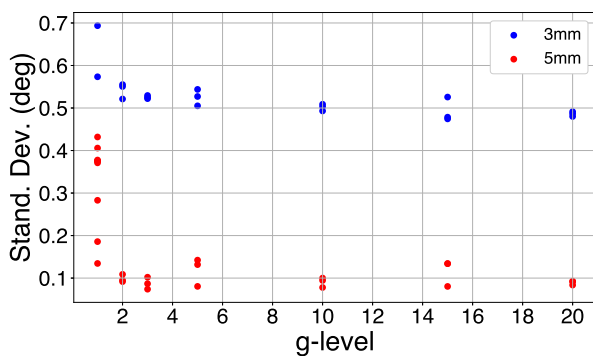
(a) Standard deviation against gravity



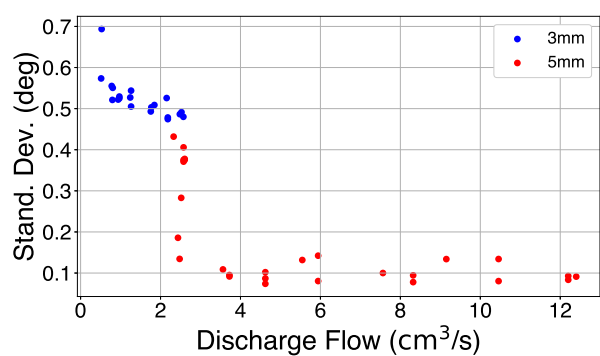
(b) Standard deviation against the discharge flow

Figure B.20: Scatter plot of the standard deviation in the angle of repose of volcanic sand against gravity and the discharge flow, for varying openings.

River-Volcanic Mixture



(a) Standard deviation against gravity

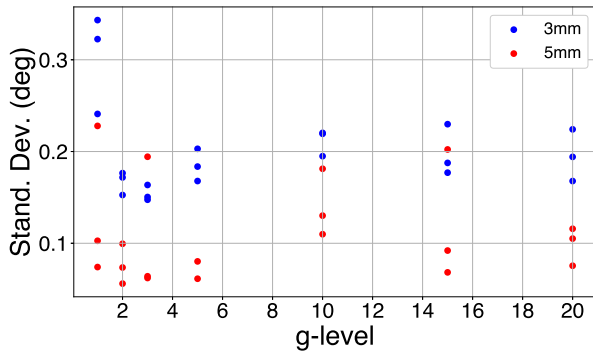


(b) Standard deviation against the discharge flow

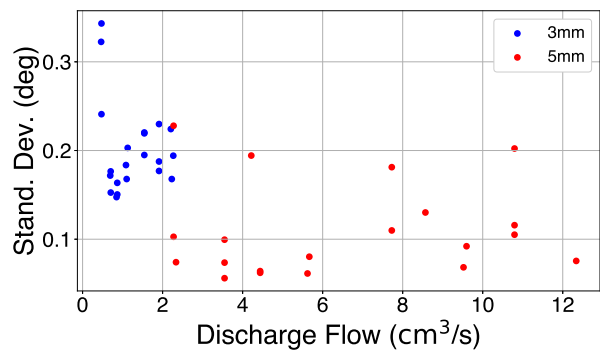
Figure B.21: Scatter plot of the standard deviation in the angle of repose of the river-volcanic mixture against gravity and the discharge flow, for varying openings.

Glass-Volcanic Mixture

For the overall slope.



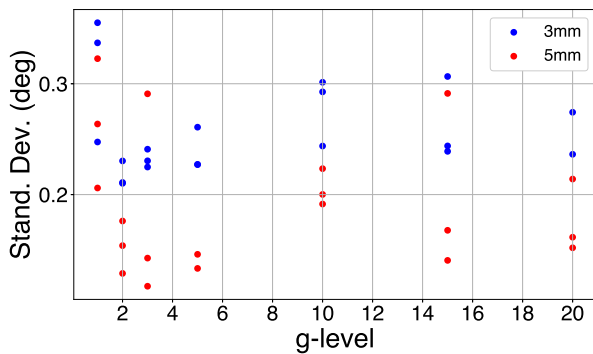
(a) Standard deviation against gravity



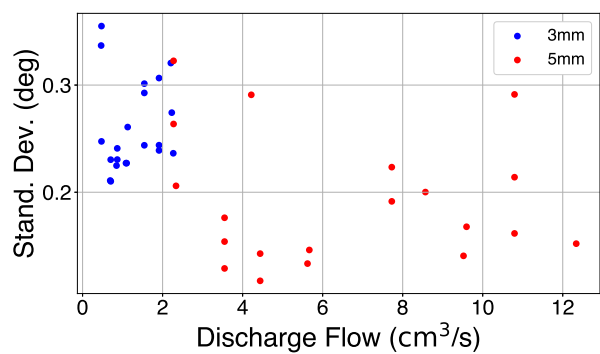
(b) Standard deviation against the discharge flow

Figure B.22: Scatter plot of the standard deviation in the angle of repose of the glass-volcanic mixture against gravity and the discharge flow, for the overall slope for varying openings.

For the upper half of the slope.



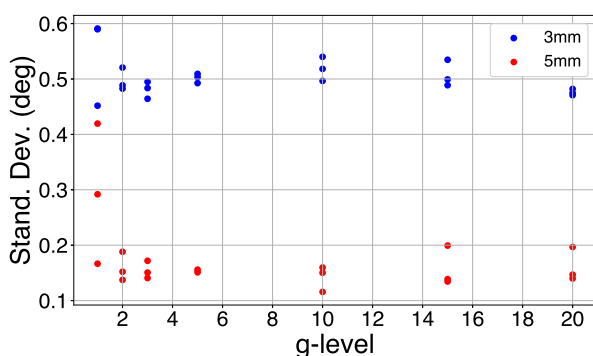
(a) Standard deviation against gravity



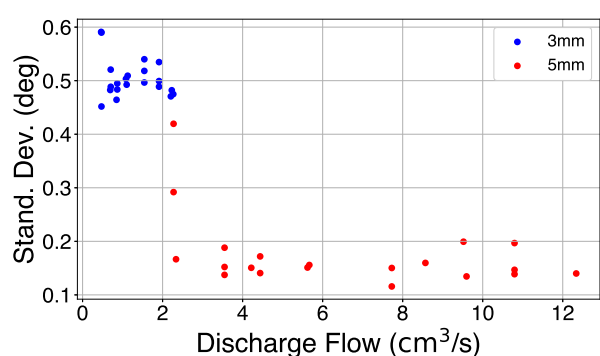
(b) Standard deviation against the discharge flow

Figure B.23: Scatter plot of the standard deviation in the angle of repose of the glass-volcanic mixture against gravity and the discharge flow, for the upper slope for varying openings.

For the bottom half of the slope.



(a) Standard deviation against gravity



(b) Standard deviation against the discharge flow

Figure B.24: Scatter plot of the standard deviation in the angle of repose of the glass-volcanic mixture against gravity and the discharge flow, for the bottom slope for varying openings.

For All Materials

For the overall slope.

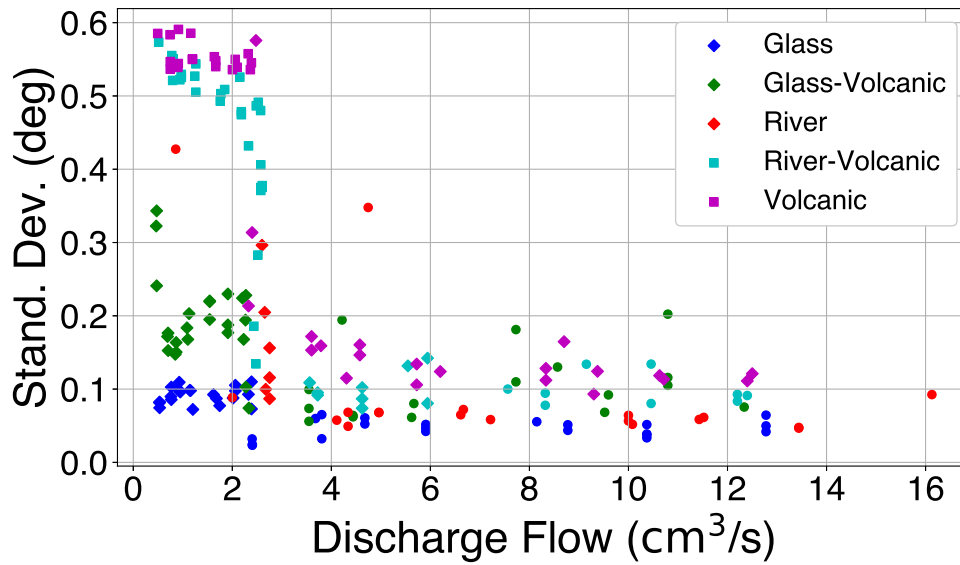


Figure B.25: Scatter plot of the standard deviation in the angle of repose against the discharge flow. This is for the overall slope, for all materials and all openings.

For the upper half of the slope.

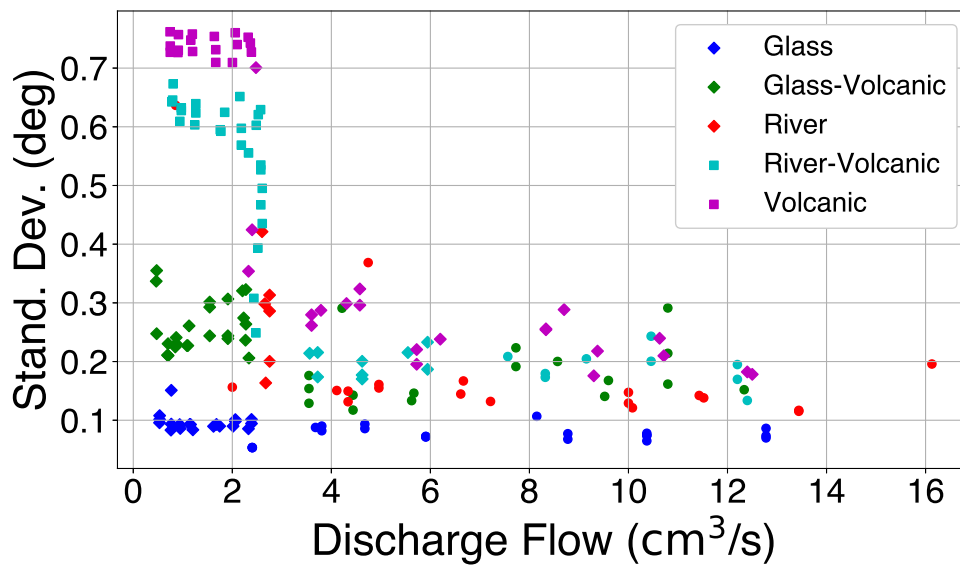


Figure B.26: Scatter plot of the standard deviation in the angle of repose against the discharge flow. This is for the upper half of the slope, for all materials and all openings.

For the bottom half of the slope.

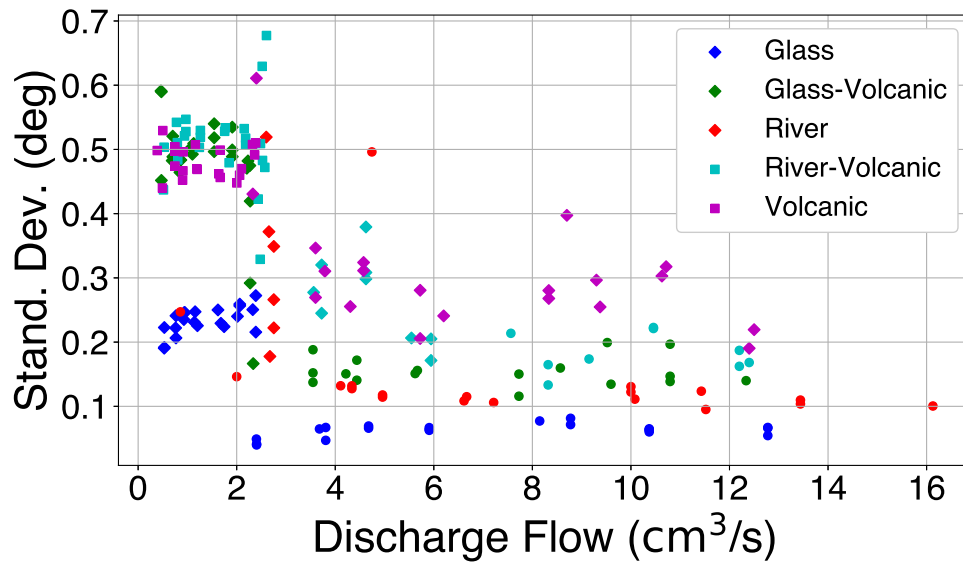


Figure B.27: Scatter plot of the standard deviation in the angle of repose against the discharge flow. This is for the bottom half of the slope, for all materials and all openings.

B.5. Mean Angle of Repose Against Discharge Flow & Gravity per Avalanche Regimes

Glass Beads

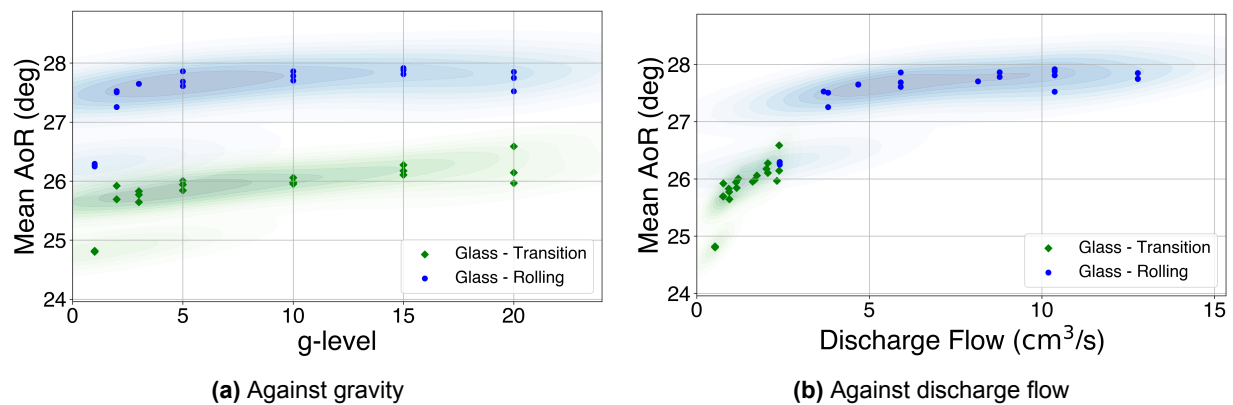
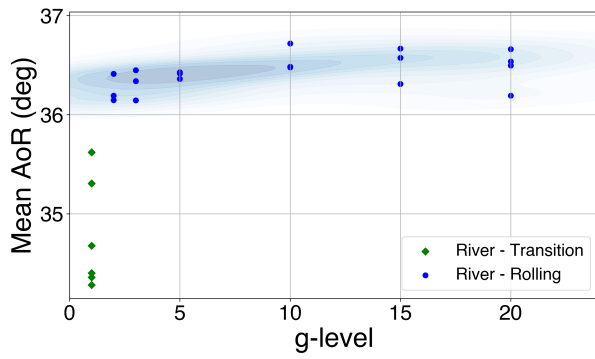
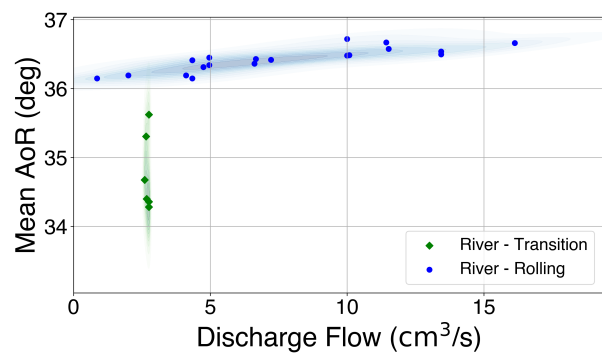


Figure B.28: Average overall angle of repose against gravity and the discharge volume flow, with varying avalanching regimes, for glass beads.

River Sand



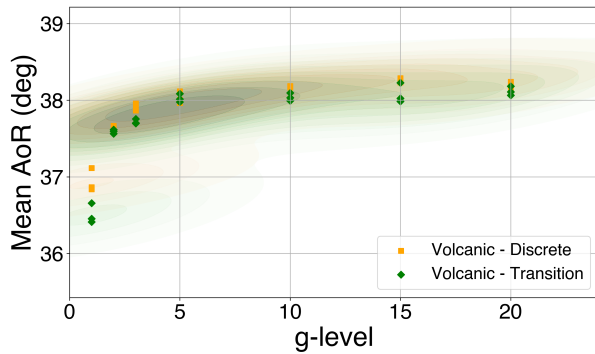
(a) Against gravity



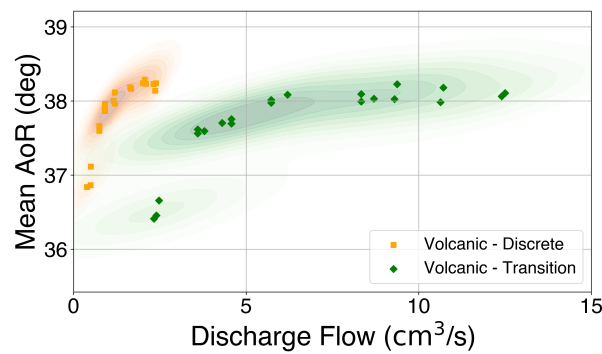
(b) Against discharge flow

Figure B.29: Average overall angle of repose against gravity and the discharge volume flow, with varying avalanching regimes, for the river sand.

Volcanic Sand



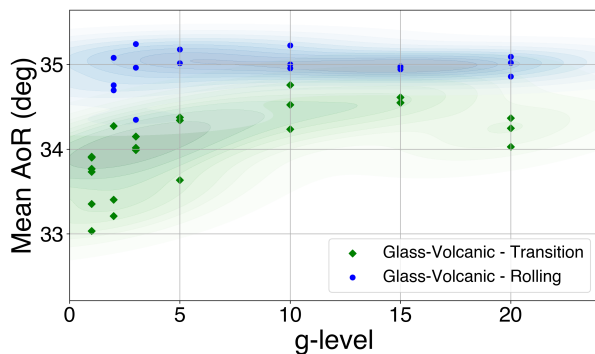
(a) Against gravity



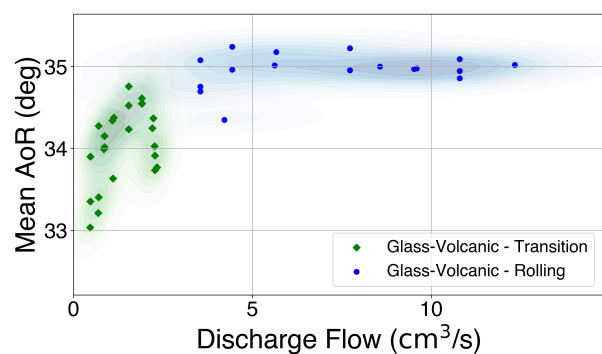
(b) Against discharge flow

Figure B.30: Average overall angle of repose against gravity and the discharge volume flow, with varying avalanching regimes, for the volcanic sand.

Glass-Volcanic Mixture



(a) Against gravity



(b) Against discharge flow

Figure B.31: Average overall angle of repose against gravity and the discharge volume flow, with varying avalanching regimes, for the glass-volcanic mixture.

River-Volcanic Mixture

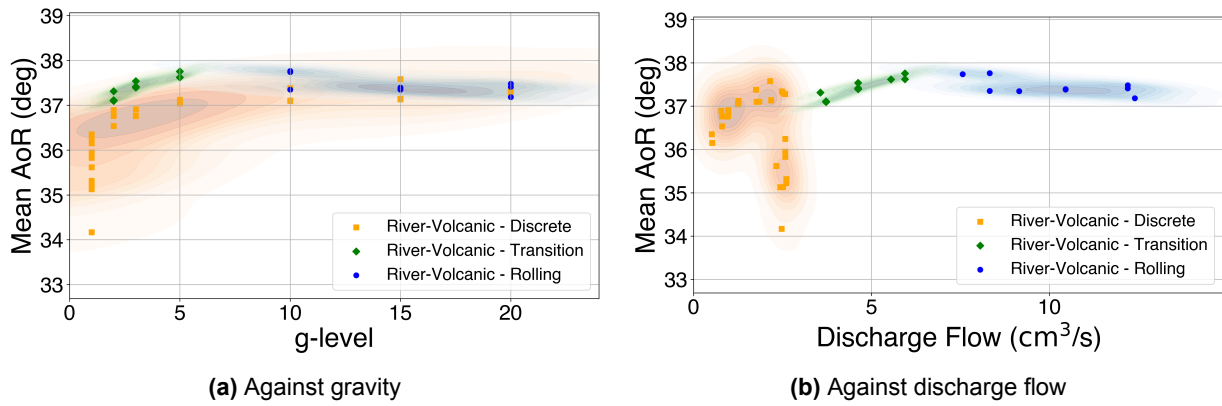


Figure B.32: Average overall angle of repose against gravity and the discharge volume flow, with varying avalanching regimes, for the river-volcanic mixture.

B.6. Static & Dynamic Angles of Repose

Here are the plots of the static and dynamic angles of repose against gravity and the discharge flow per avalanching regime.

Glass Beads

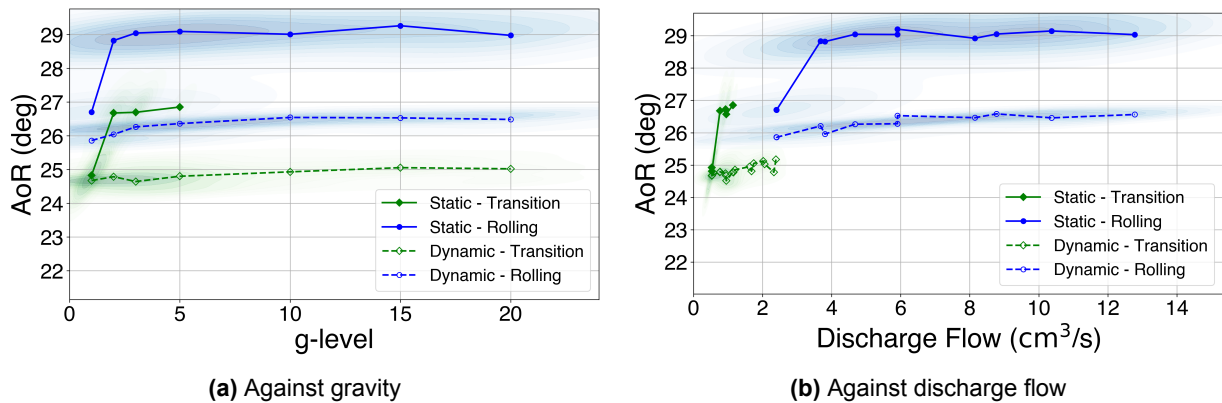
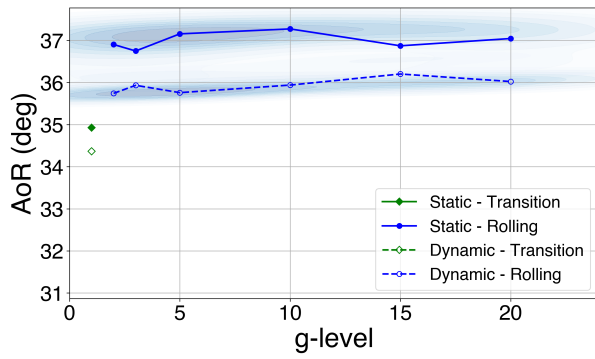
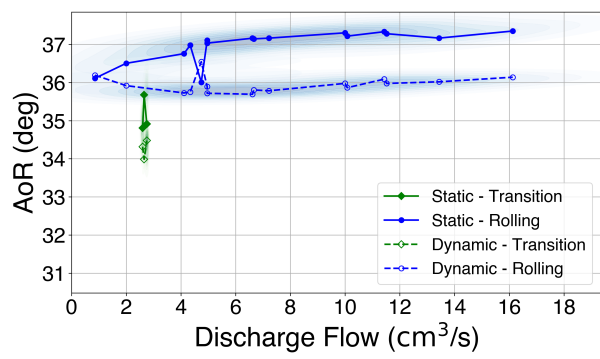


Figure B.33: Static and Dynamic AoR against gravity and discharge for glass beads.

River Sand



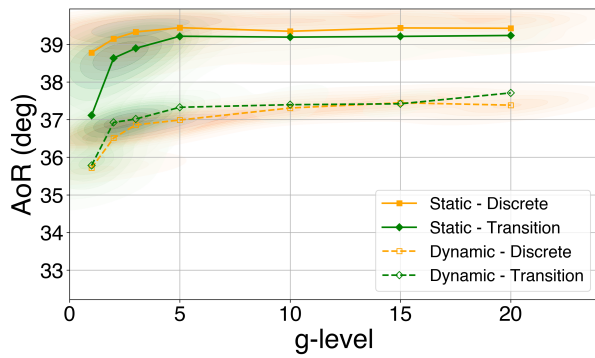
(a) Against gravity



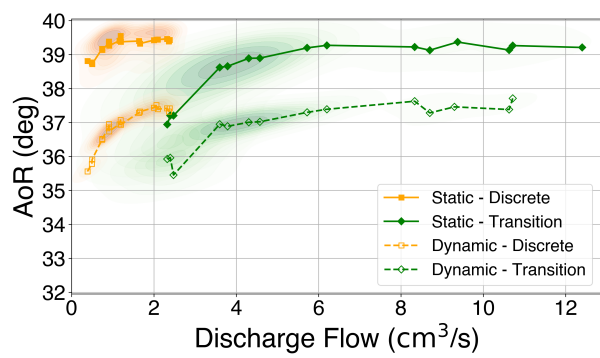
(b) Against discharge flow

Figure B.34: Static and Dynamic AoR against gravity and discharge for river sand.

Volcanic Sand



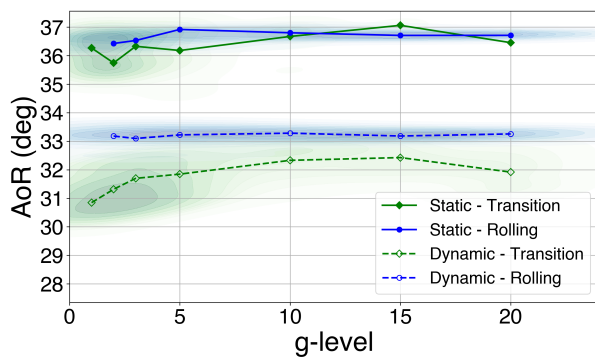
(a) Against gravity



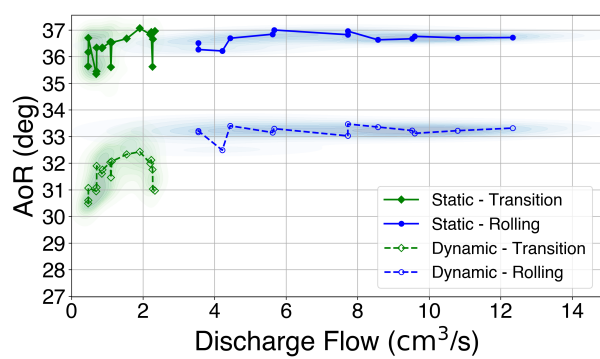
(b) Against discharge flow

Figure B.35: Static and Dynamic AoR against gravity and discharge for volcanic sand.

Glass-Volcanic Mixture



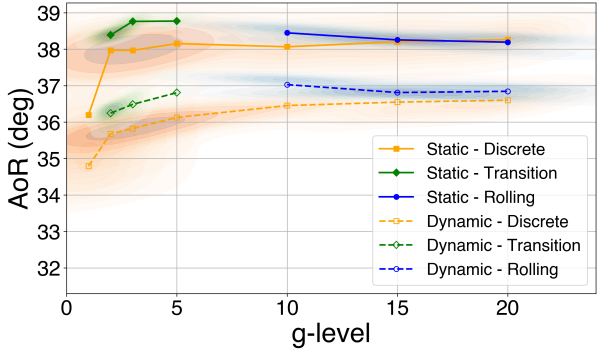
(a) Against gravity



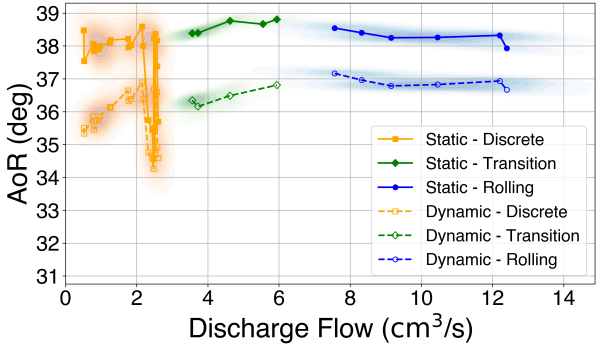
(b) Against discharge flow

Figure B.36: Static and Dynamic AoR against gravity and discharge for the glass volcanic mixture.

River-Volcanic Mixture

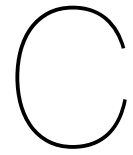


(a) Against gravity



(b) Against discharge flow

Figure B.37: Static and Dynamic AoR against gravity and discharge for the river volcanic mixture.



Effect of Gravity on Particle Separation

The two mixtures used in the experiments displayed particle separation. The glass-volcanic mixture showed particle segregation, and the river-volcanic mixture showed particle stratification. These patterns have been studied in the literature but never while varying the gravity environment (see Chapter 2). These observations are included in this appendix as they do not serve in directly answering the research question of this research. However, they do represent an addition to the literature to be explored in future research.

The effect of varying gravity on the particle separation patterns is observed in this chapter through the visual comparison of still images taken from the experimental videos.

Changes in Particle Stratification of the River-Volcanic Mixture

The stratification patterns of the river-volcanic mixture are shown in Figure C.1 and Figure C.2. As a reminder, higher gravity results in a higher discharge flow. These piles formed under different regimes: a discrete regime for the 3mm set, and a transition (from 1g to 5g) to rolling regime (from 5g to 20g) for the 5mm set. Again, stratification occurs in mixtures where particles of smaller diameter have the smaller AoR, and the particles of larger diameter have larger AoR, creating repetitive layers of each material.

The main observations for the 3mm opening are:

- The stratification layers become thinner and less defined as gravity increases.
- The length of the lighter river sand stripes decreases with increasing gravity, creating an almost segregated appearance at 20g.

The main observations for the 5mm opening are:

- The stratification clarity of the layers becomes less defined, appearing blurry or non-existent at higher gravity levels.
- The layer length varies. At 1g, the stratified layers are longer than in the 3mm-20g experiment, despite having a similar discharge flow. Additionally, more river sand particles settle in the bottom half of the pile at 1g, while at 20g, most river sand accumulates at the top.

The following interpretations can be made:

- The length of stratified layers is primarily influenced by gravity rather than discharge flow. At higher gravity, smaller river sand particles experience more friction against the layer beneath, forcing them to settle earlier along the slope, while larger volcanic particles continue moving further.
- The clarity of stratification patterns depends on both discharge flow and avalanching regime. Stratification primarily occurs in the discrete regime, where thinner layers form at higher discharge flows. The faster avalanches from the transition and rolling regimes do not let the stratification process happen

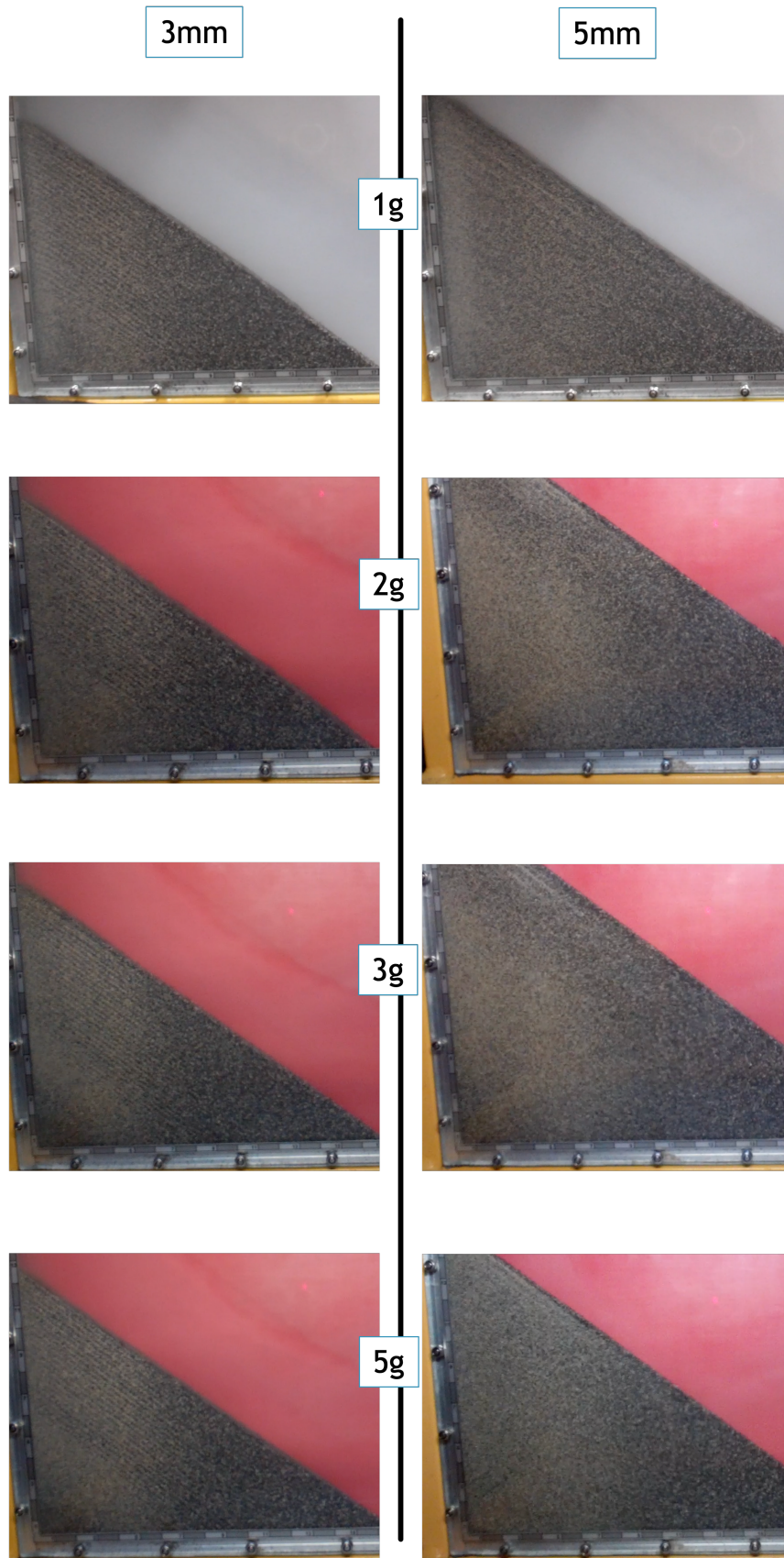


Figure C.1: Visual changes in the particle stratification patterns in the river-volcanic sand mixture when varying the gravity level (from 1g to 5g) for cells with a 3mm opening on the left, and a 5mm opening on the right.

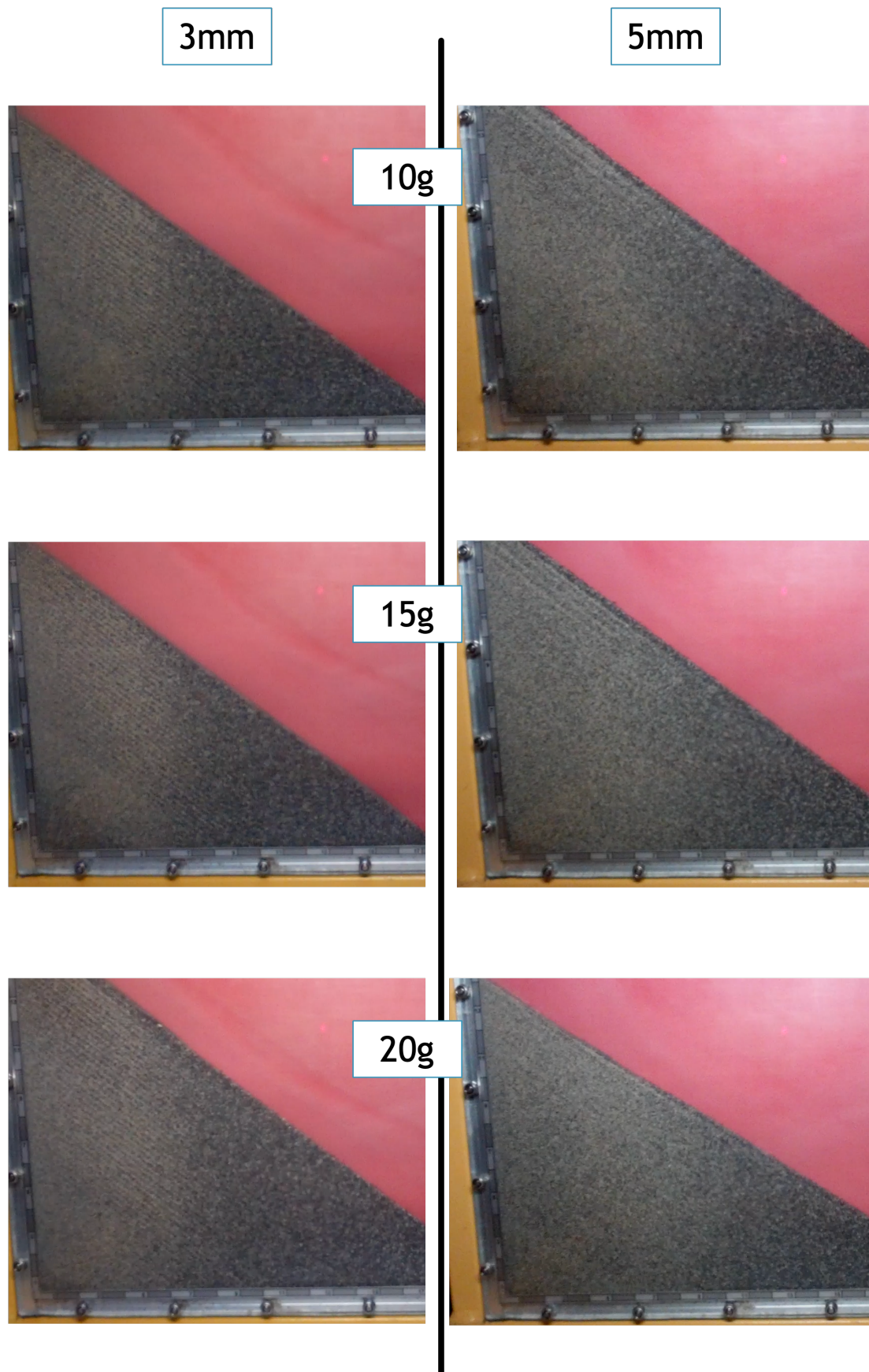


Figure C.2: Visual changes in the particle stratification patterns in the river-volcanic sand mixture when varying the gravity level (from 10g to 20g) for cells with a 3mm opening on the left, and a 5mm opening on the right.

Changes in Particle Segregation of the Glass-Volcanic Mixture

The segregation patterns of the glass-volcanic mixture are visible in Figure C.3 and Figure C.4. The 3mm piles were formed in a transition regime and the 5mm piles were formed in the rolling regime. As a reminder, segregation occurs in mixtures where particles of smaller diameter and larger AoR stop on the upper half of the pile, while particles of larger diameter and smaller AoR stop on the bottom half.

The main observations are shared for both openings:

- Segregation is less pronounced at 1g compared to 20g. At higher gravity, particles are more compacted against the underlying layer. Smaller volcanic particles with higher AoR experience greater friction and stop earlier, allowing larger glass particles to roll further downslope, increasing segregation.
- No significant visual difference is observed between the 3mm and 5mm openings at the same gravity level, indicating that higher discharge flow does not visibly affect segregation.
- Similar to the river-volcanic mixture, increased discharge flow and pile formation in transition or rolling regimes result in the disappearance of stratification (in the river-volcanic mixture) and a stronger segregation pattern (in both mixtures).

The following interpretations can be made:

- Higher gravity enhances segregation by increasing friction between avalanching particles and the underlying layers. This effect causes smaller particles with higher AoR to stop earlier than larger particles.
- The degree of segregation is primarily influenced by gravity rather than discharge flow, as shown by the lack of visible differences between the 3mm and 5mm openings at the same gravity levels.
- Formation under transition and rolling regimes favours particle segregation, likely due to faster particle movement inhibiting stratification.

Note that these observations are made qualitatively as there is no quantified measure of the segregation state in the material.

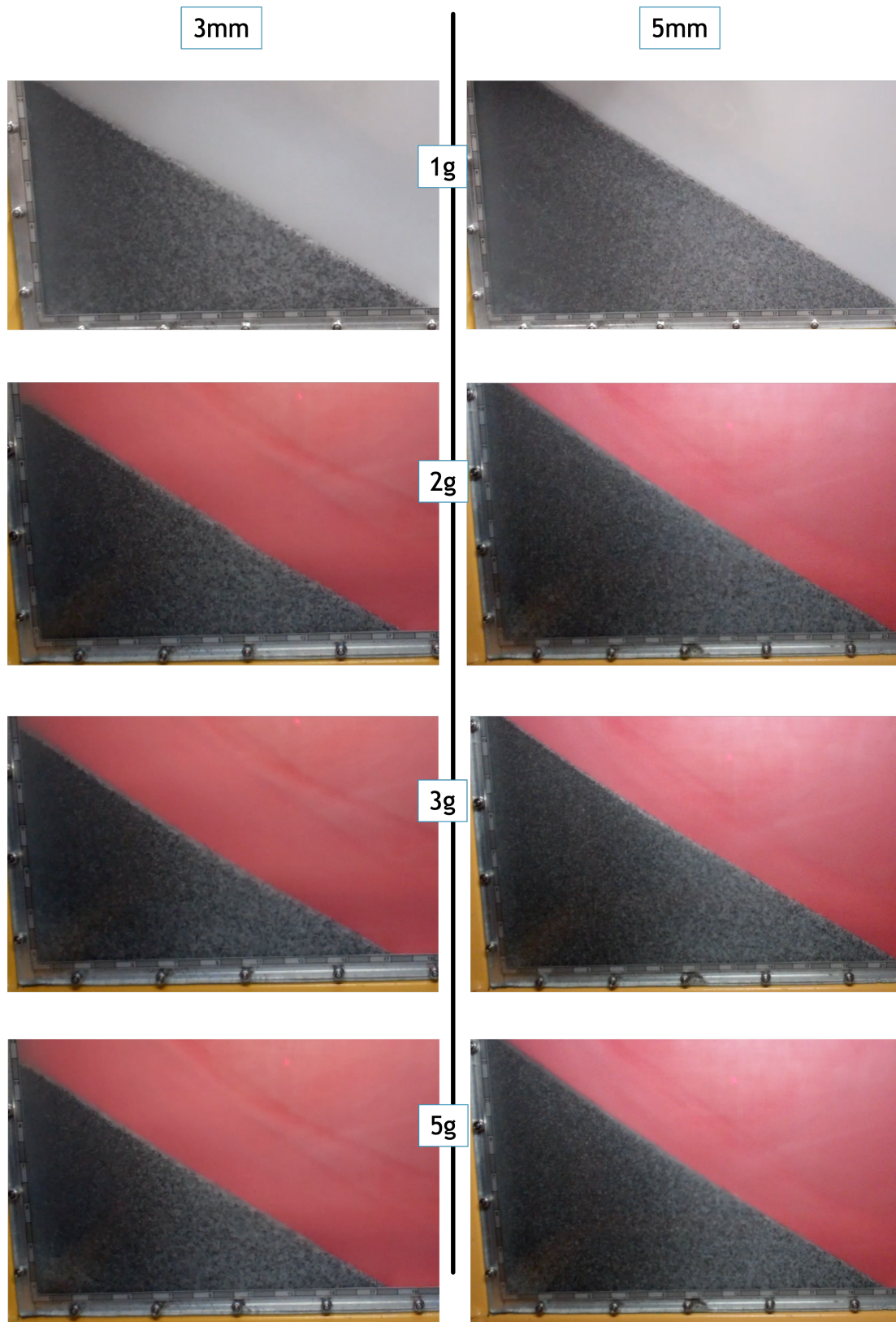


Figure C.3: Visual changes in the particle segregation patterns in the glass beads-volcanic sand mixture when varying the gravity level (from 1g to 5g) for cells with a 3mm opening on the left, and a 5mm opening on the right.

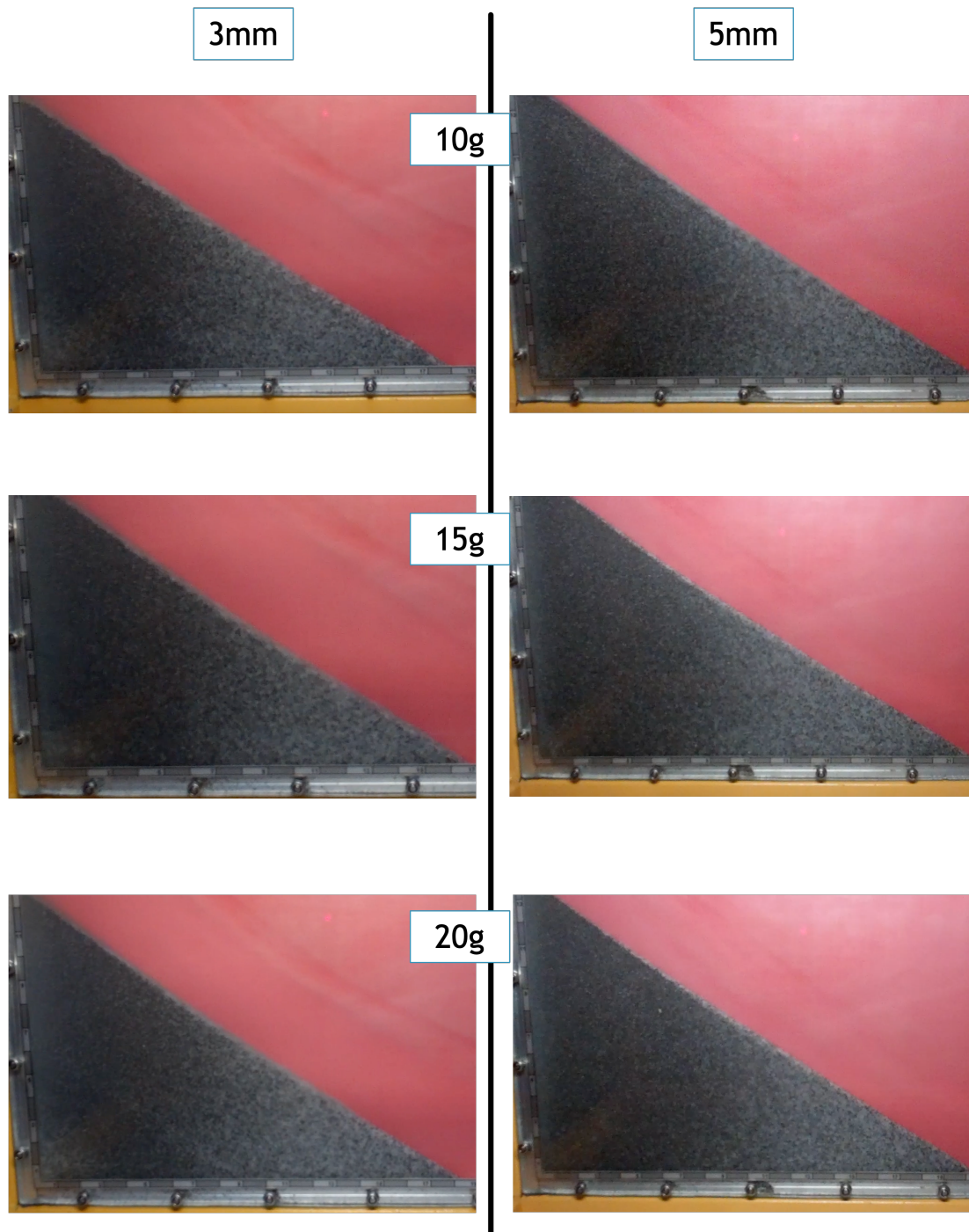


Figure C.4: Visual changes in the particle segregation patterns in the glass beads-volcanic sand mixture when varying the gravity level (from 10g to 20g) for cells with a 3mm opening on the left, and a 5mm opening on the right.

Summary of the Findings on the Effects on the Static and Dynamic Angles of Repose

Effects of the discharge flow:

- A higher discharge flow reduces the thickness of the stratification layers, weakening the clarity of stratification patterns.
- Increasing discharge flows induce changes in avalanching regime, which in turn affects the particle separation patterns.

Effects of the avalanching regime:

- Stratification primarily occurs in the discrete regime.
- The faster avalanches from the transition and rolling regimes do not let the stratification process happen.

Effects of gravity:

- Higher gravity weakens stratification and enhances segregation, by increasing friction between avalanching particles and the underlying layers. This effect causes smaller particles to stop earlier than larger particles, even if the larger particles have a higher AoR.
- The degree of segregation is primarily influenced by gravity rather than discharge flow, as shown by the lack of visible differences in particle segregation between the 3mm and 5mm openings at the same gravity levels.